II-A2a

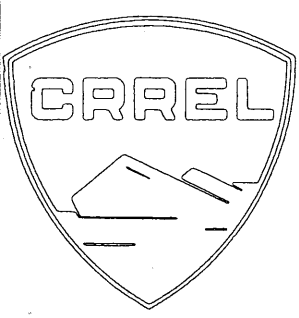

COLD REGIONS
SCIENCE AND ENGINEERING
Monograph II-A2a

SEISMIC EXPLORATION IN COLD REGIONS

Hans Roethlisberger

October 1972

CORPS OF ENGINEERS, U.S. ARMY
COLD REGIONS RESEARCH AND ENGINEERING LABORATORY
HANOVER, NEW HAMPSHIRE

The findings in this report are not to be construed as an official Department of the Army position unless so designated by other authorized documents.

SEISMIC EXPLORATION IN COLD REGIONS

Hans Roethlisberger

October 1972

DA PROJECT 4A062112A894

CORPS OF ENGINEERS, U.S. ARMY
COLD REGIONS RESEARCH AND ENGINEERING LABORATORY
HANOVER, NEW HAMPSHIRE

PREFACE

The monograph on exploration geophysics in cold regions is presented in two parts for the sake of convenience. This first part covers seismic explorations in cold regions, including related techniques based on elastic waves. Electrical, magnetic and gravimetric explorations in cold regions will be the subject of a second volume.

The present volume was prepared by Dr. Hans Roethlisberger, while engaged as contract scientist with the U.S. Army Cold Regions Research and Engineering Laboratory (USA CRREL). The author, a specialist in glaciology and geophysics, is associated with the Laboratory of Hydraulics, Hydrology and Glaciology at the Federal Institute of Technology in Zurich, Switzerland. Valuable suggestions were received from Dr. Charles R. Bentley, Professor of Geophysics, the University of Wisconson, Madison, Wisconsin, who reviewed the manuscript under a separate contract with USA CRREL.

Much of the writing of this monograph was performed under DA Project IN025001A130 and IT062112A130, *Cold Regions Research*, Task 01, *Research in Snow, Ice and Frozen Ground*, and subsequently Task 01, *Applied Research and Engineering*. The monograph is published under DA Project 4A062112A894, *Engineering in Cold Environments*, Task 20, *Cold Regions Systems Analysis, Systems Engineering, Production and Assessment Studies for Military Installations.*

CONTENTS

	Page
Preface	ii
List of symbols	viii
Editor's foreword	xiv
Introduction	1
Principles	1
Material properties	2
Elasticity and velocity	2
Body waves in isotropic media	2
Body waves in anisotropic media	2
Surface waves	5
Waves in slender bars	6
Waves in thin floating plates	6
Methods for determining seismic properties	6
Velocity	6
Attenuation	8
Seismic velocities in ice and snow	11
Single crystal ice	11
Non-porous isotropic polycrystalline ice	14
Bubbly ice	16
Velocity vs temperature	18
Velocity vs pressure	22
Anisotropic polycrystalline ice	22
Velocity and inclusions	24
Velocities in snow	26
Velocities in sea ice	31
Seismic velocities in frozen ground	35
Attenuation	39
Equipment, logistics and operation	40
Seismic surveys on snow and ice	40
Seismic surveys on frozen ground	42
Reflection soundings	44
The reflection technique on glaciers	44
Theory of reflection soundings on glaciers	51
Homogeneous isotropic layer of uniform thickness	51
Three-dimensional reflections in a homogeneous isotropic mass	54
Depth computation when the velocity is a function of depth	59
Depth determination on ice shelves	61
Anisotropy	64
Energy of reflected waves	66
Applications and results of reflection soundings on glaciers	71
Continental ice sheets	71
Ice shelves and floating ice islands	75
Valley glaciers	79
Reflection soundings in frozen ground	81
Refraction soundings	84
Method	84
Velocity and depth in homogeneous layers	84
Continuous velocity increase with depth	86
Velocity decrease with depth	91

CONTENTS (Cont'd)

Page

Energy of refracted waves 92
Applications 93
Glaciers 93
Frozen ground 100
Surface waves and waves in thin floating ice 105
Surface waves 105
Waves in thin floating ice 105
Body waves 106
Plate waves 106
Flexural waves 107
Air-coupled waves 107
Reflected waves 108
Some special applications of elastic waves 110
Echo sounding 110
Well-logging by ultrasonic pulses 110
Glacier-flow studies by an ultrasonic pulse technique 110
Acoustic surveys of the frozen zone around a freezing shaft 110
Attenuation and particle motion 111
Continuous seismic waves 111
Ice tremors 111
Selected bibliography 113
Appendix A: Computation of ray velocity as a function of direction for uniaxially anisotropic media 125
Appendix B: Various methods for determining elastic and seismic properties of ice, in particular those applicable on floating ice sheets 127
Appendix C: Spatial solutions for reflection soundings 129
Appendix D: Glossary 135
Abstract 139

ILLUSTRATIONS

Figure

1. Ratio of the velocity of a Rayleigh wave to the velocity of a shear wave as a function of Poisson's ratio ν 5
2. Time-distance graph for ultrasonic pulse measurements in circular ice rods of 7 cm diameter and variable length, TUTO Tunnel 9
3. Resonance curves for high density snow samples vibrating laterally 10
4. Elastic moduli (stiffness constants) c_{ik} vs temperature 12
5. *P*-wave velocities in the principal directions of single-crystal ice vs temperature 13
6. Ray velocity vs direction in single-crystal ice 14
7. *P*-wave velocity V_P of ice vs density ρ 18
8. *P*-wave velocity V_P vs temperature 19
9. Shear wave velocity V_S vs temperature 20
10. *P*-wave velocity vs amount of heat introduced into the sample 21
11. Ray velocity diagram in Pertinax, a hard impregnated cardboard 23
12. Theoretical velocity V_P vs content of rock (granite) inclusions in ice 25
13. Theoretical velocity V_S vs content of rock (granite) inclusions in ice 25
14. Velocity of an elastic compression wave in snow as a function of density 26
15. *P*-wave velocity V_P vs snow density, comparison of seismic and ultrasonic data 27
16. Shear wave velocity V_S vs snow density, comparison of seismic and ultrasonic data 27

ILLUSTRATIONS (Cont'd)

Figure Page

17. Wave velocities in snow from seismic data and velocities computed from various theories, vs snow density, selected sites 28
18. *P*-wave velocity vs density in milled and age-hardened snow (except naturally compacted snow where indicated), measured on samples with ultrasonic pulses (50 kHz) 30
19. *P*-wave velocity in snow as a function of time during the period of intergranular bond formation (age-hardening) 30
20. Poisson's ratio for dry snow as a function of density, seismic and ultrasonic measurements 31
21. Young's modulus E of sea ice determined by various dynamic methods, in function of total porosity n or brine volume n_b. Additional theoretical curves and an experimental one for snow are given for comparison..... 32
22. Seasonal variation of longitudinal plate velocity 34
23. Sound velocity in frozen, synthetic cores of various porosities as a function of temperature..... 35
24. Summary plot of dynamic elastic properties of frozen soils and of ice versus temperature 37
25. Relationship of soil type and Young's modulus determined by sonic tests, at -6.7°C 38
26. Patterns for geophone set-up for reflection soundings on glaciers..... 44
27. Reflection chart for ice, Poisson's ratio $\nu = \frac{1}{3}$..... 46
28. Reflection seismogram on shallow ice (70 m) at the edge of the Greenland ice sheet (Camp TUTO)..... 47
29. Series of seismograms of successive shots at increasing distance mounted to illustrate the time distance relationship..... 47
30. Travel time curves from Site 2, Greenland, showing direct *P* and S-wave, various reflected waves and refracted wave P_G 48
31. Seismic reflection records showing normal surface wave attenuation, prolonged surface noise, and reflection R_e from a basal layer arriving 0.2 sec before the main bottom echo 49
32. Shot point displacement $\overline{SS'}$ and shift of reflecting element..... 50
33. Reflection and refraction at a plane interface 52
34. Reflection at a plane boundary parallel to the surface 53
35. Diagrams for calculating three-dimensional reflection soundings 55
36. Reflections from different parts of the glacier bed as a source of error..... 57
37. Multiple reflections at a sloping interface 58
38. *P*-wave velocity and vertical travel time as a function of depth of snow..... 60
39. Schematic seismic record and notation for single and multiple reflections at the bottom and surface of an ice shelf and at the bottom of the sea 62
40. Seismic reflection records from Ross Ice Shelf 63
41. Travel time vs distance diagram for ice plate of 1 m thickness 65
42. Normed travel time difference for converted wave of type *PS* and reflected *P*-wave as a function of shot distance 66
43. Ratio of the amplitude of first (A_x) and double (A_{2x}) reflections as a function of ice depth 67
44. Reflection coefficients for plane waves in ice incident on a plane boundary between ice and various solids 69
45. Energy of waves reaching the glacier bed 70
46. Seismic traverses in Greenland..... 72
47. Seismic traverses in Antarctica 73

CONTENTS (Cont'd)

ILLUSTRATIONS (Cont'd)

Figure — Page

48. Travel time isograms (millisec) for detailed seismic reflection surveys carried out 3 years apart at the same location on the Greenland Ice Cap 75
49. Reflection impulses of two surveys three years apart 76
50. Seismic reflection records for short spreads from ice shelf in Antarctica 77
51. Detailed reflection survey on the glacier de Tacul, France 80
52. Comparison of cross section of Glacier d'Argentière from seismic reflection soundings and drilling 81
53. Wide angle reflection shots on a flood plain near Thule, Greenland 82
54. Path of wave refracted at the critical angle 84
55. Time-distance diagram of direct and refracted waves 84
56. Travel time curve and paths when the velocity increases with depth 87
57. Empirical depth-velocity curve 89
58. Paths of surface reflected waves 90
59. Section of a refraction record showing surface reflected waves P_n (Antarctica) 91
60. Energy of the refracted wave on a continental ice sheet as a function of distance from the shot 93
61. Long refraction travel-time graph from the Antarctic Peninsula 94
62. Velocity columns in Antarctica from refraction soundings 94
63. Wave velocity as a function of depth 96
64. Depth of penetration of *P*-waves as a function of shot point to seismometer distance in two locations in Antarctica 97
65. Section of a refraction seismogram from Byrd Station showing different polarized shear waves 97
66. *P*-wave velocity in snow (ice) at the depth of 50 m as a function of mean annual temperature 97
67. Accumulation rate as a function of the *P*-wave velocity V_x at a distance of 200 m 98
68. Seismic travel-time curves near Fairbanks, Alaska, from a refraction profile on 4.6 m of dry alluvium, overlying about 12 m of water-saturated sediments above permafrost (V_P = 3280 m/sec) 100
69. Refraction soundings through frozen ground to bedrock 101
70. Accuracy and alternative interpretations of refraction data in the Thule area ... 103
71. Dispersion curves of the lowest modes of elastic wave propagation in sea ice . 106
72. Elastic waves produced in sea ice by a surface explosion 108
73. Multiple converted reflections (*PS*) of ultrasonic pulses in lake ice 109

TABLES

Table

I. Conversion table for elastic constants 3
II. Experimental values of the elastic moduli (stiffness constants) c_{ik} of ice 11
III. Experimental values of the elastic compliance constants s_{ik} of ice at –16°C ... 12
IV. Velocities of elastic waves in the principal directions of single crystals or ice with common vertical c-axis orientation at –16°C 13
Va. Computed elastic properties and velocities of bubble-free polycrystalline ice with randomly oriented crystals, based on the elastic properties of single crystal ice 15
Vb. Full set of elastic constants for selected cases of Table Va 15

CONTENTS (Cont'd)

TABLES (Cont'd)

Table		Page
VI.	Comparison of properties of isotropic polycrystalline ice	16
VII.	Velocities V_P and V_S of isotropic non-porous polycrystalline ice at -16°C	16
VIII.	Temperature coefficients of V_P and V_S from laboratory measurements on single crystal ice computed for isotropic ice aggregates	18
IX.	Deviation of compressional velocity V_P from V_P vertical in the horizontal and an oblique direction	23
X.	Velocities and Poisson's ratio in pack ice	34
XI.	*P*-wave velocities in permafrost	36
XIIa.	Reflection coefficients for ice and various substances	68
XIIb.	Reflection coefficients for various combinations of substances	68
XIII.	Ice and water depths determined by various computation methods from seismic reflections (Ross Ice Shelf)	78
XIV.	Early seismic soundings on glaciers in the Alps	79

LIST OF SYMBOLS

Additional symbols of transitory use are not listed, such as various constants, integers used for identification and numbering, proportionality factors, substitutions in algebraic expressions, geometrical symbols for points, lines, angles given in the Figures, etc. All symbols are explained in the text where they occur.

A	amplitude
A_0	initial amplitude
A_n	amplitude after n cycles
C	Lamé constant
C	matrix of the elastic constants C_{ik}
C	phase velocity of flexural wave in floating ice
E	Young's modulus
E	energy per unit area at reflecting interface
E_e	energy per unit area of emergent wave
E_i	energy per unit area of incident wave
$E(R)$	energy of reflected wave
$E(2R)$	energy of double reflected wave
$E(r)$	energy per unit area at distance r
E_x	energy per unit surface area at distance x
F	modulus or algebraic expression of such related to the velocity of elastic waves
G	shear modulus : modulus of rigidity = Lamé constant
G_0	shear modulus of non-porous solid in equation for porous substance
I	matrix of units
I	energy of plane wave at arbitrary point
I'	energy of spherical wave
I_0	energy of plane wave at reference point
I'_0	initial energy per steradian
I_n; $n = 1, 2...$	identification for n-fold reflected wave not leaving the ice (shelf)
K	reflection coefficient

LIST OF SYMBOLS (Cont'd)

M	P-wave modulus = longitudinal elastic modulus under triaxial conditions
M_0	P-wave modulus for non-porous solid in equation for porous substance
P_n; $n = 1, 2...$	surface reflected wave reaching the surface for the nth time
R	curvature of the surface
R_P	identification of P-wave reflection
R_S	identification of S-wave reflection
R_{PS}	identification of P-S converted reflection
R_{SP}	identification of S-P converted reflection
S	matrix of the compliance constants S_{ik}
T	temperature
U	group velocity of flexural wave in floating ice
V	velocity of unspecified type of elastic wave
V_L	longitudinal wave velocity in a slender specimen
V_P	P-wave = compressional (longitudinal) wave velocity in an unbounded mass
V_{PL}	plate wave = compressional (longitudinal) wave velocity in a thin plate
V_R	Rayleigh surface wave velocity
V_S	S-wave = shear wave velocity
V_{SH}	velocity of horizontally polarized shear wave, or polarization perpendicular to crystallographic c-axis or structural axis of rotational symmetry
V_{SV}	velocity of vertically polarized shear wave, or polarization parallel to crystallographic c-axis or structural axis of rotational symmetry
V_T	torsional wave velocity in a slender specimen
$V_{(H)}$	velocity of wave traveling in horizontal direction, or in direction perpendicular to the crystallographic c-axis or a structural axis of rotational symmetry
$V_{(V)}$	velocity of wave traveling in vertical direction, or in the direction of the crystallographic c-axis or a structural axis of rotational symmetry
V_a	velocity of sound in air
V_i	P-wave velocity in porous ice
V_i	mean vertical P-wave velocity in an ice shelf (snow plus ice)

LIST OF SYMBOLS (Cont'd)

V_{ice}	constant vertical *P*-wave velocity below reference horizon (datum plane) in an ice mass
$\overline{V}_{ice}$	mean vertical *P*-wave velocity below reference horizon (datum plane) in an ice mass
V_r	velocity at depth
V_w	velocity of sound in water
V_x	velocity at depth of maximum penetration obtained from tangent to travel time curve at distance *x*
V_z	velocity at depth *z*
V_0	velocity at the ground surface, or at the source
V_n; $n = 1, 2...$	velocity in nth layer
V'	velocity in substratum
V_2'	up-dip velocity
V_2''	down-dip velocity
a	accumulation
c_{ik}	elastic moduli (stiffness constants) of anisotropic substance
d	diameter of circular specimen
d	depth to reference horizon
e_k	components of the strain tensor
f	frequency
f_0	resonance frequency
Δf	half-width of resonance curve
g	G^{-1}, reciprocal of shear modulus
g	gravitational constant
h	thickness of rectangular specimen
h	depth
h_i	thickness of ice shelf
h_w	thickness of water layer under ice shelf
k	bulk modulus
k	rate of velocity increase with depth

LIST OF SYMBOLS (Cont'd)

k_0	bulk modulus of non-porous solid in equation for porous substance
ℓ	length of specimen
n	porosity = ratio of pore volume to total volume (in sea ice ratio of brine volume plus air volume to total volume)
n_a	air content = ratio of air volume to total volume
n_b	brine content = ratio of brine volume to total volume
n_w	water content = water volume to total volume
p	ice content = ratio of ice volume to total volume
p_k	components of the stress tensor
r	distance from a reference point or a center
s	shot distance
s_{ik}	elastic constants (compliance constants) of anisotropic substance
t	time
t_D	travel time at distance D
t_{PS}	travel time for reflected wave converted at the interface from a P- to an S-wave
t_{SP}	travel time of S-P converted reflection
t_d	travel time from surface to reference horizon (datum plane)
$t_{\text{in wm}}$; $n = 1, 2\ldots$, $m = 1, 2\ldots$	travel time of multiple reflected wave traversing 2 n times the ice and 2 m times the water layer (ice shelf)
t_r	travel time of reflected wave
t_r	reflection time observed at a distance from the shot point
$t(z)$	travel time from the surface to the depth z
t_0	reflection time at shot point
t_0	time intercept in travel-time curve (refraction)
t_0'	time intercept in travel-time curve (refraction) corrected for temperature
Δt	stepout time for inclined reflector
Δt_0	spread correction (stepout time) for horizontal reflector
u, v, w	inclined coordinate system

LIST OF SYMBOLS (Cont'd)

x, y, z	Cartesian coordinate system
x	distance between shot point and detector
x_c	critical distance (refraction)
z	vertical depth
z_{x1}	depth of maximum penetration of refracted wave reaching the surface at the distance x1
Δ	difference (differential) of ...
Δ	time interval
ϕ	direction of minimum (maximum) *P*-wave velocity relative to the axis of rotational symmetry of anisotropy
ϕ	direction of dip (azimuth)
α	attenuation coefficient
α	angle between specimen and axis of rotational symmetry of anisotropy
α	apex angle of cone of c-axis distribution
α	dip of rock surface with respect to snow surface in profile direction
α_P	angle of incident or emergent *P*-wave
α_S	angle of incident or emergent *S*-wave
α_i	angle between the wave path and the vertical in the ice layer of an ice shelf
α_w	angle between the wave path and the vertical in the water layer below an ice shelf
α_n; $n = 1, 2, \ldots$;	angle of incidence or emergence in the nth layer
β	damping coefficient
β	dip of rock surface with respect to snow surface in profile direction
γ	critical angle of incidence (refraction)
δ	complementary angle to angle of incidence = angle between ray and interface
δ_n; $n = 1, 2 \ldots$	travel time difference between direct and nth surface reflected wave
δ'	content by volume of inclusions (spheres)
ϵ	a small dimensionless constant
θ	dip of reflecting interface
θ	angle of ray to vertical at depth
κ	compressibility = k^{-1} (reciprocal of bulk modulus)

LIST OF SYMBOLS (Cont'd)

λ	wavelength
λ_0	wavelength
ν	Poisson's ratio
ρ	density
ρ_i	density of ice
ρ_w	density of water
ρ'	density of substratum
ϕ	direction of dip
ω	angular velocity
$\tan \delta$	loss factor

EDITOR'S FOREWORD

Cold Regions Science and Engineering consists of a series of monographs written by specialists to summarize existing knowledge and provide selected references on the cold regions, defined here as those areas of the earth where operational difficulties due to freezing temperatures may occur.

Sections of the work are being published as they become ready, not necessarily in numerical order but fitting into the following plan, which may be amended as the work proceeds. The monograph series was planned and directed by F.J. Sanger as editor until 1970.

I. Environment

A. General – Characteristics of the cold regions
   1. Selected aspects of geology and physiography of the cold regions
   2. Permafrost (Perennially frozen ground)
   3. Climatology
      a. Climatology of the cold regions: Introduction, Northern Hemisphere I
      b. Climatology of the cold regions: Northern Hemisphere II
      c. Climatology of the cold regions: Southern Hemisphere
      d. Radioactive fallout in northern regions
   4. Vegetation
      a. Patterns of vegetation in cold regions
      b. Regional descriptions of vegetation in cold regions
      c. Utilization of vegetation in cold regions

B. Regional
   1. The Antarctic ice sheet
   2. The Greenland ice sheet

II. Physical Science

A. Geophysics
   1. Heat exchange at the ground surface
   2. Exploration geophysics in cold regions
      a. Seismic exploration in cold regions
      b. Electrical, magnetic and gravimetric exploration in cold regions

B. Physics and mechanics of snow as a material

C. Physics and mechanics of ice
   1. Snow and ice on the earth's surface
   2. Ice as a material
      a. Physics of ice as a material
      b. Mechanics of ice as a material
   3. The mechanical properties of sea ice
   4. Mechanics of a floating ice sheet

D. Physics and mechanics of frozen ground
   1. The freezing process and mechanics of frozen ground
   2. The physics of water and ice in soil

III. Engineering

A. Snow engineering
   1. Engineering properties of snow
   2. Construction
      a. Methods of building on permanent snowfields
      b. Investigation and exploitation of snowfield sites
      c. Foundations and subsurface structures in snow
      d. Utilities on permanent snowfields
      e. Snow roads and runways
   3. Technology
      a. Explosions and snow
      b. Snow removal and ice control
      c. Blowing snow
      d. Avalanches
   4. Oversnow transport

B. Ice engineering
   1. River-ice engineering
      a. Winter regime of rivers and lakes
      b. Ice pressure on structures
   2. Drilling and excavation in ice
   3. Roads and runways on ice

C. Frozen ground engineering
   1. Site exploration and excavation in frozen ground
   2. Buildings on frozen ground
   3. Roads, railroads and airfields in cold regions
   4. Foundations of structures in cold regions
   5. Sanitary engineering
      a. Water supply in cold regions
      b. Sewerage, and sewage disposal in cold regions
      c. Management of solid wastes in cold regions
   6. Artificial ground-freezing for construction

D. General
   1. Cold-weather construction
   2. Materials at low temperatures
   3. Icings developed from surface water and groundwater

IV. Remote Sensing

A. Systems of remote sensing
B. Techniques of image analysis in remote sensing
C. Application of remote sensing to cold regions

T.C. JOHNSON

SEISMIC EXPLORATION IN COLD REGIONS

by

Hans Roethlisberger

INTRODUCTION

In exploration geophysics use is made of the differences in certain physical properties of different types of rock or ground. The properties are those associated with some remote effect which can be measured, usually at the earth's surface, sometimes in existing tunnels or drill holes, or from the air. The aim is to gain information on the geometry and the physical properties of the substrata without excavation or drilling.

Many manuals, textbooks and handbooks on geophysical instruments and methods exist. Geophysical exploration methods as such are therefore not described in detail here. Some general information on methods is nevertheless given to serve as a background for the non-geophysicist. The main objective of the Monograph is to describe deviations from the standard techniques when operating in cold regions, specifically on snow, ice and permafrost. Special applications to problems peculiar to these areas and materials are also treated. The physical properties of cold regions materials relevant to the geophysical methods are reviewed.

In this first part of *Exploration Geophysics* seismic methods and related techniques based on elastic waves are treated.

PRINCIPLES

In the seismic method elastic waves are usually produced at a known position, the source, at an exactly known instant. They are picked up at various distances by vibration-sensitive detectors called seismographs. The most common way of exciting elastic waves is by explosive charge, but at short distances the impact of a hammer may do. Special devices producing especially high frequency vibrations or wave pulses of controlled frequency are sometimes used.

The phenomenon primarily observed is the propagation of the waves, in particular the travel time. Additional information may be gained from the direction and frequency of the motion at the seismograph station, and from the amplitude. Part of the waves penetrate the ground to some depth, but reach the surface again after reflection and refraction at the interfaces between bodies (layers) of different properties. The velocity of the seismic wave, a typical property of a given material for the particular wave type involved, must be known if travel-time observations are to be used.

MATERIAL PROPERTIES

Elasticity and Velocity

Body waves in isotropic media

Two different types of waves are dealt with in seismic work: body waves and boundary waves (guided waves). In an extended homogeneous isotropic solid, considered as a continuous medium, two types of body waves exist: compressional-dilatational waves commonly called longitudinal, primary or *P*-waves (sometimes also referred to as bulk waves), and the slower shear waves, also called transverse, secondary or *S*-waves. The velocity of the body waves can be computed from the elasticity and the density by a simple equation of the form $V = \sqrt{F/\rho}$, where V = velocity, ρ = density, and F is an elastic modulus or constant, or an algebraic expression. Various interrelated constants are in use in elasticity theory. A pair of these quantities describes a homogeneous and isotropic material sufficiently, and all the other constants can be computed if only two are given. Table I contains all the equations needed to make any desired conversion of elastic constants. The quantities to be computed are listed at the top of each column, while the given pairs of constants are found at the beginning of each line.

The velocities of the two types of body waves, the *P*- and *S*-waves, are respectively:

$$V_P = \sqrt{\frac{M}{\rho}} = \sqrt{\frac{E}{\rho} \cdot \frac{1 - \nu}{(1 + \nu)(1 - 2\nu)}}, \tag{1}$$

$$V_S = \sqrt{\frac{G}{\rho}}. \tag{2}$$

Additional equations relating V_P and V_S with arbitrary pairs of elastic quantities may readily be obtained from Table I, leading to combinations of eq 1 and 2 such as

$$V_S = V_P \cdot \sqrt{\frac{1 - 2\nu}{2(1 - \nu)}}, \tag{3}$$

or

$$\nu = \frac{1}{2} \cdot \frac{V_P^2 - 2V_S^2}{V_P^2 - V_S^2}. \tag{4}$$

Body waves in anisotropic media

When using seismic methods in cold regions one probably has to deal with anisotropic substances more often than in temperate climates. The equations relating velocities to elasticity are far more complicated for an anisotropic material than for an isotropic material. Three types of body waves exist, one of pseudo-longitudinal type and two polarized pseudo-shear waves becoming true longitudinal and true shear waves in certain singular directions of propagation, or under certain conditions. In the theoretical treatment of anisotropy it is important to distinguish between the velocity of the wave normal and the ray velocity. In seismic prospecting, where we are dealing with point sources, it is the ray velocity which is of interest.

Table I. Conversion table for elastic constants (from Gassmann[69]).

Given	To be computed					
	Young's modulus E	*Bulk modulus* k	*P-wave modulus* M	*Lamé constant* C	*Shear modulus* G	*Poisson's ratio* ν
E, k			$\frac{3k(3k+E)}{9k-E}$	$\frac{3k(3k-E)}{9k-E}$	$\frac{3kE}{9k-E}$	$\frac{1}{2}-\frac{E}{6k}$
E, M		$\frac{3M-E+w_1}{6}$		$\frac{M-E+w_1}{4}$	$\frac{3M+E-w_1}{8}$	$\frac{E-M+w_1}{4M}$
E, C		$\frac{E+3C+w_2}{6}$	$\frac{E-C+w_2}{2}$		$\frac{E-3C+w_2}{4}$	$\frac{w_2-E-C}{4C}$
E, G		$\frac{EG}{3(3G-E)}$	$\frac{G(4G-E)}{3G-E}$	$\frac{G(E-2G)}{3G-E}$		$\frac{E}{2G}-1$
E, ν		$\frac{E}{3(1-2\nu)}$	$\frac{(1-\nu)E}{(1+\nu)(1-2\nu)}$	$\frac{\nu E}{(1+\nu)(1-2\nu)}$	$\frac{E}{2(1+\nu)}$	
k, M	$\frac{9k(M-k)}{M+3k}$			$\frac{3k-M}{2}$	$\frac{3}{4}(M-k)$	$\frac{3k-M}{3k+M}$
k, C	$\frac{9k(k-C)}{3k-C}$		$3k-2C$		$\frac{3}{2}(k-C)$	$\frac{C}{3k-C}$
k, G	$\frac{9kG}{3k+G}$		$k+\frac{4}{3}G$	$k-\frac{2}{3}G$		$\frac{3k-2G}{2(3k+G)}$
k, ν	$3k(1-2\nu)$		$\frac{3k(1-\nu)}{1+\nu}$	$\frac{3k\nu}{1+\nu}$	$\frac{3k(1-2\nu)}{2(1+\nu)}$	
M, C	$\frac{(M+2C)(M-C)}{M+C}$	$\frac{M+2C}{3}$			$\frac{M-C}{2}$	$\frac{C}{M+C}$
M, G	$\frac{G(3M-4G)}{M-G}$	$M-\frac{4}{3}G$		$M-2G$		$\frac{M-2G}{2(M-G)}$
M, ν	$\frac{(1-2\nu)(1+\nu)M}{1-\nu}$	$\frac{(1+\nu)M}{3(1-\nu)}$		$\frac{\nu M}{1-\nu}$	$\frac{(1-2\nu)M}{2(1-\nu)}$	
C, G	$\frac{G(3C+2G)}{C+G}$	$C+\frac{2}{3}G$	$C+2G$			$\frac{C}{2(C+G)}$
C, ν	$\frac{C(1+\nu)(1-2\nu)}{\nu}$	$\frac{C(1+\nu)}{3\nu}$	$\frac{C(1-\nu)}{\nu}$		$\frac{C(1-2\nu)}{2\nu}$	
G, ν	$2G(1+\nu)$	$\frac{2G(1+\nu)}{3(1-2\nu)}$	$\frac{2G(1-\nu)}{1-2\nu}$	$\frac{2G\nu}{1-2\nu}$		

$$w_1 = + \sqrt{(M-E)(9M-E)},$$

$$w_2 = + \sqrt{(E+C)^2 + 8C^2}.$$

A convenient way to present ray velocity data is by plotting them in polar coordinates in the direction of the rays. The resulting (three-dimensional) figure is the wave surface, which consists of three sheets corresponding to the three body waves. The wave surface is the envelope of plane waves going at a given instant in all directions through the origin, after the lapse of one time unit. It can also be interpreted, with some reservation, as the wave front of a disturbance originating from a point source, after the unit time has elapsed, in which case it separates disturbed from undisturbed portions of the medium. A difficulty with this interpretation may be encountered in the case of the pseudo-shear wave, as for instance in single-crystal ice. It is important in this respect to be aware that the equations are developed for plane waves. While a wave which is not plane can usually be replaced by a finite number of waves consisting of plane elements, there are cases where this is not feasible, namely when a small change of direction of the propagation of the wave causes a sudden change of propagation characteristics. This is the case where the wave surface shows cusps (Fig. 6; p. 14). Evidently, internal conical refraction occurs, from Huygen's principle.

In order to relate stress and strain in anisotropic substances the components of the stress tensor, p_{xx}, p_{yy}, p_{zz}, p_{yz}, p_{zx}, and p_{xy}, are numbered p_1 to p_6, in this order, and the strain-tensor components e_{xx}, e_{yy} etc are numbered likewise in the same order. The stress components are now expressed by

$$p_i = \sum_{k=1-6} c_{ik}\, e_k, \text{ or in matrix notation } p = Ce, \tag{5a}$$

the strain components by

$$e_i = \sum_{k=1-6} s_{ik}\, p_k, \text{ or in matrix notation } e = S\,p. \tag{5b}$$

The elastic moduli or stiffness constants c_{ik} are converted to the compliance constants* by matrix inversion, $CS = I$.

Of particular interest is a special case of anisotropy which is rotationally symmetric. Such a medium is called uniaxially anisotropic, transversely isotropic or axisymmetric. Good examples of this type of substance are crystals of the hexagonal system (e.g. ice), but uniformly layered media behave in exactly the same way if the thickness of the layers (more precisely the thickness of a pack of layers which repeats itself over and over again) is sufficiently small compared to the wavelength. Five elastic stiffness constants (or compliance constants) are needed to describe the elastic behavior of a uniaxially anisotropic medium. They form the matrix

$$\begin{pmatrix} c_{11} & c_{12} & c_{13} & 0 & 0 & 0 \\ c_{12} & c_{11} & c_{13} & 0 & 0 & 0 \\ c_{13} & c_{13} & c_{33} & 0 & 0 & 0 \\ 0 & 0 & 0 & c_{44} & 0 & 0 \\ 0 & 0 & 0 & 0 & c_{44} & 0 \\ 0 & 0 & 0 & 0 & 0 & c_{66} = (c_{11} - c_{12})/2 \end{pmatrix}$$

*Voigt[184] uses moduli for s_{ik} and constants for c_{ik}.

From the five elastic constants and the density of a medium the three sheets of the wave surface can be computed. Since the wave surface is of rotational symmetry and symmetric in respect to the base plane it is, for graphical presentation, sufficient to give the ray velocities in one quadrant of a plane containing the axis of symmetry (Fig. 6). The wave polarized perpendicular to the axis of rotation is a true shear wave; this is the wave which corresponds to the "ordinary" wave in optics. The theory of the propagation of elastic waves in anisotropic media has been treated by Musgrave[131 132] and Helbig[86] among others. A selection of the equations from Helbig's work (mostly taken from the much earlier treatment of the same subject by Rudzki), especially well suited for the computation of ray velocities by electronic computer, is given in Appendix A.

Surface waves

The boundary waves, as opposed to the body waves, are important as surface waves or when dealing with bodies of limited extent of which at least one dimension is of the same order of magnitude as, or less than, the wavelength. In regular seismic work the surface waves are not directly used, but may be bothersome when they are strong and interfere with signals on the record which should be used. The velocity V_R of the Rayleigh surface wave at the free surface of a semiinfinite elastic solid is expressed by

$$\kappa_1^6 - \delta\kappa_1^4 + (24 - 16a_1^2)\kappa_1^2 + (16a_1^2 - 16) = 0, \tag{6}$$

where

$$\kappa_1 = \frac{V_R}{V_S},$$

and

$$a_1^2 = \frac{1 - 2\nu}{2 - 2\nu} = \frac{V_S^2}{V_P^2}.$$

The ratio $\kappa_1 = V_R/V_S$ vs Poisson's ratio ν is given in Figure 1. In any material the velocity of the Rayleigh wave is less than that of the S-wave. The amplitude decays rapidly with distance from the surface (depth) and at the depth of one wavelength is only a fraction of the value at the surface. Far more complicated surface waves develop in a layered substance; they are dispersive. An application exists in the case of floating ice sheets.

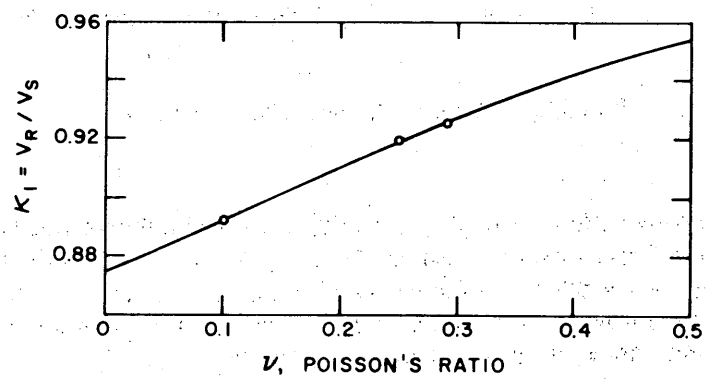

Figure 1. Ratio of the velocity of a Rayleigh wave to the velocity of a shear wave as a function of Poisson's ratio ν. (From Mason[124].)

Love waves exist in layered structures when the shear wave velocity increases with depth, and also when the increase is continuous; they are dispersive. The velocity of very short waves approaches the shear wave velocity of the top layer, whereas infinitely long waves travel at the speed of the shear wave in the substratum.

Waves in slender bars

Especially simple equations are valid when one or two dimensions of bodies of limited extent are much smaller than the wavelength. For a slender rod or prism the longitudinal velocity V_L of an extensional disturbance is

$$V_L = \sqrt{\frac{E}{\rho}}, \tag{7}$$

while a torsional wave in a circular rod travels at the speed $V_T = V_S$ of a body wave of shear mode,

$$V_S = \sqrt{\frac{G}{\rho}}. \qquad \text{(see eq 2)}$$

For cross sections other than circular a correction factor is needed. The relationship between the velocities of the longitudinal body wave (V_P) and the one-dimensional longitudinal wave in a slender bar (V_L) is given by:

$$\frac{V_P}{V_L} = \sqrt{\frac{(1 - \nu)}{(1 + \nu)(1 - 2\nu)}}. \tag{8}$$

Another type of wave is the flexural one. These are dispersive and no simple equation can be given for their velocity. However, they are important for determining Young's modulus from standing waves, i.e. flexural vibrations of bars or rods where specific frequencies occur in resonance (eq 11).

Waves in thin floating plates

When the wavelength is large compared to the thickness of the plate there is a wave similar to the longitudinal wave in a rod, called the longitudinal plate wave. Its velocity is

$$V_{PL} = \sqrt{\frac{E}{\rho(1 - \nu^2)}}, \tag{9}$$

while the velocity of shear waves is $V_S = \sqrt{G/\rho}$ as before. Flexural waves also occur. They are dispersive as in the case of the rod or bar. Some details are given on p. 107.

Methods for Determining Seismic Properties

Velocity

In applied seismic work it is common to determine, in the field, the velocities in the various materials present. While direct measurements on outcrops can be useful, it is in most cases possible to obtain the velocities as a byproduct of the soundings, i.e. by standard methods from refraction or reflection profiles. The disadvantage in this case is that the material involved is not directly accessible and its conditions are very often not exactly known.

Details about the determination of seismic properties by the refraction and reflection methods are given in the chapter on soundings.

An alternative to in situ measurement is laboratory testing, offering the advantage that the samples can be inspected and the conditions can be controlled. Laboratory studies are especially useful when the effects of specific parameters are investigated, such as composition, temperature, pressure and moisture content. Investigations on samples have their limitations, however. It is sometimes impossible to obtain undisturbed samples, the velocity changes being caused by fissures or moisture migration. In the case of synthetic samples it is difficult to make them isotropic. In addition there are cases where a heterogeneous material may be treated seismically as homogeneous, since the wavelength and the observed paths are much larger than the nonhomogeneous units, while the samples are smaller and therefore not representative of the bulk. Many glacial deposits as well as layered snowpacks are good examples of such material.

Careful interpretation is essential when laboratory results are used in field seismic explorations. Although the velocity can be computed from elastic moduli and the density, it is usually not possible to obtain accurate velocities from static tests, because of the effects of elastic relaxation and creep. Dynamic tests are therefore preferred for seismic applications. One type of dynamic test consists of inducing vibrations in the samples and determining resonance frequencies. Circular rods (cores) and rectangular bars are most frequently used, and longitudinal, torsional or flexural vibrations are applied. With sample lengths on the order of a few centimeters to one meter most commonly used, the resonance frequencies are usually in the audible range, and the technique is also referred to as the sonic method.

The longitudinal velocity V_L in a slender bar is found from the length ℓ of a rod or prismatic specimen with free ends and the resonance frequency f_0 of longitudinal vibrations by

$$V_L = 2\ell f_0. \tag{10}$$

For the flexural (lateral) vibration of a very thin rectangular bar supported at the nodal points (0.22ℓ from the ends), the equation reads

$$V_L = \frac{4\sqrt{3}\,\pi\ell^2}{m^2 h} f_0, \tag{11a}$$

where $m = 4.730$ for the first mode of flexural vibration, and h = thickness of the bar. For circular rods the equation reads

$$V_L = \frac{8\pi\ell^2}{m^2 d} f_0, \tag{11b}$$

where d = diameter of the rod. Pickett[143] gives equations and diagrams to account for the finite length to diameter ratio of the specimens. For a ratio of 10:1 the correct value of V_L is about 2.5% higher than obtained from eq 11b, and for a ratio of 5:1 about 10%. The corrections are a little higher for equal ratios of length to thickness in the case of square prisms. The shear velocity is obtained from torsional vibrations of circular rods with free ends by

$$V_S = 2\ell f_0, \tag{12}$$

but can also be measured with rectangular bars if appropriate correction factors are used. For square prisms the factor is $\sqrt{1.183}$. Magnets are often attached to the ends of the specimen for exciting the vibration and picking up the response. Free vibrations or resonance frequencies of forced vibrations are observed. A correction must be made for the mass of the magnets.[109]

The velocity V_P of the longitudinal body wave is given by eq 8, $V_P = V_L \sqrt{(1-\nu)/(1+\nu)(1-2\nu)}$. Two experiments, with either longitudinal or flexural, and torsional, vibrations, are therefore needed to determine the seismic velocity V_P by the sonic method. Some authors prefer to compare elastic moduli, which are readily obtained from eq 6 and 2: $E = V_L^2\rho$; $G = V_S^2\rho$.

A different way of determining velocity in samples is by travel-time measurements of sonic or ultrasonic pulses. This method is directly comparable with seismic travel-time determinations, apart from the difference in wavelength. It has big advantages over the resonance frequency method, but the equipment is more expensive. The main advantage is that arbitrarily shaped specimens can be measured. The *P*-wave is most commonly observed, for instance with concrete testing equipment, but transducers can also be obtained which produce an almost pure shear wave. It is generally true that the shortest wavelengths give the highest accuracy. There are practical limitations, however, because with very short wavelengths scatter occurs at the grain boundaries. The wavelength should be on the order of the grain size or larger, but it should not be much larger than the smallest dimension of the sample.

The relationship of wavelength and sample dimensions may be discussed a little further in the case of a cylindrical rod. Let us assume that measurements are made in the longitudinal direction of a circular core, with centered transducers on both ends. The length of the core is ℓ, the diameter d. The direct wave which has traveled over the distance ℓ along the axis of the core is followed by a *P*-wave reflected at the surface, which is out of phase because of the reflection at the free surface, and has traveled the distance $\sqrt{\ell^2 + d^2} \simeq \ell + d^2/2\ell$ for small ratios of d/ℓ. When the difference in travel distance $d^2/2\ell$ becomes small compared with the wavelength λ, say $d^2/2\ell < \epsilon\lambda$ with ϵ (a small dimensionless constant) probably 0.1 or smaller, then the direct and reflected waves may interfere with each other and with multiple reflections so much that the arrival of the direct *P*-wave cannot be picked accurately. Figure 2 gives the results obtained with pulses of about 20 kHz on ice cores 7.5 cm in diameter, i.e. $\lambda = 2.5d$. The measurements were started on long cores which were successively cut down in length. The graph of travel time versus distance shows the direct *P*-wave up to core lengths of about 35 cm corresponding to $\epsilon \simeq 0.04$. At greater distances the first breaks indicate a velocity of about $V_L = \sqrt{E/\rho}$, but the scatter is considerable. It is conceivable that with a proper choice of transducers it might be possible to determine V_L as well as V_P on rods using compressional ultrasonic pulses; however, a much better way of obtaining two elastic parameters is to excite the shear mode beside the compressional one.[19]

On floating ice sheets there exist some additional possibilities of inferring elastic properties from in situ tests. A list of these field methods together with the aforementioned seismic and laboratory techniques are given in Appendix B.

Attenuation

Velocity is the most important material property pertaining to elastic waves, but there is also a difference in attenuation characteristics in different materials. It can be expressed as loss factor $\tan\delta$. A convenient way of determining $\tan\delta$ in the laboratory is from free vibrations.[135 136] After exciting a specimen in resonance the power is switched off and the vibration is allowed to decay. The vibration attenuates with the damping coefficient β:

$$A = A_0\, e^{-\beta t} \sin \omega t, \tag{13}$$

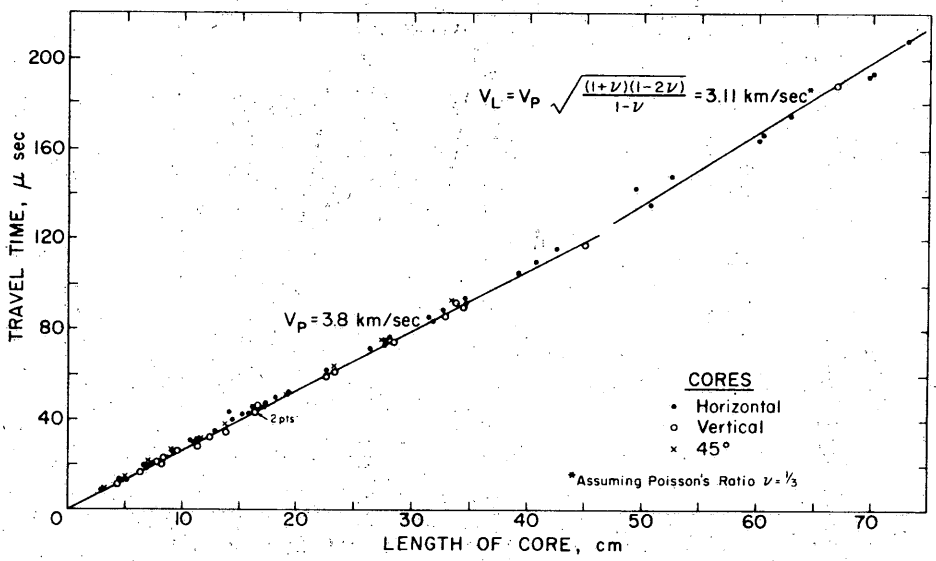

Figure 2. Time-distance graph for ultrasonic pulse measurements in circular ice rods of 7 cm diameter and variable length, Tuto tunnel. (Author's data, unpublished.)

where A = amplitude at time t, A_0 = initial amplitude, and $\omega = 2\pi f$, with f = frequency; $\beta = (1/n)f \cdot \ln(A_0/A_n)$ where A_n is a peak of the decaying vibration after n cycles. The loss factor is given by

$$\tan \delta = \frac{2\beta}{\omega}. \tag{14}$$

It can also be obtained from the resonance curve of forced vibrations (Fig. 3):

$$\tan \delta = \frac{1}{\sqrt{3}} \cdot \frac{\Delta f}{f_0}, \tag{15}$$

where f_0 is the resonance frequency and Δf is the half width of the curve. A difficulty in these laboratory studies is the air friction, which might be significant in the case of flexural vibrations. Also the coupling with the transducers should be taken into account.[117]

In seismic work it is attenuation with distance which is important. The attenuation coefficient a is defined by

$$I = I_0 \, e^{-ax} \tag{16}$$

where I_0 is the energy of a plane wave at some initial point and I the energy at distance x from this point in the direction the wave travels. The energy of a wave is proportional to the square of its amplitude, and therefore

$$A = A_0 \, e^{-ax/2}. \tag{16a}$$

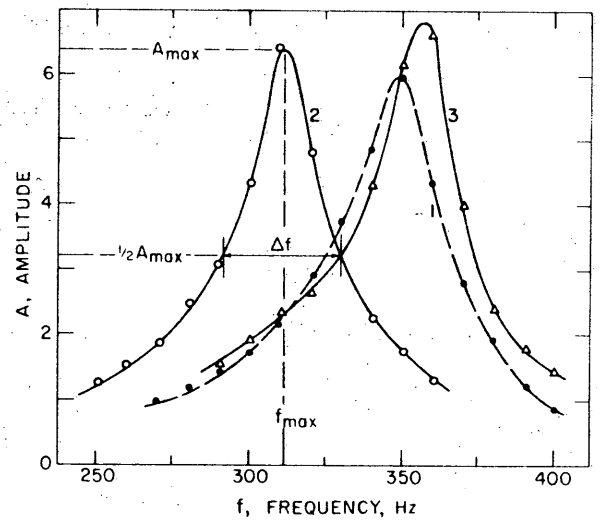

Figure 3. Resonance curves for high density snow samples vibrating laterally. (From Nakaya[135].)

(Some authors use $a/2$ as attenuation coefficient.) The distance can be expressed by travel-time, $x = Vt$, and a relation between a and the damping coefficient β from above is obtained: $\beta = V(a/2)$. The loss factor in terms of a becomes

$$\tan \delta = \frac{Va}{\omega} = \frac{Va}{2\pi f} = \frac{\lambda}{2\pi} a, \tag{17}$$

where λ is the wavelength.

When dealing with a point source, as is usual in seismics, the propagation of spherical instead of plane waves has to be considered. As a spherical wave spreads out from its source, the energy must be distributed over an area that increases as the square of the sphere's radius. The energy I' per unit area at a distance r from a point source of which the initial energy per unit solid angle (steradian) is I'_0 is therefore

$$I' = \frac{I'_0}{r^2} e^{-ar}, \tag{18}$$

while the total fall-off of the amplitude owing to spreading and absorption follows the formula

$$A' = \frac{A'_0}{r} e^{-ar/2}. \tag{18a}$$

Determining a in the field is not as simple as it may seem from the equations, because of the uneven energy distribution at the source, boundary effects at the ground surface, reflection and refraction at discontinuities and variable coupling of the instruments with the ground. One way to obtain fairly reliable information on a is to analyze multiple reflections as described on p. 66-71. A list of possibilities for extracting attenuation data from observations on floating ice sheets is contained in Appendix B.

Seismic Velocities in Ice and Snow

Single crystal ice

Ice belongs to the hexagonal crystallographic system, and the elastic behavior shows rotational symmetry with the c-axis as axis of rotation. Five independent elastic stiffness constants c_{ik} or elastic compliance constants s_{ik} describe the elastic behavior of the ice (p. 4).

Large ice crystals for experimentation are found in nature in old glacier ice, or are grown artificially in the laboratory. Velocities identical to those in single crystal ice can also be expected in bubble-free lake ice with common vertical c-axis orientation of all the grains, since the different orientation of the a-axes from grain to grain does not affect the rotationally symmetric elastic behavior. A certain deviation may nevertheless exist due to the imperfect structure of the lake ice.

Experimental results of laboratory determinations of the constants c_{ik} are given in Table II for temperatures of –16°C and –10°C. Different methods have been used by the various authors in different frequency ranges. The first three groups of authors worked with single crystals grown in the laboratory, while Brockamp and Querfurth used polycrystalline lake ice with parallel c-axis orientation. For most values agreement exists within the limit of error between the various determinations. The somewhat larger differences in the case of c_{13} and c_{44} might, according to Bass et al.[11], be explained by dispersion. Imperfect crystal structure may be another reason for deviations, especially in the case of the lake ice.[34] Some corresponding values of the constants s_{ik} are presented in Table III. The change of the elastic moduli c_{ik} with temperature is given in Figure 4. (For the constants s_{ik} see Bass et al.[11])

Table II. Experimental values of the elastic moduli (stiffness constants) c_{ik} of ice (10^{10} dynes/cm^2).

Reference	*Jona and Scherrer*[100]	*Green and Mackinnon*[81]	*Bass et al.*[11]	*Brockamp and Querfurth*[34]	*Bennett*[19a]
Method	*Optical diffraction patterns (Schaefer-Bergmann)*	*c_{33} and c_{44} by ultrasonic pulse technique, rest from Penny's relations*	*s_{ik} by resonance of vibrating rods and plates*	*Ultrasonic pulse technique*	*Ultrasonic pulse technique*
Frequencies	*15-18 MHz*		*10-50 kHz*	*2-12 MHz*	*~600 kHz*
Temperature	*–16°C*	*–16°C*	*–16°C*	*–16°C*	*–10°C*
c_{11}	13.845 ± 0.08	13.33 ± 1.98	13.3 ± 0.8	13.63 (±0.04)	14.06 ± 0.08
c_{12}	7.07 ± 0.12	6.03 ± 0.72	6.3 ± 0.8	6.69 (±0.05)	7.15 ± 0.15
c_{13}	5.81 ± 0.16	5.08 ± 0.72	4.6 ± 0.9	5.15	5.88 ± 0.25
c_{33}	14.99 ± 0.08	14.28 ± 0.54	14.2 ± 0.7	14.85 (±0.03)	15.24 ± 0.12
c_{44}	3.19 ± 0.03	3.26 ± 0.08	3.06 ± 0.015	3.04 (±0.015)	3.06 ± 0.034
$c_{66}=\frac{1}{2}(c_{11}-c_{12})$	3.39 ± 0.07	3.65 ± 1.05	3.5 ± 0.6	3.47 (±0.013)	3.05 ± 0.036

The velocities in the principal directions, i.e. parallel and perpendicular to the c-axis, which is for convenience assumed to be vertical, depend on single moduli: $V = \sqrt{c_{ii}/\rho}$. (In some of the experiments velocities were measured and this relation has been used to compute the constants c_{ii}.) Table IV gives some velocities based on the values of c_{ii} of different authors, at –16°C (ρ = 0.919 g/cm^3). The *P*-wave velocities determined indirectly by Bass et al. appear to be too low compared

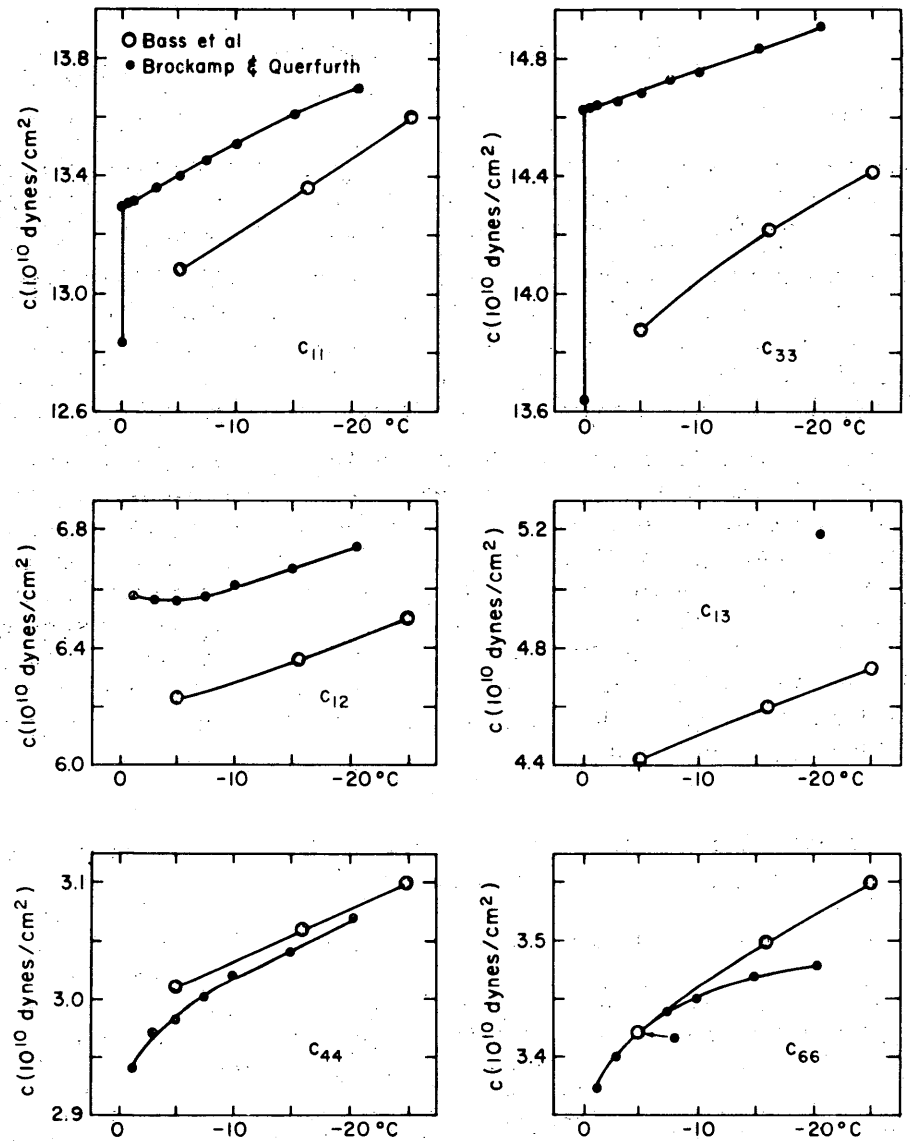

Figure 4. Elastic moduli (stiffness constants) c_{ik} vs temperature. (After Bass et al.[11] and Brockamp and Querfurth[34].)

Table III. Experimental values of the elastic compliance constants s_{ik} of ice at −16°C (10^{-12} cm²/dyne). (After Bass et al.[11])

s_{ik}	Jona and Scherrer[100] (conversion from c_{ik})	Bass et al.[11]
s_{11}	10.4 ± 0.3	10.13 ± 0.05
s_{12}	−4.3 ± 0.3	−4.16 ± 0.15
s_{13}	−2.4 ± 0.1	−1.93 ± 0.21
s_{33}	8.5 ± 0.4	8.28 ± 0.04
s_{44}	31.4 ± 0.3	32.65 ± 0.15
$s_{66} = 2(s_{11} - s_{12})$	29.4 ± 1.2	28.58 ± 0.4

Table IV. Velocities of elastic waves in the principal directions of single crystals or ice with common vertical c-axis orientation at –16°C (m/sec).
V_{SV} indicates a vertically polarized and V_{SH} a horizontally polarized shear wave, while (*V*) and (*H*) indicate vertically and horizontally traveling waves respectively.

Wave type	*Computation*	*Jona and Scherrer*[100]	*Bass et al.*[11]	*Brockamp and Querfurth*[34]	*Bennett*[19a]
$V_{P(H)}$	$\sqrt{c_{11}/\rho}$	3882 ± 11	3804 ± 114	3857 ± 3.4	3932 ± 5
$V_{P(V)}$	$\sqrt{c_{33}/\rho}$	4039 ± 11	3931 ± 97	4024 ± 5.3	4037 ± 1
$V_{S(V)} = V_{SV(H)}$	$\sqrt{c_{44}/\rho}$	1863 ± 9	1825 ± 4	1824 ± 4.4	1836 ± 5
$V_{SH(H)}$	$\sqrt{c_{66}/\rho}$	1921 ± 20	1952 ± 167	1946 ± 3.6	1947 ± 5

with those obtained by direct ultrasonic pulse measurements by other authors. There is a slight velocity decrease with rising temperature followed by a steep drop in the last tenths of a degree C when the melting point is reached (Fig. 5). At temperatures between about –5°C and –20°C the following temperature coefficients are applicable:[34]

$$\Delta V_{P(H)}/\Delta T = -2.8 \text{ m/sec °C}$$

$$\Delta V_{P(V)}/\Delta T = -1.7 \text{ m/sec °C}$$

$$\Delta V_{S(V)}/\Delta T = -1.5 \text{ m/sec °C}$$

$$\Delta V_{SH(H)}/\Delta T = -1.2 \text{ m/sec °C}.$$

In an arbitrary direction forming the angle ϕ to the c-axis, the computation of velocities from the elastic constants is more involved (Appendix A). The results based on the constants by Bass et al. of Table II and density $\rho = 0.91$ g/cm^3 are given graphically in Figure 6. The *P*-wave velocities are too low compared with those of other authors, as indicated above, but the general shape of the curves is correct, showing a minimum at about 50° for the pseudo *P*-wave and a pronounced maximum with cusps for the pseudo *S*-wave between 40° and 50°. The difficulties encountered with cusps when working with point sources instead of plane waves are pointed out on page 4.

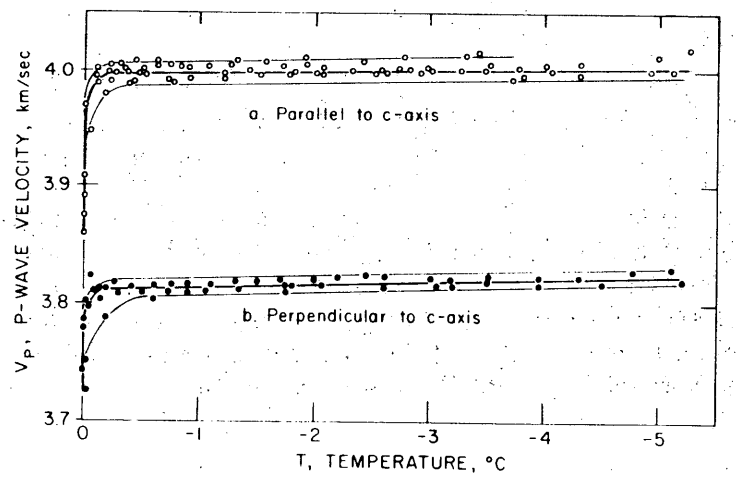

Figure 5. P-wave velocities in the principal directions of single-crystal ice vs temperature. (From Brockamp and Querfurth[34]*.)*

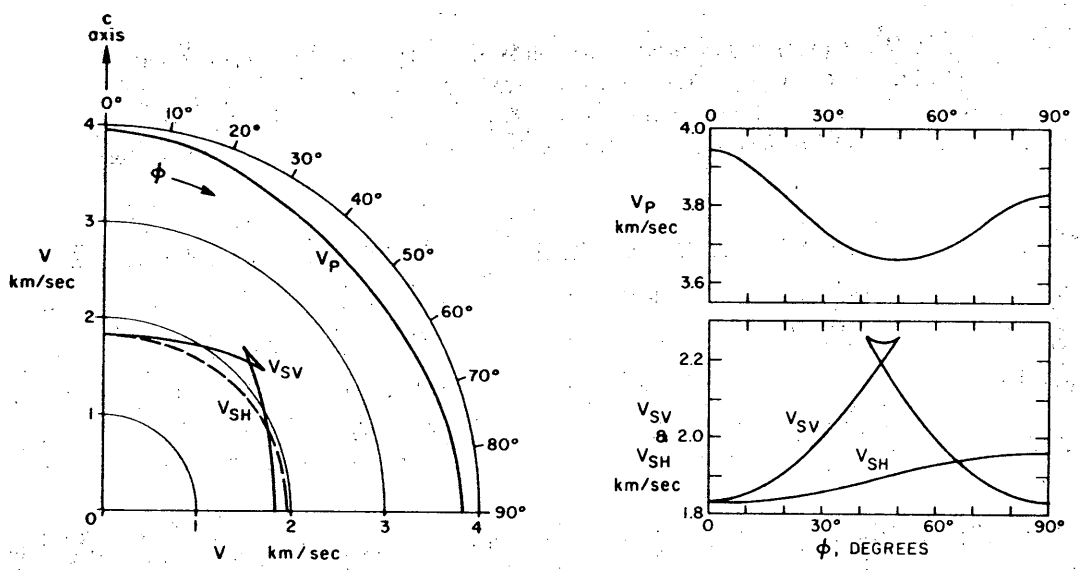

a. *Polar coordinates.* b. *Cartesian coordinates.*

Figure 6. Ray velocity vs direction in single-crystal ice based on the elastic moduli of Bass et al.[11] *at –16°C (the values of V_P are too low, but the shape of the curve is shown correctly). (After Roethlisberger*[167]*.)*

Non-porous isotropic polycrystalline ice

An aggregate of randomly oriented crystals can be regarded as a homogeneous and isotropic body in which only two types of waves occur, *P* and *S*. It is possible to compute their velocities from the elastic moduli of the crystalline substance, but it is very complicated to do it accurately. Approximate equations for computing a mean value of the *P*-wave modulus *M* and the Lamé constant *C* for a uniaxially anisotropic substance are:[184]

$$M = \tfrac{1}{15}\,(8c_{11} + 3c_{33} + 4c_{13} + 8c_{44}) \tag{19}$$

and

$$C = \tfrac{1}{15}\,(c_{11} + c_{33} + 5c_{12} + 8c_{13} - 4c_{44}). \tag{20}$$

With these equations, and with the conversions of Table I and eq 1 and 2, the elastic constants and velocities of Table Va for isotropic bubble-free polycrystalline ice were computed. Because of the conversion of the constants s_{ik} into c_{ik} the values based on Bass et al. are least accurate. In the penultimate line the arithmetic means of the values from Jona and Scherrer and Bass et al. are given for the temperature of –16°C. They are almost identical with the values based on Brockamp and Querfurth, while the latest figures by Bennett[19a] given in the bottom line are about as close to the values from Jona and Scherrer – though for different temperatures. The complete set of elastic moduli and velocities for idealized non-porous isotropic polycrystalline ice is given in Table Vb based on the data by Brockamp and Querfurth (A) and Bennett (B).

Table Va. Computed elastic properties and velocities of bubble-free polycrystalline ice with randomly oriented crystals, based on the elastic properties of single crystal ice.

References	Temp °C	Density ρ g/cm^3	Young's modulus E 10^{10} dynes/cm^2	Shear modulus G 10^{10} dynes/cm^2	Poisson's ratio ν	P-wave velocity V_P m/sec	S-wave velocity V_S m/sec
Jona and Scherrer[100]	−16	0.919	9.40	3.55	0.324	3851	1965
Bass et al.[11]	− 5	.917	9.26	3.56	.302	3698	1970
	−16	.919	9.43	3.62	.304	3736	1985
	−25	.920	9.55	3.66	.305	3766	1995
Brockamp and Querfurth[34]	− 5*	.917	9.28	3.53	.314	3770	1962
	−16	.919	9.424	3.585	.3143	3796	1975
	−20.5	.9195	9.48	3.60	.315	3805	1979
Mean Jona and Scherrer and Bass et al.	−16	.919	9.415	3.585	.314	3794	1975
Bennett[19]	−10	.918	9.403	3.545	.3263	3870	1965

*c_{13} = 5.19 observed at −20.5° only; computed with mean relative temperature correction of other c_{ik}: c_{13} = 5.05 at −5°C and 5.16 at −16°C.

Table Vb. Full set of elastic constants for selected cases of Table Va.

A: Brockamp and Querfurth[34] at −16°C. B: Bennett[19a] at −10°C.

	E	k	M	C	G	ν
	10^{10} dynes/cm^2					
A	9.42	8.46	13.24	6.07	3.585	.3143
B	9.40	9.02	13.75	6.66	3.545	.3263

Bruggeman[39] has shown that the Voigt method of averaging the elastic moduli according to eq 19 and 20 can be quite inaccurate for crystalline substances with a very strong anisotropy of the unit crystal, like zinc. For ice, which is not nearly as strongly anisotropic, only small differences were obtained between elastic moduli and velocities computed by the Voigt and the Bruggeman method, as illustrated in Table VI.

Non-porous isotropic polycrystalline ice in the ideal form is hardly found in nature, but certain types of glacier ice can come very close. This is especially the case for the ice in dry polar ice sheets at some depth, which has not yet undergone much mechanical deformation, but is at sufficient pressure so that the porosity is negligible. (Ice deformed by glacier flow usually shows preferred crystal orientation and thereby anisotropy.) Bentley[25] gives a value for V_P of 3851 m/sec for isotropic ice at −26.4°C from field observations in Antarctica. Allowing for residual porosity of, say, 0.005% at 300-m depth, one obtains (for porosity and temperature effects see below) 3866 m/sec for non-porous ice. This value may be compared with those in Table Va and further with the results of laboratory measurements by Bennett[19a] on porous samples; his straight-line fit extrapolated to the

density of pure ice gives 3846 m/sec at –10°C. The various figures for V_P adjusted to the common temperature of –16°C are given together with V_S in Table VII. The shear wave velocity for isotropic ice cannot be obtained as readily from field data as the *P*-wave velocity, because of higher sensitivity to a very weak anisotropy of the surface layers. Also the laboratory result of Bennett may not be free from effects of anisotropy.

Table VI. Comparison of properties of isotropic polycrystalline ice, computed according to the Voigt and the Bruggeman theories, based on the c_{ik} by Jona and Scherrer at –16°C.

Computation method	E 10^{10} *dynes/cm*^{2}	M 10^{10} *dynes/cm*^{2}	G 10^{10} *dynes/cm*^{2}	ν	V_P *m/sec*	V_S *m/sec*
Voigt theory*	9.40	13.63	3.55	0.324	3851	1965
Bruggeman theory[39] (simple means)	9.30	13.65	3.50	0.327	3854	1952
Bruggeman theory[39] (Voigt means)	9.32	13.66	3.51	0.327	3855	1954

*Eq 19 and 20

Table VII. Velocities V_P and V_S and Poisson's ratio of isotropic non-porous polycrystalline ice at –16°C.

	V_P *m/sec*	V_S *m/sec*	ν
Computation from single crystal (Brockamp and Querfurth)	3794	1975	.314
Computation from single crystal (Bennett)	3884	1972	.326
Bentley field data	3853		
Bennett laboratory samples	3860	1944	.330
Average	3848		

Bubbly ice

Glacier ice is usually bubbly, but can contain bodies of clear ice of limited extent. Lake ice is either completely clear with occasional bubbles, or very bubbly in the case of snow-ice, which is frozen slush. A convenient way to distinguish snow from ice is to say that snow is permeable to air and ice is not. In the cold, dry snow of the polar ice sheets the transition from permeable snow to impermeable ice occurs at a density of about 0.8 g/cm^3 at a depth of 50 to 150 m, depending on temperature and accumulation rate. The density increases further with depth, but at a lesser rate, to approach the density of bubble-free ice asymptotically. At depths below 300 m there is only a very small difference in density from one location to another.

The effect of porosity is to lower the velocity of elastic waves. In the equation $V_P = \sqrt{M/\rho}$ and $V_S = \sqrt{G/\rho}$ the elastic moduli M and G apparently decrease more rapidly than the density ρ when the porosity increases. Mackenzie[123] has developed equations for computing the elastic constants of a solid containing spherical holes. For holes of uniform radius they can be written:

$$G = G_0 \left(1 - \frac{5M_0}{k_0 + 2M_0} n\right), \tag{21}$$

$$k = \frac{k_0(M - k_0)(1 - n)}{M_0 - k_0(1 - n)}, \tag{22}$$

where n = porosity, and where the suffix 0 indicates the non-porous and the unsuffixed symbols the porous solid. Mackenzie has given additional terms of higher orders of n depending on the standard deviation of the volumes of the holes. The effect is small and can be neglected for ice, where n is small and the holes are usually of comparable size.*

From eq 21 and 22 we obtain with the elastic constants of Table Vb for lines A and B, respectively,

$$\text{A: } G = 6.79(0.528 - n)\ 10^{10} \text{ dynes/cm}^2 \tag{23a}$$

$$\text{B: } G = 6.67(0.531 - n)\ 10^{10} \text{ dynes/cm}^2 \tag{23b}$$

and

$$\text{A: } k = \frac{4.78(1 - n)}{0.565 + n}\ 10^{10} \text{ dynes/cm}^2 \tag{24a}$$

$$\text{B: } k = \frac{4.73(1 - n)}{0.524 + n}\ 10^{10} \text{ dynes/cm}^2. \tag{24b}$$

These equations have served to compute the theoretical velocity V_P given by curves 1A and 1B in Figure 7, making use of the relations of Table I and eq 1 and 2. Some experimental results by Robin[156] are plotted beside the theoretical curves, as well as the linear empirical relationship of curve 5 given by Bennett[19] (eq 25), corrected for temperature. Curve 1B, based on Bennett's measurements on single crystal ice, and curve 5, based on a large number of measurements on samples of polycrystalline ice, agree better with Robin's data than curve 1A based on the measurements on lake ice by Brockamp and Querfurth. At high densities between 0.85 and 0.919 (porosities of up to 7.5%) the theoretical curve 1B further shows agreement in the slope with Bennett's empirical curve. At lower densities the curves diverge. (This divergence becomes even more pronounced in snow of still lower density as shown below.) Bennett's empirical straight line fitted to a large number of values appears to be the most satisfactory relationship between velocity and density. It is expressed (at –10°C) by

$$V_P = 3160\rho + 945 \text{ m/sec.} \tag{25}$$

The shear wave velocity obtained on the same specimens is given by

$$V_S = 1370\rho + 680 \text{ m/sec.} \tag{26}$$

* For alternative equations and additional reference see ref. 56a.

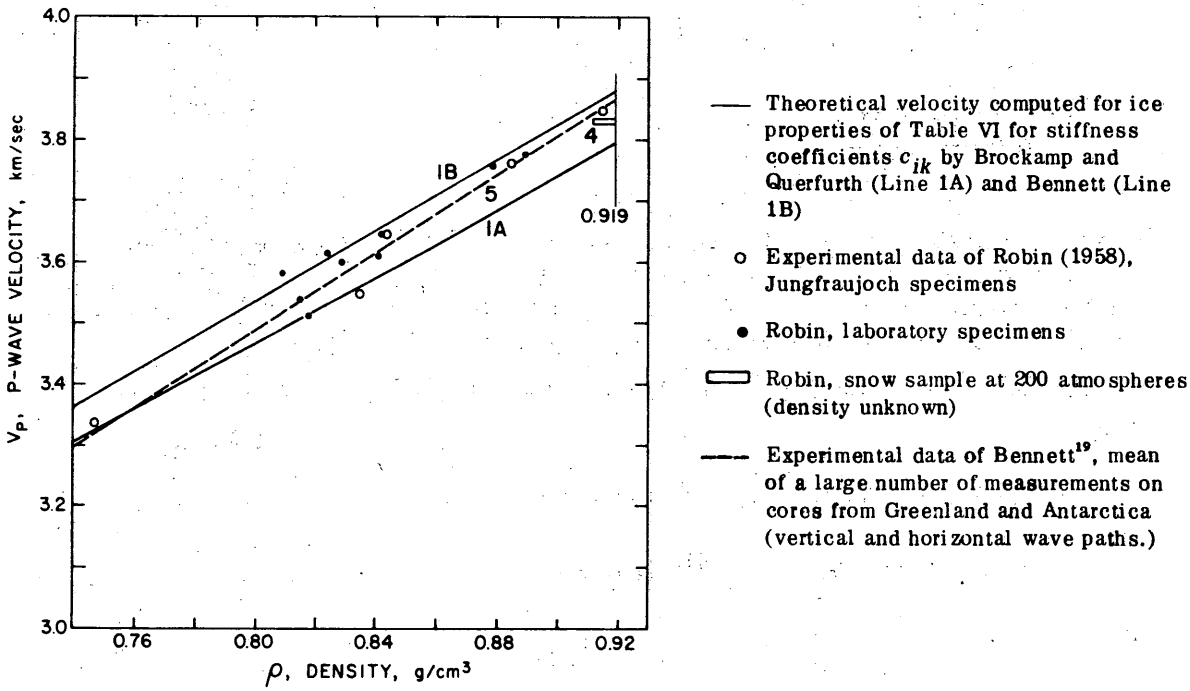

Figure 7. P-wave velocity V_P of ice vs density ρ at –16°C corrected for temperature with the coefficient –2.3 m/sec °C.

Velocity vs temperature

The velocity-temperature relationship has been experimentally determined with ultrasonic measurements by Robin, who has found a temperature coefficient of –2.3 m/sec °C for the *P*-wave for ice of a high density. Using the results of the computation of the velocities in Table Va the temperature coefficients of Table VIII are obtained. The coefficients of Brockamp and Querfurth compare very well with the –2.3 m/sec °C of Robin. There is an indication that the coefficient decreases in its absolute value with decreasing temperature. For V_S a temperature coefficient of –1.1 m/sec °C seems appropriate.

Table VIII. Temperature coefficients of V_P and V_S from laboratory measurements on single crystal ice computed for isotropic ice aggregates, m/sec °C.

	$\Delta V_P/\Delta T$		$\Delta V_S/\Delta T$	
Temp range °C	*Bass et al.*[11]	*Brockamp and Querfurth*[34]	*Bass et al.*[11]	*Brockamp and Querfurth*[34]
– 5 to –16	–3.5	–2.4	–1.4	–1.2
–16 to –20.5		–2.0		–0.9
–16 to –25	–3.3		–1.1	
– 5 to –20.5		–2.3		–1.1
– 5 to –25	–3.4		–1.2	

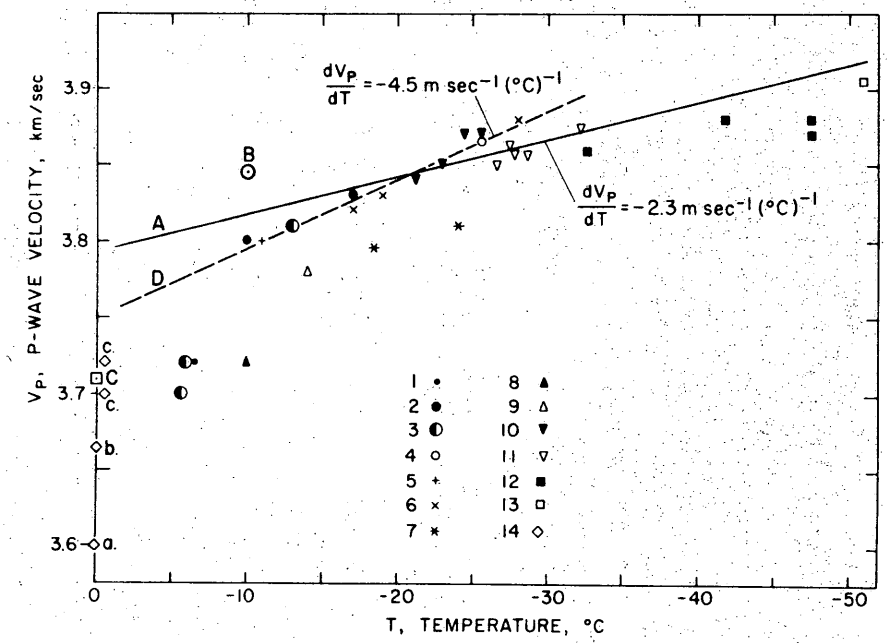

Seismic measurements:

1. Greenland ice sheet, Brockamp et al.[32], after Thyssen[182]
2. Greenland ice sheet, Joset and Holtzscherer[103]
3. Baffin Island, Roethlisberger[160]
4. Greenland ice sheet, Bentley et al.[20]
5. Novaya Zemlya, Wölcken, after Thyssen[182]
6. Greenland ice sheet, Brockamp and Kohnen[35], after Thyssen[182]
7. Ellesmere Island, Hattersley-Smith[84], Weber and Sandstrom[186]
8. Edge of Greenland ice sheet, Roethlisberger[162]
9. Edge of Greenland ice sheet, Bentley et al.[20], Goldthwait[76]
10. Antarctic Peninsula Plateau, Bentley[23]
11. Byrd Plateau, Bentley[23]
12. Victoria Plateau, Bentley[23]
13. Polar Plateau, Bentley[23]
14. Various mountain glaciers, a) Thyssen[182], b) Vallon[183], c) Clarke[46]

Ultrasonic measurements:

Line A Robin[156]
Point B Bennett[19]
Point C Thyssen[182]
Line D Thyssen's empirical relationship.

Figure 8. P-wave velocity V_P vs temperature.

The laboratory experiments can be further compared with seismic results on dry polar ice sheets, where there is generally a thick zone of fairly isotropic ice of approximately uniform high density and uniform temperature at depths below about 300 m. The velocities in this zone reach a maximum, because the temperature increases at still greater depth, causing the velocities to drop. Data from the maximum velocity zone obtained from seismic refraction lines are given in Figure 8 (symbols 1-14) together with ultrasonic laboratory results (line A and points B and C) and a straight line Thyssen[182] had fitted to a selection of field data. Some shear velocity data are presented in Figure 9. There are various reasons that the observed velocities deviate from an ideal curve, namely:

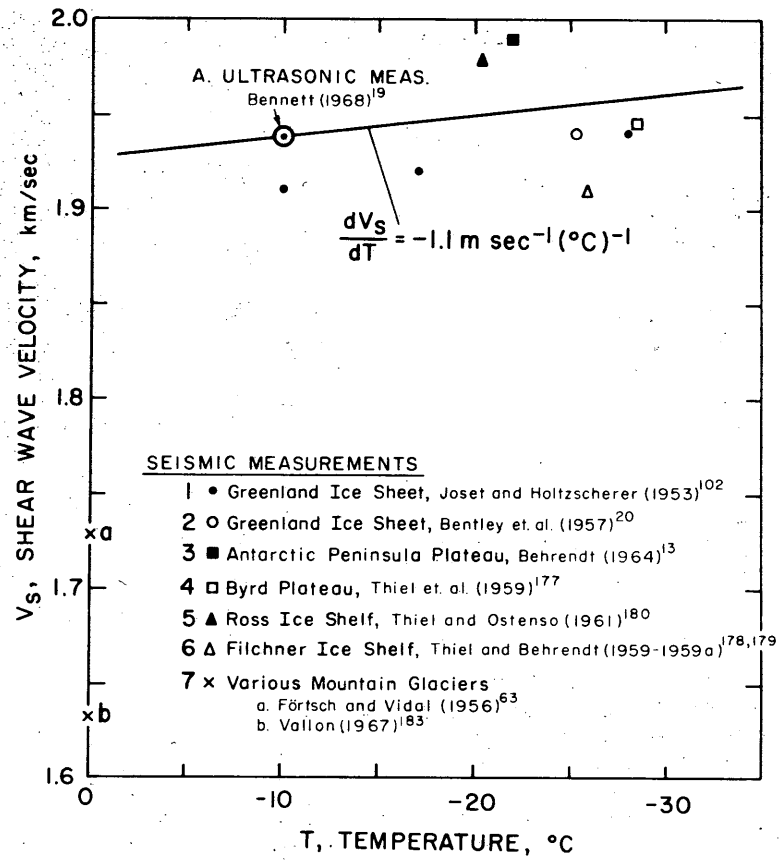

Figure 9. Shear wave velocity V_S vs temperature.

1. The timing device of the equipment may not have been calibrated under field conditions.

2. The temperature estimates may be inaccurate.

3. The refraction line may have been too short to reach the maximum velocity.

4. The dependency of the velocity on the ratio of wave length to the effective thickness of the maximum velocity layer has not been considered, as discussed by Thyssen[182] (see p. 86).

5. The ice at the depth of the maximum velocity may have been anisotropic.

As the melting point is approached, the velocity drops rapidly, as indicated in Figures 8 and 9, and more clearly shown on Figure 5 for single crystal ice. Robin has found that the velocity in melting samples may change with time and can vary considerably from one sample to another in spite of equal density. He has suggested that the liquid at the grain boundaries is the controlling factor, which in turn depends on the purity of the ice (more specifically on the distribution of impurities). On melting specimens of glacier ice he has measured a velocity of 3683 m/sec on a clear sample and 3510 m/sec on a sample of density 0.844 g/cm^3. Thyssen[182] has obtained mean values of 3710-3740 m/sec on melting samples from a few meters depth on the tongue of a temperate glacier. It seems reasonable to assume that a much more uniform velocity should occur at depth in a temperate glacier. Air porosity must become very small as, in the case of cold ice, due to pressure. But also the liquids should not be spread out at the grain boundaries, but confined to the corners, the effect on velocity therefore being relatively small. A fairly constant value of velocity in a temperate glacier at depth can therefore be expected. A value of 3600-3620 m/sec most frequently stated by various authors is probably the best figure now recommendable, but higher values (around 3660 m/sec) have also been reported from very careful studies[58, 183] and are equally justified (see also ref. 56a: 3630 m/sec at 60m depth, 3700 m/sec for $\bar{V}_p$ in a vertical direction).

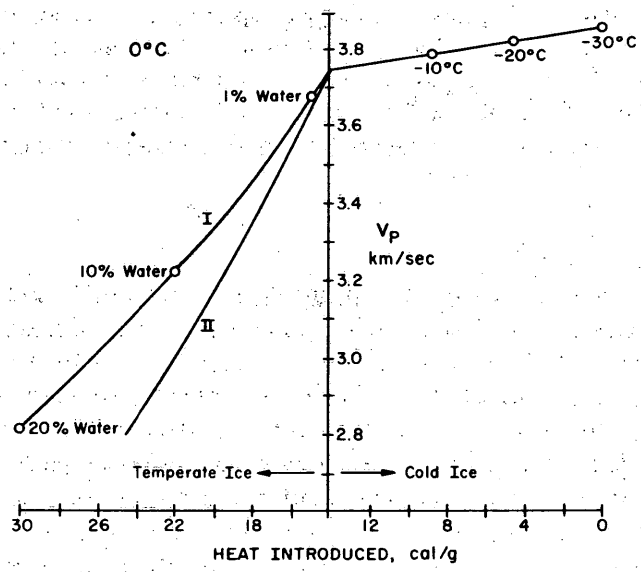

Figure 10. P-wave velocity vs amount of heat introduced into the sample. Explanation of curves I and II in text. (From Thyssen [182])

Thyssen[182] has discussed the role of water in temperate ice. Rather than plotting velocity vs temperature, he uses in the abscissa of Figure 10 the heat introduced into a hypothetical specimen, starting the mental experiment at –30°C. Below freezing he uses his empirical relationship (Fig. 8, line D):

$$V_P = 3.75 - 4.5 \cdot 10^{-3}\, T \text{ (km/sec)}, \tag{27}$$

where T means temperature in °C. The initial velocity at –30°C is obtained from this equation. In the temperate ice he gives curve II based on experimental data by Langleben and Pounder[116] on sea ice with small brine contents at low temperature, and curve I based on the equation given by Willie et al.[193]

$$\frac{1}{V_P} = \frac{n_w}{V_w} + \frac{1 - n_w}{V_i}, \tag{28}$$

where n_w is the water volume relative to total volume including ice, air and water (brine volume related to the actual density), V_w the velocity of sound in water, and V_i the compressional velocity in ice without water but containing the same volume of air as the wet sample. Temperature is given as an additional parameter on the curve below freezing to the right, and water volume at melting temperature, to the left. According to the graph the velocity of 3600 m/sec commonly used on temperate glaciers would indicate a water content of about 2% by volume, but considering the uncertainty of the velocity of water-free ice at the melting point, this is not conclusive.

Very low velocities have frequently been reported at the glacier surface in the ablation zone. The reasons are decreasing density as the bubbles expand on pressure release, internal melting due to solar radiation, and crevassing. Because of the latter a velocity of only 3000 m/sec over a distance of 200 m has been observed by Süsstrunk[173], whereas the proper value of 3600 m/sec was observed from 500 to 700 m.

It may seem paradoxical that the wave velocities in polar glaciers should be better known than those in temperate glaciers of the lower latitudes. However, the temperate glaciers are far less homogeneous, and the terrain is usually so rugged that the error in velocity is negligible compared with the deviations of the true glacier bed from the geometrical model used for evaluation of soundings. It seems that little emphasis has therefore been placed on exact velocity determinations in temperate ice.

Velocity vs pressure

The primary effect of pressure is to reduce porosity, first elastically and then by creep until the bubble pressure reaches the hydrostatic pressure in the ice. With decreasing porosity the density and the velocity increase. But also in clear ice a slight increase of velocity should be expected with increasing pressure. It is estimated that the effect of reduced porosity and the pressure effect in thick ice sheets are of the same order as, or smaller than, the temperature effect at depth; otherwise the velocity increase should be perceptible in very long refraction profiles. The pressure effect at about 200 atmospheres was found to be smaller than the accuracy of the measurement in a laboratory experiment.[56] Uniaxial compression gave an average increase of V_P with stress on the order of 4.8 ± 2 m/sec bar in other experiments.[122] The exact pressure effect should be known together with the temperature effect to compute the exact velocity below the maximum velocity layer in ice sheets.

Anisotropic polycrystalline ice

A mass of ice is anisotropic when there is preferred crystallographic orientation, since the single ice crystal shows noticeable anisotropy (Fig. 6). Glacier ice with a maximum degree of orientation, i.e. all c-axes parallel, would to a first approximation show the same degree of anisotropy as a single crystal, but lesser velocities due to porosity. (No complete analogy is to be expected, because there is no reason that the elastic moduli c_{ik} should be proportionally changed by bubbles.)

An approximate method of computing the elastic behavior of polycrystalline ice with preferred crystal orientation, in particular the resulting velocity distribution in space, consists of averaging the reciprocal wave normal velocity (called slowness). Rüter[168] has applied this method to compute compressional wave normal velocities (also referred to as phase velocities) for actual orientations taken from fabric diagrams. Bennett[19] gives more accurate approximations based on the square of the slowness, but uses the more convenient first power in the actual computations. In the case of the shear wave he accounts for the fact that the resulting polarized wave is affected by the slownesses of both the true and the pseudo-shear wave of an arbitrarily oriented crystal. (Averaging the slownesses of the two shear waves separately is too inaccurate.) He presents the results of a systematic computation of two types of preferred orientation showing axial symmetry, the first where all the c-axes are evenly distributed in the surface of a cone, the second where they are evenly distributed within the cone. Because of the axial symmetry of the crystal orientation the resulting polycrystalline aggregate is also transversely isotropic like the unit crystal. For small apex angles the shape of the curves representing velocity versus direction of propagation is not altered, but the degree of anisotropy decreases as the apex angle increases. At large apex angles the character of the anisotropy changes, so that (if cone axis is vertical) $V_{P(V)}$ and $V_{P(H)}$ become minima of the P velocity and $V_{S(V)} = V_{SV(H)}$ becomes the maximum of the S-wave velocity. The transition occurs at considerably smaller apex angles in the case of the surface cones than in the case of the solid cones. Table IX gives a few results on the degree of anisotropy for solid cones (axes evenly distributed within the cone). The figures refer to directions in which the wave normal is vertical to the wave front, so that the wave normal and ray velocities are identical. In an arbitrary direction the results from slowness averages have to be converted for use in relation with wave fronts; graphical or analytical methods are available[86].

Table IX. Deviation of compressional velocity V_P from V_P vertical in the horizontal and an oblique direction.

For ice showing preferred orientation with the directions of the c-axes evenly distributed within a vertical cone of apex angle α ($\alpha = 0°$: single crystal ice). Angle ϕ between vertical (cone axis) and the oblique direction, in which V_P becomes an extremum. (After graphs by Bennett[19].)

α	$100\,\frac{V_{P(H)} - V_{P(V)}}{V_{P(V)}}$ %	ϕ	$100\,\frac{V_{P(\phi)} - V_{P(V)}}{V_{P(V)}}$ %
0°	−3.9	52°	−6.7
20°	−3.1	53°	−5.0
30°	−2.2	54°	−3.4
40°	−1.4	56°	−1.7
45°	−1.0	70°	−1.0
60°	−0.4	42°	+0.4

Ice with a highly preferred orientation has been encountered at the edge of the Greenland Ice Cap in the experimental ice tunnels of camp TUTO. A *P*-wave velocity distribution with a high peak value in the vertical direction, a somewhat lower peak value for horizontal propagation and a minimum in an oblique direction has been observed when travel-time measurements were carried out with pulsed vibrations,[164] in general accord with the computations.[68]

Anisotropy of large bodies of otherwise isotropic material can also be caused by layering (Fig. 11), but there are other kinds of structural anisotropy as well. The high degree of anisotropy in the top snow layers of Antarctica observed by Bennett[19] ($V_{P(V)} \approx 2V_{P(H)}$ within 3 m of the surface at the South Pole) must be caused by structural anisotropy. It disappears rapidly with depth to give way to a slight preferred crystal orientation which has been observed in drill holes in Antarctica as well as Greenland. At depths of many hundreds of meters very pronounced crystal orientations causing a relatively high degree of anisotropy exist.[25a] The alternation of porous and non-porous layers (foliation) in the ice near the surface of a temperate valley glacier has been shown to give a measurable anisotropy effect of a few percent.[56a]

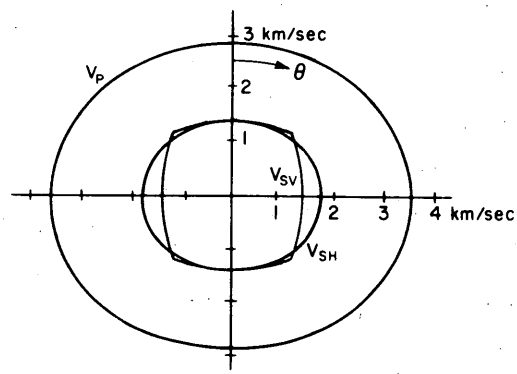

Figure 11. Ray velocity diagram in Pertinax, a hard impregnated cardboard. (After Helbig[86].)

Velocity and inclusions

Bruggeman[40] has shown that the elastic moduli of a mixed material consisting of two or a multitude of solids depend on the structure, even when the final product is isotropic. One approach to compute elasticity and velocity in a mixed substance is to assume that spheres of one component are embedded randomly in a matrix consisting of the other component. The equations, only valid for low contents of spheres, i.e. as long as the spheres do not influence each other, are:

$$1 - \delta' = \frac{g' - g}{g' - g''} \left(\frac{g''}{g}\right)^{2/3}_{i}; \tag{29}$$

$$\frac{1 - \delta'}{\kappa - \kappa'} = \frac{1}{\kappa'' - \kappa'} + 4 \int_0^{\delta'} \frac{d\delta'}{4\kappa' + 3g}; \tag{30}$$

$$\rho = \delta' \rho' + (1 - \delta') \rho'' \tag{31}$$

where

δ' = content by volume of the spheres

$g = \frac{1}{G}$ with G = shear modulus

$\kappa = \frac{1}{k}$ with k = bulk modulus and

ρ = density of the mixed substance.

The primed symbols are used for the embedded material, the double primed symbols for the matrix. *P*-wave velocities computed with the above equations are given in Figure 12, *S*-wave velocities in Figure 13.

Bruggeman's[40] second method consists of computing the five elastic moduli of a laminar substance from the equations:

$$c_{11} - \frac{c_{13}^2}{c_{33}} = \sum_i a_i \left(C_i + 2G_i - \frac{C_i^2}{C_i + 2G_i}\right); \tag{32}$$

$$\frac{1}{c_{33}} = \sum_i a_i \frac{1}{C_i + 2G_i}; \tag{33}$$

$$\frac{c_{13}}{c_{33}} = \sum_i a_i \frac{C_i}{C_i + 2G_i}; \tag{34}$$

$$\frac{1}{c_{44}} = \sum_i a_i \frac{1}{G_i}; \tag{35}$$

$$\tfrac{1}{2}(c_{11} - c_{12}) = c_{66} = \sum_i a_i G_i; \tag{36}$$

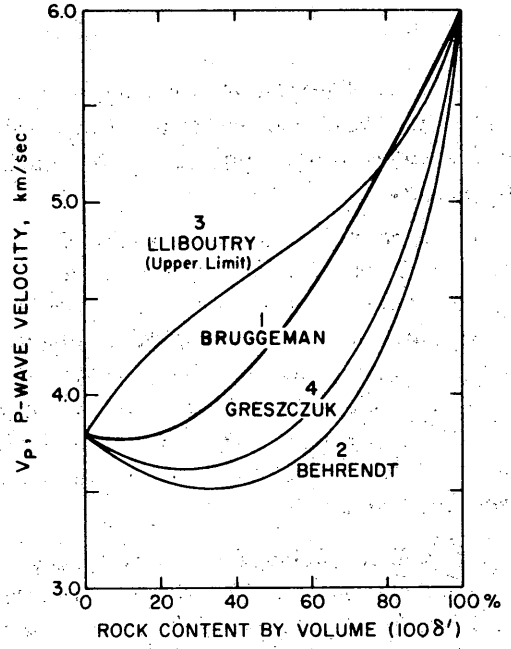

1. Bruggeman (eq. 29, 30, 31)
2. linearity for 1/k and 1/G (Behrendt[12])
3. linearity for 1/k and G (Lliboutry[120])
4. linearity for 1/k and ν (Greszczuk[82]).

Figure 12. Theoretical velocity V_P vs content of rock (granite) inclusions in ice. Properties of rock: $V_P' = 6.0$ km/sec, Poisson's ratio $\nu' = 0.23$, density $\rho' = 2.68$ g/cm³; properties of ice: $V_P'' = 3.8$ km/sec, $\nu'' = 0.331$, $\rho'' = 0.92$ g/cm³.

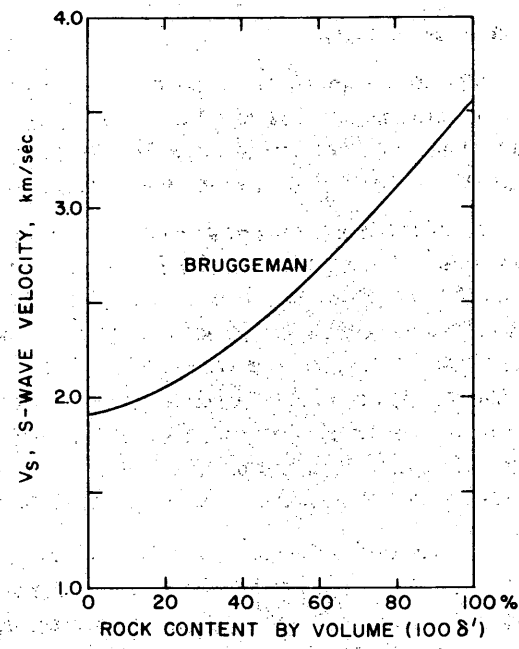

Figure 13. Theoretical velocity V_S vs content of rock (granite) inclusions in ice. Properties of components see Fig. 12. (Bruggeman theory, eq 29 and 31.)

$$\rho = \sum_i a_i \rho_i \qquad (37)$$

where C_i and G_i are the Lamé constants of substance (i) and a_i is the content by volume of substance (i), $\sum_i a_i = 1$. The equations are written for an arbitrary number i of components. The laminar material is anisotropic, but it can be converted into an isotropic material with eq 19 and 20, which is an approximation, or the more accurate solution by the same author.[39]

The velocity in mixed solids has also been figured out by much simpler approximate computations assuming linearity for various elastic constants, i.e. assuming that either certain stresses or strains are changed in proportion to the rock content (Lliboutry,[120] p. 701). The discrepancy between the result of the extreme assumptions is very large (Fig. 12), and none of the approximate methods can be recommended. Behrendt's[12] computation of $V_P = 3640$ m/sec, $V_S = 1880$ m/sec and $\nu = 0.32$ for ice containing 13% of morainic material was obtained with the method of curve 2 and is probably too low. Systematic experimental data seem to be lacking.

Not much is known about the effect of clay particles in ice, but it can be assumed that a fair amount of clay inclusions might lower the velocities considerably at temperatures close to the melting point.

Velocities in snow

The velocities in snow depend strongly on the density, but the structure (bonding of the grains) can be an important factor. In naturally compacted snow in situ, at least under dry polar conditions, the structures are quite uniform from the beginning and converge further with age and increasing density. Velocities can therefore be well related to density.

A summary of *P* velocity vs density data by various authors, obtained by a variety of methods, is presented in Figure 14. Further data on *P* velocities and a graph on *S* velocities assembled by Bennett[19] are given in Figures 15 and 16. A discrepancy exists between most of the seismic refraction and ultrasonic laboratory results obtained on cores, the latter being lower. This may reflect that the seismic arrival times used are related to waves traveling selectively in snow masses of above-average velocity, while average densities are used for the plot. Alternatively, it may be the consequence of the anisotropy of the surface layers (p. 29), the velocity being higher in the vertical than in the horizontal direction[19]. In that event the waves would penetrate deeper than assumed, and the observed velocity would be assigned to a too low density.

In Figure 17a the data from four selected sites (Site 2, Byrd Station, Camp Century and the South Pole) where particularly reliable seismic refraction velocities and densities are available are compared again. (The graph might be further improved by using original data.) The four curves compare well over the whole range of densities, indicating that a fair depth-density relationship can be obtained from seismic refraction data with an estimated accuracy of about ±0.01 g/cm³.

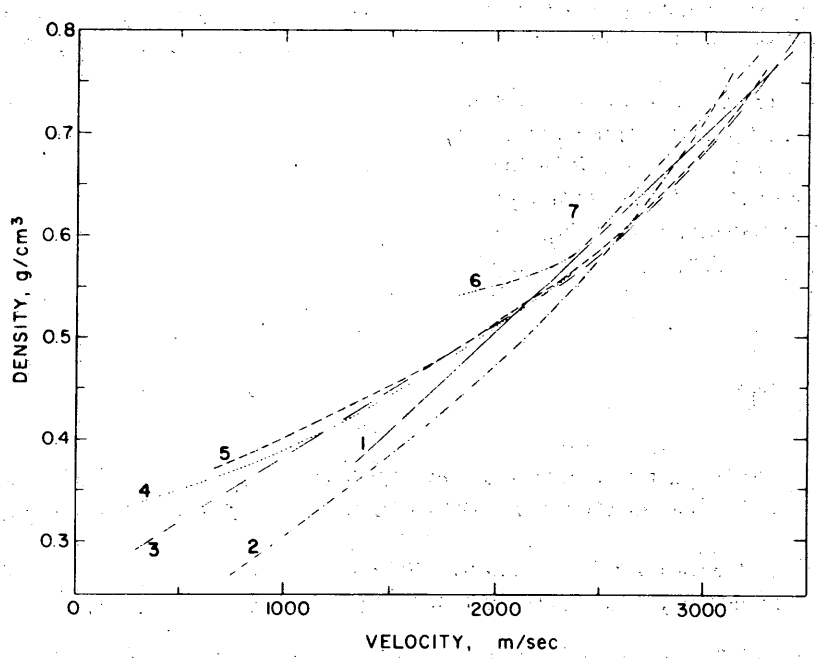

1. Robin – Jungfraujoch
2. Robin – laboratory
3. Crary, et al. – Ross Ice Shelf
4. Roethlisberger – Greenland
5. Bentley, et al. – Greenland
6. Robin – Maudheim
7. Lee – processed snow

Figure 14. Velocity of an elastic compression wave in snow as a function of density. (From Mellor[125].)

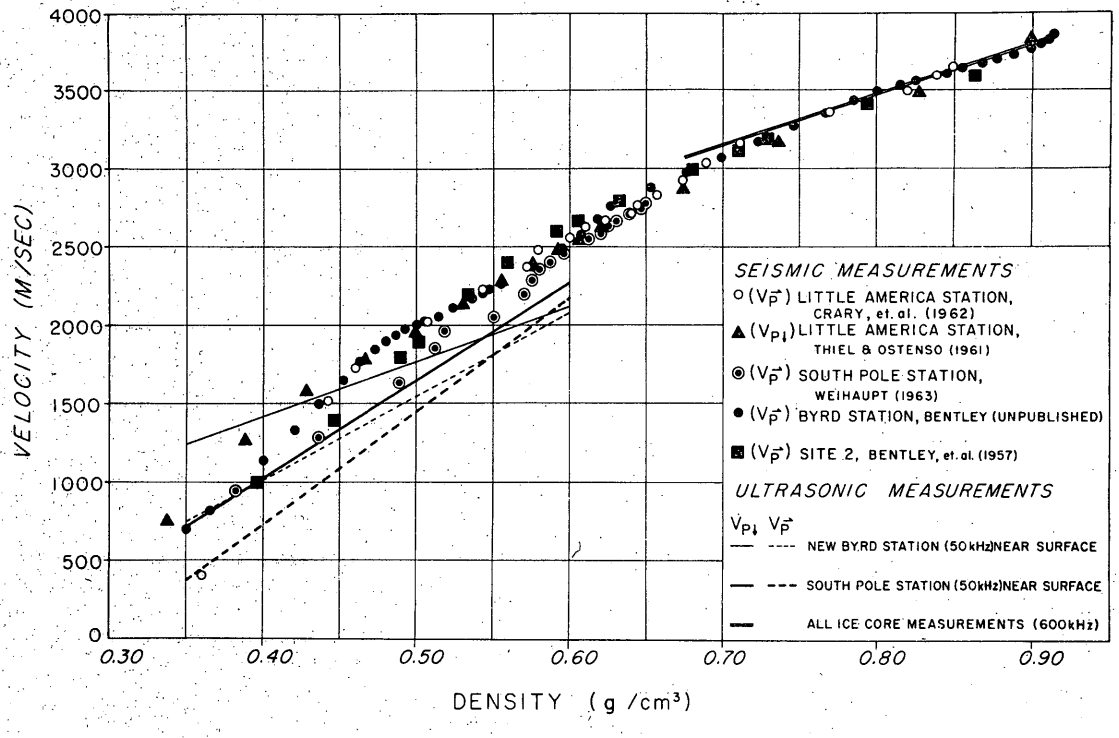

Figure 15. P-wave velocity V_P vs snow density, comparison of seismic and ultrasonic data. (From Bennett[19].)

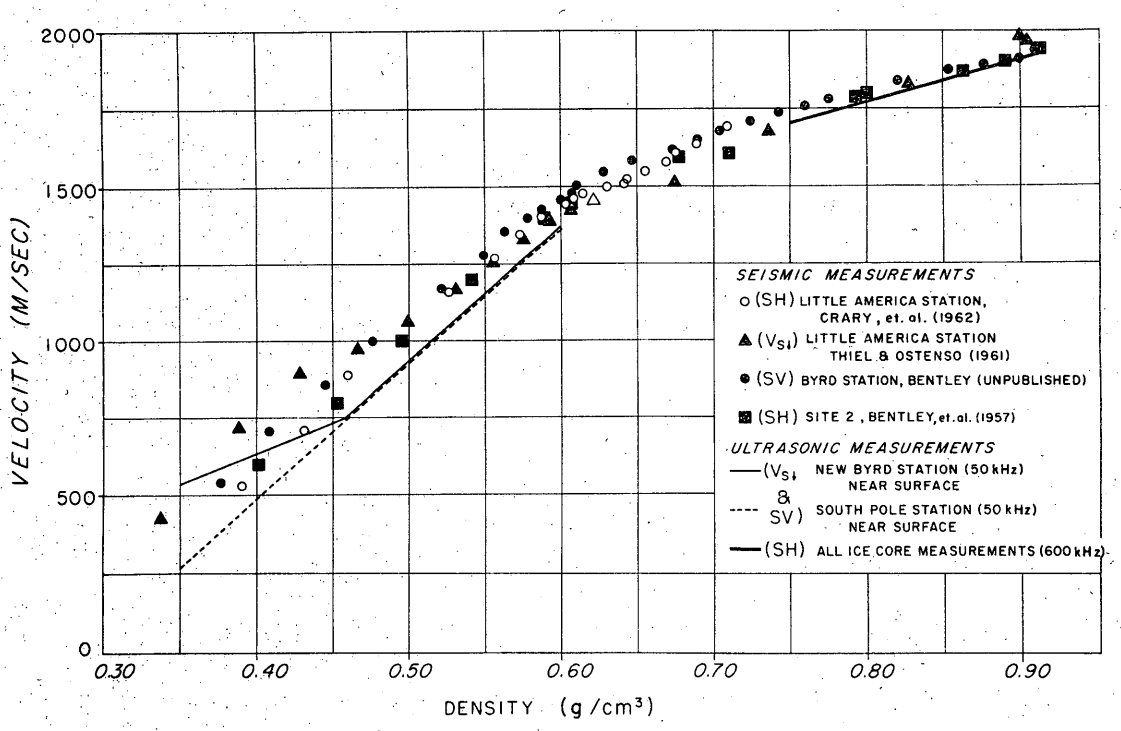

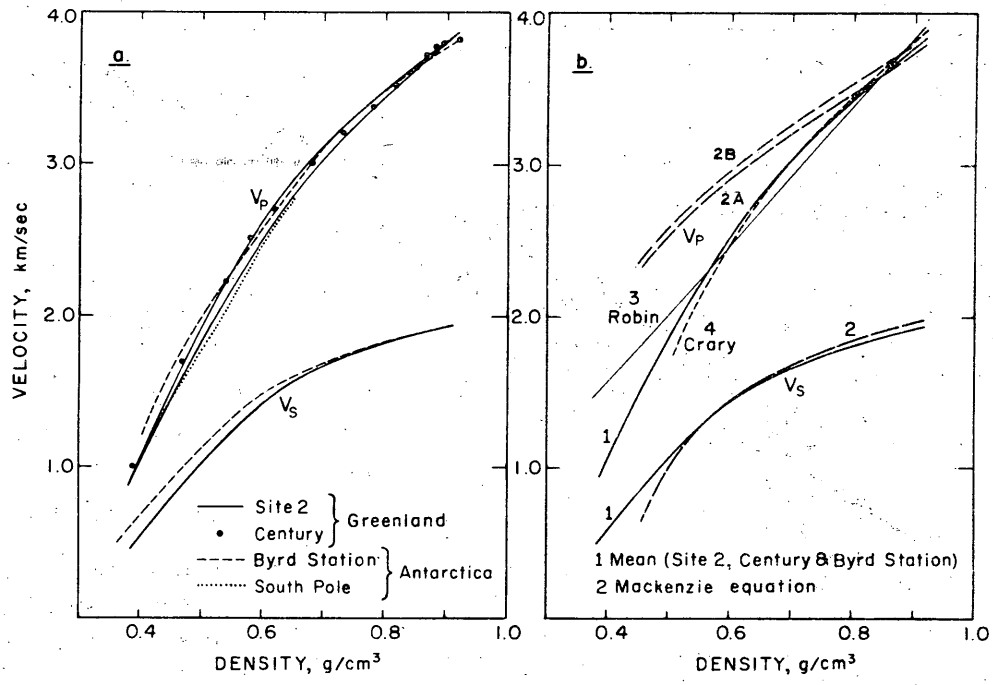

Figure 17. Wave velocities in snow from seismic data and velocities computed from various theories, vs snow density, selected sites. a) Site 2 velocity after Bentley et al.[20] and Roethlisberger et al.[166], density supplied by Langway; Century velocity after Clarke[44], density supplied by Gow; Byrd Station velocity after Bennett[19], density after Bender and Gow.[18] South Pole velocity after Weihaupt[190], density after Giovinetto.[74] b) Comparison of the mean velocity vs density relationship of Fig. 17a with various computed curves. (Explanations in text.)

In Figure 17b the mean velocity – density curves (1) for the three representative stations of Figure 17a (without South Pole), corrected for temperature as outlined below, are compared with computed curves. Curves (2) were obtained with the Mackenzie theory (p. 16-17, giving the theoretical effect of spherical holes of uniform size in an isotropic elastic material, applied to idealized polycrystalline ice with random crystal orientation based (A) on the Brockamp and Querfurth data at –16°C, and (B) on the Bennett data corrected for temperature (Table Vb). Curve (3) is based on the velocity-density-temperature relationship given by Robin.[56] He has fitted the straight line expressed by the following equation to results from ultrasonic velocity measurements, carried out at Jungfraujoch with a limited number of firn and ice specimens showing uniform texture:

$$V_P = \frac{\rho - 0.059}{2.21} 10^4 \quad \text{(m/sec)} \tag{38}$$

(ρ in g/cm³). Assuming that the temperature coefficient is the same for snow as for ice (a procedure which is not necessarily correct) he has further obtained

$$V_P = \frac{\rho - 0.059}{2.21} (1 - 0.00061\,T)\ 10^4 \quad \text{(m/sec)} \tag{39}$$

where T = temperature in °C. Equation 39 has been used to compute line 3 for the same temperature of –16°C as curve 2 is given. The same temperature coefficient (1 – 0.00061 ΔT), with ΔT the temperature difference between the site and –16°C, has been used to correct curves 1, 2B and 4 to –16°C. Curve 4 is based on the function

$$V_P^2 = (22.52\rho - 0.87 - 3.79\rho^{-1})\ 10^6 \quad (\text{m}^2/\text{sec}^2) \tag{40}$$

given by Crary[54] for the Victoria Land Plateau, Antarctica (average temperature about –46°C). A similar relation has been obtained on the Ross Ice Shelf,[53]

$$V_P^2 = (11.72\rho + 10.83 - 6.75\rho^{-1})\ 10^6 \quad (m^2/sec^2) \tag{41a}$$

for the density range 0.5 to 0.92 g/cm³ at –27°C, and

$$V_P = 7744\rho - 1965 \quad (m/sec) \tag{41b}$$

for densities below 0.5 g/cm³. Equations 40 and 41a are based on a linear relationship of E, and of $(1-\nu)/(1-2\nu)(1+\nu) = M/E$, with density, where E = Young's modulus, ν = Poisson's ratio and M = longitudinal modulus under triaxial condition. This linearity was deduced from the experimental seismic results.

The Mackenzie equations, curves 2, give a good fit for V_S and appear to predict V_P fairly well for high densities (compare Fig. 7). It is not surprising that the theory, based on isolated spherical bubbles, fails at densities below 0.8 or 0.75 g/m³, where it is known that the pores are communicating. The linear relationship of Robin, curve 3, has been widely applied in the literature (eq. 39). It can be seen from Figure 17b that there is a systematic deviation of the velocity-density relationship from linearity. It seems that Robin's equation has almost been used as a law, although it was never meant to be one. Crary's empirical curve (4) is steeper throughout than the mean Greenland-Byrd curve, but is quite close to it for densities above 0.55 g/cm³. The large difference in temperature (–40 to –50°C on the Victoria Land Plateau as against –24 to –26°C in Greenland and at Byrd) probably accounts for the systematic difference as further discussed below.

The role of the structure in snow is different from that in ice. Crystal orientation is not nearly as important as in ice, but bonding of the grains is the decisive factor. This is best shown by comparing velocities of naturally compacted snow with artificially disaggregated and redeposited (milled) snow. Figure 18 gives data obtained on specimens with the ultrasonic method. It is interesting to note that after 2-3 years the milled snow shows higher velocities than the naturally deposited snow. A further example of the aging is given in Figure 19. Hobbs[87] has applied the theory of sintering to the aging effect on the E modulus of snow.

A slight difference in bonding (bubble shape) in snow of equal density may also exist in nature. Old snow (low accumulation rate) would show higher sphericity of the bubbles and therefore higher velocities. Since the aging process depends strongly on temperature, higher sphericity may be expected at higher temperatures. This might account for the low velocities in the snow at the South Pole, while the slightly higher velocities in the snow of Byrd Station as compared to Site 2 and Century might reflect the much lower accumulation rate (i.e. greater age at equal density) at temperatures only 1 to 2 degrees lower (Fig. 17a).

Anisotropy must also be considered, as shown by Bennett (1968). He reports compressional velocities V_P (vertical) twice as large as V_P (horizontal) within 3 m of the surface at the South Pole and 1½ times as large within 4 m of the surface at Byrd Station. The difference between V_P vertical and horizontal diminishes rapidly with depth, but is still detectable 28 m below the surface. The large $V_{P(V)}/V_{P(H)}$ ratio is explained by structural anisotropy, which is also apparent from directional permeability.[17] It is astonishing that V_P vertical is larger than V_P horizontal which is the opposite from what is usually found in layered media (Fig. 11). Larger horizontal than vertical velocity has also been inferred from Rayleigh wave analysis on the Ross Ice Shelf by Robinson.[158] Towards the transition from snow to ice, crystal orientation sets in, which may account for velocity differences of V_{SV} and V_{SH} (vertically and horizontally polarized shear wave) at large distances of refraction shots.[19 23 25a]

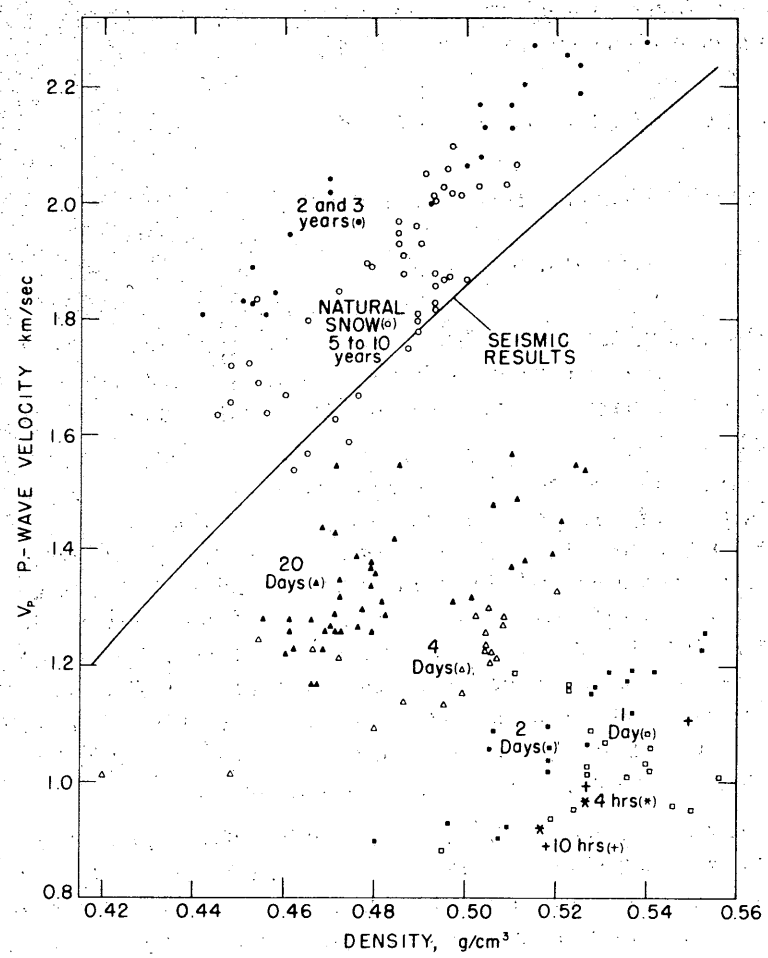

Figure 18. P-wave velocity vs density in milled and age-hardened snow (except naturally compacted snow where indicated), measured on samples with ultrasonic pulses (50 kHz). Age groups are indicated by symbols and the time between deposition and measurement is written within each group. (Author's data, unpublished.)

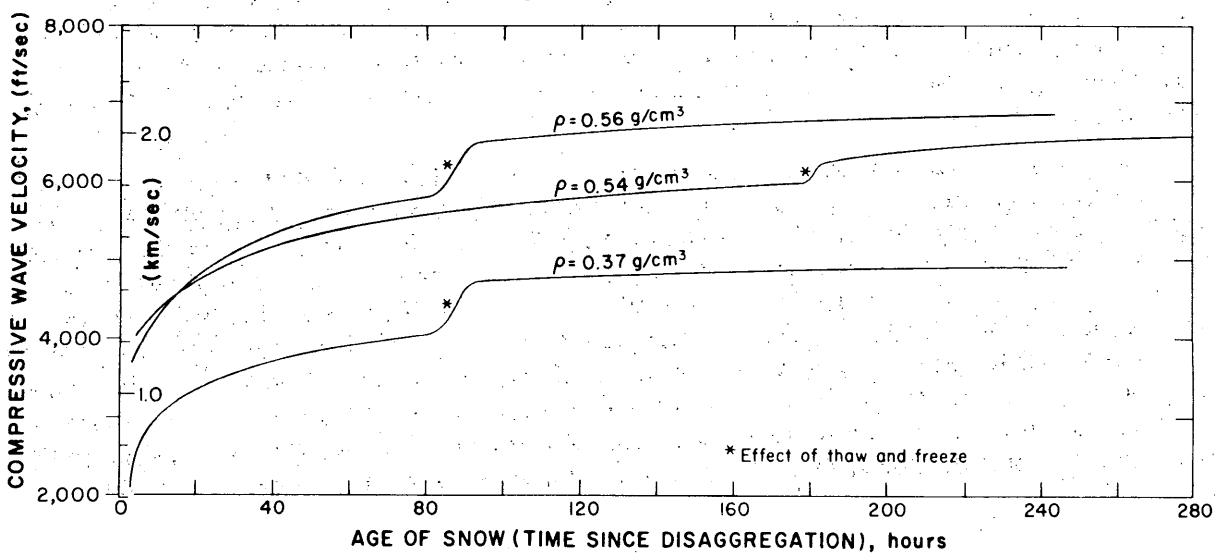

Figure 19. P-wave velocity in snow as a function of time during the period of intergranular bond formation (age-hardening). (After Lee, from Mellor.[125])

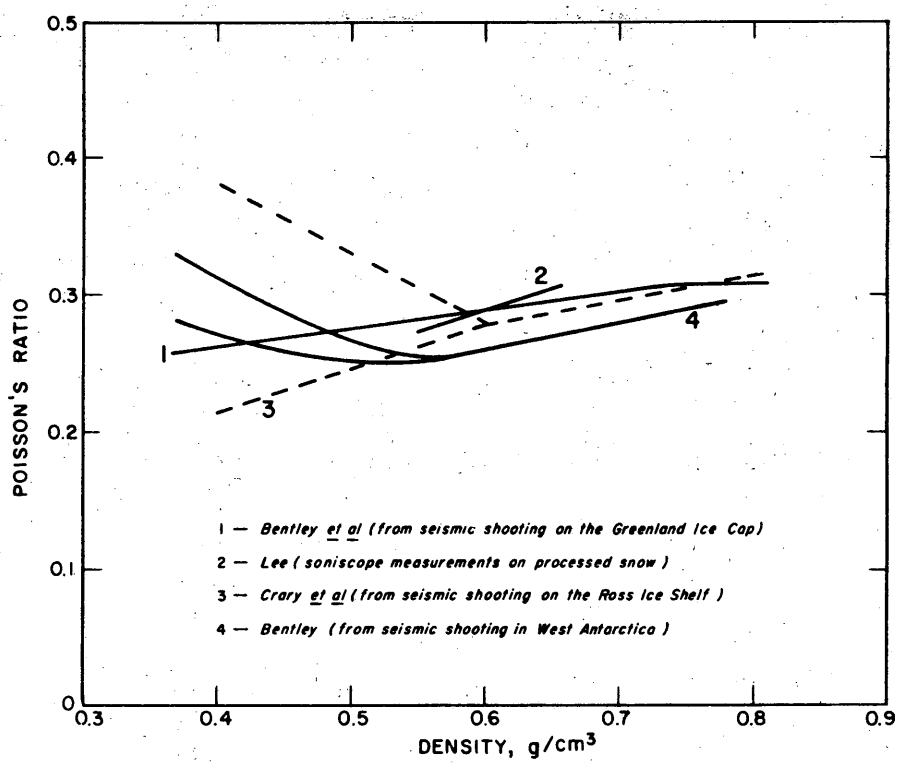

Figure 20. Poisson's ratio for dry snow as a function of density, seismic and ultrasonic measurements. (From Mellor[125].)

In the accumulation zone of a temperate glacier as well as a cold glacier at elevations where considerable melting occurs the velocity distribution is very much different from the dry cold ice caps. Very strong layering occurs, and the velocity distribution changes with season as the water content of the snow changes. The increase of density with depth and therefore of velocity with depth is faster than in cold polar snow, and it is quite erratic. It is therefore necessary to determine the velocity-depth relationship for each location.

A number of detailed studies, summarized by Mellor[125] in Monograph III-AI, p. 21-23, have been carried out on snow with sonic methods. The results are usually presented in terms of Young's modulus. The dependency of Poisson's ratio on density, deduced from seismic in situ measurements and ultrasonic laboratory studies, is given in Figure 20.

Velocities in sea ice

Sea ice is a mixed substance with a complicated structure. The components are ice, brine, air and, at low temperature, small quantities of crystallized salts of various chemical composition. The structure is changing with time, and the changes depend on temperature. Age and temperature history are therefore important factors in the study of sea ice. The brine content n_b, which can in turn be expressed in terms of salinity and temperature[67] is a convenient parameter to which velocities in sea ice may be related. For practical reasons the air is often considered a part of the brine content[116] since the bubbles are usually contained in the brine, and air replaces brine when specimens are partially drained. It would be clearer, however, to use brine volume n_b for the liquid alone and refer to porosity n when liquid plus air (n_a) are meant. However, it is no easy task to determine the porosity of samples from which brine was partially drained if the temperature has changed as well.

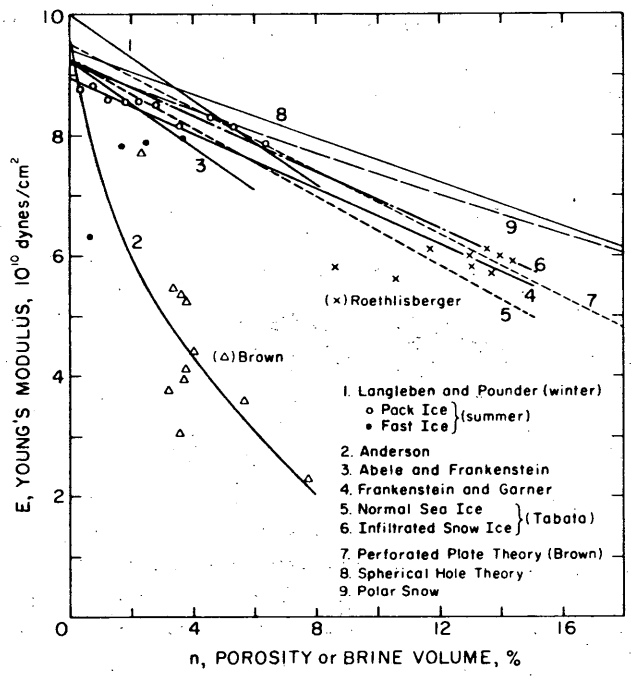

Figure 21. Young's modulus E of sea ice determined by various dynamic methods, in function of total porosity n or brine volume n_b. Additional theoretical curves and an experimental one for snow are given for comparison. (After Langleben and Pounder[116]; Brown[38]; Anderson[4]; Abele and Frankenstein[1]; Frankenstein and Garner[68]; Tabata, from Weeks and Assur[188]; spherical hole theory: eq (IB-22/23); polar snow from Fig. B-18b; author's data, unpublished.)

Body wave velocities in sea ice have been measured on floating sea ice by standard seismic techniques and by ultrasonic pulse methods. Further information on the elastic parameters has been obtained from plate waves, flexural waves (dispersion analysis and air coupled waves), and resonance frequency tests on samples. Only in rare cases has it been possible to obtain two elastic parameters on exactly the same ice under identical conditions, and with comparable accuracy. It is therefore difficult to compare the results by different investigators when different parameters have been measured. From the rare cases where two parameters have been observed it is nevertheless known that Poisson's ratio varies only between certain limits, say 0.2 to 0.4, and much less under comparable conditions. Constant values of $\nu = 0.33$ (Pounder and Stalinsky[147]) and $\nu = 0.295$ (Langleben and Pounder[116] and Pounder and Langleben[149]) have been used in the literature for conversions, while in other cases the observed values were taken.[38] If we compute Young's modulus from *P*-wave velocity V_P and an assumed value of $\nu = 0.33$, then a correction of up to 35% would be necessary if Poisson's ratio varied between 0.2 and 0.4. When the computation is based on the plate velocity V_{PL}, then the analogous corrections would be less than 8%.

A summary of values of Young's modulus *E* versus total porosity *n* (in some cases brine volume n_b) is given in Figure 21. The average *E* versus porosity or *E* versus brine volume curves of the various authors have primarily been replotted, but some of the individual determinations (or averages of groups of tests) are given as individual points. The data by Langleben and Pounder, and Frankenstein and Garner, were obtained by means of ultrasonic pulse measurements on samples. In converting

to Young's modulus Frankenstein and Garner have used a value of $\nu = 0.25$ for Poisson's ratio, which gave them very high values for E. Curve 3 has been reduced for $\nu = 1/3$ at $n = 0$ and $\nu = 0.3$ at $n = 150‰$; curve 4 has been reduced for $\nu = 1/3$ throughout. (The resulting correction is too large for part of the original data, because an impure P-wave has been measured in the more slender specimens. The correct line for the Frankenstein and Garner results would therefore be somewhat higher.) Brown's and Anderson's data are based on plate wave velocities and flexural wave velocities measured in the field, and on sonic measurements on specimens, and Tabata's results entirely on sonic measurements. The formerly unpublished data added by the author were obtained from ultrasonic measurements in situ, which were carried out shortly before breakup in North Star Bay, Thule, Greenland, in June 1959. Temperatures (between –0.5 and –1.4°C) were also measured in situ with thermocouples, while the salinity was determined on cores, taking precautions to lose as little brine as possible. The transducers were placed in 1 and 1½-in. brine-filled holes. The same type of transducers could be used in winter, frozen in at different levels. They were used in this manner in glacier ice.[164]

In Figure 21 a striking discrepancy is immediately apparent between the findings of different investigators: at certain porosities the highest values are almost four times as large as the smallest ones. On the other hand, the scatter of the results of individual investigators has been found to be small. Various possibilities exist to explain the major discrepancies, none of them being very satisfactory:

1. *Use of the wrong value for Poisson's ratio.* Even with extreme assumptions (which might hardly be justified) the discrepancy cannot be fully explained.

2. *Anisotropy.* Anisotropy effects must be expected, since a preferred orientation of the ice crystals exists (horizontal c-axes) and the sea ice structure is highly anisotropic (vertical plates). The difference in horizontal and vertical directions observed by Frankenstein and Garner confirms the existence of anisotropy. Anisotropy effects might cause differences in, say, Young's modulus when different methods have been used, but hardly to the observed degree.

3. *Frequency.* It is noteworthy that all the high values of E have been obtained by ultrasonic methods, while the lowest values were computed from sonic tests, plate waves in the low frequency sonic range, and from air-coupled waves of much lower frequencies. Some of the sonic results, however, fall into the range of the high values. Mobility of brine at high porosities may be a reason for low velocities at low frequency.

4. *Structure.* Some structural effect has been demonstrated by Tabata (curves 5 and 6), but it is doubtful that the very low values of Brown and Anderson could have been caused by structure difference.

It is interesting to note that the high values of E from ultrasonic measurements are quite close to those computed from P-wave velocities in glacier ice at equal porosities, and also to the results of theoretical computations, particularly to the ones obtained with the "perforated plate theory",[38] approximated by a straight line. Apart from the influence of porosity Pounder and Langleben[149] [116] have found that biennial and older polar ice gave values of Young's modulus averaging 3.6% lower than those for annual sea ice of similar brine content, a difference which is not very significant if compared with the large discrepancies between various investigators.

The P-wave velocity is related to Young's modulus by $V_P = 1.225\sqrt{E/\rho}$ if $\nu = 1/3$ is used for Poisson's ratio. From the experimental results on E from Figure 21 it is found that V_P decreases from about 3800 m/sec at $n = 0$ to about 3400 m/sec at 100‰ porosity (brine volume), but that it may be considerably lower. The plate velocity is 13% smaller than the compressional body wave velocity: $V_{PL} = 0.87\,V_P$, again for $\nu = 1/3$, which gives 3300 m/sec for $n = 0$ and 2950 m/sec or lower for $n = 100‰$. Using $\nu = 0.3$ gives corresponding values for V_P and V_{PL} of 3600 to 3200 and 3250 to 2900, respectively, or lower.

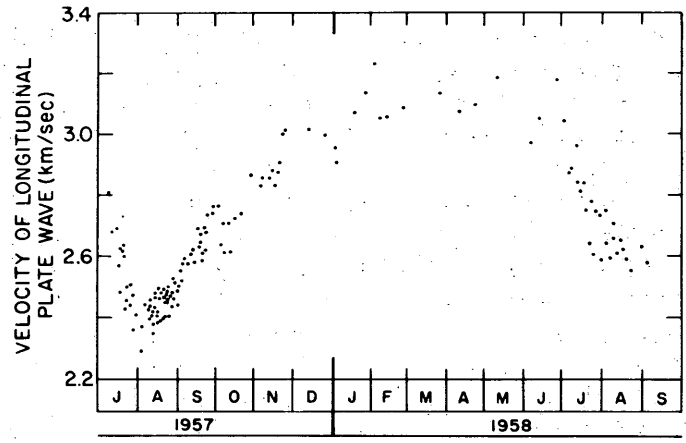

Figure 22. Seasonal variation of longitudinal plate velocity. (After Hunkins, from Weeks and Assur[188].)

The seasonal variation of the plate velocity in pack ice is shown in Figure 22. Table X gives seismically observed values of V_{PL}, V_P and V_S for the same pack ice at various dates, as well as Poisson's ratio computed from eq 4 and a formula relating V_{PL} and V_S:

$$\nu = 1 - 2\left(\frac{V_S}{V_{PL}}\right)^2 . \qquad (42)$$

Considering the relatively low salinity of pack ice and the low temperature in winter the figures for V_P and V_{PL} are low compared with the ultrasonic results. Lower seismic than ultrasonic velocities in specimens have also been observed by Pounder and Langleben.[149] Their values obtained on biennial ice near Isachsen in April-May supplement Table X nicely: V_P = 3110 m/sec, V_{PL} = 2920 m/sec, V_S = 1788 m/sec, $\nu = 1 - 2(V_S/V_{PL})^2 = 0.254$. Poisson's ratio is lower than the value of 0.33 for freshwater ice, as in bubbly ice and snow. Lin'kov,[119] on the other hand, has reported high values of Poisson's ratio between 0.33 and 0.39, while Langleben and Pounder[116] give an average of 0.295 and Pounder and Langleben have found 0.299. Porous materials in general show a low Poisson's ratio; however, if the pores are completely filled with a liquid, this does not affect the shear modulus, while the moduli related to a volume change become larger. Thus Poisson's ratio will be larger in the liquid-filled substance than in the air-filled one.

Table X. Velocities and Poisson's ratio in pack ice. (After Hunkins[93].)

Date	*P-wave velocity* V_P *m/sec*	*Plate wave velocity* V_{PL} *m/sec*	*S-wave velocity* V_S *m/sec*	*Poisson's ratio, computed from* $\frac{\frac{1}{2}(V_P/V_S)^2 - 1}{(V_P/V_S)^2 - 1}$	$1 - 2(V_S/V_{PL})^2$
25-27 Aug 1957	2802	2457	1552	.278	.202
15-16 Sept 1957	2974	2541	1578	.306	.229
3-4 Jan 1958	3401	3181	1862	.290	.315
24-31 Mar 1958	3504	3129	1826	.312	.319
17-20 Apr 1958	3504	3088	1857	.312	.277

When relating elastic moduli with velocity the density must also be known. Sea ice below the water table contains a very small amount of air bubbles, and because of the brine content the density is higher than in clear ice. Densities of $\rho = 0.94 \pm 0.02$ g/cm^3 have been reported at -20° C, and about 0.91 g/cm^3 at -15° C.[116] Lower densities between 0.87 and 0.91 g/cm^3 have frequently been reported for ice at the surface and for partially drained specimens.

The technical properties of sea ice, including the elastic properties, have been thoroughly reviewed by Weeks and Assur[188] in Monograph II-C3. Further details on elasticity are contained in their review.

Seismic Velocities in Frozen Ground

The seismic velocities in soils and rocks are affected by cold temperature only when there is water to freeze. Since most soils and rocks contain water, they usually show a different velocity below the freezing point than above it. The transition, however, can occur gradually below 0° C, when the water is saline, or because of the interfacial forces in fine-grained soils.

Velocities in frozen soils or rocks are higher than in the same material in the unfrozen state. The change of velocity that occurs in a given soil or rock type is a function of the degree of saturation, i.e. the ratio of ice-filled pores to air-filled pores, and of the ratio of frozen to unfrozen water. In addition, the distribution of the ice may be different (depending on the soil and rate of freezing), and the different structure and texture adds an additional complication. No strict rules can be given to predict velocities exactly or to relate velocities to type and condition of frozen ground. From existing observations it is nevertheless possible to form an idea of upper limits and common values of certain types of frozen ground.

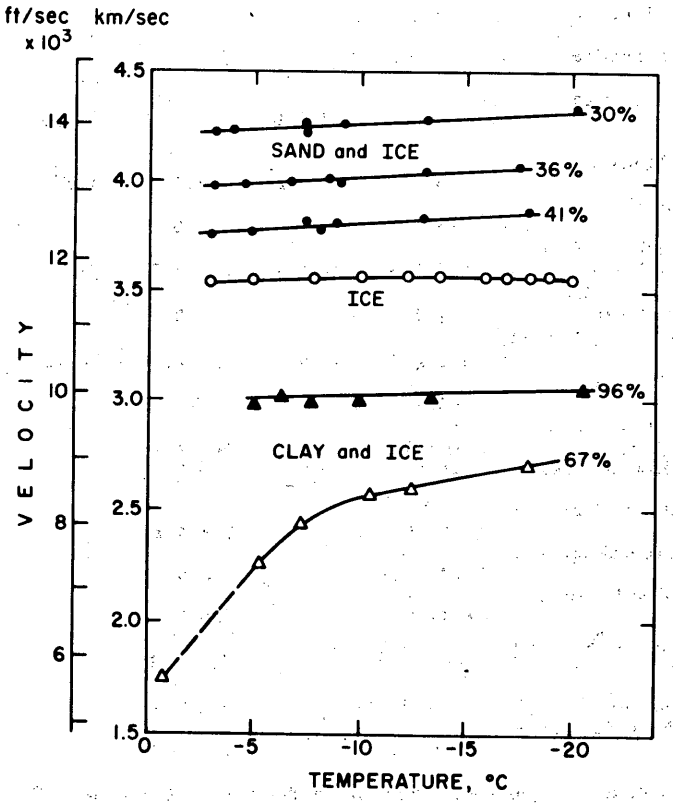

Figure 23. Sound velocity in frozen, synthetic cores of various porosities (%) as a function of temperature (after Müller,[130] from Barnes[9]).

Compressional-wave velocities V_P from seismic field observations have been compiled by Barnes[9] (Table XI). The largest increase in V_P from the unfrozen to the frozen state occurs in the unconsolidated quaternary sediments as one would expect. Coarse-grained materials show generally higher values than fine-grained ones, especially at temperatures close to 0° C. The highest values go with the lowest temperature. Velocities in hard rocks are generally high for the rock type involved. The dry to slightly damp weathered surface materials of Antarctica are listed as unfrozen, although the mean annual temperature of the area is -20° C.

The temperature effect has been more clearly demonstrated with laboratory experiments (Fig. 23 and 24).

P-wave velocities in Permafrost, (After Barnes 1965 with some additions).

Rock Types	Locality and Reference	Seismic Velocity (kilo ft/sec) Frozen	Unfrozen	Seismic Velocity (km/sec) Frozen	Unfrozen	Est Grou Tem °C
Quaternary sediments						
Silt and organic matter	Fairbanks Area, Alaska[a]	5-10	1.8-4	1.5-3.0	0.6-1.2	-1
Alluvial clay	Northway, Alaska[b]	7.8		2.4		-2
Silt and gravel	Fairbanks Area, Alaska[c]	7.7-10		2.3-3.0		-1
Aeolian sand	Tetlin Junction, Alaska[c]	8		2.4		-3
Floodplain alluvium	Fairbanks Area, Alaska[c]	8-14	6.1-7	2.4-4.3	1.9-2.1	-1
Tundra silts, sands, and peats						
(Gubik Formation, probably saline)	Barrow Area, NPR-4, Alaska (Woolson 1962)	8-8.8		2.4-2.7		-9
(Gubik Formation, probably saline)	Skull Cliff Area, NPR-4, Alaska (Woolson 1962)	7.4-8.9		2.3-2.7		-9
(Gubik Formation, less saline)	Topagoruk Area, NPR-4, Alaska (Woolson 1962)	8-12		2.4-3.7		-9
Gravel	Fairbanks Area, Alaska[a]	13.0-15.2	6-7.5	4.0-4.6	1.8-2.3	-1
Outwash gravel	Tanacross, Alaska[c]	7.6-10		2.3-3.0		-3
Glacier moraine	Delta Junction, Alaska[c]	7.6-13.2		2.3-4.0		-2
Unclassified sediments	Isachsen, Canada (Hobson 1962)	8.8		2.7		-10
Glacier outwash	Thule, Greenland (Roethlisberger 1961, 1961a)	14.9-15.5		4.5-4.7		-11
Glacier till	Thule, Greenland (Roethlisberger 1961, 1961a)	15.4-16.0		4.7-4.8		-11
Glacier till	McMurdo Sound, Antarctica (Bell 1966)	9.8-13.8	1.6-5	3.0-4.3	0.5-1.5	-20
Loess (dry)	McMurdo Sound, Antarctica (Bell 1966)		1		0.3	-20
Exfoliated granite (dry)	McMurdo Sound, Antarctica (Bell 1966)		4		1.2	-20
Shattered rock (dry)	McMurdo Sound, Antarctica (Bell 1966)		2.6-8		0.8-2.5	-20
Mesozoic sediments						
Mudstone (Ogotoruk Formation)[d]	Ogotoruk Creek, Alaska (Barnes 1960)	14.2	11[d]	4.3	3.4[d]	-5
Mudstone (Ogotoruk Formation)[d, e]	Ogotoruk Creek, Alaska (Barnes 1960)	13.2		4.0		-5
Shale and siltstone (Schrader Bluff Formation)[e]	Fish Creek Test Well 1, NPR-4, Alaska (Chalmers 1949)	8.9-9.8	6.6-7.6	2.7-3.0	2.0-2.3	-8
Shale and sandstone (Chandler Formation)[e, f]	Umiat Test Well 2, NPR-4, Alaska (Legge 1947/48)	12.7		3.9		-7
Shale and sandstone (Nanushuk Group)[e, g]	Simpson and Minga Wells, NPR-4, Alaska (Wiancko 1950)	8.1-8.4	5-7	2.5-2.6	1.5-2.1	-9
Sandstone (Colville Group)	Umiat Area, NPR-4, Alaska (Woolson 1962)	10.7		3.3		-7
Sandstone and shale (Nanushuk and Colville Group)	Meade-Oumalik Area, NPR-4, Alaska (Woolson 1962)	10-14		3.0-4.3		-9
Sandstone (Isachsen Formation)	Isachsen, Canada (Hobson 1962)	11.1		3.4		-10
Paleozoic and older sediments						
Shale (Dundas Formation)	Thule, Greenland (Roethlisberger 1961, 1961a)	12.5-15		3.8-4.6		-11
Sandstone (Narssârssuk Formation)	Thule, Greenland (Roethlisberger 1961, 1961a)	17.0-17.4		5.2-5.3		-11
Quartzite (Wolstenholme Formation)	Thule, Greenland (Roethlisberger 1961, 1961a)	18.4-19		5.6-5.8		-11
Dolomite (Narssârssuk Formation)	Thule, Greenland (Roethlisberger 1961, 1961a)	18.9-19.3		5.8-5.9		-11
Metamorphic rocks						
Schist (Birch Creek Schist)	Fairbanks Area, Alaska[a]	13-16		4.0-4.9		-1
Gneiss	Thule, Greenland (Roethlisberger 1961, 1961a)	20-20.8		6.0-6.3		-11

[a] Obtained from H.G. Taylor, 1938, Report on geophysical work by the seismic method in placer deposits of Fairbanks District o Alaska, unpublished report to U.S. Smelting, Refining & Mining Co.

[b] Unpublished data from J.H. Swartz and E.R. Shephard, U.S. Geol. Survey. 1946

[c] Data by author in 1952

[d] The Materials Testing Laboratory, U.S. Army Engineer District, Alaska, tested cores from this well and found that 5 porosity measurements averaged 6.4% and that dynamic measurements on unfrozen cores gave elastic moduli which may be used to comp a velocity in the unfrozen rocks of about 11,000 fps

[e] Measurements by velocity logs of wells; rest measured by refraction

[f] Porosity measurements of 44 cores from Umiat Test Well #2 averaged 13.5% (Collins 1958)

[g] Porosity measurements of 15 cores from Simpson Test Well #1 averaged 30.8 % (Robinson 1959)

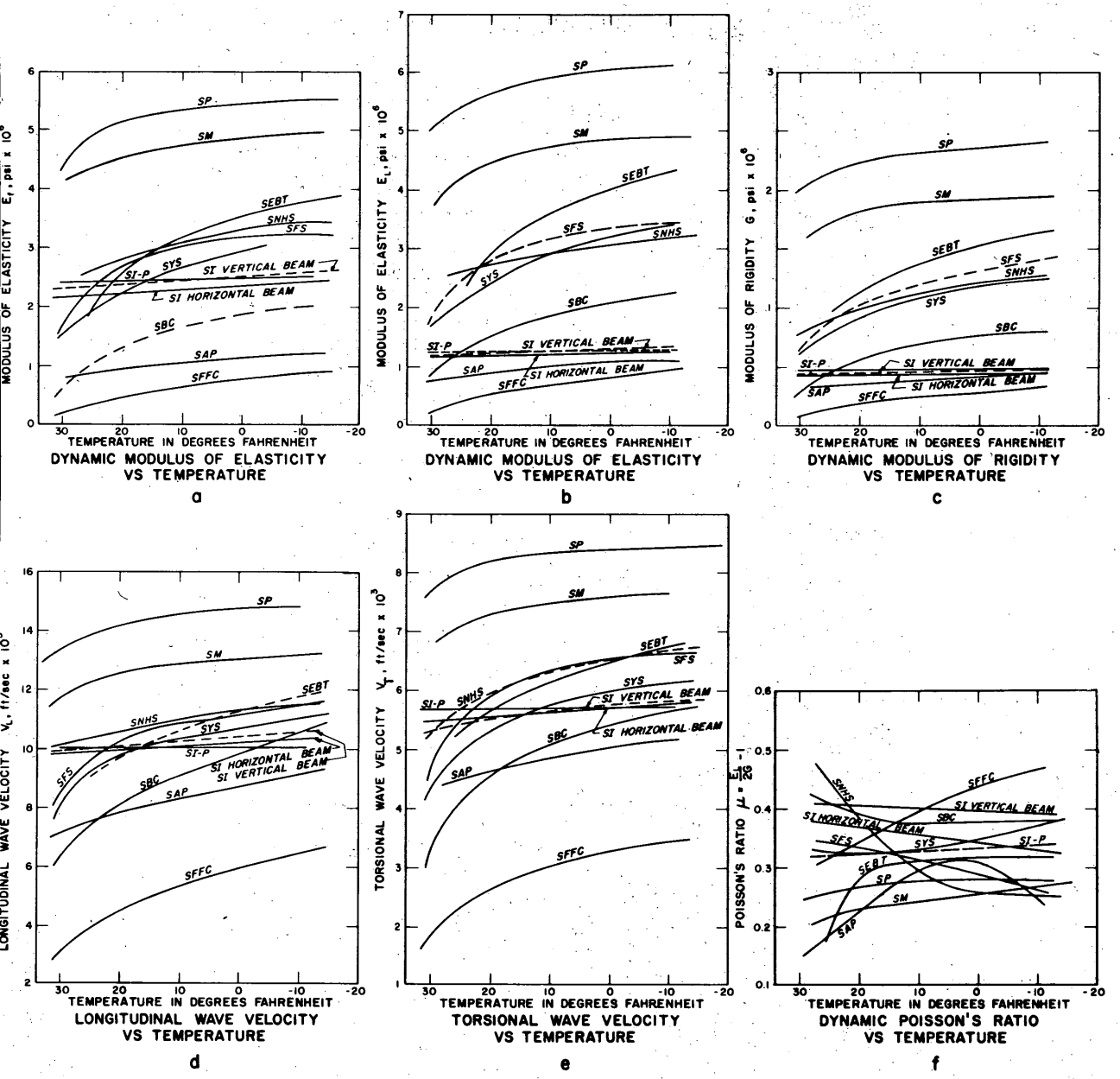

LEGEND

SP	— Peabody Gravelly Sand	SYS	— Yukon Silt
SM	— Mc Namara Concrete Sand	SBC	— Boston Blue Clay
SEBT	— East Boston Till	SFFC	— Fargo Clay
SNHS	— New Hampshire Silt	SAP	— Alaskan Peat
SFS	— Fairbanks Silt	SI	— Laboratory Frozen Ice
		SI-P	— Portage Lake Natural Ice

NOTES

This figure summarizes all data obtained in this investigation. Each curve represents test results of two to six specimens.

Curve of Poisson's Ratio vs temperature is based on values taken from average curves in graphs b and c.

Figure 24. Summary plot of dynamic elastic properties of frozen soils and of ice versus temperature (Kaplar[109]). E_f from flexural, E_L from longitudinal vibrations of square prisms at the resonance frequency, $V_f = \sqrt{E_f/\rho}$, $V_L = \sqrt{E_L/\rho}$. G from torsional vibrations, $V_T = \sqrt{G/P}$. The temperature gradient during freezing of the specimens was perpendicular to the prism axis in the horizontal and parallel to it in the vertical beams.

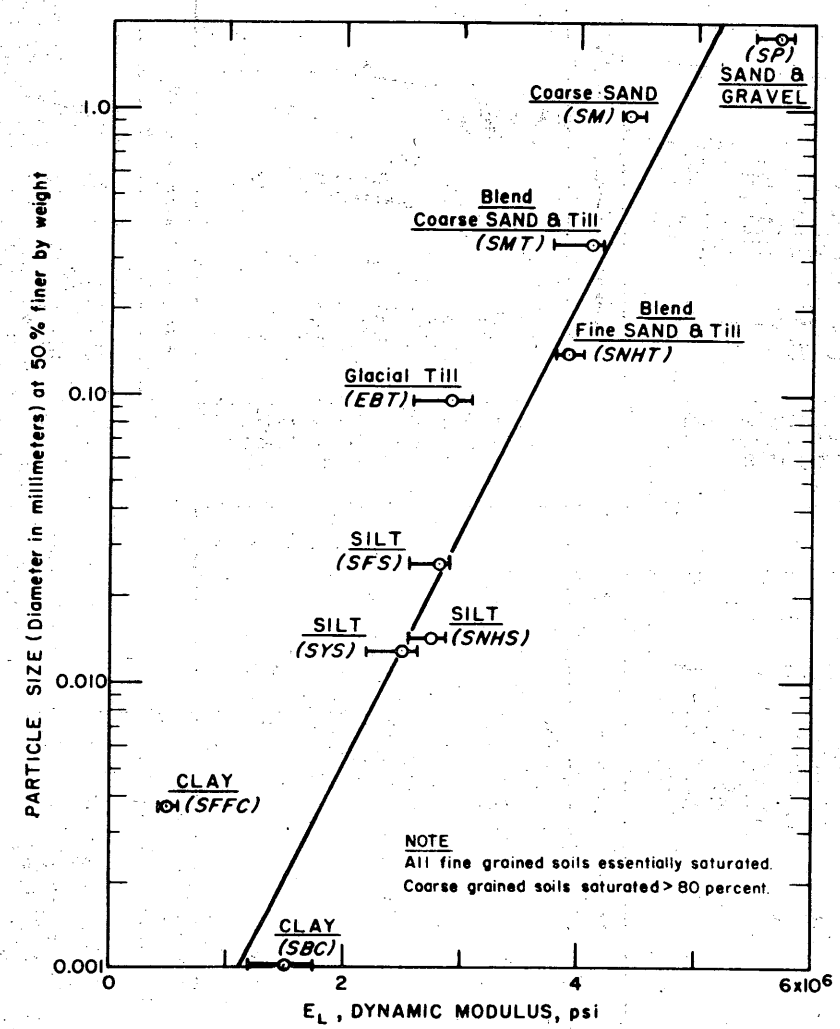

Figure 25. Relationship of soil type and Young's modulus determined by sonic tests, at -6.7°C (from Kaplar[110]).

The figures demonstrate further that the velocities V_L and V_T of the fine-grained specimens are lower than those of the coarse-grained ones. Kaplar's[109] experiments generally show a much larger temperature coefficient of velocity at high temperatures than at low ones, and this effect is more pronounced and appears over a larger temperature range for the fine-grained samples than for the coarse ones. Similar results have been reported by Zykov.[196] Only one clay sample in Müller's experiment (Fig. 23) shows this effect, while the velocity in the sand samples increases linearly with temperature. Figure 25 shows further the importance of the grain size of frozen soil to Young's modulus, and thus for seismic velocity. At least a rough correlation between grain size and velocity seems to exist, while plotting velocity vs ice content has so far not been very successful.[9,130] The expression given by Müller[130] for frozen quartz sand,

$$\frac{1}{V_P} = \frac{p}{2500} + \frac{1-p}{6250} \tag{43}$$

where p is the volume ratio of ice to total volume, is a rough approximation which clearly gives too low values for V_P at very high ice contents. Experimental data for the case where the liquid

filling the pores is brine have been presented by Desai and Moore.[56] In a brine-soaked sandstone specimen the strongest velocity increase was observed over the temperature range from a few degrees below 0°C to -16°C.

Very little information is available on anisotropy of frozen ground. Barnes and MacCarthy[6] have reported a case where V_P (vertical) was larger than V_P (horizontal).

Attenuation

Some little information is available on the attenuation coefficient α as defined by eq 16. At frequencies of about 100 Hz in the cold ice of the Antarctic ice sheet Robin[56] has obtained an attenuation constant of 0.65 km^{-1}, or 1 decibel per 356 m (p. 68). This is too large according to Bentley[25b] who estimates α to be on the order of 0.2 km^{-1}, at 100-150 Hz. Westphal[191] has investigated the attenuation of pressure pulses at higher frequencies in a temperate glacier and has obtained values of 0.024 m^{-1} (0.1 dB/m) at 2.5 kHz and 0.43 m^{-1} (1.9 dB/m) at 15 kHz (half these values in his definition of the attenuation, based on amplitudes). He has been able to show that scattering at the grain boundaries is the dominant source of attenuation of high-frequency acoustic waves. Millecamps and Lafargue[126] have reported sound absorption of 3 dB/m at 65 kHz in temperate glacier ice.

From these figures the following loss factors tan δ are obtained: 0.004 (Robin), 0.0008-0.0012 (Bentley), 0.0055 and 0.017 (Westphal) and 0.0063 (Lafargue). A smaller loss factor is to be expected for cold polar ice than for temperate ice, so that from this comparison also Robin's value appears to be too high. Much larger values of tan δ have been reported by Nakaya[135, 136] for snow, obtained by flexural vibration of small specimens. Only at very low temperatures can his results be compared with those from seismic observations.

Akimov[2] gives 10-15 dB/m at 100 kHz in frozen quick sand, and values orders of magnitude larger in unfrozen materials. The attenuation figures by Johnson and Fischer[99] obtained by different techniques are wrong, since the modes of vibration have not been properly identified (p. 111). One of their experiments showed that shear waves in ice are strongly damped at a frequency of 80 Hz and below, less at higher frequencies.

EQUIPMENT, LOGISTICS AND OPERATION

Seismic Surveys on Snow and Ice

Although the basic technique for seismic exploration work is the same in cold regions as in temperate climates, and standard equipment is used as a rule, it is worthwhile to mention here a number of instrumental and operational problems and special procedures a geophysicist without previous polar experience may want to know before he goes to the field.

The best type of equipment is high frequency gear able to pick up frequencies between 30 and 500 Hz. Signals on the order of 100 to 200 Hz and higher have consistently been recorded in reflection work even on thick continental ice sheets. But high frequencies are also encountered in refraction work, higher than what is customarily experienced in a temperate environment. Simple equipment is adequate for most glacier soundings; no automatic gain control, suppression and mixing are needed. A very small number of channels is adequate to provide satisfactory results, but it may of course be more economical to use a larger number of channels and save on the explosive. Filters and double registration with two stages of amplification have always been a big asset. (Kapitza and Sorokhtin[107] for instance recommend a band pass filter of 150 - 200 Hz for reflection work on the high Antarctic plateau; on the American traverses 215 - 320 Hz, the highest band pass available, gave best results.) The Southwestern Industrial Electronics portable CP-15 high resolution reflection seismograph system has been used very successfully in most of the work done by USA SIPRE and USA CRREL. In the IGY operations in Antarctica the portable 24-trace equipment of the 7000 B series manufactured by Texas Instruments Incorporated (formerly Houston Technical Laboratory) was equally adequate. Some of the very small shallow refraction seismographs for engineering work which have recently come on the market may be adapted to glacier work, but they usually cover a frequency band too low and a time span too short to be of much use unless they are drastically modified. It is obvious that special equipment is needed for special applications, like very low frequency seismographs to measure flexural waves of floating ice. For long refraction profiles on thick ice sheets it may be necessary to have suitable radio communication for transmitting the time break.

Considering the great homogeneity of snow and ice it is worth the effort to take special care for a high accuracy in timing. To give an example, the fork in the unit used by the Ross Ice Shelf traverse party[53] was found on calibration in the field to be fast by 2.5 parts per 1000. While this would be of no concern in regular seismic work, and could certainly also be tolerated as far as depth soundings are concerned, it could become important if an attempt were made to obtain highest possible precision in, say, velocity determinations. Proper calibrations in the field have unfortunately not been carried out by all investigators on the assumption that the timing unit of commercial equipment is sufficiently reliable for the soundings, which it usually is. Standard frequencies which can be used for calibration are broadcast by radio station WWV (Fort Collins, Colo.) on 2.5, 5, 10, 15, 20 and 25 MHz, and by WWVH (Puunene, Hawaii) at 5, 10 and 15 MHz. Tones of 600 Hz and 440 Hz are alternately transmitted every 5 minutes for durations of 3 minutes on the hour and 2 minutes thereafter.[77]

Most equipment is adapted to reasonably low temperature, but problems may develop in the severe cold of polar ice sheets or in winter, especially in the mechanical parts, such as the paper-driving mechanism, the time signal generator of the recorder, or the converter in the power supply unit. Robin[56] has even experienced breakage of seismometer springs due to low temperature. Certain geophones should therefore be equipped with a clamping mechanism when they are transported at very low temperatures. In most traverses this has not been found necessary. Robin reports

further that the amplifiers showed a gradual loss of capacity of electrolytic condensers, while the galvanometers became difficult to focus owing to the different thermal expansion of glue and mirrors. In the camera the rubber rollers became hard while distorted, which resulted in a movement of the recording paper in jerks. A metallic roller helped.

Batteries become inefficient in the cold, lead-acid batteries less so than nickel-cadmium ones. If temperatures are expected to drop below -10°C it is advisable to set up the instruments in a heated tent or vehicle. Care has to be taken to avoid condensation; this is best achieved by putting instruments in a plastic bag when they are brought from the cold into a warmer place.

Wind-induced vibrations have to be excluded by placing the geophones in shallow holes and covering them with snow; marking flags and other objects which might stand nearby must be removed. Advantage should be taken of the fact that the ground noise is generally low. If there is a layer of soft annual snow on solid ice the geophones are usually placed on the ice. Under melting-freezing conditions the geophones and electric lines may freeze into the ice, especially under strong solar radiation, and may be lost if not disengaged before they are completely frozen in.

When setting up the instruments in cramped space, it is profitable to use some sort of a shock mounting because of microphonic amplifiers: the mechanical vibrations produced by the recorder timing system and power supply unit may be picked up by the amplifiers. Placing the amplifier and recorder cabinets on a foam rubber mat and keeping them from touching each other is adequate. The cabinets may not automatically be grounded, in which case it is very important to connect them with a wire. Some investigators have cut down the noise by using separate batteries to isolate camera, amplifier or power supply and by wrapping the camera in aluminum shielding.

A relatively large shot point distance from the spread is required for shallow reflection soundings on ice. A long telephone line from the blaster to the seismograph station is therefore necessary, as for refraction work. Relatively long spreads are often appropriate in addition to the long shot point distance, so that geophone cables with a long outlet spacing from 20 to 60 m should be taken.

Drilling is not necessarily required for placing the charges, which may, on solid ice, be put right at the surface without any tamping. A more economical use of the explosives is made, however, if they are placed in hand-drilled holes. The CRREL 1½-in. ice auger and 3-in. coring auger are efficient tools, but a high grade steel pipe with four to six large, sharpened teeth rather strongly offset alternately to the inside and outside of the pipe will also do. On snow, the charges should be set sufficiently deep to have good sound transmission, generally at 2-4 m depth. Special problems have been encountered on the high Antarctic plateau, where Kapitza and Sorokhtin[107] have shown that shot hole depths of at least 40 m are necessary to avoid the strong seismic background noise initiated by explosions closer to the surface (see also sample records in Bentley,[23] p. 346).

For the study of physical properties, shear waves should also be recorded. Geophones which can operate in the horizontal direction are therefore needed. Various techniques have been used to intensify the shear wave at the source, such as striking a wooden post placed in an auger hole with a sledge hammer in a direction normal to the line, exploding a blasting cap next to a steel plate set vertically into the snow parallel to the line of the spread, blasting at the wall of a pit, hitting the wall of a pit horizontally with a hammer or a suspended weight, or blasting with permacord stretched across the line of the spread.[20 93 177]

The weight of portable equipment is on the order of 200 kg; the accessories, augers, explosives, photographic supplies, generator for charging the battery etc. weigh about the same. A total of 500 kg of technical equipment is a reasonable figure for an operation of a few weeks for a reflection survey. The heaviest single piece of equipment is on the order of 25-30 kg.

TNT or equivalent military explosives, 60% dynamite (gelatin-based cold region type), and Nitramon have most frequently been used for explosives. The weight of a single charge for a reflection survey varies from a fraction of a kilogram to about 1 kg of TNT or equivalent (50 - 200 g of gelatin for distances of 300 to 1000 m and ice thickness of 100 to 700 m, placed in drill holes or a bare ice surface, according to Süsstrunk[173]). In Antarctica 1-lb charges have been almost standard. In deep refraction work on continental ice sheets shots of over 100 kg have been fired to cover distances of more than 10 km (250 kg at 18 km, Behrendt[13]).

It takes at least two men to operate the seismic equipment – the operator of the amplifiers and recorder, and the operator of the blasting unit (unless the blasting is done from the seismograph station) – but it is not economical to work in very small groups. Süsstrunk[173] figured that it takes eight men (including the surveyor) for commercial reflection soundings with portable equipment in the mountains. It is then possible to shoot 30 to 35 records per day, furnishing about 100 reflecting elements of the glacier bed. Far fewer records are taken per day in reflection surveys on ice sheets where the station has to be moved after every few shots; while for refraction studies one to two dozen records can be achieved. These figures may help to estimate the amount of explosives, oscillograph paper and photo chemicals to take along when planning a seismic survey. Records are usually 0.5 to 1 m long depending on paper speed and depth.

Proper consideration should be given to climatological factors which might affect the quality of the results when planning a seismic operation. This does not only mean to think about the weather. It has been observed for instance at Byrd Station, Antarctica, that the surface noise was considerably greater in spring (October) than in the fall (March).[177] Weihaupt[189] mentions that Crary's party was able to obtain reflections in 1958-59 when traversing the old trail in warmer months in an area of the Victoria Land Plateau where it had previously been impossible to get results. Working on solid ice surfaces can become quite difficult when the first severe frost sets in because of the cracking of the ice, as experienced by Crary[52] on the shelf north of Ellesmere Island. Snow at the surface may be beneficial in damping Rayleigh waves and giving protection from high frequency vibrations induced by wind. Also, there are fewer open running melt streams when there is snow at the surface. However, deep snow is a nuisance because the geophones have to be buried.

Seismic Surveys on Frozen Ground

A seismic survey on frozen ground is similar to the normal operation, but what has been said about the effect of severe cold etc. for the work on snow and ice is also true on frozen ground. High frequency equipment is advisable as in snow and ice operations if the frost table is close to the ground surface. For large scale seismic explorations, such as a survey for oil, a major difficulty is putting the shot hole down, i.e. drilling in permafrost.[114] Cooled compressed air was found very satisfactory for returning the drill cuttings to the surface.[194] One way of getting around this difficulty is to blast in water; this is particularly easy when working offshore on the frozen sea or on frozen bays and lakes, but there are other problems involved, such as rough ice and interference of the strong multiple reflections between the ice cover and the bottom of the water.[88]

For shallow refraction work for engineering purposes there is no need to drill into frozen ground, since at least under summer conditions it is fully adequate to place the charge at the frost table. If there is a poorly saturated frozen surface layer it may be necessary to get the charge down to denser material. But in summer the conditions are ideal since there is water-saturated material right above the frost table guaranteeing a good energy transfer into the high velocity

permafrost. There is practically no weathering layer (except the thin active layer) to worry about, this being the reason for the desirability for high frequency equipment. Best results were obtained with repeated shots in the same hole. The amount of explosive necessary for surface shots is of course relatively high: about 6 kg were used for a 1-km refraction shot[162 163] and 45 kg for 5.5 km.[88] A further disadvantage of the method is that a large area is hit by flyrock, which makes the method quite impractical for standard reflection work. It seems, however, that Hobson[88] was not bothered by this problem since he does not mention it.

A strong static signal on all traces, knocking them out for a period of time at the shot instance, has been experienced by the author, probably related to the dry air and high insulation of the rock outcrop where the geophones were placed. The signal interfered with the high accuracy velocity determination the measurements were intended for.

A full appraisal of the effect of the cold regions environment for large scale seismic exploration in the Canadian Arctic Islands, containing various recommendations, has been given by Hobson.[88]

REFLECTION SOUNDINGS

The Reflection Technique on Glaciers

There is a basic difference between regular seismic reflection work in stratified rock and soundings on glaciers, because of the unique homogeneity of large ice masses, and also because of a large change, as a rule, in at least one of the important properties (velocity and density) at the glacier bed. The elastic body waves are in this case strongly reflected at the interface, and reflection events of unusual sharpness can therefore be recorded in glacier work. Shortcuts in processing seismic data, specific procedures, and special applications are widely practical, which differ from the routine described in textbooks and manuals. Deviations from the regular work are mainly considered here, and the description of the reflection method in this Monograph is confined to soundings on glaciers, the standard application to multilayered rock strata being covered by textbooks.

Because of the sharpness of the reflection, it is usually not necessary to use a large number of closely spaced geophones as in oil exploration. Relatively long spreads are more appropriate, with geophone spacings at 20 to 60 m. Shorter spacings of 10 m (which can always be obtained with the same geophone cable) may be an advantage when the echoes are weak, as experienced by Robin[156] in a difficult area of Antarctica.

Common features of the boundary at the bed of a glacier are its irregularity and the fact that it is often impossible to predict the direction of dip. Rather than shooting two perpendicular lines, it is common to use L-spreads or grid patterns (Fig. 26). The latter are used for detailed soundings on valley glaciers, where the geophones are placed at the corners of squares or rectangles or in the isometric pattern proposed by Vallon.[183]

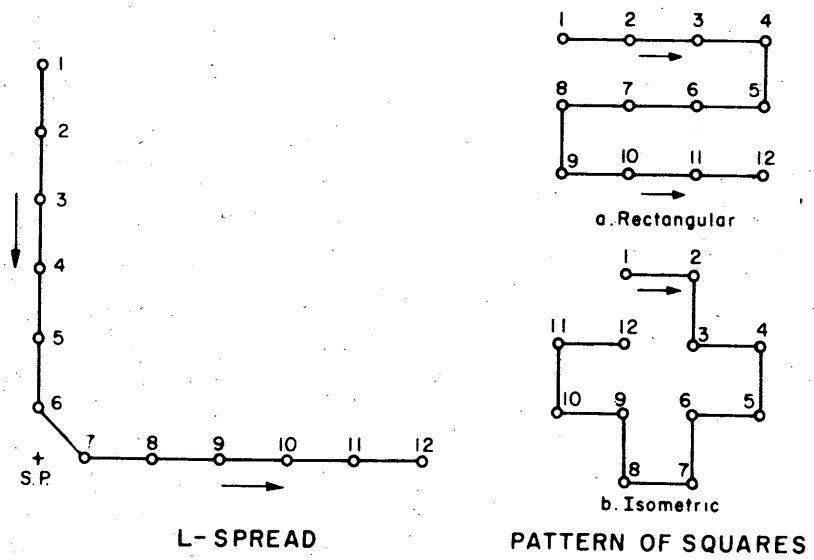

Figure 26. Patterns for geophone set-up for reflection soundings on glaciers.

Typical spreads which have been used on continental ice sheets for reflection soundings or combined reflection-refraction work are:

12 geophones spaced at 30-m intervals, linear spread, shot point 60 m from each end (Greenland, Roethlisberger et al.[166])

2 × 12 geophones spaced at 30-m intervals, L-spread, every 4th geophone placed horizontally in the direction of the line (W. Antarctica, Bentley and Ostenso[21])

24 geophones at 30-m intervals, linear spread of about 700 m total length, shot holes at 50 m from each end or at center (Ross Ice Shelf, thickness 100 to 700 m, same setup with all detectors horizontal, Crary[53])

6 geophones at 10 m, linear spread, shot distance usually 100 m; T-spread used tentatively (Queen Maud Land, Antarctica, Robin[156])

It may be noticed that geophones have sometimes been placed horizontally, sometimes in the longitudinal direction of the line, sometimes in the transverse direction, depending on the objective.

It is usually known beforehand whether the ice is deep or shallow. This is important, because a basically different shot point location is indicated depending on this condition. On deep ice the shot is placed close to the spread, and the reflection is recorded after the surface waves (ground roll) have decayed. On shallow ice less than about 200 to 400 m thick, a wide-angle reflection technique must be used where the shot is placed at a distance of about 1.2 times the depth, or more, from the seismometers in order that the reflection signal be received before the arrival of the direct shear and Rayleigh waves.

Even though we assume that it is known beforehand whether the ice is shallow or deep, the actual depth can be within a large range. Proper identification of the reflection signal from the first shots at a location is then the clue to a successful sounding operation. This is not always simple, since there are a number of events on a record to choose from.

On shallow ice a few shots are fired at variable distance, and a time-distance graph is plotted, on which the proper identification can readily be made. Figure 27 gives an example of a normed graph, where the ratio of travel-time to vertical reflection time is plotted versus the ratio of distance to ice thickness. Theoretical curves and observed travel times are given. The systematic deviations in this example can be explained by a slight dip of the interface and anisotropy of the ice, but disregarding the deviations the graph gives proof of the proper identification of the main event, the single *P* reflection. In addition to the direct *P*-wave and the single reflection R_P (which have both been recorded in great numbers but are not plotted), the direct *S*-wave, some doubtful double reflections R_{2P} and numerous shear reflections R_S have been identified, as well as some reflections where the wave is converted at the interface from *P* to *S* or *S* to *P*. R_{PS} and R_{SP} clearly deviate from each other in some cases because of the dip.

The surface wave arriving shortly after direct *S* has been left out. It is doubtful that the $S\bar{P}S$, "internally refracted wave"[26] has a physical meaning: multiple *PS/SP* events were probably taken for $S\bar{P}S$ where this signal has been reported to occur. Erratic signals can immediately be recognized from the graph and may then be traced to their proper source, like a reflection on a crevasse (phase change) or an inner moraine, or spontaneous cracking of the ice. With a little experience the reflection signal can then be identified without having to plot every record. Figure 28 gives an example of a typical good record on very shallow ice showing various events. Far more complicated situations are encountered on ice shelves, where strong sea bottom reflections and multiple reflections within the water can make the identification of all the events very difficult indeed.

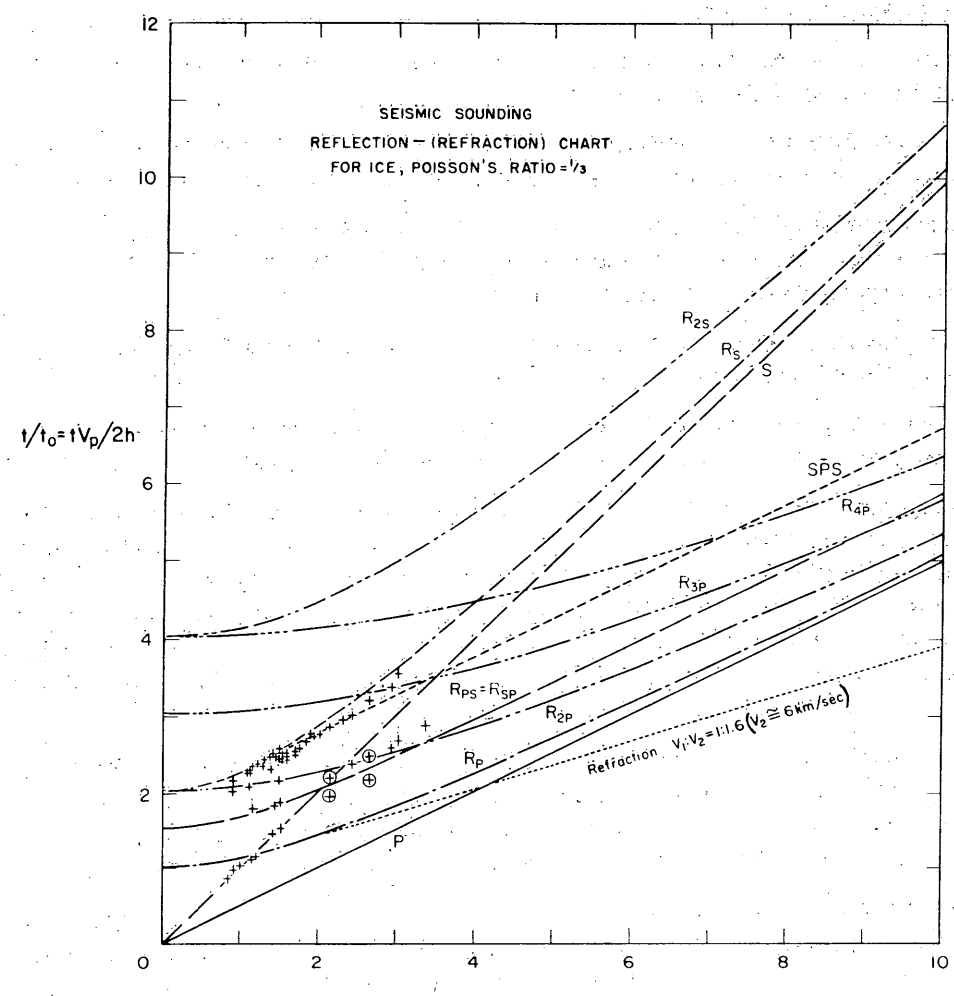

x = shot to geophone distance
h = ice thickness (depth)
t = travel time
t_0 = travel time for vertical P-wave reflection
V_P = velocity of P-wave
P = direct P-wave
S = direct S-wave
V_1, V_2 = velocities in ice and substratum

R_{1P} = single P-wave reflection
R_{2P} = double P-wave reflection
R_{nP} = n-fold P-wave reflection
R_{nS} = n-fold S-wave reflection
R_{SP} = S-wave reflected as P-wave
R_{PS} = P-wave reflected as S-wave
$R_{S\bar{P}S}$ = internally-refracted wave (Berckhemer and Oliver[26])

Figure 27. Reflection chart for ice, Poisson's ratio ν = 1/3. (From Roethlisberger[161].)

On thick ice the reflection signal can be obtained after the ground roll from the explosion has decayed. This is the common technique, since less explosive is needed than for wide angle reflections, and it is a much simpler operation when the shots can be fired close to the station than far away. But good reflections can be obtained at larger shot point distances as well, as demonstrated by Joset and Holtzscherer[102] and Bentley et al.[20] (Fig. 29). Figure 30 illustrates the events that have been identified in a survey on the Greenland ice sheet, ice thickness 1800 to 2000 m.

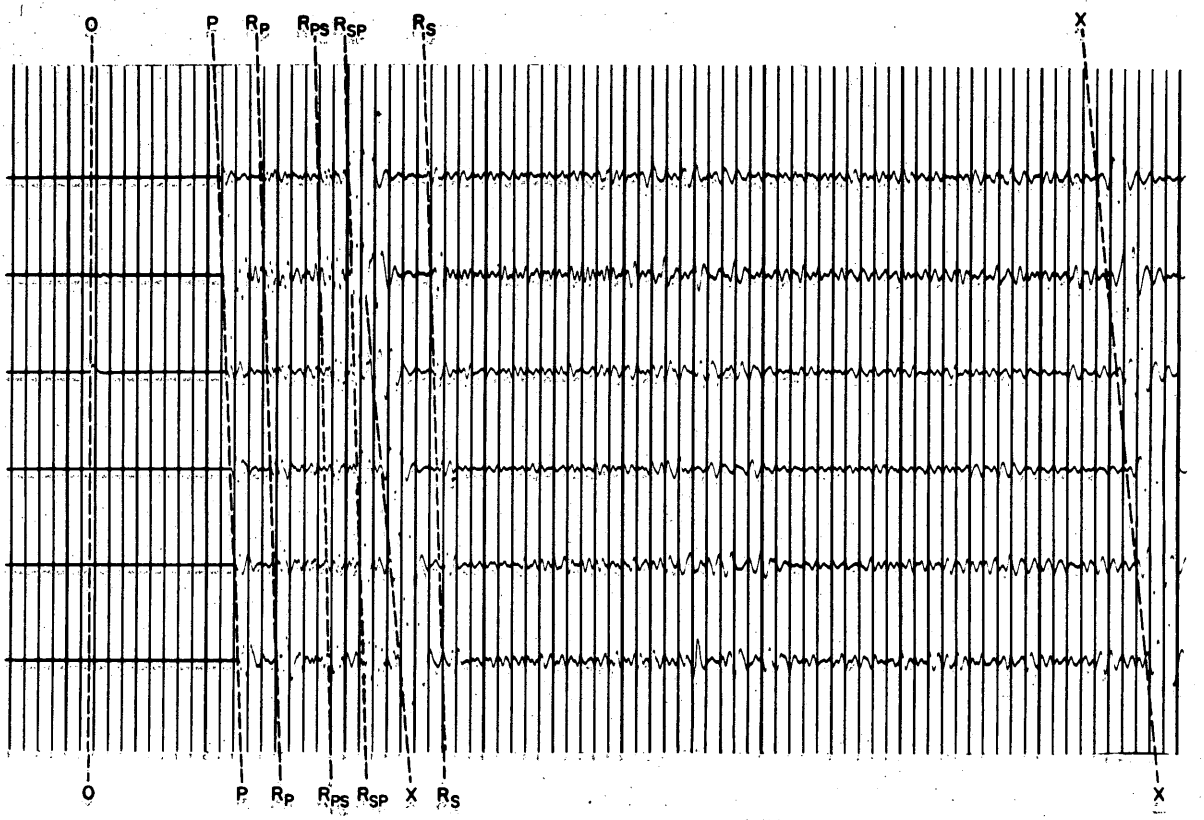

Figure 28. Reflection seismogram on shallow ice (70 m) at the edge of the Greenland ice sheet (Camp TUTO). 0 = shot instance, P = first break of P-wave; R_P, R_S, R_{PS} and R_{SP} reflections, X = repeated erratic pulses from unknown source interfering with S-wave. Time line interval: 5 millisec. (From Roethlisberger.[161])

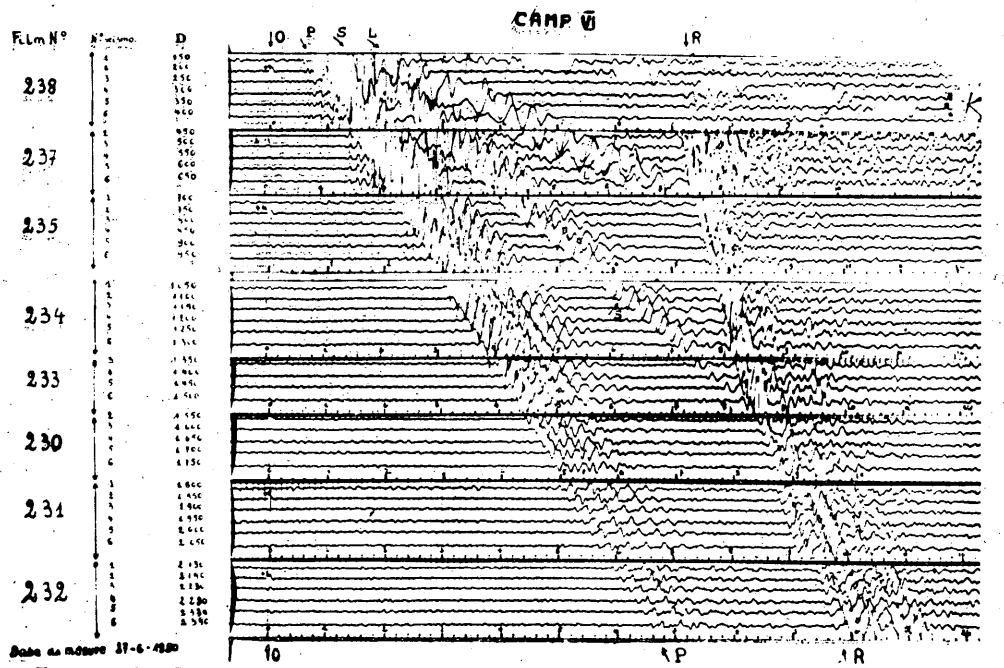

Figure 29. Series of seismograms of successive shots at increasing distance mounted to illustrate the time distance relationship. 0 = shot instance, P = P-wave, S = shear wave, L = surface wave, R = P-wave reflection. (From Holtzscherer and Robin.[91])

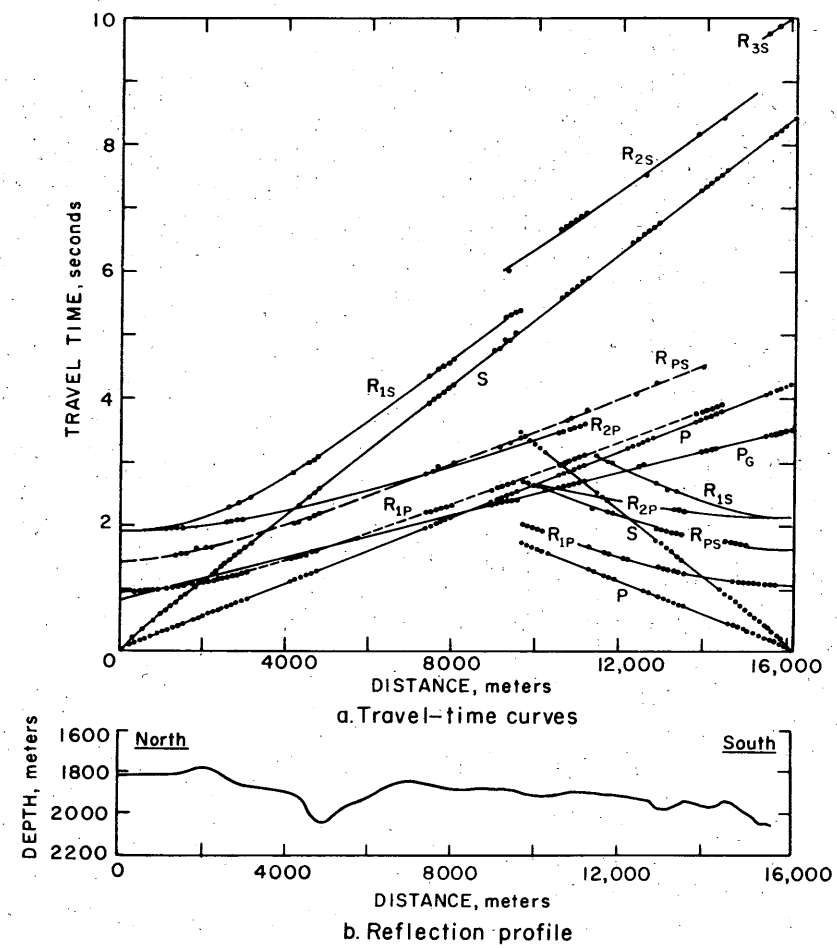

Figure 30. Travel time curves from Site 2, Greenland, showing direct P *and* S *wave, various reflected waves and refracted wave* P_G. *(From Bentley et al.*[20]*)*

There are certain conditions where the ground roll decays slowly, the danger then being that the single reflection may be obscured and the double reflection taken as the single one. A thickness of twice the correct value will be the result. In many places great difficulty has been experienced in obtaining the reflection signal at all, either because it was too weak or because of sustained ground roll. A large variety of filter settings and shooting techniques then have to be tried.

The shooting methods are especially important. Some authors recommend small charges combined with higher amplifier gain, others the opposite, claiming that a higher charge improves the ratio of reflection to noise. This may depend on snow conditions. In any event, a better energy transfer is always obtained by setting the charge deeper. Robin[156] has pointed out that the depth could profitably be taken in a certain relationship to the wavelength to obtain constructive interference rather than the opposite. In practice it was found that a depth of 1 to 2 m was satisfactory in Greenland,[166] while 4 m was needed in the St. Elias Mountains,[46] 4 to 10 m in various areas of Antarctica[21] and 40 m in the interior of Antarctica.[23 107] The main difficulty in Antarctica is the very strong sustained ground roll which decays only very slowly with time (Fig. 31). Sometimes it helps to recharge the cavity of a former explosion (use of a "sprung" hole). This seems to

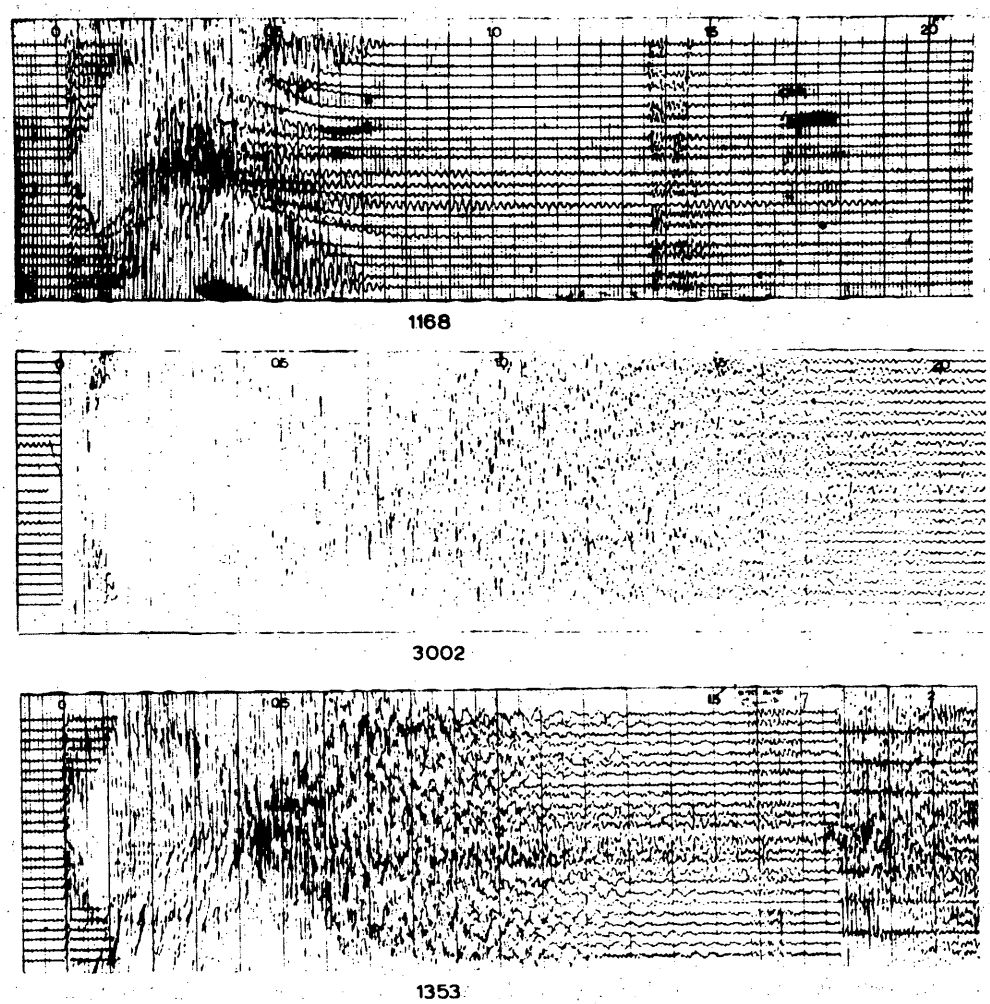

Figure 31. Seismic reflection records showing: (1168) normal surface wave attenuation, (3002) prolonged surface noise, and (1353) reflection from a low velocity basal layer arriving 0.2 sec before the main bottom echo. (From Bentley and Ostenso.[21])

give a better energy transfer at the same time, up to a factor of five.[177] But often only very deep shot holes have given results. With shot holes 28 to 41 m deep, reflections from excellent to poor quality were identified at 11 stations out of 14 on the McMurdo - South Pole traverse.[157] It can be assumed that placing the geophones equally deep in drill holes would give a further improvement. Air blasts have also been tried, for instance in a 7-shot pattern 2 m above the surface.[21] It has been observed that for a charge of fixed size, the air shot produced reflections with greater amplitude than the buried charge, but at the disadvantage of producing an air wave and increased surface wave disturbance.[177]

Where surface noise is a problem, the use of filters usually improves the reflection signal, otherwise it is better to use a frequency band as wide as possible. Band pass filter settings of 30 - 215 Hz,[189] 40 - 90 Hz,[46] 70 - 140 Hz,[142] 75 - 300 Hz, 70 - 425 Hz[166] and various other settings have been reported. The corrections for the filter delay can be quite large[44 142] and it is therefore better not to use filters for high precision. Under the very difficult conditions of the high Antarctic plateau a narrow band pass filter of 150 - 200 Hz had led to an enhancement of the signal from 3 to 4 times compared with the surface noise,[107] but often still higher frequencies are even better.[23]

Some special problems are encountered with the seismic sounding method when working on mountain glaciers with a rugged bed. This type of work has some importance in relation to engineering applications. To determine the cross section of a valley glacier is a good example. We are dealing here usually with the shallow ice again, and the speciality of the soundings is that they are truly three-dimensional. A pattern of squares is used to set up the geophones (Fig. 26), and the shot points have to be located far enough from the geophones. (Since crevasses may cut off most of the energy of the *S*- and surface waves, reflections may be obtained at shorter distances than would otherwise be possible.) Because it is easier to move the shot point than the station, a large number of shots are fired in various directions and distances around the station, so that reflections from different places on the bed will be received. It is very important that proper consideration be given to the best location of each station setup, so that optimum information on the shape of the bed can be gathered without having to shift the station too often. No information can be obtained about the bed directly under the station, which is obvious from the fact that no close shots can be used. A fresh setup is therefore needed at least once for the survey of a complete cross section, unless the station can be placed close to the center of the glacier and a whole cross section can be covered by shooting a fan across the glacier either upstream or downstream of the station. Most researchers seem to have placed the shot points either on the main axes through the geophone grid or on lines through the diagonals.[160 173 183] It is by no means necessary to restrict oneself in the choice of the shot point location, however. The shots can be placed anywhere on the glacier where a suitable reflection occurs, as further elaborated in the section on depth computation.

For the arrangement and spacing of the shots, it is interesting to note further that a displacement by a fixed distance will result in only a small shift of the reflecting element if the reflection occurs on a convex section of the bed (a knob), and in a large shift if it occurs at a concave interface (a bowl) (Fig. 32). Consequently, the blank zone under the geophone stations is small or large depending on whether the station is located over a convex or concave section of the bed, respectively. The most important principle to be followed in a survey is to check continuously that reflections are obtained, and to evaluate part of them immediately to find out which areas have been covered and which have been missed.

The accuracy of a survey is primarily limited by the accuracy of the determination of the travel time of the reflected wave, which in turn depends on the sharpness of the break. Under most favorable conditions the break can probably be measured to 1/10 of a wavelength of the first cycle, which gives, at a frequency of 400 Hz, a time accuracy of ± 0.25 millisec corresponding to about ± 1 m in the reflected path, or 0.5 m in depth. This is an ultimate accuracy which can probably never be realized. Robin[156] estimates the accuracy in the time measurement alone as 2 millisec (corresponding to about 4 m) at some Antarctic inland stations to 10 millisec (about 19 m). Combining these and various other sources of error, his estimates of accuracy range from ± 6 m at 250-m ice depth to ± 47 m at 2000 m of ice. Bentley[23] estimates that ± 10 m is a representative

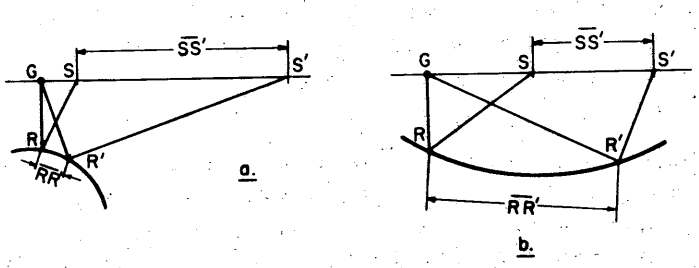

Figure 32. Shot point displacement $\overline{SS'}$ and shift of reflecting element. a. over a knob; b. over a bowl.

figure for the relative accuracy between two stations of the same area of a continental ice sheet, while ± 40 m is the total error for thick ice of the surveys in west Antarctica in the areas where there is a low velocity layer at the base.[21] Kapitza and Sorokhtin estimate the error of seismic soundings at 4 - 5%. For soundings on valley glaciers Süsstrunk[173] gives 1% error in the time measurement and the spatial graphical solutions, and about 3% error due to irregularities of ice and boundary. This latter figure was obtained by comparison of the seismic results with 16 soundings by thermodrill on the Gorner Glacier in Switzerland, with ice thickness up to 500 m. Paterson and Savage[142] have reported differences of 3 to 7 m on Athabasca Glacier in a similar comparison. Clarke[44] estimates the error in depth on a wide valley glacier at ± 10 m, going up to + 25 m (± 10 m) if a complete cycle is missed, while Vallon[183] points out that on a deep narrow mountain glacier with an irregular bed the individual sounding may easily be off by as much as 50 m. Further comparisons of seismic soundings with drilling are given in Figure 52.

The seismic reflection method with standard equipment is limited in its application to ice which has at least a certain thickness. If the glacier is too shallow then the reflection occurs too soon after the direct pulse, of which the duration is at least a few cycles. A further increase of the shot point distance in the wide angle reflection technique employed on shallow ice gives a relatively high amplitude of the reflection, but also moves it still closer to the direct wave. A depth of some 50 m is therefore the limit for a high frequency seismograph system, and more for a system with a lower frequency band. The limit depends further on the character of the interface and substratum. There is no reason that higher frequencies could not be used for still shallower ice (sonar), but since the range of portable thermal drilling equipment extends from 0 to about 60 m there is not much need for developing the technique.

It should finally be mentioned that the geophone and shot positions have to be properly surveyed to an accuracy which should be better than the one given by the time measurement, which is ± 1 m on ice and ± 0.3 m on firm snow (soft snow should be avoided anyway). For soundings where no high precision is needed it is possible to obtain the shot distance from the travel time and the velocity. Firing a cap in the air is another technique that has been used for quick distance determination.[20]

Theory of Reflection Soundings on Glaciers

Homogeneous isotropic layer of uniform thickness

In the theory of both the reflection and the refraction methods the principles of geometric optics are used, with the complication that two types of waves exist, *P* and *S*. In a homogeneous isotropic medium the ray is a straight line normal to the wave front, i.e. identical to the wave normal. The basic law describing how the ray of a wave changes direction at an interface between two homogeneous isotropic media is Snell's law:

$$V_1/V_2 = \sin\alpha_1/\sin\alpha_2 \qquad (44)$$

where V_1 is the velocity of the incident wave, V_2 the velocity of the emergent wave after reflection or refraction, and α_1 and α_2 the angles between the incident and emergent rays, respectively, and the normal to the interface. In the most general case an incident wave of one type (*P* or *S*) produces four emergent waves, namely reflected *P* and *S* and refracted *P* and *S*. The solid lines in Figure 33 illustrate the case of a *P*-wave in a low velocity medium incident at the boundary to a high velocity medium. The same four paths are also followed by the three other incident waves given with dashed lines.

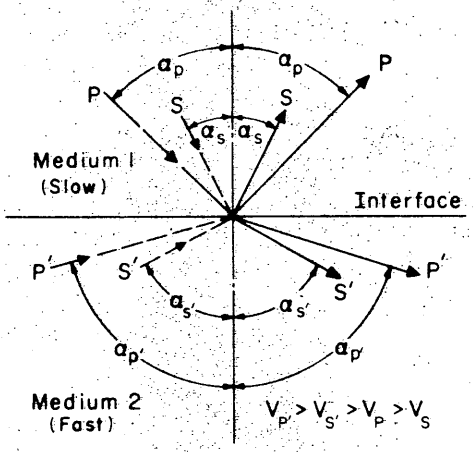

Figure 33. Reflection and refraction at a plane interface.

For our specific problem of reflections we note that the angle of incidence is equal to the angle of reflection for P reflected as P, or S reflected as S, while for the wave which is converted at the boundary the formula

$$\frac{V_P}{\sin\alpha_P} = \frac{V_S}{\sin\alpha_S} \tag{45}$$

holds where α_P and α_S are the angles of incidence of the P- and S-wave respectively. Note that the angles between ray and normal to the interface are used, which are identical to the angles between wave front and interface. In ice the ratio of V_P to V_S is close to 2 (Poisson's ratio = 1/3) and therefore

$$\sin\alpha_P = 2\sin\alpha_S. \tag{45a}$$

The simplest case for the computation of depth is the plane-parallel plate of thickness h. Shallow and thick ice are treated as two separate cases because of the different technique involved as far as the shot distance is concerned:

Case 1. Wide-angle reflection on shallow ice (Fig. 34a). From simple geometric considerations the travel time of a reflected wave is given by

$$t_r = \frac{1}{V}\sqrt{s^2 + (2h)^2} \tag{46a}$$

so that

$$h = \frac{1}{2}\sqrt{(Vt_r)^2 - s^2} = \frac{V}{2}\sqrt{t_r^2 - t^2} \tag{46b}$$

where h = depth, s = shot distance, t_r = travel time of the reflected wave, t = travel time of the direct wave and V = velocity (V_P or V_S). For an n-fold multiple reflection the depth equation is given by

$$h = \frac{1}{2n}\sqrt{(Vt_{nr})^2 - s^2} \tag{47}$$

The condition that the reflection signal occurs on the record before the S-wave pulse (p. 45) is formulated by

$$\frac{1}{V_P}\sqrt{s^2 + (2h)^2} \quad \frac{s}{V_S} \tag{48a}$$

which leads, for Poisson's ratio of 1/3, i.e. $V_P = 2V_S$, to

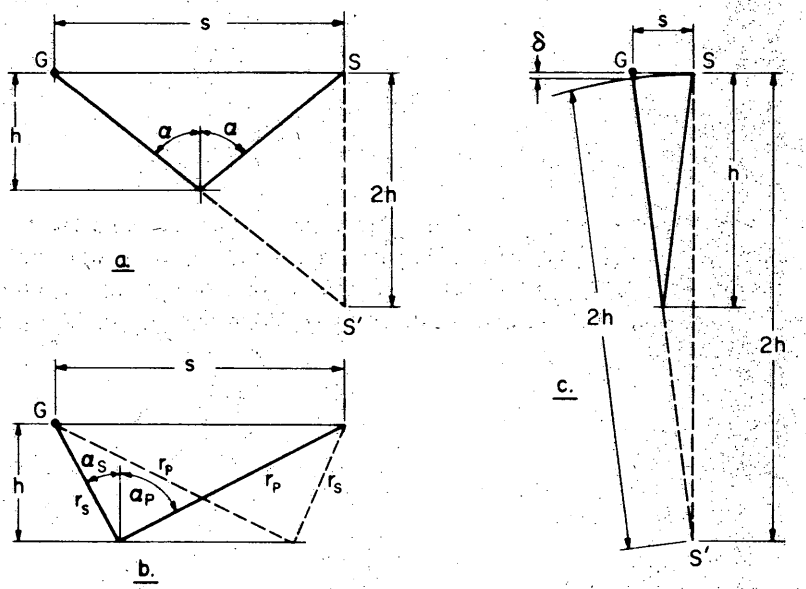

Figure 34. Reflection at a plane boundary parallel to the surface. a.) Wide angle reflection (shallow ice). b.) Reflection of converted wave R_{PS} *(solid line) and* R_{SP} *(dashed line). c.) Reflection when the shot distance is small (thick ice).*

$$s > 1.15h + \Delta \tag{48b}$$

where Δ/V_P is the time needed to identify the R_P event. For the reflections where the *P*-wave is converted to an *S*-wave at the interface or vice versa the trigonometric equations

$$s = h(\tan\alpha_S + \tan\alpha_P) \tag{49a}$$

and

$$t_{PS} = h\left(\frac{1}{V_S \cos\alpha_S} + \frac{1}{V_P \cos\alpha_P}\right) \tag{49b}$$

are obtained from geometrical considerations (Fig. 34b), while eq 45a gives an additional relation between α_P and α_S. No simple explicit solution for h as a function of β and $t_{PS} = t_{SP}$ can be given. The simplest way of finding depth from $R_{PS} = R_{SP}$ is to use a chart (Fig. 27).

Case 2. Thick layer, shot point near the geophone spread (Fig. 34c). Equation 46b can be written as

$$h = \tfrac{1}{2} V t_r \sqrt{1 - \left(\frac{s}{V t_r}\right)^2}$$

and the approximation

$$h \cong \tfrac{1}{2} V t_r \left[1 - \tfrac{1}{2}\left(\frac{s}{V t_r}\right)^2\right] = \tfrac{1}{2} V (t_r - \Delta t_0) \tag{50}$$

is obtained. The term

$$\Delta t_0 = \frac{(s/V)^2}{2t_r} \tag{50a}$$

is the spread correction (stepout time); after subtracting it from the observed travel-time the depth can be obtained from $h = Vt_r/2$ for all geophones of a spread. In an area of uniform thickness the spread correction remains the same and can be tabulated for a whole survey; on thick ice it varies from 0 to a few milliseconds. The same result as in eq 50 can be obtained from the graph in Figure 34c, where

$$h = \tfrac{1}{2}(Vt_r - \delta) \tag{50b}$$

and

$$\delta = \sqrt{4h^2 + s^2} - 2h \tag{50c}$$

which can be approximated by

$$\delta \cong \frac{s^2}{4h} \cong \frac{s^2}{2Vt_r} = \Delta t_0 V. \tag{50d}$$

Three-dimensional reflections in a homogeneous isotropic mass

Glacier beds are seldom parallel to the surface; for the exact evaluation the coordinates of the reflection point, dip and strike should be found. The linear arrays of the geophones are replaced by *L*-spreads (sometimes *T*-spreads), or the geophones are set up in a tetragonal grid pattern (Fig. 26). Various approximate and rigorous solutions of the problem exist. The most practical solution in a particular operation depends on the application and on the available means for computation or construction. All methods have in common that the reflection is assumed to occur on a plane interface and that a single mirror image of the shot point therefore exists which is the same for all geophones.

In the most general case the geophones are located on a sloping surface, the shot is arbitrarily placed and the reflecting plane shows arbitrary dip and strike (Fig. 35). The mirror image is located on spheres with the geophone at the center, the radius of the spheres being given by velocity multiplied by reflection time. The intersection of three spheres gives the spatial solution for the mirror image. A completely analytical method has been described by Doell.[56] First the three simultaneous equations for the spheres are solved:

$$(x_p - x_i)^2 + (y_p - y_i)^2 + (z_p - z_i)^2 = (Vt_i)^2 \qquad i = 1, 2, 3 \tag{51}$$

where x_p, y_p, z_p are the coordinates of the image point P, x_i, y_i, z_i the coordinates of geophone G_i, V the velocity and t_i the reflection time observed at geophone G_i. Subtracting the second of the three equations (51) from the first and the third from the second yields two linear equations in the unknowns x_p, y_p and z_p. One or the other of the unknowns can now easily be eliminated, and x_p and y_p are expressed by z_p. Substitution for x_p and y_p in one of the equations (51) leads to a quadratic equation in z_p which has to be solved, taking into account that the reflection must occur inside the glacier (positive value of the radical).

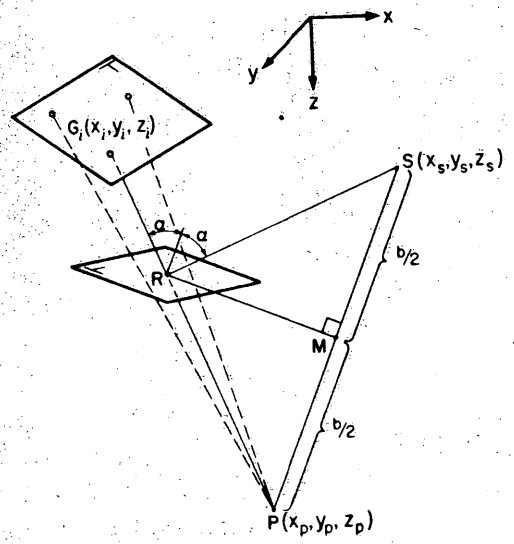

a. *3-dimensional space diagram.*

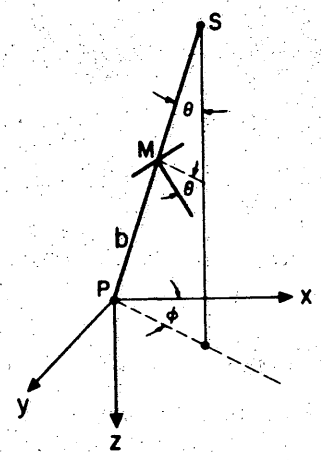

b. *Diagram for calculating dip, θ, and direction (azimuth) of dip, ϕ.*

Figure 35. Diagram for calculating three-dimensional reflection soundings.

The length of the line $\overline{SP}$ between shot point S and image point P is

$$\overline{SP} = b = \sqrt{(x_p - x_s)^2 + (y_p - y_s)^2 + (z_p - z_s)^2} \tag{52a}$$

and its direction cosines are

$$\ell = \frac{(x_p - x_s)}{b}; \qquad m = \frac{(y_p - y_s)}{b}; \qquad n = \frac{(z_p - z_s)}{b}. \tag{52b}$$

The reflecting plane is the perpendicular bisector of this line, given in normal form as

$$\ell(x - x_s) + m(y - y_s) + n(z - z_s) = \frac{b}{2}. \tag{53}$$

The line $\overline{G_iP}$ (for example $i = 1$) whose equations are

$$\frac{(x - x_1)}{(x_p - x_1)} = \frac{(y - y_1)}{(y_p - y_1)} = \frac{(z - z_1)}{(z_p - z_1)} \tag{54}$$

intersects the reflecting plane at R, the point of reflection. Simultaneous solution of eq 53 and 54 yields the coordinates of R. The dip of the reflecting plane is given by

$$\theta = \cos^{-1} n = \cos^{-1} \frac{z_p - z_s}{b} \tag{55a}$$

or for small θ more appropriately by

$$\theta = \tan^{-1} \frac{\sqrt{(x_p - x_s)^2 + (y_p - y_s)^2}}{z_p - z_s} \quad . \tag{55b}$$

The direction of dip (azimuth) relative to the x-axis is

$$\phi = \pm \tan^{-1} \frac{y_s - y_p}{x_s - x_p} \qquad \text{when } x_s - x_p \geq 0 \tag{56a}$$

$$\phi - \pi = \pm \tan^{-1} \frac{y_s - y_p}{x_s - x_p} \qquad \text{when } x_s - x_p < 0 \tag{56b}$$

where ϕ is positive when measured clockwise (Fig. 35b).

The rigorous analytical method described above was impractical before the time of electronic computers, and is still not satisfactory in the field where it is often important for a few preliminary results to become available immediately. The mathematically most elegant method is not the most useful one under field conditions. It is therefore appropriate to devote some space to the earlier treatments of the problem of three-dimensional evaluation of reflections.

The distance to the reflector is often large compared to the geophone spacing, in which case the rays are almost parallel at adjacent geophones, and the direction cosine relative to an axis through two geophones given by $V\,\Delta t_r/d$ where Δt_r is the difference in reflection time and d the true distance between the two geophones. A second direction cosine is obtained relative to a second axis through two geophones preferably at a right angle to the first axis. Using proper sign convention and transformation equations the direction cosines are transformed into a rectangular coordinate system (x, y, z) with horizontal x, y plane, and the coordinates of the mirror image point are obtained from the true distance between geophones and image point (obtained by multiplying the reflection time by velocity). This technique has been described by Roethlisberger,[160] who also gives the special transformation equations to be used when the geophones are placed on a steep slope using a theodolite. (In this case the geophones may not form an exactly rectangular pattern on the dipping slope, but the horizontal projection is rectangular.) The coordinates of the reflection point and dip and strike of the reflecting plane are obtained from geometry (App. C), either by computation (Fig. C1), or graphically (Fig. C2). When working with a square geophone pattern it is an advantage to find a mean solution for all four geophones forming a square. This technique has been described by Lliboutry.[120] The full solution including the position of the image point can be determined graphically (Fig. C2).

The computation methods are adequate when sufficient data are processed by computer. Graphical methods are more appropriate if only a few points have to be analyzed as under field conditions where the essential objective is to appraise continuously the areas that are actually covered in a detailed sounding operation over rough bed topography.

The main concern in evaluation, whether done analytically or graphically, is whether or not the reflections at a group of geophones are received from the same area of the bed. A simple control is to check whether the mean travel times of diagonal pairs in a geophone square are about equal.[160] Lliboutry[120] has proposed using the traces of the four planes determined by the intersections of the spheres (eq. 51, $i = 1$ to 4) on a horizontal plane for a test. These traces form a square, which should be small if the reflections occur on elements of the bed which are close together. However, Vallon[183] has shown that already a small error in reflection time can have a fairly large effect on the size of the test square. He has found that an error of 1 millisec in time can cause a side length of the test square as large as 500 m with side lengths of the geophone square

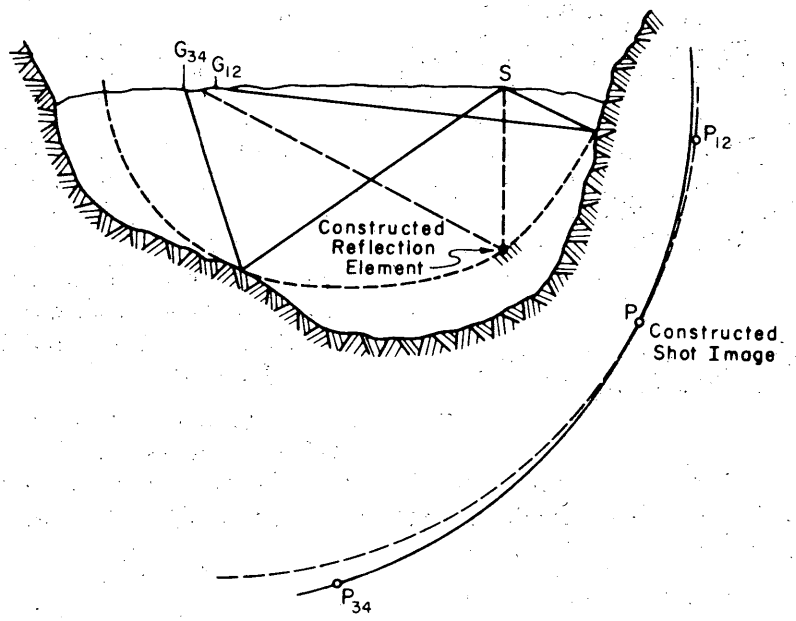

Figure 36. Reflections from different parts of the glacier bed as a source of error. (From Vallon[183].)

of 30 m. In his work on a very deep, narrow valley glacier he has concluded that only about 15 out of 142 cases, showing side lengths of over 600 m, were definitely caused by inconsistent reflection signals from widely different parts of the bed. On the other hand, as also pointed out by Vallon, it can happen that the interpretation is in error in spite of a satisfactory square, if the geophones are reached in pairs (Fig. 36). A comparison of the results from adjacent geophone squares will nevertheless reveal this type of error. It is sometimes possible to evaluate more than one single-reflection impulse from one geophone location.[44]

The computation of depth and dip can be considerably simplified when the short shot distance is used (deep ice). The angle α between one leg of an L-spread and the rock surface in a plane normal to the interface is obtained from

$$\sin\alpha = \frac{(Vt_r)^2 - (Vt_0)^2 - s^2}{2s\,Vt_0} \tag{57}$$

where t_0 is the reflection time at the shot point and t_r the reflection time at distance s from the shot; α is taken positive for a down-slope in the direction of the spread. This formula reduces to

$$\sin\alpha = V\frac{t_r - t_0}{s} = V\frac{\Delta t - \Delta t_0}{s} \tag{57a}$$

when s and α are small; Δt_0 and Δt are the normal and the observed stepout times, respectively. The dip β in the direction of the other leg of the spread is obtained accordingly. The true dip θ of the rock surface with respect to the snow surface and the direction ϕ of dip with respect to the leg on which α was measured, where $|\alpha| > |\beta|$, are obtained from the equations

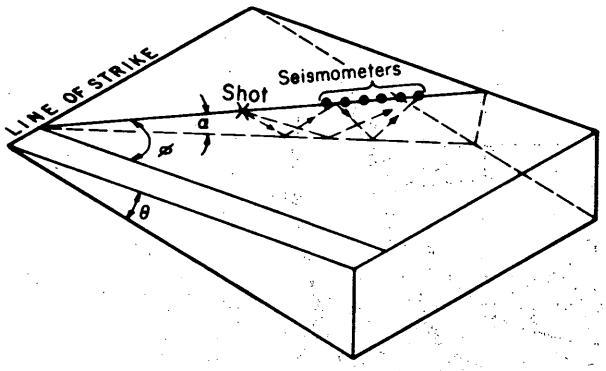

Figure 37. Multiple reflections at a sloping interface. (From Robin.[156]*)*

$$\cot\phi = \frac{\sin\alpha}{\sin\beta} \tag{58a}$$

$$\sin\theta = \frac{\sin\alpha}{\cos\phi} \tag{58b}$$

and the vertical depth z is given by

$$z = h/\cos\theta. \tag{58c}$$

(The equations based on tangents by Thiel et al.[177] are correct when the apparent dips α' and β' in vertical planes through the spread are used.)

Multiple reflections will now be considered. Poulter[145] has developed the theory for multiple reflections in a wedge-shaped ice body, and his results have been summarized by Robin.[156] The dip θ of a plane tilted subsurface when the top surface is a horizontal plane (Fig. 37) is given by

$$\frac{\sin i\,\theta}{\sin k\,\theta} = \sqrt{\frac{(Vt_i)^2 - s^2}{(Vt_k)^2 - s^2}} \tag{59}$$

where V and s are velocity and shot distance as before and t_i and t_k are the respective travel-times for the multiply reflected impulses of number i and k. For the first reflection R_1 and the first multiple R_2 the travel-times are t_1 and t_2, and the formula becomes

$$2\cos\theta = \frac{t_2}{t_1}\sqrt{\frac{1 - (s/Vt_2)^2}{1 - (s/Vt_1)^2}}. \tag{59a}$$

When s/Vt_1 is small it is

$$\cos\theta = \frac{t_2}{2t_1}. \tag{59b}$$

The true dip θ determined in this way on a single leg of a spread can be combined by eq 58b with the apparent dip α to find the angle ϕ between the spread and the direction of true dip. The accuracy with which α and θ can be obtained with short spreads is not sufficient to give a good value of ϕ in this manner, however. Another representation of the problem of multiple reflections for small relative shot distances has been given by Clarke.[46]

Only the reflections of P- or S-waves have been considered so far, the latter being seldom observed. The converted reflections P to S or S to P also have some practical importance. The problem of spatial converted reflections R_{SP} has been solved by Sandstrom.[169] The solution is presented in Appendix C1, eq 102. Solutions for R_{PS} could be developed along similar lines. Sandstrom has only observed converted reflections R_{SP}, while Bentley et al.[20] have concluded that in their case it was the R_{PS} impulse which was recorded, because it was usually only visible on the traces from horizontal geophones. Roethlisberger[161] has obtained both events in a case

where the two signals were split up owing to dip of the interface, but R_{SP} was more consistent and stronger (Fig. 28).

Depth computation when the velocity is a function of depth

The assumption of homogeneity throughout the ice mass is not justified when the top layer is snow (firn) with variable velocity increasing with depth. This is the case in most surveys on continental ice sheets. On thick ice when the shot distance is small the rays are almost perpendicular to the surface layer. A reference horizon (datum plane) is chosen where the velocity becomes approximately constant. The time t_d for travel across the layer above this horizon is taken into account. (A correction in the shot distance also has to be made if this distance is large.) Because of the depth of the charge below the surface a lesser time correction than t_d has to be made for the time from shot to reference horizon, or the time interval t_d is used minus the up-hole time (time from shot to detector at the surface directly above the shot). The time t_d is found by numerical integration of

$$t_d = \int_0^d \frac{dz}{V_z} \tag{60}$$

where d is the depth to the reference horizon and V_z is an empirical function obtained from a refraction survey of the surface layer. The ice thickness is computed for a plate below the reference horizon and the thickness of the surface layer is added:

$$h = \left(\frac{t_r}{2} - t_d\right)\overline{V}_{ice} + d \tag{61}$$

where $\overline{V}_{ice}$ is the mean velocity in ice. The case of a dipping subsurface is treated accordingly, where a correction in t_d and d is only necessary when the dip is large. The snow and low velocity ice layer is similar to the weathering layer in standard reflection work. Pratt[150] has treated this question in far greater detail than is done here or in textbooks, taking the curvature of the rays into account.

Typical values that have been used for t_d and d in Antarctica are: $t_d = 0.057$ sec and $d = 200$ m, and $t_d = 0.102$ sec and $d = 325$ m.[13, 157] The time t_d is approximately constant for areas with equal depth-density relationship and can therefore often be used unchanged throughout a survey in one area. Clarke[44] has approximated the empirical depth-velocity relationship by a simple function where the velocity increases linearly with depth:

$$V_z = V_0 + kz \quad \text{for} \quad 0 \leq z \leq d \tag{62a}$$

where V_0 is the velocity at the surface,

$$V(z) = V_{ice} \quad \text{for } z \geq d \tag{62b}$$

and therefore

$$k = \frac{V_{ice} - V_0}{d}. \tag{62c}$$

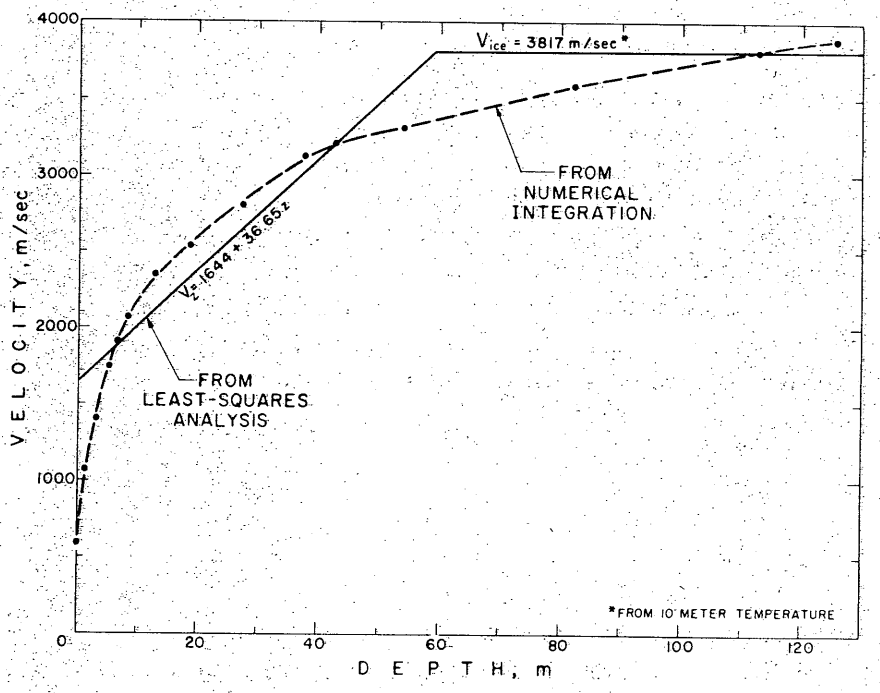

a. P-wave velocity as a function of depth in snow, comparison of results obtained from refraction data by numerical integration and an approximation with linear increase of velocity with depth.

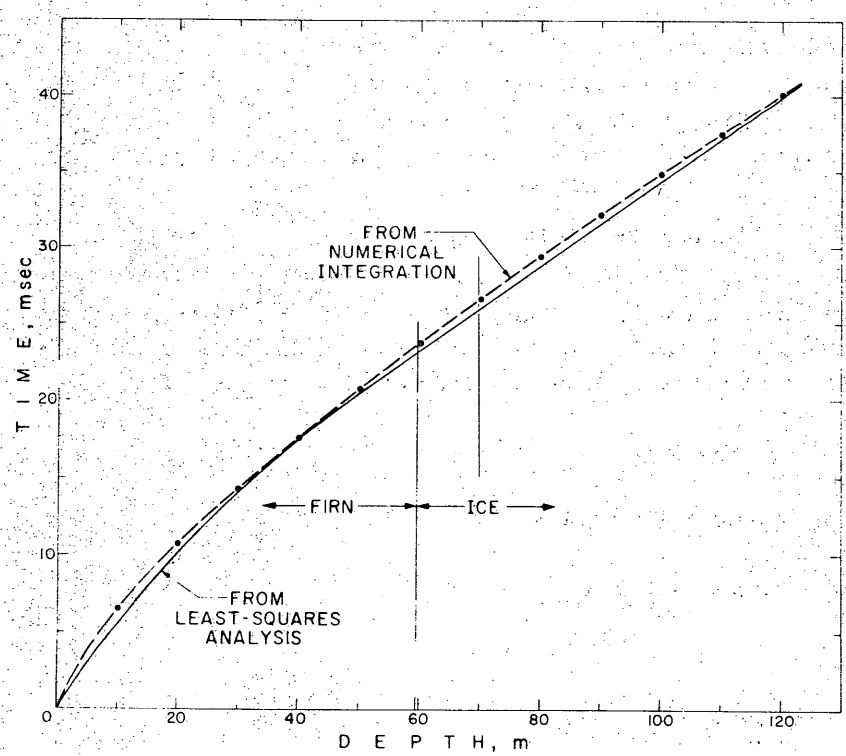

b. Vertical travel time as a function of depth for the velocity-depth curves of Figure 38a.

Figure 38. P-wave velocity and vertical travel time as a function of depth of snow. (From Clarke.[44])

The time-depth function for a vertically traveling wave is given by

$$t(z) = \int_0^z \frac{dz}{V_0 + kz} = \frac{1}{k} \ln \left(1 + \frac{kz}{V_0}\right) \qquad \text{for } 0 \le z \le d. \tag{63}$$

The travel-time from the surface to the reference horizon is

$$t_d = \frac{d}{V_{ice} - V_0} \ln \frac{V_{ice}}{V_0}. \tag{64}$$

A comparison of the time-depth function obtained by numerical integration and eq 63 is given in Figure 38b for the true velocity-depth function and the approximate function with linear velocity increase of Figure 38a. It is seen that the approximate integration gives very satisfactory results for t_d.

Further velocity changes with depth may occur below the reference horizon with increasing pressure and because of increasing temperature at greater depth. If the reference horizon is not taken too deep the velocity will show a slight further increase and then slowly start to decrease, the effect of temperature becoming larger than that of pressure. The mean velocity in ice is needed to compute the ice thickness below the reference horizon (eq 61). A standard procedure in seismic work to obtain the mean velocity $\overline{V}$ is to plot t_r^2 against s^2, where t_r is the travel time of the reflection pulse and s the distance between shot and geophone. A straight line with slope $1/\overline{V}^2$ is obtained when the reflecting interface is a plane and there is no dip in the direction of the spread (eq 46a). For higher accuracy, shot points in addition to the one close to the spread are moved out along the axis of the spread. The mean velocity $\overline{V}_{tot}$ of snow and ice together is obtained when plotting t_r^2, and it has to be corrected to obtain $\overline{V}_{ice}$ directly. The "$T\,\Delta\,T$" method described in geophysical textbooks serves when there is dip and the interface is not plane, and sufficient shots are available for statistical treatment. Since the interface is hardly ever plane under a glacier, a special reflection survey should be carried out for highest precision, keeping the reflection point as constant as possible. Both shot point and geophone have to be moved (see Dobrin,[57] p. 122-123).

Mean ice velocities $\overline{V}_{ice}$ depend on the depth chosen for the reference horizon and the temperature profile of the ice sheet, among further factors possibly influencing velocity at depth like crystal orientation and inclusions. Typical values are:

3660 m/sec, Salmon Glacier, British Columbia[58]
3700 m/sec, Kaskawulsh Glacier, Yukon Territory
3820 m/sec, Ross Ice Shelf, Antarctica[53]
3845 m/sec, Site 2, Greenland[20]
3840-3870 m/sec, Antarctic Peninsula[13]
3905 m/sec, Polar Plateau, Antarctica[157]
3921 m/sec, Polar Plateau, Antarctica[157]

The question of the best values of velocity for Antarctica has been discussed by Bentley.[23] Clarke[44] has used mean ice velocities estimated from temperature at 10-m depth in Greenland.

Depth determination on ice shelves

Reflections occur at the ice/water interface and at the bottom of the sea. This leads to a large number of possible combinations of single and multiple reflections (Fig. 39). The variety

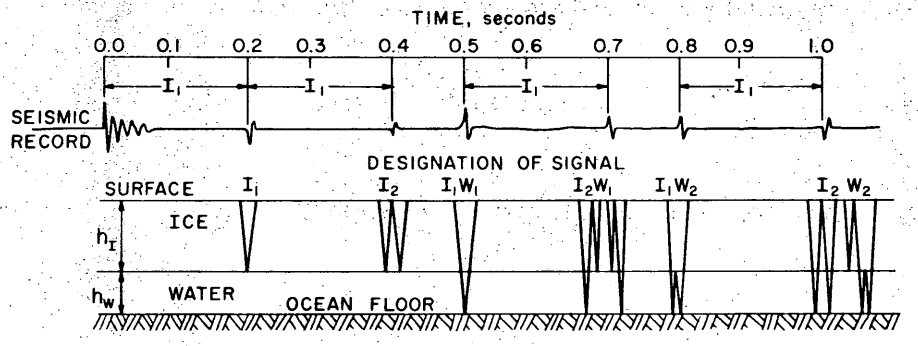

Figure 39. Schematic seismic record and notation for single and multiple reflections at the bottom and surface of an ice shelf and at the bottom of the sea. (After Crary et al.[53])

is even larger because of the occurrence of *P*- and *S*-waves in the ice. Crary et al.[53] have listed a number of ways to determine the thickness of an ice shelf from the travel times of all these various reflections, and they have applied many of them to the Ross Ice Shelf. The methods are:

1. The standard *P*-reflection technique of ice sheets is sometimes applicable, but often the ice is too thin. Single (I_1) and multiple reflections (I_2, I_3, etc.) have been obtained and used to determine the mean velocity on the thicker sections of ice shelves. On the Ross Ice Shelf

$$h\,(\text{in meters}) = \left(\frac{t_{i1}}{2} - 0.0345\right) 3820 + 100 \tag{65}$$

gives the depth h where t_{i1} is the travel-time of the first *P*-reflection at the ice/water boundary.

2. The most consistently observed and strongest reflection is the one from the water/sediment interface ($I_1 W_1$). The formulas relating distances and times, given below, are not subject to easy application.

$$x = 2h_i\left(\tan a_I + \frac{h_w}{h_i}\tan a_w\right) \tag{66a}$$

$$t_{i\,1w\,1} = \frac{2h_i}{V_i}\left(\sec a_i + \frac{h_w \cdot V_i}{h_i \cdot V_w}\sec a_w\right) \tag{66b}$$

where x = distance between shot and detector, h_i = ice thickness, h_w = thickness of the water layer, a_i and a_w = angle between the wave path and the vertical in the ice and water layers respectively, and V_i and V_w = the mean *P* velocities in ice and water. On the Ross Ice Shelf V_w = 1442 m/sec was used, taken from Hydrographic Office data. To evaluate the field data, charts were made up using eq 66a, b and

$$\overline{V}(t_{i\,1w\,1})^2 = (h_i + h_w)^2 + x^2. \tag{67}$$

The mean velocity $\overline{V}$ also depends on the ratio of ice to surface layer thickness (snow and low density ice) so that different charts had to be used for different ice thicknesses. Pratt[150] has also treated the problem of sea bottom reflections in great detail, developing the equations in series.

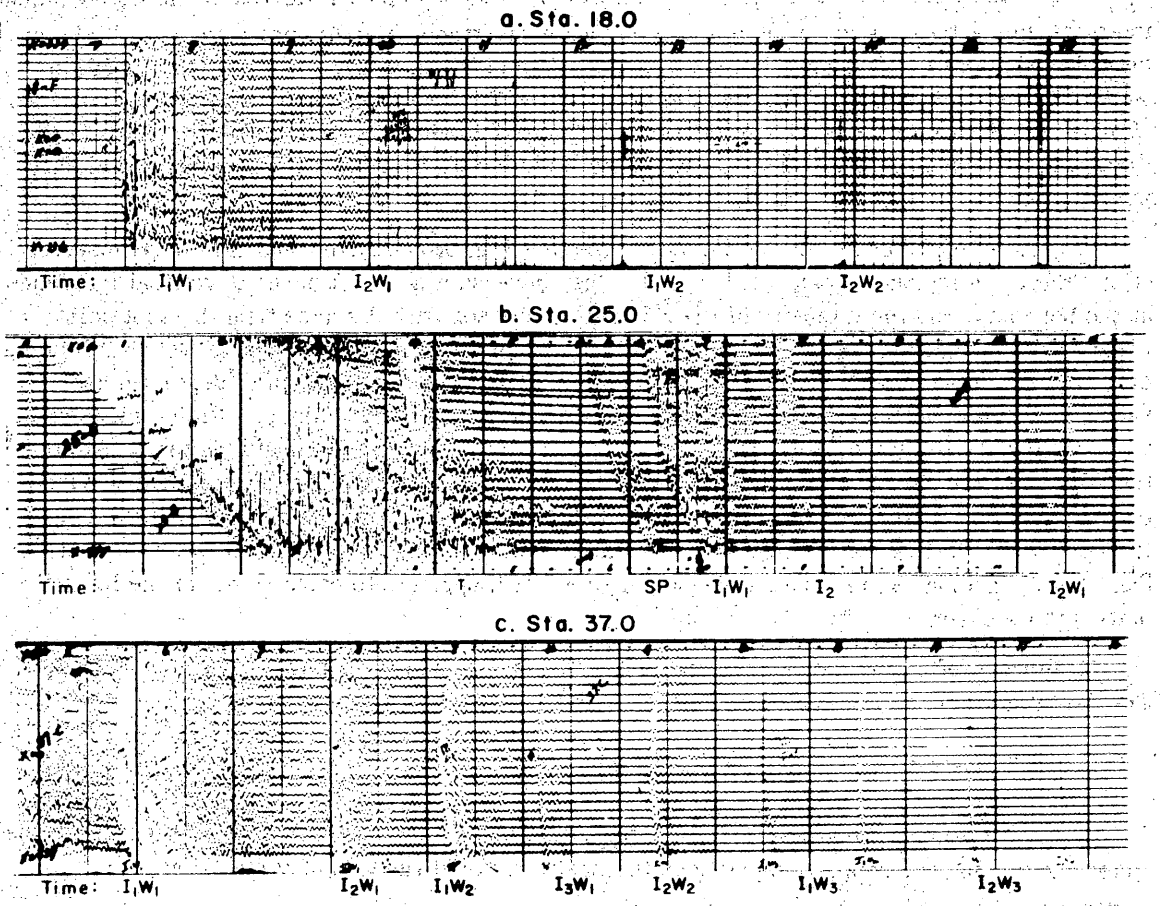

Figure 40. Seismic reflection records from Ross Ice Shelf. a) Ice thickness = 377 m, water depth = 376 m. b) Ice thickness = 694 m, water depth = 191 m. c) Ice thickness = 384 m, water depth = 244 m. (From Crary et al.[53])

In spite of a great effort to apply various corrections he found this method inaccurate. He shows analytically that a large spread is required. Poulter[145] has described a mechanical method to determine depth of ice and water.

3. Multiple reflections of waves traveling through both the ice and water layer can usually be identified. By proper combination of two such waves the travel time for a path only in ice or in water can readily be obtained (Fig. 39); for determination of the ice thickness with eq 65 it is:

$$t_{i1} = t_{i2w1} - t_{i1w1}$$

$$= t_{i2w2} - t_{i1w2} \qquad (68)$$

The I_2W_1 reflection follows shortly after the main I_1W_1 reflection and is often obscured by reflection noise, probably from sub-bottom reflections, but both I_1W_2 and I_2W_2 are usually well recorded (Fig. 40a). Identification is done in a t^2 versus x^2 plot where V is higher for I_2W_1 and lower for I_1W_2 than for I_1W_1 or I_2W_2. On good records identification is further helped by the phase relationship. I_1W_1, I_2 and I_1W_2 are in phase with the direct P-wave, while I_1 shows a 180° phase change.

I_2W_2 shows the phase change or not, depending on whether it is only reflected at the water/sediment interface and at the surface, or also at the ice/water interface. Interference effects are to be expected in this case. The analysis becomes more difficult when either the ice/water (eq 59) or water/sediment interface, or both, is dipping. Poulter[145] gives a thorough mathematical analysis of multiple reflections between non-parallel planes (p. 58) which is then applied to multiple reflections between surface and sea bottom on the Ross Ice Shelf, albeit under erroneous velocity assumptions.

4. Converted *PS* or *SP* reflections at the ice/water interface have frequently been observed (Fig. 40b) as in ice masses on solid ground. The conversion does not occur at vertical incidence at the boundary, and the intensity of the *PS* event increases with distance from the shot point accordingly. Identification of *PS* is also readily possible from the t^2 vs x^2 plot which falls on a curved line. Formulas of the form of eq 66 are obtained for the computation of depth (eq 49). Charts for various average velocities of the *P*- and S-waves corresponding to various thicknesses were used in the Ross Ice Shelf survey by Crary et al. to analyze the time and distance data obtained from the recordings. An approximation can be made by extrapolation of the time-distance curve or t^2 vs x^2 curve to the intersection with the ordinate and using t at $x = 0$ and $\overline{V}_P$ and $\overline{V}_S$ for vertically traveling waves from surface to interface, or a chart of travel time versus depth.[177] Sandstrom's method (App. C) might also be applied, with appropriate corrections for the low velocity surface layer.

5. *S*-wave reflections were observed, but still less frequently than the *P*-wave reflections. The depth on the Ross Ice Shelf has been given by

$$h \text{ (in meters)} = [(t_s/2) - 0.0525]\,1925 + 75 \ . \qquad (69)$$

6. At the edge of the ice shelf further combinations of waves are possible by shooting in the water and placing the geophones partly on the shelf, partly at the foot of it on the bay ice.[177]

7. On relatively thin ice with no low velocity surface layer (ice island T-3) a strong signal was observed in which the frequency could be related to thickness, the so-called Crary wave (p. 108).

The water depth below the ice is obtained from the very strong I_1W_1 reflection, using a velocity of 1442 m/sec after subtracting the time spent in the ice. The dip of the water/sediment boundary can easily be obtained too[53] when the ice/water interface is horizontal, as is generally the case. Sample records for various ice thicknesses and water depths are given in Figure 40.

Anisotropy

The assumption of an isotropic substance has been made in the equations for depth and dip up to this point. This assumption may not be justified if the highest precision is wanted, since the layered snow near the surface as well as ice with a preferred crystallographic orientation are anisotropic. By taking the anisotropy into account it may also be possible to extract some information on preferred *c*-axis orientation in big ice masses from a reflection survey.

The simplest case is a horizontal plate of an axisymmetric medium with vertical axis of anisotropy. Three types of waves must now be considered, the pseudocompressional *P*, the horizontally polarized true shear wave $S_1 = S_H$, and the vertically polarized shear wave $S_2 = S_V$ (Fig. 6). For reflections without conversion R_P, R_{SH} and R_{SV} the angle of incidence is equal to the angle of emergence, as in the isotropic case. The velocity however changes with direction and the t_r^2 vs s^2 plot deviates from a straight line. The relation $(Vt)^2 = 4h^2 + s^2$ (eq 46a) can be used to determine the velocity as a function of direction.

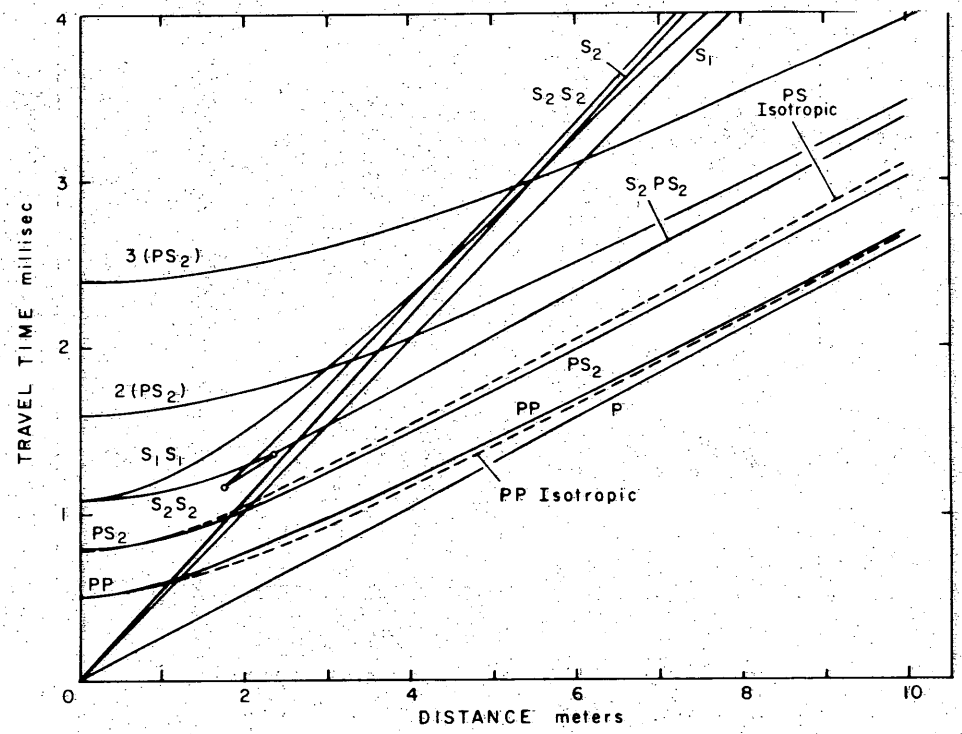

Figure 41. Travel time vs distance diagram for ice plate of 1 m thickness. Solid lines for vertical c-axes orientation computed with elastic constants by Bass et al.[11] at -16°C, dashed lines for polycrystalline isotropic ice with $V_P = 2V_S = 3823$ *m/sec. (From Roethlisberger.[167])*

For the converted waves PS_V and S_VP (S_H is not converted) the relation between angle of incidence and angle of emergence is given again by Snell's law, but for the velocities of the wave normals instead of the rays. The horizontal components of the wave normals have therefore to be equated in the computation. This was done by Roethlisberger[167] for an ice plate where all *c*-axes are vertical (as is sometimes found in lake ice). The travel time vs distance diagram is given in Figure 41. The maximum deviation in travel time from the isotropic case is about 4% for the *P*, 3% for the *SH*, 15% for the *SV*, and 3% for the converted *PS* reflection. The *SV* reflection is most affected, but also the time difference between the *P* and *PS* reflections is quite sensitive to this type of anisotropy, showing a reduction of 9% at large distances (Fig. 42). Similar effects but smaller deviations can be predicted for highly oriented glacier ice where the *c*-axes are closely grouped around a vertical axis, but when they are evenly distributed in a cone of wide apex angle (60°) the sign of the deviations changes.[19]

The computation of ray paths and travel times becomes far more complicated when the axis of anisotropy is not perpendicular to the interface.[70] In the general case the incident ray, the normal to the interface and the emergent ray are no longer in one plane. Further theoretical difficulties are encountered when the preferred orientation does not show rotational symmetry. Considering the smallness of the velocity differences to be expected in nature and the fact that the interface is seldom an ideal plane, there is little hope of solving a complicated case of anisotropy by seismic reflection studies; but it should be possible to estimate the degree of anisotropy and its general symmetry. The most promising quantity to be measured is the travel time of the *SV*

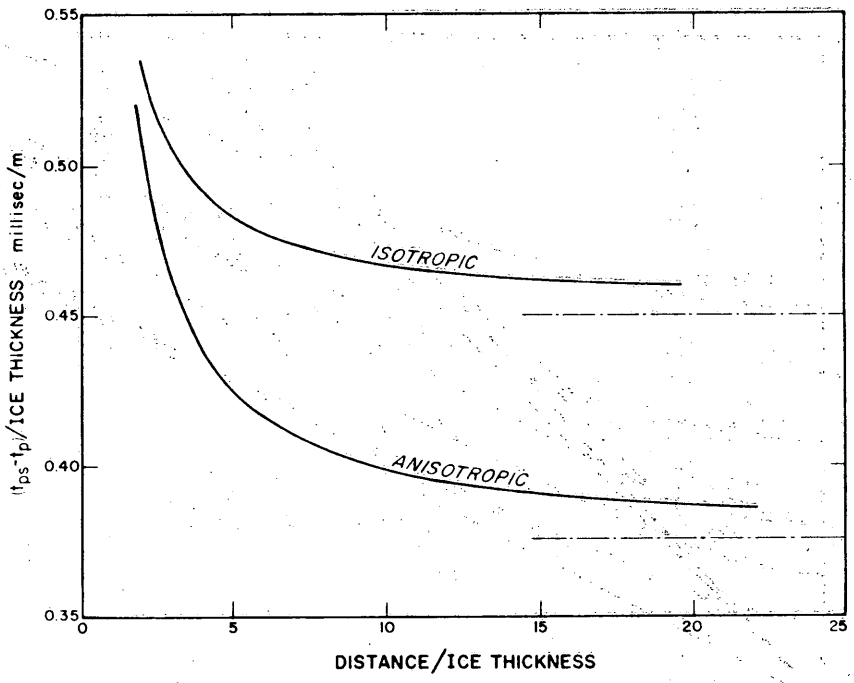

Figure 42. Normed travel time difference for converted wave of type PS *and reflected* P*-wave as a function of shot distance. (From Roethlisberger.*[167])

wave versus shot distance and the travel time difference between the *P* and *PS* or *SP* reflection at large shot distances.

Energy of reflected waves

Some additional information is contained in the reflected pulse, besides the travel time and the direction of the motion, namely its intensity, and this can be used to obtain information on the substratum below the reflecting boundary. The energy of a wave is proportional to the amplitude squared, or to the square of the amplitude of the measured component, if the direction of motion is sufficiently constant in a set of measurements. One has to be aware of the effects of automatic gain control (AGC) when using equipment where this cannot be switched off: only small amplitudes can be used so that AGC does not interfere.

The energy distribution around the source should first be neglected. Only the loss through attenuation and the loss by reflection then have to be dealt with. Two or more homogeneous isotropic media are considered. I_0 is the initial energy per unit solid angle (steradian) moving out in all directions from a point source. Then if α is the attenuation constant, the energy I' per unit area at distance r from the source is given by eq 18:

$$I' = \frac{I'_0}{r^2} e^{-\alpha r} .$$

The loss upon reflection perpendicular to a plane interface is given by

$$E_e = KE_i \tag{70}$$

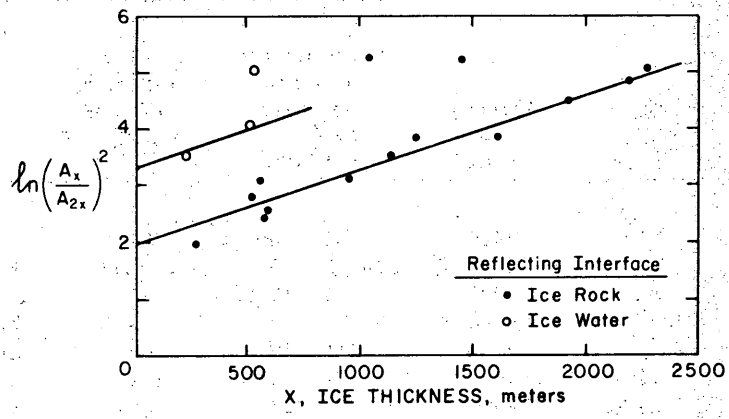

Figure 43. Ratio of the amplitude of first (A_x) and double (A_{2x}) reflections as a function of ice depth. The slope of the main straight line shows the attenuation of P-waves in ice, while the intercepts at zero distance indicate the average reflection coefficients. (From Robin.[156])

where E_i is the energy per unit area of the incident wave and E_e the energy per unit area of the emergent wave. K is the reflection coefficient given by

$$K = \left(\frac{V'\rho' - V\rho}{V'\rho' + V\rho}\right)^2 \tag{71}$$

where V is the velocity (V_P or V_S) and ρ the density as before, and the primed symbols are used for the lower and the unprimed ones for the upper medium. (The product V_P by ρ is termed the acoustic impedance.) The energy per unit area at the surface of a plate of thickness h for a wave reflected once (shot at the surface) is

$$E(R) = \frac{I_0' K}{(2h)^2} e^{-2ah} \tag{72a}$$

and the energy of a doubly reflected wave

$$E(2R) = \frac{I_0' K^2}{(4h)^2} e^{-4ah} \tag{72b}$$

which leads to the energy ratio for the first and double reflection of

$$\frac{E(R)}{E(2R)} = \frac{4}{K} e^{2ah}. \tag{73}$$

Similar equations are obtained for further multiple reflections. Robin[156] has used the amplitude ratios of first and double reflections at variable ice thickness to find K and a experimentally (Fig. 43). He finds for the attenuation constant in Antarctica (-19 to -40°C) a value of

Table XIIa.. Reflection coefficients for ice and various substances. (From Robin.[156])

Specimen	Density (ρ) (g/cm^3)	Velocity (V_P) (m/sec)	Characteristic acoustic impedance (ρV_P) (g/cm^2 sec)	Reflection coefficient of energy K	Remarks
Sea water	1.02	1450	1.5×10^5	0.16	
Moraine (wet)	1.5 - 2.4	1000 - 2000	$1.5 - 4.8 \times 10^5$	0 - 0.16	Estimated
Ice	0.9	3830	3.5×10^5	–	
Moraine (frozen)	1.0 - 2.5	3800 - 5000	$3.8 - 7.5 \times 10^5$	0 - 0.13	Estimated
628	2.74	4520	12.4×10^5	0.31	Granulite
840	2.68	4610	12.4×10^5	0.31	Greywacke
647 (sedimentary)	2.70	4920	13.3×10^5	0.34	Siltstone
647 (sill)	2.88	6165	17.8×10^5	0.45	Basaltic sill
841	2.81	5050	14.2×10^5	0.37	Quartz microdiorite
397	2.68	5440	14.6×10^5	0.38	Greywacke
62	2.93	5130	15.0×10^5	0.39	Quartz diorite
388	2.77	5830	16.2×10^5	0.42	Slate
NN (Förstefjell sill)	2.94	6390	18.8×10^5	0.47	Dolerite
671	3.00	6520	19.5×10^5	0.48	Dolerite

Table XIIb. Reflection coefficients for various combinations of substances. (From Robin.[156])

Specimen	Water	Ice	Moraine (wet)	Moraine (frozen)	Sedimentary rock	Gabbroic rock
Water	–	0.16	0 - 0.27	0.19 - 0.45	0.62	0.74
Ice	0.16	–	0 - 0.16	0 - 0.13	0.31	0.48
Moraine (wet)	0 - 0.27	0 - 0.16	–	0 - 0.19	0.20 - 0.62	0.37 - 0.74
Moraine (frozen)	0.19 - 0.45	0 - 0.13	0 - 0.19	–	0.06 - 0.28	0.20 - 0.45
Sedimentary rock	0.62	0.31	0.20 - 0.62	0.06 - 0.28	–	0.05
Gabbroic rock	0.74	0.48	0.37 - 0.74	0.20 - 0.45	0.05	–

$\alpha = 6.5 \times 10^{-4}$ m^{-1}, or 1 decibel per 356 m. This is about three times as large as newer results from Bentley.[25] Typical values of K are given in Table XIIa, b from which Robin has concluded:

> "One point with practical application which is apparent from the table is that if the first echo is weaker than a subsequent echo for a shot on inland ice, then the first echo almost certainly originates from the top of a morainic layer. If the first echo is a little stronger than the second it could come from the top of a layer of frozen moraine with sedimentary rock below. Any echoes from gabbroic sills intruding into sedimentary rocks below the bed of the glacier will however be appreciably weaker than one of the earlier echoes either from the bottom of the ice or of the moraine, so are unlikely to be mistaken for the primary echo."

Brockamp[36] has concluded from the large reflection coefficient that no thick layer of ground moraine exists in central Greenland.

At oblique incidence the energy of the incident wave is partitioned among four emergent waves (Fig. 33). This problem has been brought into a suitable analytical form by Nafe,[134] and Roethlisberger[165] has used his equations to compute a wide variety of cases of ice in contact with solids. Figure 44 gives a few examples. Similar figures have been presented by Crary[50] for the ice/air and

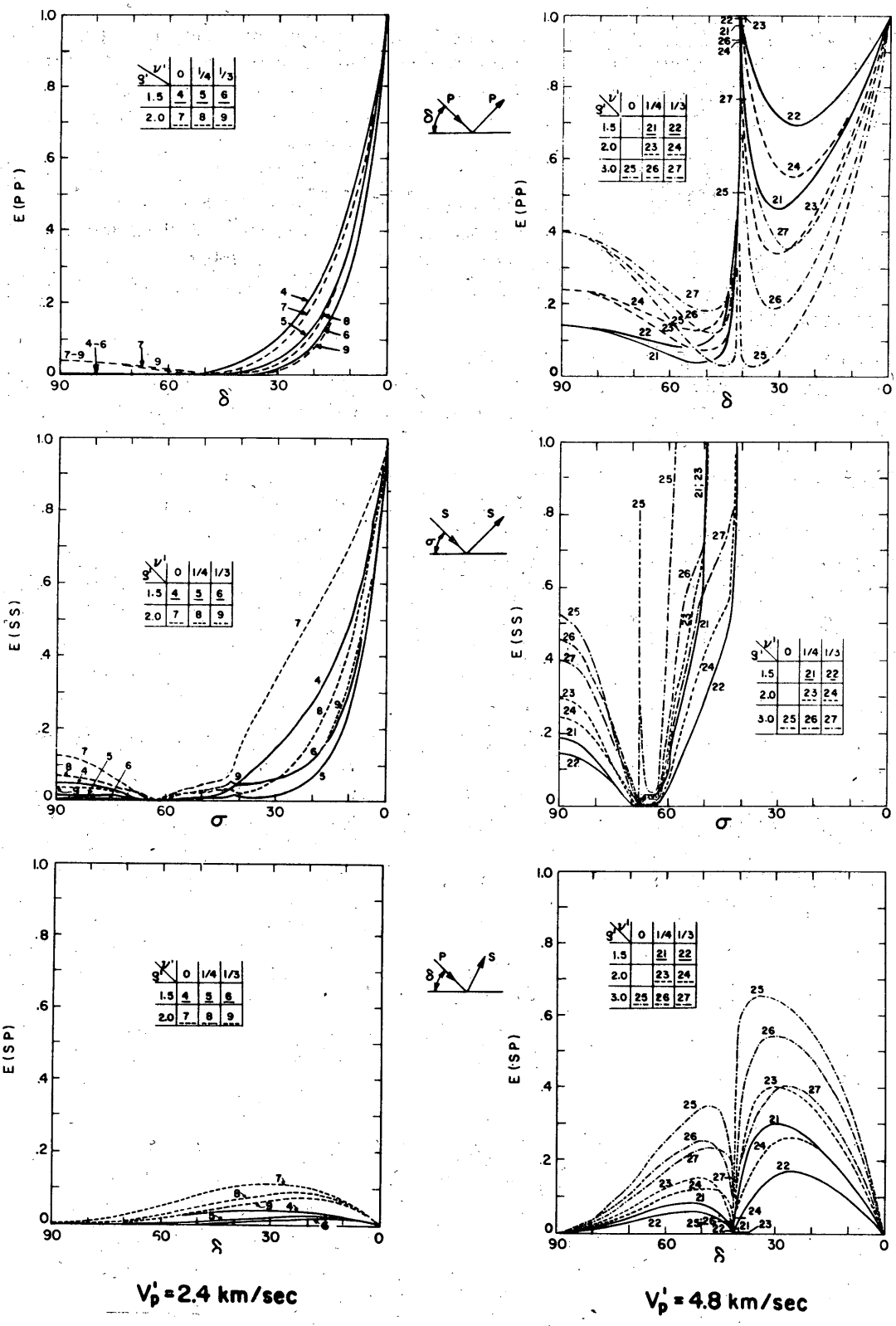

Figure 44. Reflection coefficients for plane waves in ice incident on a plane boundary between ice (V_P = 3.6 km/sec, ν = 1/3, ρ = 0.9 g/cm³) and various solids with P-wave velocities of V'_P = 2.4 km/sec on left and V'_P = 4.8 km/sec on right, and various Poisson's ratios ν' and densities ρ' as indicated in tables. (Numbers of curves in boxes.) (From Roethlisberger.[168])

ice/water interfaces. The computation is only valid for plane waves, and it must be applied with reservation where abrupt changes of energy ratios (reflection coefficients) occur. The following conclusions can be reached based on the cases of Figure 44 and additional ones for $V_P' = 1.2$, 3.6, 4.2 and 6.0 km/sec. For the *P*-wave reflection the coefficients decrease at small angles of incidence ($90° - \delta$) with increasing angles and at 30° ($\delta = 60°$) are in many cases about half the value at 0° ($\delta = 90°$). At very large angles, approaching 90°, they approach unity, and they show an additional peak at lesser angles if the velocity in the substratum is higher than in ice.* The reflection coefficients of the *S*-wave drop more rapidly with increasing angle of incidence but become unity at angles beyond critical, and the energy ratios of the *PS* reflection are zero at 0° and 90° incidence of *P* and have one maximum if V_P' is smaller and two or three maxima if it is larger than the *P* velocity in ice.

This applies to single plane interfaces between solids. Robin[156] also treats the ice/water boundary for perpendicular and oblique incidence (see also Crary[50]) and gives equations for computing the energy of reflected waves at the bottom of the sea and deeper interfaces below an ice shelf.

Special phenomena are to be expected from irregularities of the interface, say an undulating boundary about a plane, or thin intermediate layers. For example, at a layer thickness of 1 quarter wavelength and equal reflection coefficients at the two interfaces (and no phase change) the two reflections will cancel each other. Complicated interferences will occur with seismic pulses containing a whole frequency band and with changing shot distances. Some specific cases in relation to field observations have been discussed by Bentley et al.[20] and Robin.[156] It is also noteworthy in this respect that a gradual change of properties, as may occur at a glacier bed by a gradual mixing of ice and ground moraine, over a distance of several wavelengths does not give rise to any reflection.[41]

The energy of reflected waves is, within certain limits, proportional to the amount of explosives, and for a particular size of charge depends on the conversion of explosive energy into elastic waves, and on the distribution of the energy as a function of direction of the rays. Robin[156] has treated both questions for the snow surface layer of Antarctica in great detail. He has observed that the energy of the *P*-waves caused by an explosion increased by a factor of about 50 for a shot at 12-m depth as compared to one at 2 m. A shot in the air was comparable to the 12-m shot in its energy conversion.

The energy distribution at some distance from the shot is then influenced by the velocity change with depth. The energy per unit area at the reflecting interface is given by

$$E = \frac{I_0'}{r^2}\left(\frac{V_0}{V_r}\right)^2 \frac{\cos\theta}{\sqrt{1 - [(V_0/V_r)\sin\theta]^2}} \qquad (74)$$

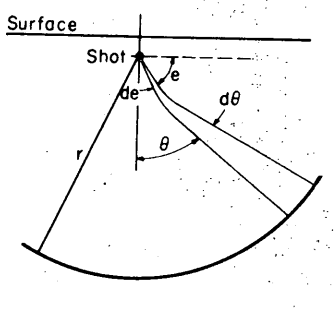

Figure 45. Energy of waves reaching the glacier bed (eq 74). (From Robin.[156])

where I_0' is the energy per steradian as before, r the distance from the shot, $V_0 = V_P$ at the shot depth, $V_r = V_P$ in ice at depth and θ the angle of the ray at depth relative to vertical (Fig. 45). The term containing θ does not vary much over the range of values normally encountered (0° to 30°), so the energy at the reflecting interface varies directly with the shot intensity and inversely with r^2 (radiation law in a homogeneous medium), and is proportional to $(V_0/V_r)^2$. That the "defocusing" factor $(V_0/V_r)^2$ is small near the snow surface and increases rapidly with depth indicates that there is an additional advantage of

* The position and width of this peak have been found to be in fair agreement with field observations by Dewart.[56]

placing the charge at some depth. Robin points out that with the "Poulter method" of air shooting, where a plane wave is formed by shooting off simultaneously several charges suspended in the air above the snow, not only is the normal "inverse square" loss reduced, but also the defocusing effect will be absent. This does not take into account all the aspects of directivity of the plane wave thus formed, namely that the area where the plane wave will be received is about equal to the area of the shot pattern, and that with only a few geophones there is little chance of getting the benefit from the outlined effects. This might explain why some investigators have been successful with the "Poulter method" while others have not.

Applications and Results of Reflection Soundings on Glaciers

Only a very general summary will be given of the worldwide application of reflection soundings on glaciers, concentrated on the applicability of the method, on certain difficulties encountered, and on certain observations which have been difficult to explain, some of them still being discussed.

Continental ice sheets

The first reflection soundings on an ice sheet were carried out in the early days of the seismic exploration method by Brockamp, Sorge and Wölcken,[82] on the Wegener expedition to Greenland in 1929 - 1931. A mechanical seismograph was used, and depths of up to about 2000 m were successfully measured. Not until 20 years later (1949-1951) was the work of the Germans in Greenland taken up by a French expedition, the Expéditions Polaires Francaises under the leadership of P.E. Victor. The seismic work was carried out by Joset (who was killed in a crevasse in the operation together with the Danish glaciologist, Jarl) and Holtzscherer.* Over 400 soundings were accomplished with new sensitive electronic equipment; the greatest depth measured was about 3000 m. A number of complete cross sections in a general east-west direction and some north-south traverses were covered in the central and southern part of Greenland. Further soundings in the northwestern part of Greenland in 1953 and since have been sponsored by the U.S. Army,[3 20 45 91] and a few soundings were accomplished by the British North Greenland Expedition in 1952 - 1954.[41] In 1958 a program was started in west Greenland by the Expédition Glaciologique Internationale au Groenland (EGIG).[35 36 37] The position of these surveys on the map is shown in Figure 46.

The first soundings on the Antarctic ice sheet were accomplished in 1951-52 by Robin[92 155 156] during the Norwegian-British-Swedish Antarctic Expedition 1949-52 and by Imbert[96] as part of the activity of the Expéditions Polaires Francaises. In 1957 began the large effort by many countries of the International Geophysical Year (IGY) and continuing projects, aiming at the determination of the ice volume of the Antarctic continent as a whole. These surveys have been summarized by Bentley.[22 23 24] The greatest ice depth has been observed between Byrd Station and the Sentinel Mountains. It is, according to Bentley and Ostenso,[21] 4270 m (4335 m is listed in the table for station 918, 80°23.6'S, 109°51'W, however). Ice thickness up to 4000 m has also been reported from east Antarctica by Sorokhtin et al.[172] Figure 47 shows which areas have been covered by seismic soundings.

It has been possible to apply the reflection method in most places, but sometimes with great difficulty, and in some areas the quality of the reflections has been very poor. Northeast Greenland is the only large area in which no reflections have been obtained.[41] It would be of considerable interest to visit this area again with more sophisticated equipment and to try wide-angle shots if no reflection can be recorded at vertical incidence.

The cold areas of the interior of Antarctica have posed a major problem because of the strong ground roll, which has been suspected by Robin[156] to occur only when V_P at the surface is less

---

* Ref. 89, 90, 92, 101, 102, 103.

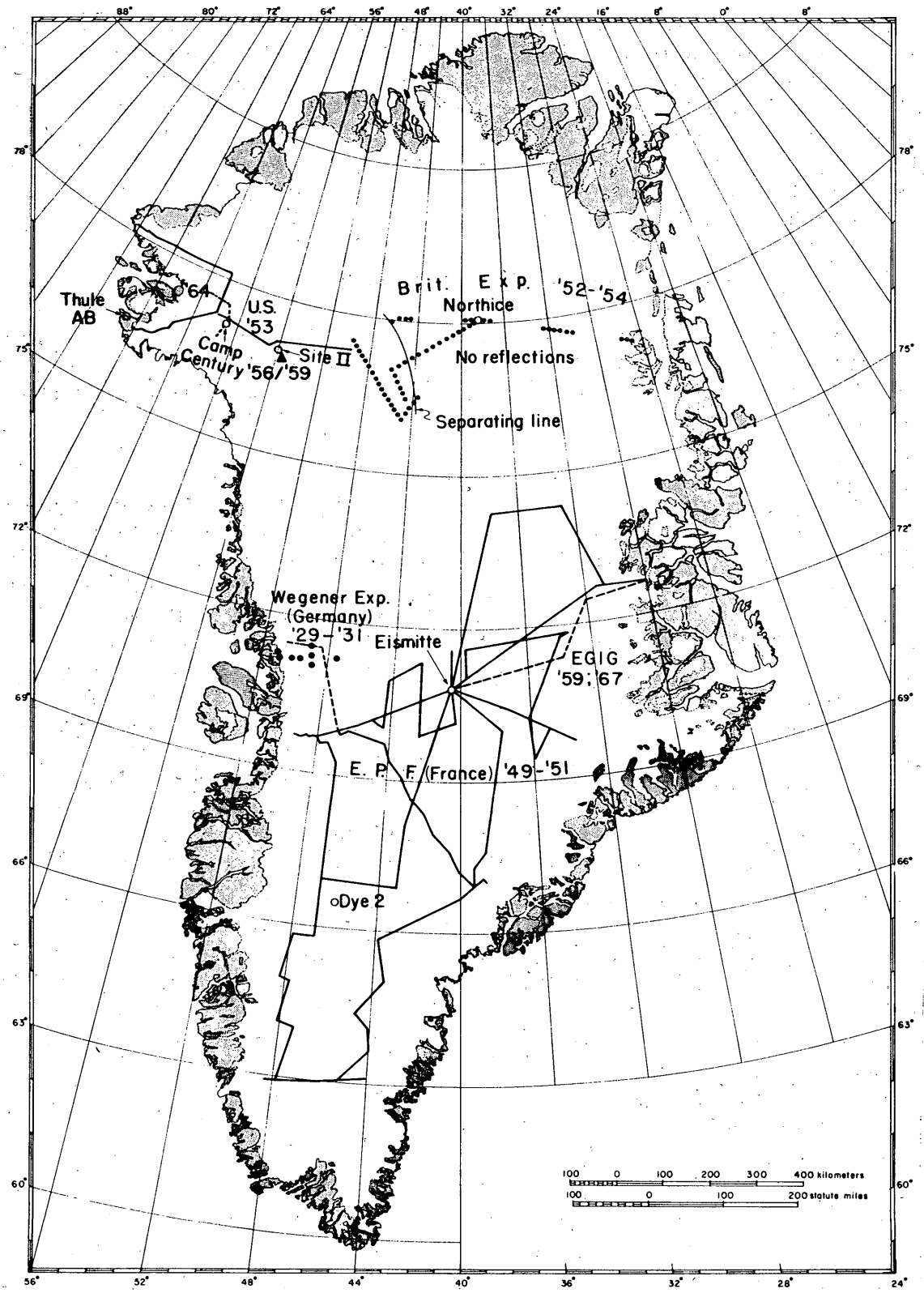

Figure 46. Seismic traverses in Greenland.

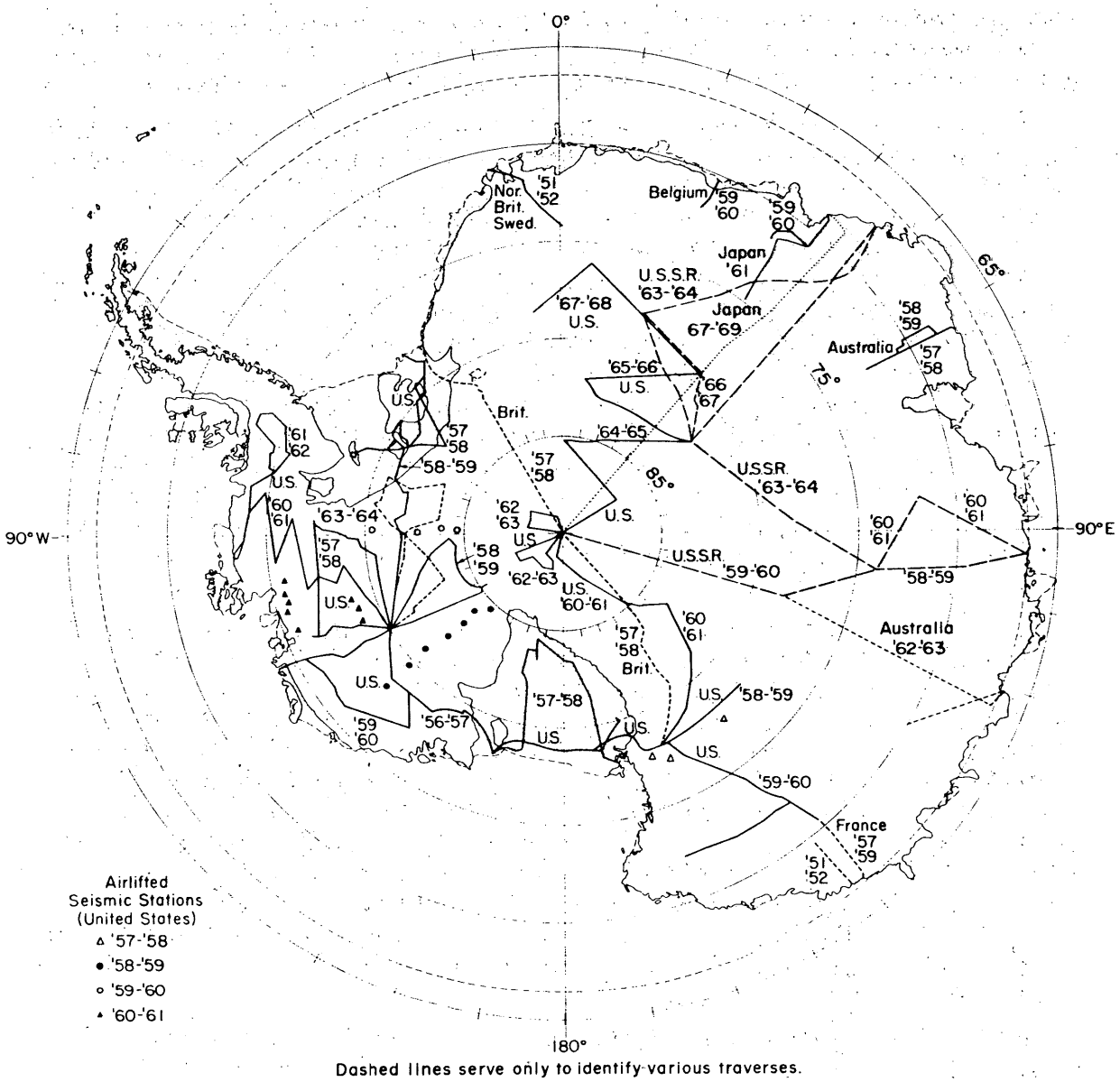

Figure 47. Seismic traverses in Antarctica. (After Bentley,[28] with additions.)

than the velocity of the surface wave, which is about equal to V_P at 7-m depth. That the phenomenon must be related to a very thin surface layer is supported by the observation of seasonal change of the intensity of the surface noise (p. 42). Bentley[28] has discussed the problem in view of dependency of the attenuation on frequency and temperature and the layering of the surface.

Reflections from more than one boundary have been reported frequently, and it has usually been possible to distinguish between sub-bottom and later reflections from other portions of the ice due to irregular topography, by analyzing frequencies, relative amplitude, and depth and dip of the interface.[12 13] Some attempts have been made to find the nature of the substratum from reflection characteristics. Bentley et al.[20] have tried to explain the relative intensities of R_P, R_{SV}, and R_{SH} and the occurrence, only at certain distances, of a long period (about 0.1 sec) constant

frequency wave train. But there has been conflicting evidence as to whether the velocity V_S in the intermediate layer is higher or lower than in ice. The existence of a layer about 100 m thick had been established independently by a difference in depth from reflection and refraction shooting.

A faint early reflection R_e which has been observed in some areas in Antarctica is of particular interest (see Fig. 31, record No. 1353). It was first thought to occur at the top of a layer in which the P velocity measured from wide-angle reflection shooting is a few percent below the velocity of cold ice,[12 21] but in view of Bentley's[25] analysis of anisotropy the velocity in the bottom layer cannot be determined accurately. The nature of the layer has been discussed by Behrendt[12 13], Bentley[25] and Lliboutry.* Ice containing rock inclusions or pure ice at the pressure melting point or showing a sudden change of crystal orientation has been suggested. Bentley[25a] has, from a detailed study of a fair number of records showing the R_e reflection, reached the conclusion that by far the majority of cases can convincingly be traced to ice containing morainal material. The strongest evidence comes from the reflectivity, which is often too high for a pure ice boundary, from the duration of the echo which indicates the presence of diverse reflecting layers, and from abrupt changes in the reflectivity and the layer thickness as well as the dip of the reflector, which can locally and regionally be related to bedrock topography. This would not be the case for a pure ice boundary. There is, however, one exception where there is a good possibility that a temperature-controlled velocity boundary is the source of an unusually short and regular R_e reflection.

While no indication of anisotropy of the ice was obtained by Behrendt,[12 13] the ultrasonic measurements of Bennett[19] on ice cores have shown that a slight variation of velocity with direction is to be expected in the top few hundred meters of the continental ice sheets. Bentley[25] has even demonstrated in a very careful study of wide-angle reflections (combined with the analysis of the refracted waves) that a very high degree of anisotropy is the rule in the still deeper layers of the Antarctic ice sheet. Even converted P- to S-wave reflections occur occasionally at normal incidence. More than half, even as much as 90%, of the ice column consists of anisotropic ice in most of the region studied. A model with a pronounced concentration of c-axes around a rotational axis makes it possible to explain most observations, whereby the axis is inclined 30° or more to the vertical, and lies in or near the flow plane at the majority of the stations. In this study use was made of the proper theory of waves in anisotropic polycrystalline ice,[19] while most discussions on anisotropy in the earlier literature have been based on the wrong assumption that the wave front of a P-wave from a point source would be an ellipse.[12 180]

Some special applications of the reflection soundings on ice sheets can be mentioned. Brockamp[33] has suggested measuring thickness variations in time by repeated detailed surveys, while Roethlisberger et al.[166] have tried to observe the *horizontal* displacement. The accuracy was found to be insufficient to furnish a value for the small displacement in 3 years at Site II, Greenland, over about 2000 m of ice, either from a comparison of the two maps (Fig. 48) or of the reflections at identical and neighboring geophone spreads (Fig. 49). It has been estimated that under more favorable conditions the method should give an accuracy of up to 30 to 50 m of horizontal displacement.

Traverses have also been carried out on a smaller ice cap, the Vatnajökull in Iceland, by a joint French-Icelandic team.[104] Depths up to 1000 m were observed. Reflections in this predominantly temperate ice mass were generally very good; in some cases more than one reflecting interface existed. One specific problem whose solution was also attempted was the question of

---

* Ref. 120 (p. 700-702), 121.

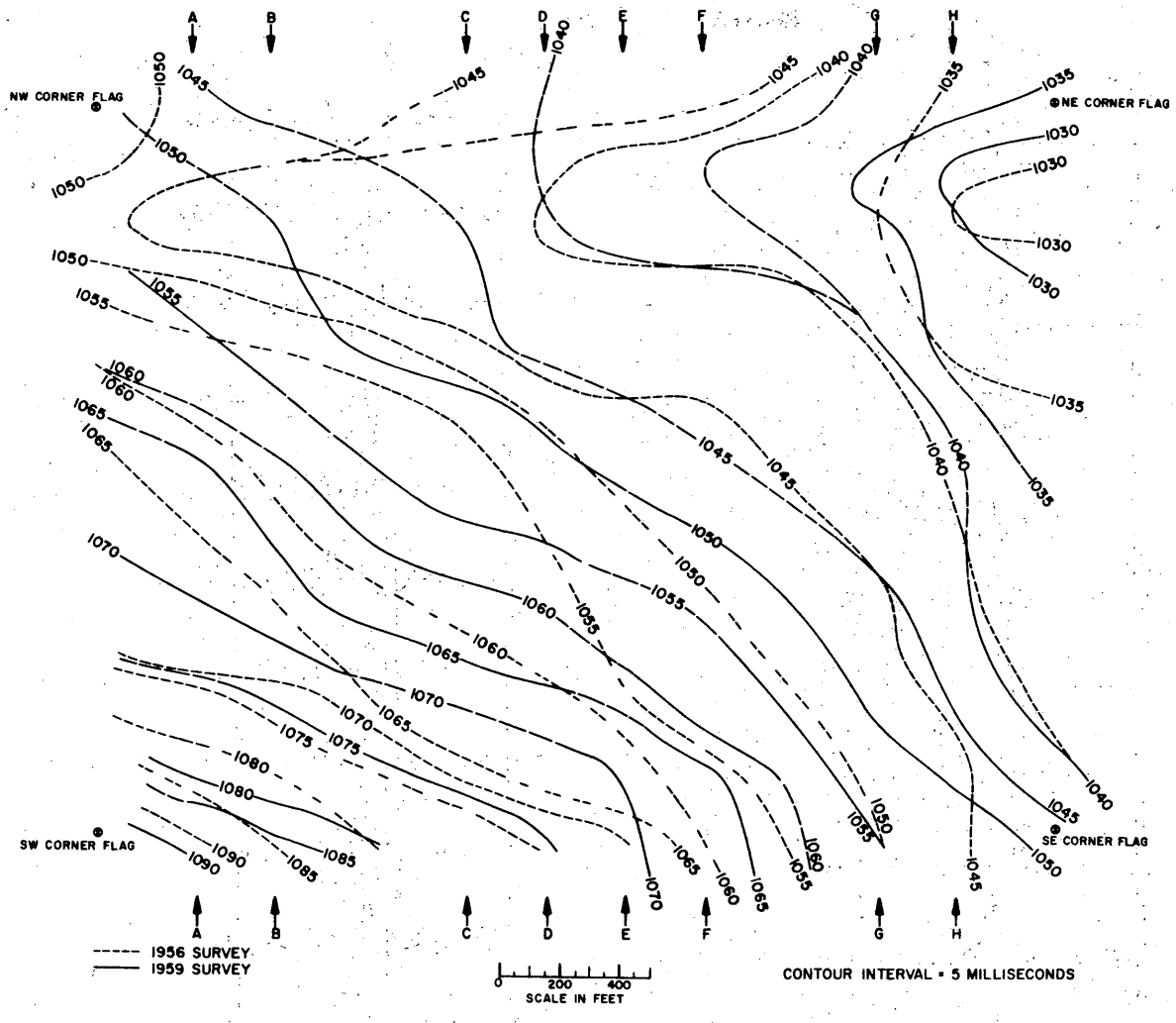

Figure 48. Travel time isograms (millisec) for detailed seismic reflection surveys carried out 3 years apart at the same location which was marked by surface flags on the Greenland ice cap near Site II. No consistent shift is apparent. (From Roethlisberger, Bentley and Bennett.[166]*)*

whether there was a water body beneath the depression of Grimsvötn or not. A negative answer was given, but the opposite can now be stated with confidence, based on the knowledge that has become available from the extensive work on shelves. The records from point 27A in the report by Joset and Holtzscherer should be reevaluated. The survey was carried out in the spring of 1951, and a *jökulhlaup* (glacier burst) from Grimsvötn with an estimated total discharge of 3.5 km^3 took place in July 1954.

Ice shelves and floating ice islands

The first seismic soundings on an ice shelf (the Ross Ice Shelf) were carried out by Poulter[144, 145] on the second Byrd Antarctic Expedition in 1934-35, i.e. shortly after the first soundings on a continental ice sheet had been accomplished in Greenland. More recently, intensive studies have been made in Antarctica and on floating ice islands of the Arctic Ocean.*

* Ref. 50, 52, 53, 156, 178, 180.

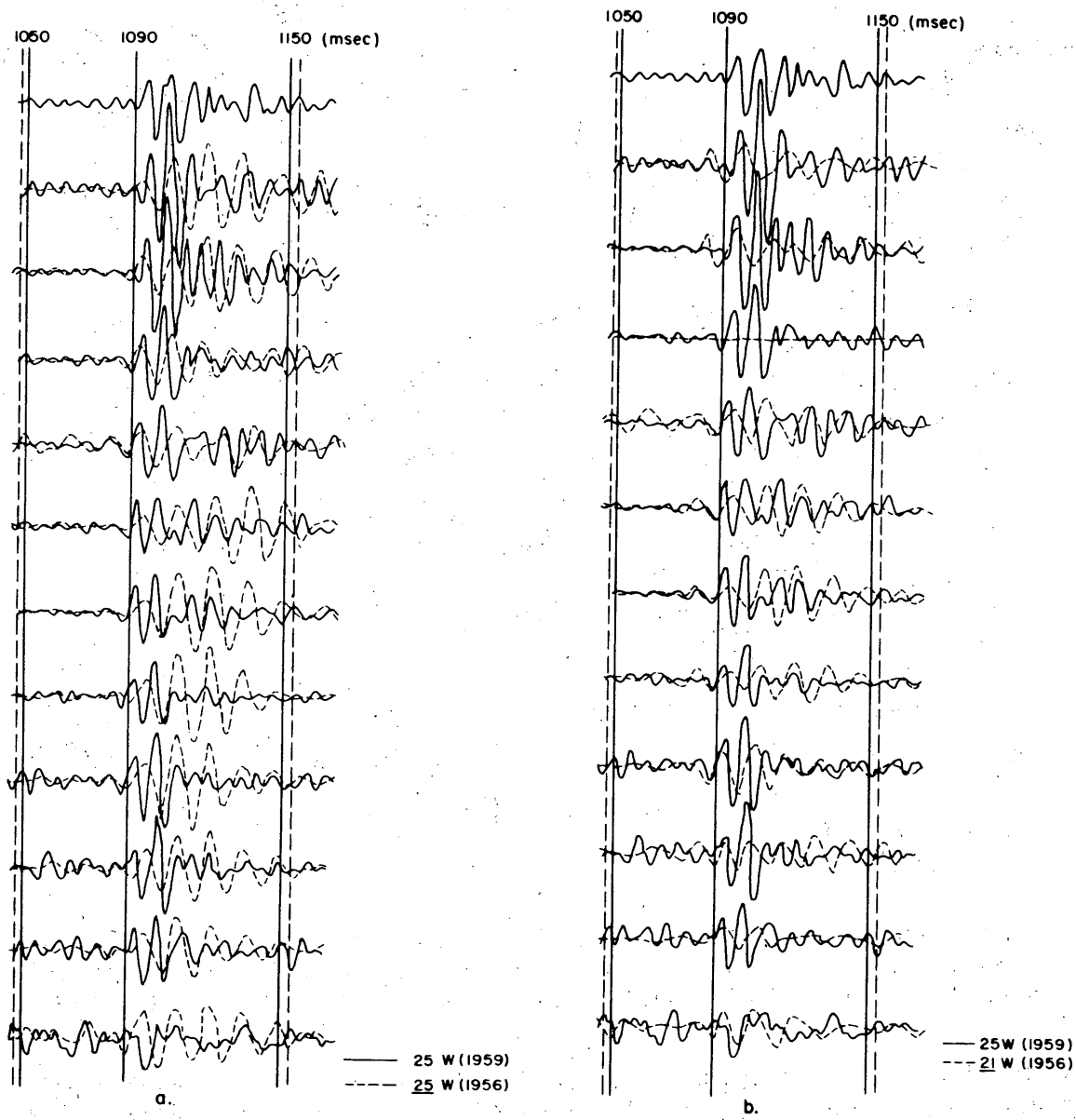

Figure 49. Reflection impulses of two surveys three years apart – a. for identical spreads, b. for adjacent spreads 200 ft apart – matching equally well in both cases. (From Roethlisberger, Bentley and Bennett.[166])

With short spreads Robin[156] obtained a faint echo from the bottom of the ice, which was often missing. However, a strong sea bottom reflection was recorded followed by medium quality echoes from lower interfaces and multiple echoes (Fig. 50). The ice-shelf thickness was determined from the seismic reflections at 180 ± 30 m, compared to 186 ± 5 m given by Schytt from elevation and density. A mean vertical velocity $\overline{V}_P$ = 3760 m/sec was determined from vertical and oblique ocean bottom reflections. (Poulter's very low velocity below sea level, explained by percolation of sea water in the ice, was found to be incorrect by all the later surveys and the deep drilling at Little America; the elaborate evaluation of multiple reflections in a wedge-shaped body therefore can not have been correct.) Cook[48] has been able to determine moderate ice thickness of around

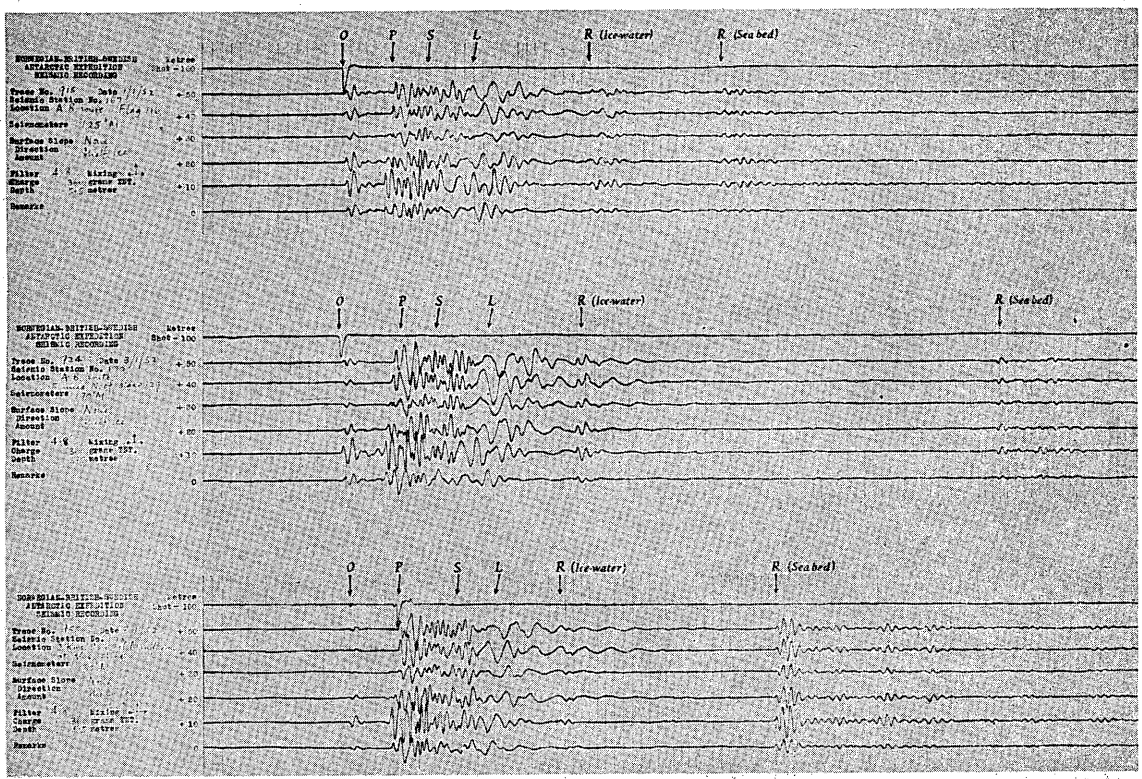

Figure 50. Seismic reflection records for short spreads from ice shelf in Antarctica. (From Holtzscherer and Robin.[91])

50 m by means of reflected *SH* waves (horizontally polarized shear waves) which he produced by placing the charges against a vertical ice wall lined up with the spread.

Crary et al.[53] have worked with a large range of spreads on the Ross Ice Shelf on variable ice thickness from below 100 m to over 700 m and have obtained a large variety of reflected impulses (Fig. 40). Table XIII gives some results obtained by using various methods of depth computation (p. 61-64). Where the comparison with the reliable *P*-reflection is possible, deviations of 30 m in ice depth are common in the methods using waves through water, and some values deviate more than 50 m. The seismic values have also been compared with ice thickness computed from elevation and estimated densities. A systematic deviation towards low seismic values was observed, but it is not certain whether this has a physical meaning or not. Thiel and Behrendt[178] have used independent methods of ice depth determination at the edge of the Filchner Ice Shelf to check the value of *P* and *S* velocities used in the survey from the edge inward. The methods compared were those where the wave travels in ice and water and those where it travels entirely in water.

The seismic reflection method for measuring water depth has also been applied on drifting ice islands on the Arctic Ocean (T-3) [49 50] and on old sea ice.[48 95 197]

Table XIII. Ice and water depths determined by various computation methods from seismic reflections (Ross Ice Shelf). (From Crary et al.[53])

Sta.	Elev. (m)	Ice thickness, various methods PP (m)	PS/SP (m)	$\overline{V}_1$ (m)	$\overline{V}_2$ (m)	M (m)	Final H (m)	Qual. H	Time I_1W_1 (sec)	Water depth (m)	Elev. ocean floor (m)	Dip ocean floor (deg) Amt.	True az.
LAS	43	–	–	–	–	–	257**	Good	0.697	393	-607	N	
1.0	197	415	–	–	–	–	415	Good	(on grounded ice)			1.0	315
2.0	48	367	374	–	–	–	369	Poor	0.354	104	-425	–	
4.0	59	–	–	336	–	–	(384)	Poor	0.557	244	-539	–	
5.0	49	–	328	333	–	–	328	Fair	0.765	416	-695	–	
6.0	51	–	–	344	–	–	344	Poor	0.534	243	-536	–	
7.0	46	–	329	–	–	–	329	Poor	–	–	–	–	
8.0	51	–	354	–	–	383	369	Good	0.917	510	-828	6.5	292^{v}
9.0	53	–	–	361	389	374	375	Good	0.778	407	-729	0.4	305^{v}
10.0	51	–	–	–	–	–	(369)	–	0.465	184	-502	–	
11.0	56	–	384	394	444†	373	384	Good	0.971	543	-871	N	
12.0	59	–	380	464†	404	357	380	Fair	0.714	359	-680	N	
13.0	62	–		366	334	371	363	Fair	1.045	604	-905	0.7	090^{v}
14.0	60	–		354*	409	–	354	Poor	0.574	268	-562	0.8	348^{v}
15.0	57	–		356	364	–	360	Poor	0.591	278	-581	N	
16.0	57	–		331	333	353*	353	Good	0.820	446	-742	N	
17.0	59	–		386	414	371	385	Fair	0.730	369	-695	N	
17.2	58	–		394	–	366	380	Poor	0.733	373	-695	N	
18.0	60	–	384	364	369	376	377	Good	0.736	376	-693	N	
18.2	64	–		389	–	408	398	Poor	0.762	387	-721	N	
19.0	65	–	424'	434	409	409	418	Good	0.764	381	-734	N	
19.2	66	–		403	–	–	403	Poor	0.770	391	-728	N	
20.0	66	–		366	434	408	404	Poor	0.798	411	-749	N	
21.0	73	–	–	442	469	–	456	Fair	0.711	329	-712	N	
22.0	82	553		534	499	519	529	Good	0.698	291	-738	0.9	193^{v}
23.0	96	627*	608'	628	635	620	627	Good	0.646	217	-748	N	
24.0	98	660*		653	735	649	660	Good	0.550	136	-698	0.7	097^{v}
25.0	103	694*	689'	663	695	695	694	Good	0.645	191	-782	0.8	074^{v}
25.1	111	771*		–	–	753	771	Good	0.755	242	-902	–	
26.0	99	681*	666'	697	745	668	681	Good	0.450	56	-638	N	

In *PS/SP* column ' indicates reflection received with vertical geophone orientation. – indicates records made with horizontal orientation but no reflections received.

$\overline{V}_1$ is ice thickness using average velocity in ice plus water obtained by least square of times on 12 longest distance geophones.

$\overline{V}_2$ is ice thickness using average velocity obtained from ΔT across entire record with shots fired at ends of spreads.

M is ice thickness as determined from multiple reflections.

† indicates a value not used in average for *H*.

* indicates that only this value was considered for *H*.

( ) indicates estimate only.

In columns giving dip of ocean floor N denotes negligible dip, less than 0.3°; – denotes that dip information is not available; v denotes dip information available in only one direction.

** Ice thickness at Little America by drilling, Ragle et al.[152]

Valley glaciers

The earliest seismic soundings on ice were carried out with a mechanical seismograph on valley glaciers in the Alps by Mothes in 1926-28[128 129] in preparation for the Wegener expedition to Greenland. Mechanical seismographs were used thereafter on many occasions before electronic equipment became available. Table XIV gives a compilation of the early work in the Alps. Some early soundings have also been carried out in North America in 1934 by Goldthwait,[75] in 1948 by Northwood and Simpson[138] and in 1949 by Poulter, Allen and Miller.[146] The more recent work accomplished in many countries in almost every area where there are glaciers would be too numerous to be listed in detail. A review on Russian work on valley glaciers, mainly during IGY, has been given by Borovinsky.[29]

The seismic reflection method has become a standard tool for glaciological and engineering applications. Figure 51 gives a good example of the results of a detailed survey on a narrow mountain glacier, and Figure 52 illustrates the accuracy of a survey in a case where drilling information became available. The method is quite universally applicable with the exception of very shallow ice less than about 50 m thick as explained above (p. 51) and in the case of particular geometrical configurations such as a glacier which is deeper than half its width. Also a subglacial gorge cut into a wider bed, a case of some importance for tunneling projects under a glacier, cannot be probed. Its existence can nevertheless be excluded if continuous profiling is possible, and conversely the gorge probably exists when no reflections are obtained over a certain area.

Strangely enough, reflection from crevasses seems to interfere little with that from the bed, although bad conditions have been reported. The paths of the direct waves are known to go around the crevasses, from the fact that very low apparent velocities are obtained for short distances, becoming increasingly higher as the shot distance is increased. It must therefore be assumed that

Table XIV. Early seismic soundings on glaciers in the Alps. (After Süsstrunk.[173])

Years	*Glaciers*	*Investigators*
1926-28	Hintereisferner (Austria)	Mothes
1929	Konkordiaplatz-Grand-Aletsch (Switzerland)	Loewe, Mothes, Sorge
1929	Pasterzegletscher (Austria)	Brockamp, Mothes
1932	Glacier du Rhone (Switzerland)	Gerecke, Müller, Jost, Occhslin
1935	Glacier du Rhone (Reflection soundings)(Switzerland)	Kreis
1936-39, 47, 48, 50	Glacier inférieur de l'Aar et Glacier du Finsteraar (Switzerland)	Florin, Jost, Kreis, Renaud, Süsstrunk
1943	Glacier du Morteratsch (Grisons, Switzerland)	Florin, Jost, Kreis, Renaud, Süsstrunk
1946	Glacier de la Plaine-Morte (Switzerland)	Florin, Kreis, Süsstrunk
1947	Grand-Aletsch (transverse profile below Konkordia)	Florin, Süsstrunk
1948	Glacier du Gorner (Switzerland)	Süsstrunk with Florin, Pahud, Renaud and Riva
1948	Glacier du Tsidjiore-Nouve (Valais, Switzerland)	Süsstrunk with Bisig
1949	Glacier du Mont-Collon (Bas-Arolla, Switzerland)	Süsstrunk
1949	Glacier du Z'Mutt (Valais, Switzerland)	Süsstrunk
1949	Bodengletscher (lower part of Gorner)	Süsstrunk
1949-50	Mer de Glace (France)	Süsstrunk

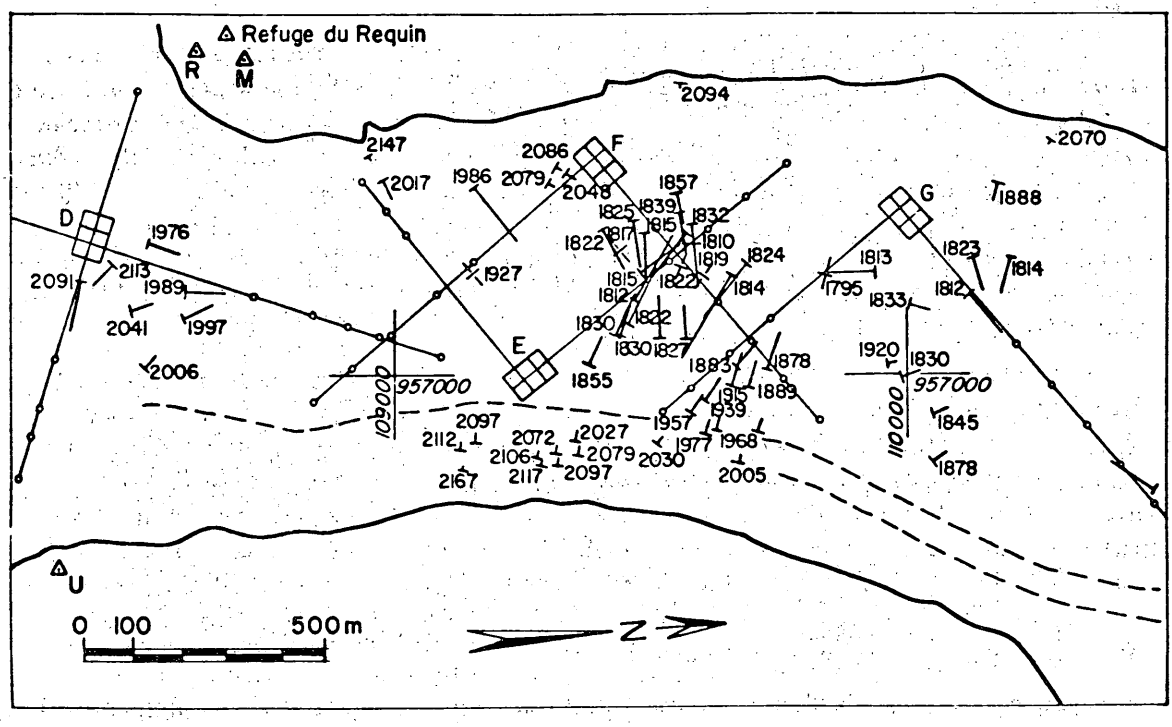

a. *Geophone arrays and shot points at the surface and dip and strike symbols with elevation in meters at the bed.*

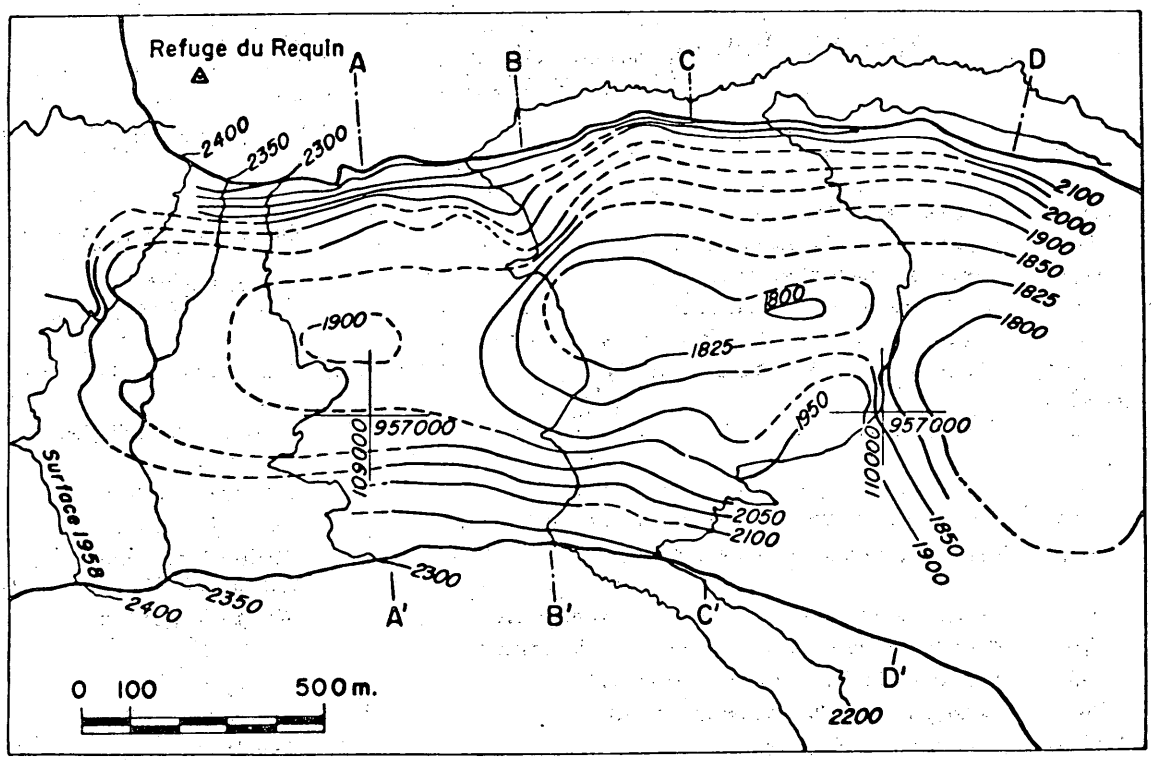

b. *Contour map of the survey area.*

Figure 51. Detailed reflection survey on the Glacier de Tacul, France. (From Vallon[183].)

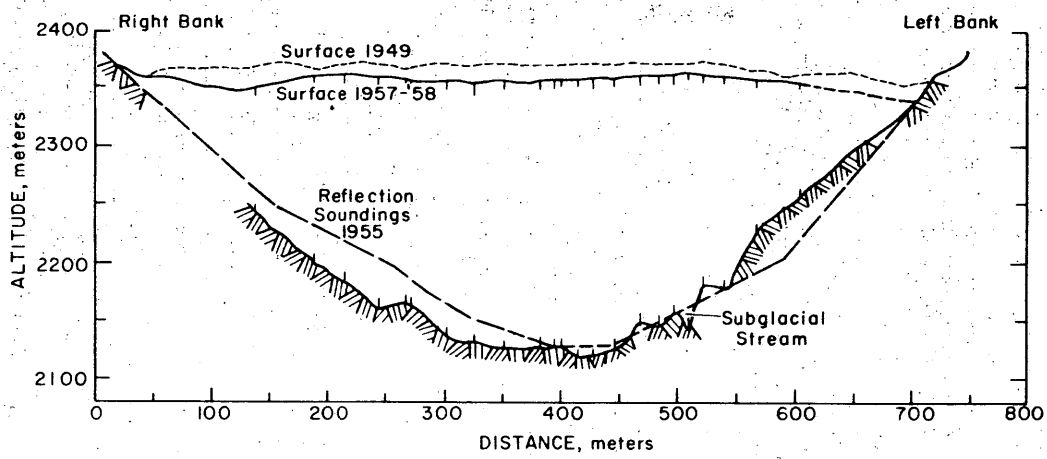

Figure 52. Comparison of cross section of Glacier d'Argentière from seismic reflection soundings and drilling. (From Lliboutry.[120])

the reflected rays are also deflected around the crevasses. This will influence the accuracy of a survey. The character of the impulse would probably be changed, by showing an emergent break, i.e. a first wave cycle of low frequency.

On various occasions in the Alps and in Asia[28] two reflections have been observed on large temperate valley glaciers. The second one must be the reflection from bedrock, the first from a boundary within the ice or from the interface between the bottom of the glacier and a thick layer of glacial outwash and ground moraine. The first reflection is often as strong as the second. It is thus much stronger than the early reflection event which has been reported from certain areas of Antarctica (p. 74), but it is not less controversial. Depending on various conceptions one has of processes in the glacier concerning ice flow, water circulation and sediment transport by water as well as on glaciation history, both explanations of the first reflection sounding—occurring on an intraglacial or on a subglacial boundary—can be more or less supported. Further detailed investigations on the early reflection horizon would seem to present a worthwhile research project. Doell[58] has reported a different type of internal reflection from an area of the Salmon Glacier, B.C. The reflecting surfaces here were found to strike transversely to the flow direction of the glacier, while they appeared to be vertical near the surface and curved to near tangency with the bed at greater depths. Up- and downslope dips were observed with respect to the glacier. Crevasses can be ruled out as an explanation because of the distribution across the glacier and almost all the way from top to bottom, and because of their absence in other parts of the glacier. The shape of the reflecting surfaces may indicate some association with stress conditions. No details on the energy of the internal reflections and whether they occur as first or second reflections are given in the publication.

Reflection Soundings in Frozen Ground

The reflection method is not basically different in its application on frozen ground and on ordinary rock strata, and it is therefore not necessary to describe it. Besides having certain implications for general operations (drilling difficulties!), a frozen surface layer may alter the frequency and particularly ground roll characteristics considerably. This is true for both seasonally frozen ground and thin permafrost. The sounding of frozen ground is an application of special interest in this Monograph but seasonally frozen ground is far too thin to be probed by the reflection method, and so is thin permafrost.

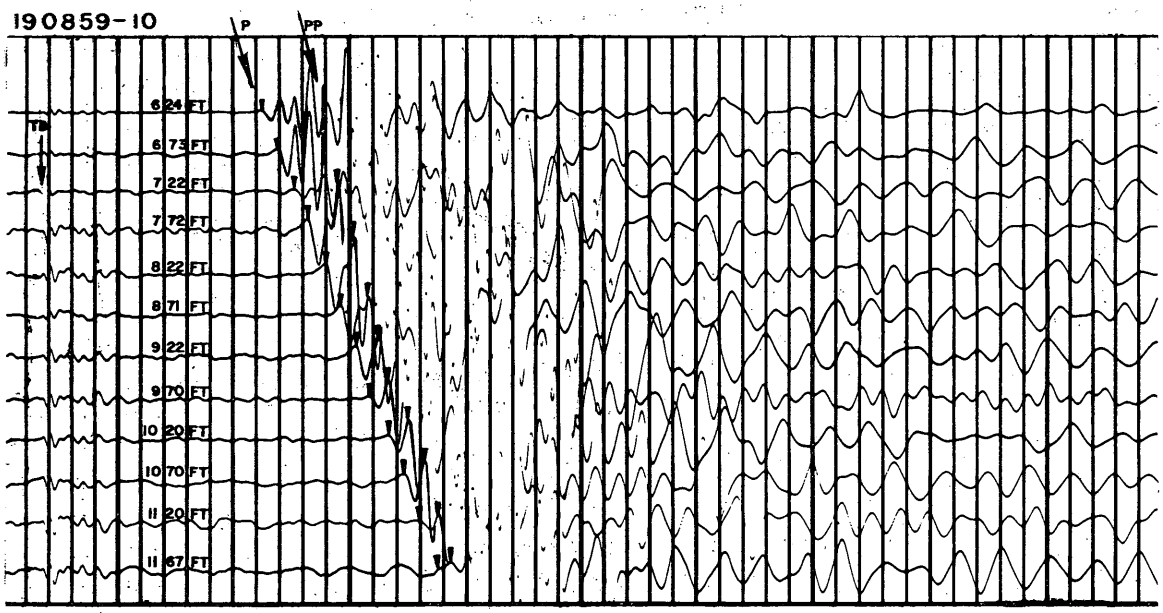

a. Sample record showing wide angle reflection event of higher amplitude than the direct wave in permafrost. Time lines in 5 millisec intervals.

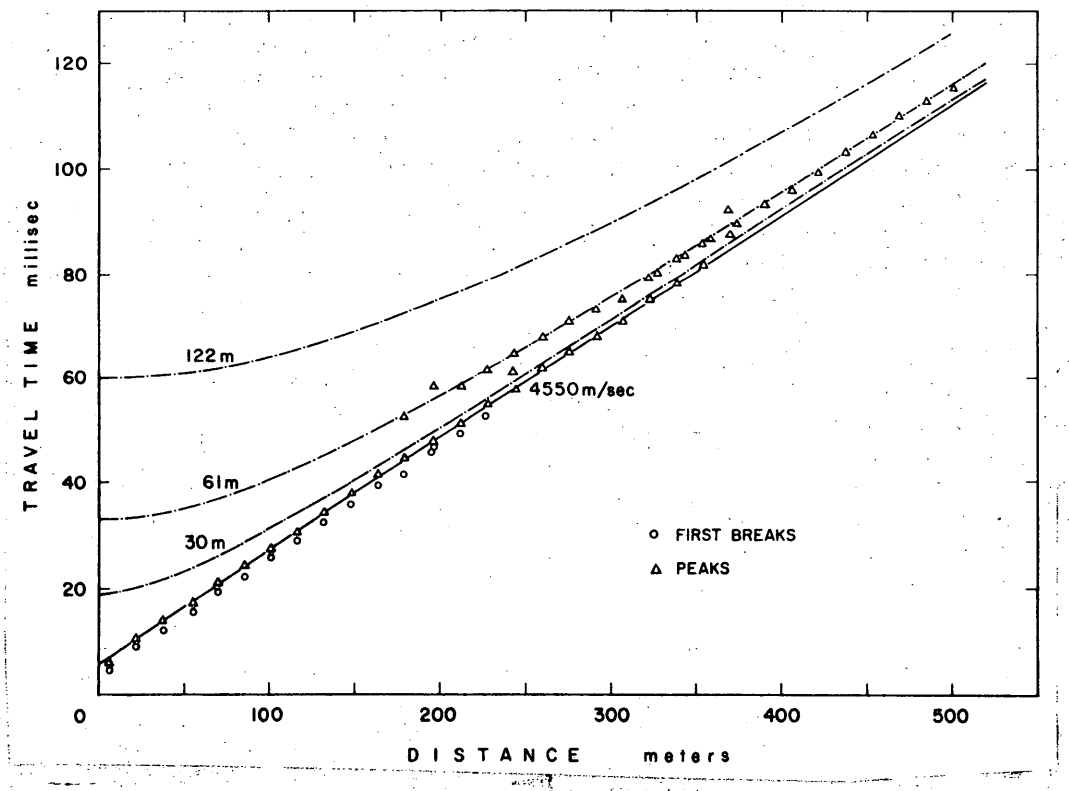

b. Time-distance diagram of wide angle reflection shots. Theoretical curves for the first peaks of reflections from 30, 61 and 122 m are compared with the measured values. The 61-m curve fits the observed travel times closely.

Figure 53. Wide angle reflection shots on a flood plain near Thule, Greenland. (From Roethlisberger.[162])

In thick permafrost the temperature increases with depth below the top layer of seasonal temperature variations, causing the velocity to decrease generally with depth. This situation is rare in temperate areas and is hardly ever as pronounced as in cold regions. From what was outlined above (p. 70) about "defocusing" of the seismic energy in snow where there is an increase of velocity with depth it can be concluded that some benefit should be occasioned by the negative velocity gradient in permafrost, in the way of a focusing effect. The rays are bent downwards, so that more energy is directed towards the deep reflector.

This effect is also felt in the horizontal direction in the opposite sense, the energy being directed away from horizontal transmission. This effect is particularly beneficial for the recording of later arrivals, as further elaborated in the chapter on refraction, but it also has some important bearing on wide angle reflections in permafrost as stated by Roethlisberger.[162] [163] A reflection signal from an extremely shallow interface at a depth of only 60 m was obtained near Thule Air Base. It was observed that the direct wave (shot at the frost table; the thin active layer is neglected) decayed very rapidly with distance, but that a somewhat later event took over with a sharp break and high amplitude (Fig. 53a). When plotting the time-distance curve it was found that the later arrival coincided very nicely with the hyperbola representing reflections at about 60-m depth (Fig. 53b). Results from a previous drill hole were available from this location, showing 62 m of frozen gravel and sand (outwash) over shale, also frozen, with some frozen clay at the top of the shale (Dundas formation). Since the refraction survey had given velocities of 4630 ± 90 m/sec for the outwash and 3960 to 4420 ± 150 m/sec for the Dundas formation (Table XI), the interface is at a discontinuity of high velocity to low, where no horizontally refracted wave occurs. There can therefore be no doubt that the observed event was a reflection. The reverse shot did not show the signal as clearly, however. Further studies with this promising technique are needed.

No successful reflection soundings of the base of the permafrost are known to the author, with the exception of a single questionable reflection by Crowley reported by Barnes.[9] This may be due to an irregular interface and more likely to a gradational velocity change. The best chance to obtain reflections from this interface would undoubtedly be in porous sand or gravel, or in porous sandstone. The wide-angle reflection technique would seem to be the most promising method to be tried.

The change of velocity with temperature is a complication in deep soundings for oil. It causes a time delay in thawed areas that, if not recognized, may cause an erroneous interpretation. The absence of the permafrost where lakes exist or have recently disappeared can in this way produce a relief in the seismic interpretation as large as 100 m.[133] No satisfactory method was found for computing a correction for velocity changes due to changes of permafrost thickness, in a survey in northern Alaska.[194]

REFRACTION SOUNDINGS

Method

The refraction method applied in cold regions is to a large extent the same as in a temperate climate. Only the basic principles will be stated with a little more emphasis on those theoretical details which have a specific application in either glacier work or soundings on frozen ground.

Velocity and depth in homogeneous layers

The theory of refraction is based on Snell's law (eq 44). Both *P*- and *S*-waves should in principle be considered as in the theory of reflection, but in practice the *P*-waves are used almost exclusively. In consequence, only the *P*-waves will be dealt with and V is used for the *P*-wave velocity without the suffix P in this chapter. The waves used are refracted from a low velocity medium into a high velocity medium and back into the low velocity one. The basic condition for the applicability of the refraction method is therefore that the lower-velocity medium must overlie a higher-velocity substratum.

The simplest case is a layer with velocity V_1 of uniform thickness on a substratum with velocity V_2, where $V_1 < V_2$. Of all the reflected and refracted waves one is refracted at the critical angle γ into the lower medium where it travels along the boundary, being continuously refracted back to the surface (Fig. 54). The critical angle is defined by

$$\sin\gamma = \frac{V_1}{V_2} \tag{75}$$

which is readily obtained from eq 44 for $\sin\alpha_2 = 1$. Because of the faster speed in the lower medium, the refracted signal will eventually reach the detector before the direct signal traveling entirely in the low speed upper medium, if the distance between the source and the detector is increased. Plotting the travel time against distance gives a graph of the type shown in Figure 55 for the simple case of Figure 54. The depth h is obtained by the equation

$$h = \frac{x_c}{2}\sqrt{\frac{V_2 - V_1}{V_2 + V_1}} \tag{76a}$$

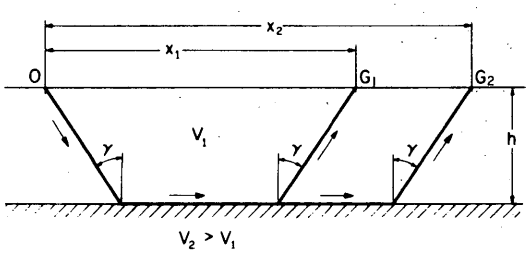

Figure 54. Path of wave refracted at the critical angle.

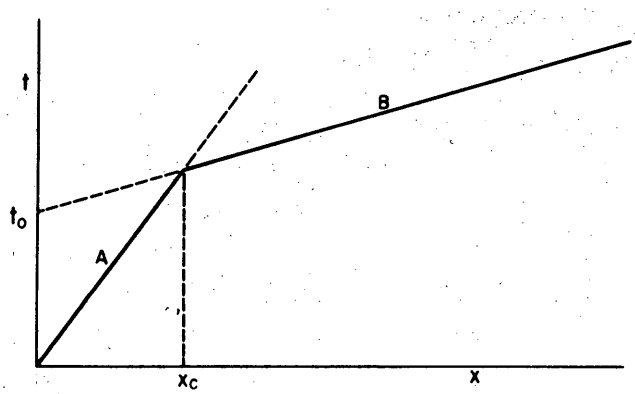

Figure 55. Time-distance diagram of direct (A) and refracted (B) waves.

where x_c is the distance at which the refracted wave overtakes the direct wave (critical distance) found from the break of the travel-time curve (Fig. 55), or from

$$h = \frac{t_0}{2} \frac{V_1 V_2}{\sqrt{V_2^2 - V_1^2}} \tag{76b}$$

where t_0 is the time intercept of the refracted branch of the travel-time curve at $x = 0$. The velocities V_1 and V_2 are found as the inverse slope of the branches A and B of the travel time curve. Equations for two or more layers and for a dipping interface are given in most geophysics textbooks. In the latter case two different apparent velocities are obtained for the refracted wave depending on the direction of the seismic profile relative to the dip; a value larger than V_2 is obtained for the up-dip velocity V_2', a smaller one for the down-dip velocity V_2''. The apparent velocities are given by

$$V_2' = \frac{V_1}{\sin(\gamma - \theta)} \tag{77a}$$

$$V_2'' = \frac{V_1}{\sin(\gamma + \theta)} \tag{77b}$$

where θ is the dip.

Special methods are available for certain typical configurations such as a low velocity surface layer of variable thickness over a high velocity reflector. (The active layer is a good example.) The depths can then be computed in a very simple way with delay-time techniques.[10 176 195] For more complicated configurations of the interface a pointwise interpretation is necessary. After the approximate depths of the different layers have been computed with the standard equations, the interfaces are adjusted section by section to fit all the observed travel time data in both shooting directions, using Snell's law and Huygen's principle. (Each point reached by a wave front may be regarded as a new center of a spherical wave. A new wave front at some later instant is then found as the envelope of all the spherical waves.) This leads to the wave-front methods where the fronts of waves at different time lapses are constructed which originate at the source (shot).[88 181] (See also Fig. 69b.) These methods are particularly appropriate for cold regions because of the ease with which later arrivals may be obtained (p. 100-103).

The refraction method gives more velocity information than the reflection method and therefore serves to identify rock types as well as depth, and to furnish velocities which are used to compute depth from reflections. Robin[156] has made a study of velocities on the Antarctic ice sheet using least-square analysis for the first impulse (first break) and first trough or peak. The standard deviation was slightly less for the first peaks than for the first breaks, and the velocity was slightly larger for the peaks. By plotting residuals it was possible to separate curvature of the time-distance curve from random scatter. Roethlisberger[162] has also used least squares to analyze data collected on frozen ground at Thule, Greenland. By using the time differences between the two directions of shooting rather than travel time it was possible to eliminate the scatter caused by the inhomogeneities at the geophone locations and thereby reduce the standard deviation. This method is particularly useful on frozen ground to eliminate the variations of an active layer which shows negligible dip over the length of the spread.

The refraction method cannot detect layers of lower velocity under high velocity upper layers. When the profile is made long enough that a still deeper layer with a higher velocity than the first

layer will show up, a faulty depth will be computed. Since decreasing velocity with depth is a typical condition of permafrost, the depth figures obtained are likely to be too high and must be used with caution.

The velocities in frozen materials are generally high, and velocity differences between contiguous layers of frozen materials are usually quite small. This is the reason that very long refraction profiles are necessary to obtain the refracted impulses as first events. This inconvenience is partly compensated by the possibility of obtaining later arrivals, which shows that equipment giving the full display of the waves registered by the geophones is superior to mere timing of the first inpulse. Because some equipment has a limited recording time when using Polaroid film for recording it may be interesting to ask what ultimate depth can be obtained by such equipment. On a glacier maximum ice thickness of about 100 to 200 m can be reached with equipment having 0.3 sec as a time limit, depending on the type of bedrock.

Anisotropy, whether by preferred crystallographic orientation in ice or layering of frozen ground, may have to be taken into account. Snell's law has in this case to be modified to accommodate the wave normal instead of the ray, as pointed out for the case of *PS* reflections (p. 65). The subject has been treated in detail by Gassmann.[70]

The velocity obtained from travel-time curves can depend on the wavelength, more precisely on the ratio of wavelength to layer thickness. Thyssen[182] has discussed this question for the case of glaciers and has given the empirical correction of

$$\Delta V = 0.5\, e^{-9\times10^{-5} fh} \quad \text{(km/sec)} \tag{78}$$

where f = frequency, h = ice thickness; the correction has to be added to the observed velocity to obtain the true body wave velocity. The correction in this form is not well founded if the travel times are taken from first breaks, except for long distances many times the ice thickness. The problem is similar to that of body waves in slender bars (p. 8), but more complicated because of the solid/solid interface at the bottom of the ice layer. The distances to which the front of the body wave can be detected should be even larger than in the case of rods or prisms. In practice the travel-time curves are often affected at short distances by a crevassed or porous surface layer, so that the velocity determination may be based on rather long distances. This is probably the main reason for the dependency of velocity on frequency found by Thyssen. His geometry factor should not be applied rigidly to cases where the surface ice is sound, and particularly when the travel-time curve is a straight line through the origin.

Continuous velocity increase with depth

A continuous velocity increase with depth is a typical condition for sedimentary deposits, where the deepest layers are the most compacted ones because of highest overburden and the best cemented ones because they are the oldest. The subject is therefore amply treated in the geophysical literature. It is nevertheless presented here in some detail because of its great importance on continental ice sheets, shelves and the accumulation area (névé fields) of mountain glaciers, where a pronounced gradual velocity increase exists in the snow and low density ice.

A medium is considered where the velocity increases in the direction perpendicular to the surface, which may for convenience be assumed to be horizontal. It is further assumed that no changes occur in the horizontal direction. The vertical direction is therefore an axis of rotational symmetry (uniaxial inhomogeneity). Only the vertical rays are straight in such a material; all other rays are curved. The rays from the source to the receiver follow the path of minimum time, which is a curve concave towards the surface. They will reach greater depths as the distance between source

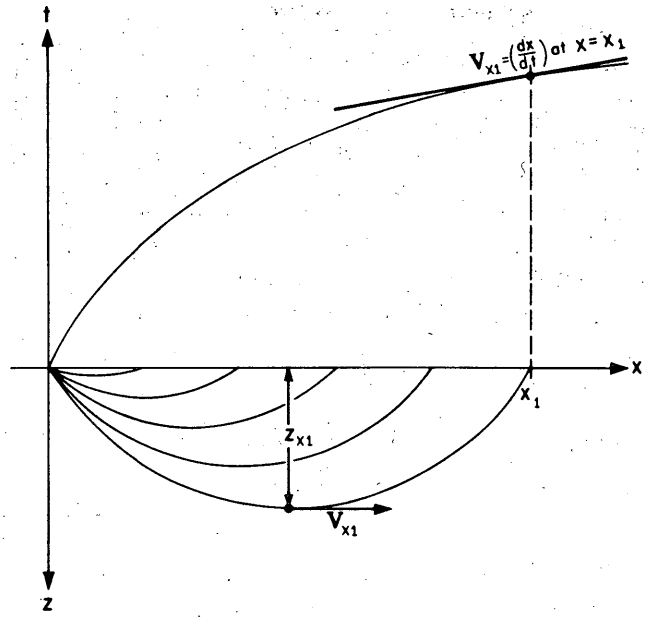

Figure 56. Travel time curve and paths when the velocity increases with depth.

and receiver increases (Fig. 56). The travel-time curve is convex in the direction of the time axis, and the inverse slope of the curve at distance x_1 gives the velocity V_{x1} at maximum penetration z_{x1}. The basic formula relating the apparent horizontal velocity, as received at the surface, to the depth of penetration of the seismic wave was derived in the early part of the century through the contributions of several authors, mainly Wiechert, Herglotz, Bateman and Slichter:

$$z_{x1} = -\frac{1}{\pi}\int_{x=0}^{x=x1} \cosh^{-1}\frac{V_{x1}}{V_x}\,dx \qquad (79)$$

where V_x is the apparent horizontal velocity given by the inverse slope of the travel-time curve as a function of the distance x. By numerical integration of eq 79 for variable x_1, the function $V(z)$ is evaluated. It is clear that errors result when the condition of continuous velocity increase is not fulfilled, i.e., where intermediate low velocity layers are present. But this is not the only case where complications may be encountered. A marked increase in velocity followed by a smaller though still positive increase can cause triplication in the travel-time curve which cannot be identified correctly by first arrivals alone. This is true for P and S curves. Crary et al.[53] estimate that the errors caused by this type of complication in the surface snow layers of Antarctica, in assigning depths to the recorded velocities, do not exceed 1 meter.

The apparent horizontal velocity vs distance function is obtained from the travel-time curve. There are several ways to proceed. The graphical determination of the slope of the travel-time curve $1/V$ is one way. At greater distances, where the curvature becomes small, a least squares method has also been used, giving a mean velocity for sections of 12 to 24 geophones. A computer program based on running means with a control that the velocity does not decrease with increasing distance is another alternative.

Equation 79 is valid for shot points at the surface. Corrections on the travel-time curve therefore have to be made when the depth of the shot point cannot be neglected. This problem is treated in some textbooks and in more detail by Pratt[150] and Brockamp and Pistor.[37] The same methods apply when use is made of a reference horizon (datum plane) below the surface layer of variable velocity (weathering layer), either in the analysis of reflection or refraction data. An alternative to numerical methods is the construction of a wave-front and ray-path diagram as shown by Redpath.[153]

A linear increase of velocity with depth is sometimes used as an approximation in place of the empirical relationship. The velocity V_z is given by eq 62a:

$$V_z = V_0 + kz$$

where V_0 is the velocity at the surface. The penetration depth for a shot-to-detector distance x is

$$z_x = \frac{V_0}{k} \left[\sqrt{1 + (kx/2V_0)^2} - 1\right]. \tag{80}$$

Combining eq 62a and 80 gives

$$V_2^2 = V_x^2 = V_0^2 + \tfrac{1}{4} k^2 x^2 . \tag{81}$$

This is the equation of a straight line in the V_x^2 versus x^2 diagram with the slope $k^2/4$ and ordinate V_0^2 at $x = 0$. A standard least-squares procedure is applicable to find the coefficients.

Clarke[45] has used one surface layer of linear velocity increase with depth ("firn") followed by ice with constant velocity, on the Greenland ice sheet. Although the approximation of velocity vs depth looks crude (Fig. 38a), the vertical travel time $t(z)$ versus depth from least-squares analysis fits that derived by numerical integration very nicely (Fig. 38b). Clarke's method is therefore very efficient for using refraction data to make surface layer corrections in reflection work. Crary et al.[53] have approximated the depth-velocity curve more closely by computing sections of linear velocity increase at 5-m increments in Antarctica. The vertical travel time in a layer from depth z_1 to z_2 is (see eq. 63)

$$t \Big|_{z_1}^{z_2} = \int_{z_1}^{z_2} \frac{dz}{V} = \frac{z_2 - z_1}{V_2 - V_1} \ln \frac{V_2}{V_1}. \tag{82}$$

A very good approximation of longer sections of the empirical depth-velocity curve has been achieved by Brockamp and Pistor[37] with an exponential expression and a power function. The exponential expression is given by

$$V(z) = a - b \cdot e^{-cz} . \tag{83a}$$

The coefficients b and c are found from a $\ln(dV/dz)$ versus z plot (Fig. 57a), then a is determined to give a best fit of $V(z)$. Two sets of the coefficients a, b, c were found to be sufficient for the complete depth-velocity curve on the Greenland ice sheet (Fig. 57a, b). The power function

$$V(z) = \alpha z^{\beta} \tag{83b}$$

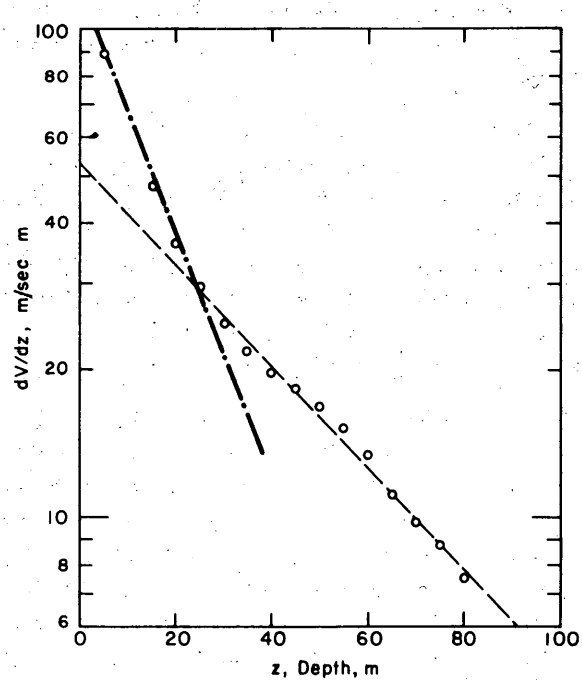

a. *Log plot of* dV/dz *versus z.*

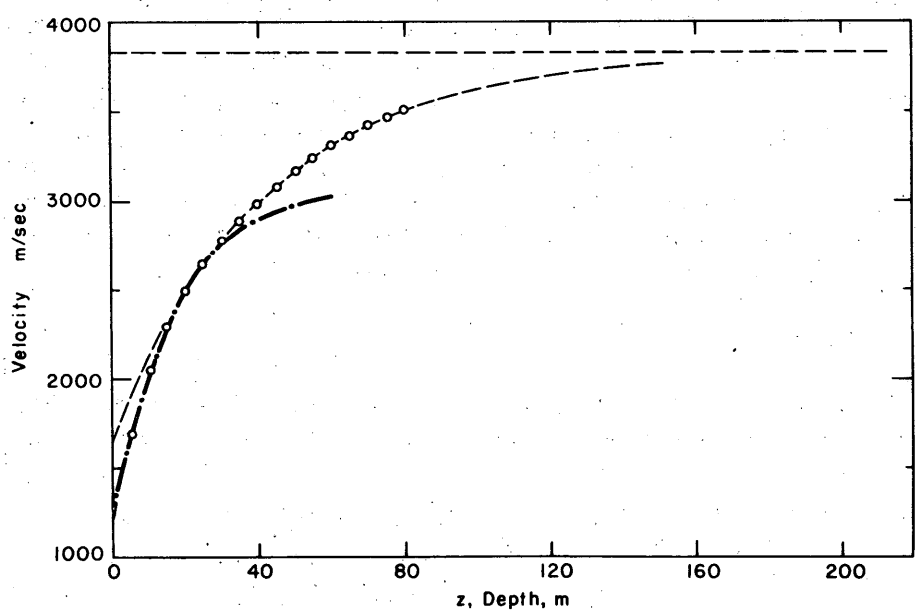

b. Approximation of observed velocities with two sectors of exponential curves.

Figure 57. Empirical-depth-velocity curve. (From Brockamp and Pistor.[57])

was found to be adequate for the depth range from 2.5 to 80 m in a number of cases, with β around 0.25 to 0.3. (A similar power function with $\beta = 1/6$ incidentally gives the velocity increase with depth for regularly packed spheres.)

Errors of $V(z)$ obtained from refraction have been determined from comparison with up-hole time; on the Ross Ice Shelf the computed time was from 0.8 to 2.1 millisec larger than the measured up-hole time. Robin[156] has estimated that the error, when using eq 79 for numerical integration, was about 5% in depth z, but less for $V(z)$ for a given z. He has also pointed out that a systematic error is to be expected for shallow depths, the reason being that, when the wavelength is large compared with the depth of penetration, a decrease in the velocity of the waves compared with that in an infinite medium must be expected. Probably a more significant source of systematic error is the strong anisotropy in the surface layer reported by Bennett.[19]

The problem of anisotropy is no easy matter. Only the simple ellipsoidal case will be considered briefly where the wave surface (and also the index surface) is an ellipsoid of revolution, and the axis of revolution is vertical. Too large values of z_x are obtained with the isotropic formulas (eq 79) if the velocity is larger in the horizontal than in the vertical direction. This is obvious from consideration of refraction at the base of a single homogeneous anisotropic layer, which must be thinner if the travel time is the same as in an isotropic layer, a statement which also holds if the uniaxially inhomogeneous mass is approached by an infinite number of homogeneous layers. Likewise, too small values of z_x are obtained if the velocity is larger in the vertical than in the horizontal direction. In the case of linear increase of velocity with depth and constant ratio of $V_{(H)}/V_{(V)}$ the rays are sections of ellipses instead of sections of circles as in the isotropic case.[71]

When the refracted wave reaches the surface it is reflected to follow a path similar to that which it has traveled before. A multitude of refracted waves is therefore traveling between two surface points A and B (Fig. 58). $P = P_1$ is not reflected except at the end point and arrives first. $PP = P_2$ is reflected once at the mid-point C, $PPP = P_3$ twice at 1/3 of the distance AB, etc. The surface reflected waves are also referred to as multiply reflected or as multiply refracted, undergoing repeated reflections at the surface. A seismic record showing typical surface reflections is given in Figure 59. Multiple surface reflections have an application when for some reason the time break is missing at large distances (Bentley et al.[20]). The time difference between the multiple reflection arrival P_n and the first arrival P_1 at the distance D serves to find the travel time of the latter if the travel-time curve is known to the distance D/n. It is

$$t_D = n t_{D/n} - \delta_n \tag{84}$$

where δ_n is the time difference between P_1 and P_n, which may be determined either from first breaks or later corresponding peaks. No phase reversal appears to take place in spite of the surface reflections (Fig. 59).

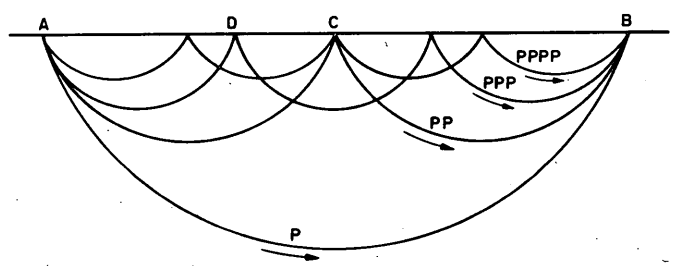

Figure 58. Paths of surface reflected waves. (From Robin.[156])

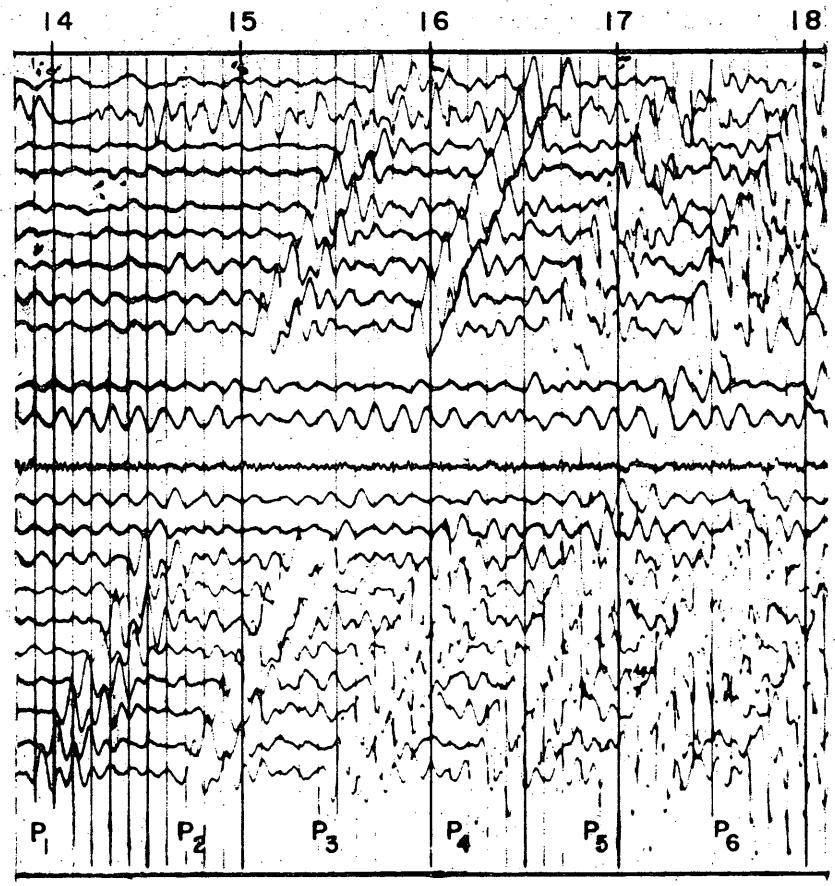

Figure 59. Section of a refraction record showing surface reflected waves P_n *(Antarctica). (From Crary.*[54]*)*

It is further worth noting that P_n makes it possible to measure the velocity at maximum penetration with considerable accuracy from one shot, since for large enough distance where the travel-time curve is straight, and for small enough n, $\delta_{n+1} - \delta_n$ is the time intercept of the straight travel-time line, whereas the various P_n give a number of points on that line.[23]

Velocity decrease with depth

A decrease of velocity with depth is typical in permafrost below a certain depth because of the increasing temperature, and for the same reason it also exists in large cold glaciers, especially ice sheets and ice shelves. Only the velocity at the top of the layer of decreasing velocity can be obtained by refraction. The average velocity for depth computations of deeper layers is uncertain and has to be obtained by other means (wide-angle reflection profiles or well-logging) or estimated from the temperature gradient and the nature of the strata. A complication when using the temperature gradient in frozen ground is that saturation may change along with temperature.[175]

Depending on the thickness of the zone of maximum velocity below the frost table, in relation to the wavelength, the refracted wave in the permafrost decays very rapidly with distance. This wave arrives first except for the direct wave through the active layer at very short distances and deeper refractions at much greater distances. Because of the rapid decay of the permafrost wave the signals of deeper refractions can be obtained easily as later arrivals, a condition hardly

ever experienced in temperate regions (Fig. 53a, 69). For continuous profiling of depth measurements of the active layer this rapid decay of the refracted wave in permafrost is less favorable, reducing the length of applicable spreads. The question of rapid decay of the permafrost wave has also been discussed in some early Russian literature. Riznichenko[154] tries to prove that no "shadow" zone is to be expected, because of the surface-reflected waves traveling entirely above the velocity inversion, but does not take into account that there is a difference between first arrivals and vibrations in general. It may well be that the strong surface-reflected waves he predicts because of the ducting effect of the low velocity surface layer exist if the active layer (plus warm surface layer of the permafrost) is thick compared with the wavelength, but is absent when the active layer is thin. The velocity in the active layer being very low, conditions for refraction work will still be very favorable even if the "direct" (active layer) wave does not decay rapidly with distance.

Energy of refracted waves

Only some specific problems will be discussed without going into the basic theory for which the pertinent geophysical literature has to be consulted.

A case of some interest is a thin high velocity layer embedded in low velocity material. An isolated ice layer in snow or a thin layer of frozen ground fits this model. The rule in such a case is that a refracted wave can be registered when the thickness is at least $\lambda/6$ where λ is the wavelength in the high velocity layer.[115]

A specific problem of importance in glacier work is how the energy is distributed in the surface layer of snow and low density ice where the velocity increases with depth (see also p. 66). It has been treated in detail by Robin.[156] He has analyzed the variation of energy of refracted waves with distance in theory and experiment using his own data from Queen Maud Land, Antarctica, and data of the French expeditions to central Greenland. The energy E_x per unit surface area at distance x from the shot is

$$E_x = \frac{I_0'}{x} \frac{V_0^2}{V_x^3} \frac{1}{\sqrt{1-(V_0/V_x)^2}} \frac{dV_x}{dx} \tag{85a}$$

where I_0' is the initial energy per unit solid angle as in eq 18 and 72, V_0 the velocity at the surface and V_x the velocity at maximum penetration (which is equal to the velocity at distance x). Good results were obtained with this equation at distances from 100 to 1500 m, but not in all cases. The curvature of the earth, or more generally of the surface, has to be taken into account at larger distances:

$$E_x = \frac{I_0'}{x} \left\{ \frac{1}{[(V_0/V_x) - (x/2R)]^2} - 1 \right\}^{-1/2} \left(\frac{V_0}{V_x^2} \frac{dV_x}{dx} + \frac{1}{2R} \right) \tag{85b}$$

where R = curvature of the surface. From this formula and allowing for attenuation, Robin has computed the curve given in Figure 60. Extrapolating from the experience of the French party in Greenland, who used 20 kg of explosive at 9.4 km, 200 kg would be needed at 12.4 km and 2000 kg at 15.7 km, which indicates that there is a limit for the application of the refraction method. Results have nevertheless been obtained to larger distances with far less explosive than indicated by Robin's theoretical considerations, his attenuation figures being too large as pointed out

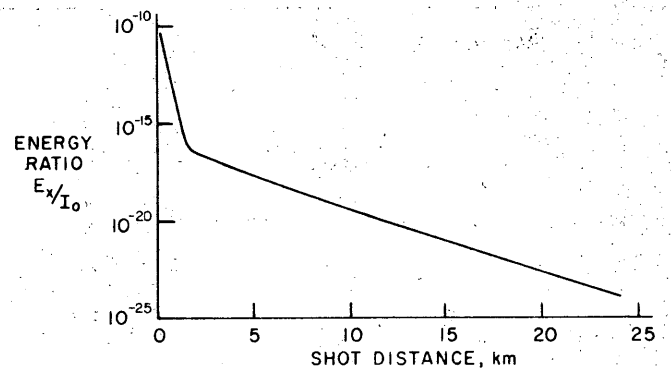

Figure 60. Energy of the refracted wave on a continental ice sheet as a function of distance from the shot. (From Robin.[156])

elsewhere (p. 39). Robinson[158] has carried out a similar study with the recent data from Antarctica and has obtained practically no attenuation, contrary to Robin.

The energy of the surface-reflected waves P_n has also been discussed. Bentley et al.[20] and Robinson[158] have shown how the amplitude at first increases with the number of multiple reflections and then decreases. Robin[156] has discussed attenuation and reflection losses and has tried to explain why under certain conditions the very strong surface noise experienced in Antarctica may develop.

Applications

Glaciers

Although the refraction method can in principle be used for depth soundings, it has only occasionally been applied on glaciers, because the reflection method is faster, more accurate and requires less explosive when it works, i.e. when the ice is thick enough. Refraction soundings for the mere purpose of obtaining ice depth are limited therefore in practice to shallow ice, particularly on névé fields, and may also be the solution on somewhat thicker ice when only low frequency equipment is available. In the very early work on glaciers[30 31 72] the basic phenomenon of refraction was of interest, and it had first to be established that the principles of geometrical optics were applicable to elastic waves. It is noteworthy that Gerecke and Müller[72] have identified refracted S-waves with their mechanical seismograph.

The most extensive refraction work was accomplished on various Austrian glaciers by a Munich group with Förtsch being the chief investigator.[62 63 64 65 73] Refraction lines up to about 1 km in length were arranged along the main axes of the glaciers and on a few cross sections. On the Hintereisferner the *P*-wave velocity below the equilibrium line (firn line) varied between 3500 and 3850 m/sec with a mean of 3680 m/sec, the *S*-wave velocity between 1600 and 1925 m/sec, with a mean of 1730 m/sec; Poisson's ratio, based on mean V_P and V_S, was 0.36. The depths, reaching maximum values of around 200 m, were computed partly from reflections at the near geophone stations, but mainly by the refraction method (wave-front method) along the line. The results have been presented in longitudinal and cross sections. A thick intermediate layer is quite consistently shown with velocities V_P between 4000 and 5000 m/sec followed by bedrock showing velocities higher than 5000 m/sec.

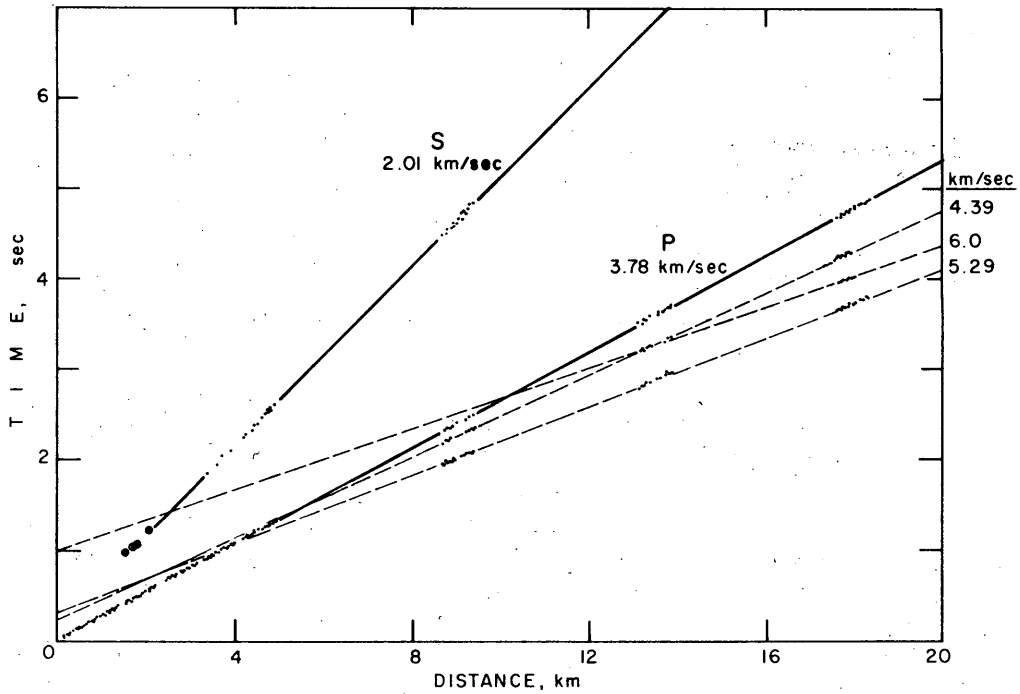

Figure 61. Long refraction travel-time graph from the Antarctic Peninsula. Arrival times are corrected for elevation and topography. (From Behrendt.[13])

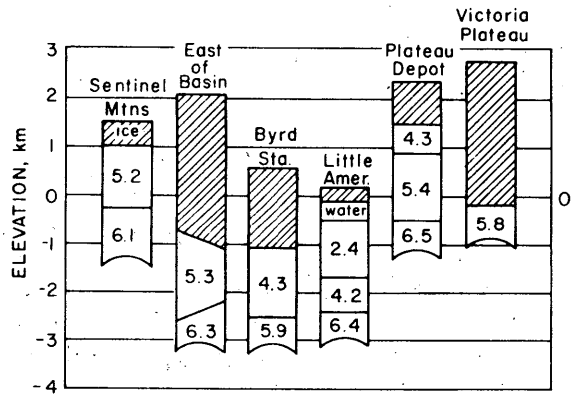

Figure 62. Velocity columns in Antarctica from refraction soundings. (From Bentley.[23])

The intermediate layer was first interpreted as frozen ground-moraine, but it is questionable whether the seismic events were properly identified to begin with. No *PS/SP* arrivals were reported by the authors, so that one may suspect that they interpreted this type of reflection signal erroneously as a refraction event. Berzon et al.[27] have reported V_P = 3500 m/sec for moraine from Tuyuksu glacier in an environment where permafrost would be more likely to be found than in the Alps. As to the subsequent interpretation as a densely packed moraine this view is equally difficult to accept because no one else has reported comparable velocities in loose materials. The question of an intermediate layer at the glacier bed deserves further investigation, since a second reflection which has occasionally been observed on temperate valley glaciers lacks a satisfactory explanation (p. 81).

The above discussion already shows that the refraction method has a much wider application than for ice depth measurements alone, since it allows investigation of the sub-bottom structure of a glacier. This can be done on a small scale, as was demonstrated at the margin of the Greenland ice sheet (Fig. 69), or on a large scale in the middle of continental ice sheets. In Greenland, Joset and Holtzscherer[102] have picked up three refracted signals under 1370 m of snow and ice giving information on the thickness of two and the velocity in three sub-bottom layers. As many layers have been identified by Behrendt[12,13] on the Arctic Peninsula (Fig. 61); Figure 62 summarizes

further results from long refraction studies in Antarctica. Although it is not possible to identify the rock types directly from the velocity, it has usually been possible to get a fairly good idea by taking the nearest outcrops and data from magnetic surveys into account as well as the reflection coefficient if available from reflection soundings (Brockamp[36]). A velocity between 4 and 5 km/sec has been found in some places directly under the ice. If this layer is thin it may consist of ground moraine which is frozen, or it might be sedimentary rock, basalt or gneiss.[12 36 102] Bentley et al.[20] have obtained an ice thickness of 1820 m at Site II on the Greenland ice sheet by reflection and 1930 m by refraction, which they explain by an intermediate layer of about 100 m thickness (depending on its velocity) (p. 73).

By extensive wide-angle reflection-shooting it was shown in the above case (Site II) and by Behrendt[12] for the Antarctic Peninsula that anisotropy of the deeper ice layers may be neglected, but Bentley[25] has shown that anisotropy effects are far more common than expected before. They should be taken into account in refraction soundings, which are more sensitive to errors in the velocity than reflection soundings.

Refraction soundings have most frequently been applied in polar glaciology to investigate snow and ice layers near the surface in areas of net accumulation, where there is a gradual increase of velocity with depth. The primary result of the refraction survey is the velocity vs depth relationship, which is needed for the reflection soundings. A summary of results from a number of places is given in Figure 63a, b. The velocity increases with depth at a diminishing rate (with the exception of the semi-temperate Hubbard Glacier) to reach the maximum at a depth of 40 to over 200 m. The distance at the surface is plotted against depth of penetration of the curved paths in Figure 64, which gives an idea of the length of refraction lines needed to reach a certain depth. The velocity at the depth of maximum penetration can be determined with very high precision with sufficiently long refraction lines, and since it could be shown that in the majority of cases the anisotropy is weak at this depth[19 23 25] the maximum velocity depends on temperature only. Seismic refraction results therefore yield temperature information at the depth of maximum penetration (eq 39). It should be noted that this is true for the *P*-wave only; the *S*-wave velocity is much more affected by the weak anisotropy present in the layer in question (Fig. 65).

Because of the close correlation of velocity with density (Fig. 17) the depth-density relationship can be extracted fairly accurately from the depth-velocity results. Temperature differences may be allowed for by using the temperature coefficient $(1 - 0.00061\Delta T)$ of eq 39. A refraction survey can thereby replace pit studies and core drilling as far as average density increase with depth is concerned, but not for studies of stratigraphy. The density at a certain depth depends, among other factors, on temperature and accumulation rate. If these two were the predominant factors it should be possible to infer the accumulation rate from known depth-density data and temperature; and because of the close correlation of density and velocity, it should then also be possible to obtain accumulation rates directly from velocity information and temperature. For equal accumulation rates the velocities at a given depth should decrease with decreasing temperature, and for a fixed temperature the velocities should increase with decreasing accumulation rate. This is to be expected because the snow will be more compacted at higher temperatures, because the rate of densification is high, or at lower accumulation rates, because it takes longer for the snow to reach the fixed depth. In Figure 66 observed velocities at the 50-m level below the surface are plotted against temperature, and accumulation rates are stated in g/cm^2 yr where known. A set of equidistant straight lines has been drawn representing lines of equal accumulation, to fit reliable data near the periphery of the group of points, and using a geometric progression for the accumulation intervals, following Gow[79] in his analysis of temperature and accumulation for

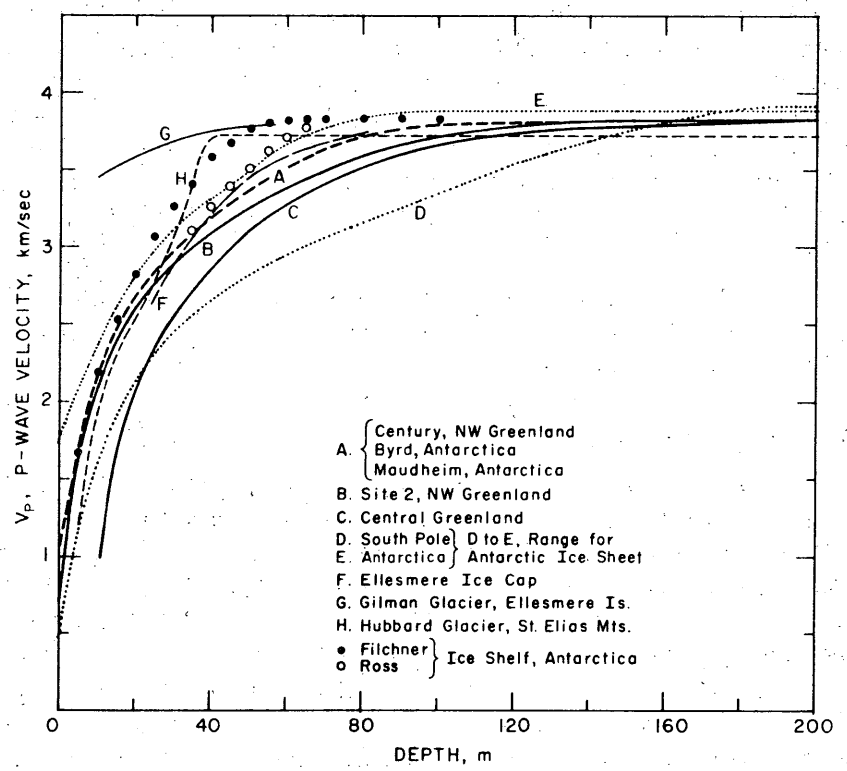

a. P-velocity as a function of depth on continental ice sheets, ice shelves and glaciers. (After Behrendt,[13] Bentley et al.,[20] Clarke,[44] Crary,[54] Robin,[156] Thiel and Ostenso,[180] Weber and Sandstrom,[186] Weihaupt.[190])

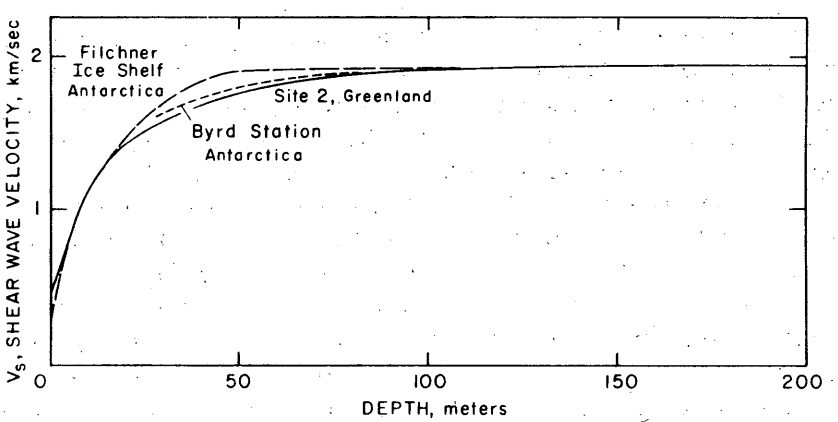

b. Shear wave velocity as a function of depth on the Greenland and Antarctic ice sheets (Bentley et al.,[20] Bennett[19]) and Filchner ice shelf (Thiel and Behrendt.[178])

Figure 63. Wave velocity as a function of depth.

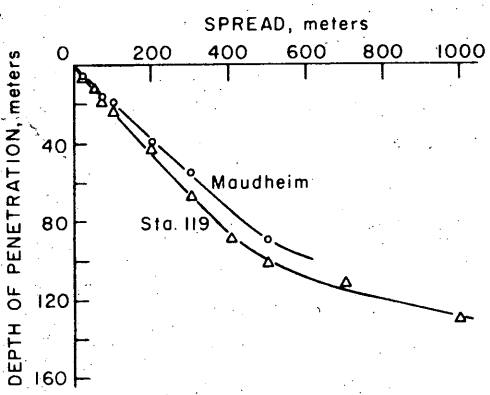

Figure 64. Depth of penetration of P waves as a function of shot point to seismometer distance in two locations in Antarctica. (From Robin.[156])

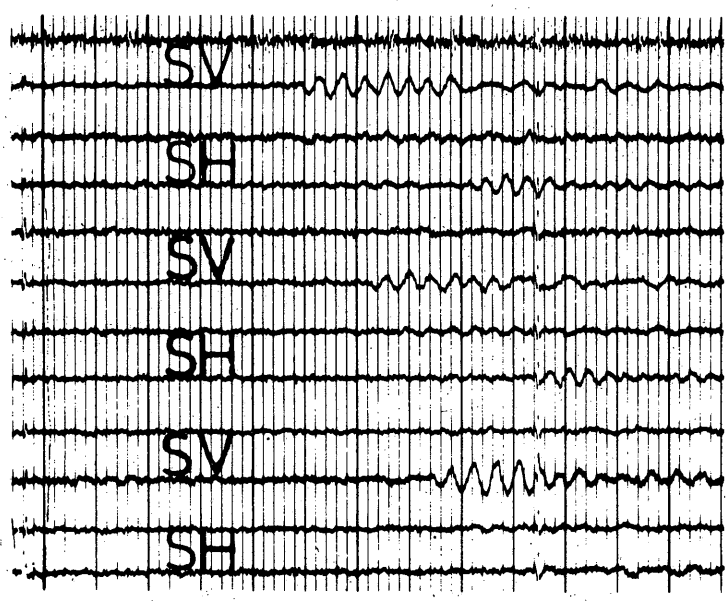

Figure 65. Section of a refraction seismogram from Byrd Station showing different polarized shear waves. Total travel time about 6.6 sec. The charge was 135 kg at 12.5 km. Timing lines are 0.01 sec apart. (From Bentley.[23])

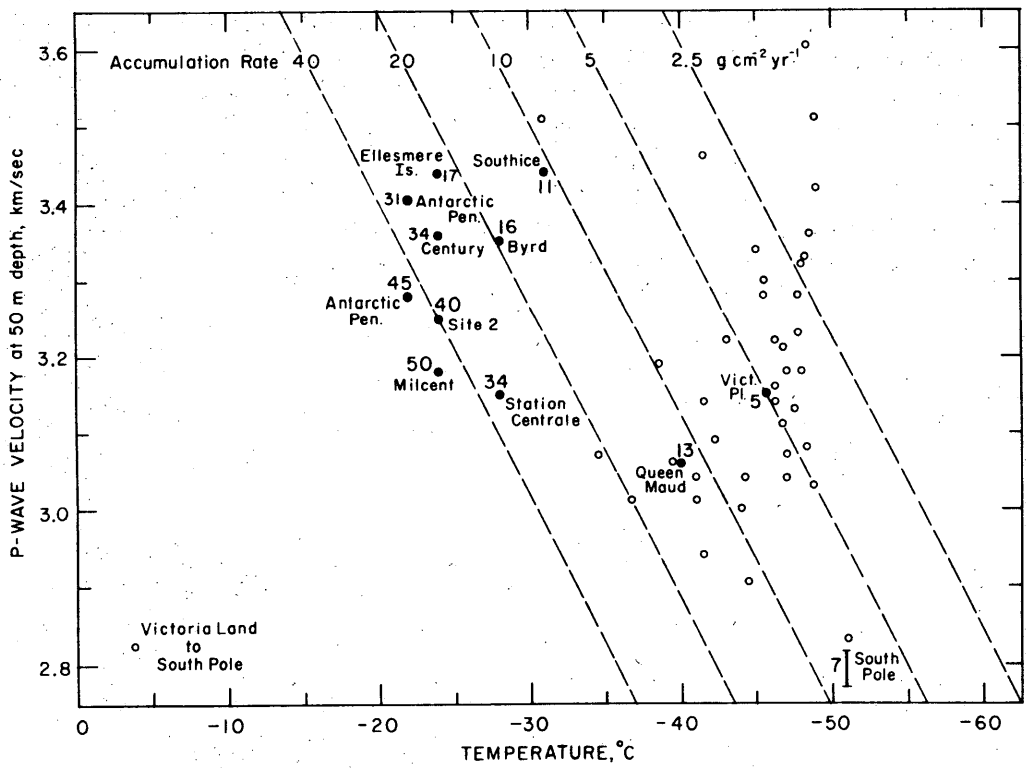

Figure 66. P-wave velocity in snow (ice) at the depth of 50 m as a function of mean annual temperature.

the three locations with similar depth-density profiles, namely Southice, Byrd Station and Camp Century. A temperature difference of 6.5°C was obtained in this way to correspond with an accumulation factor of 2, as compared to 4°C given by Gow. The suspected general relationship between velocity, temperature and accumulation rate is confirmed by the graph, but if the nomogram is used for extracting accumulation rates from known velocity at 50-m depth the accuracy is not very high in some cases. The wide scatter of the results from the Victoria Land Plateau in Antarctica is somewhat discomforting, but may in fact reflect a large variation of accumulation rates depending on local surface topography as shown by Gow and Rowland[78] for the Byrd Station area. Original density differences, dependency of the densification process on original snow structures, and horizontal strains may further help to explain the large scatter. Although the mean horizontal strains on the Victoria Land Plateau are very small (Crary,[54] Table 15), larger strains may occur in relation to the surface undulations; but also relatively large accumulated strains are to be expected even at very small strain rates when the accumulation rate is very small, due to the old age of the deeper snow layers. The nomogram of Figure 66 can be expressed by

$$V_{z=50} = 5460 + 38.2\,T - 809 \log_{10} a \qquad \text{(m/sec)} \qquad (86)$$

where T = temperature in °C, and a = accumulation rate in g/cm² yr. The coefficients of this equation should be reevaluated by a least-squares analysis based on the best available data.

In spite of the many factors which influence the depth-velocity, i.e. depth-density, relationship, it has still been possible to derive useful information on accumulation from velocity data. Behrendt[13, 14] has been able to obtain a fair correlation between accumulation rate and density at a depth of 40 m for an area of uniform temperature (±2.6°C) and variable accumulation rates from 20 to 50 g/cm² yr in Ellesworth Land and the southern Antarctic Peninsula, using density data resulting from refraction work. The standard deviation from an empirical linear relationship obtained by least-squares fit through the data was ±4.7 g/cm² yr and was less than from a more sophisticated curve based on densification theory. Equally small standard deviations were obtained for regression analysis of accumulation versus velocity V_x of the velocity vs distance curves, at fixed distances from the shot point. This information is far more readily obtained than velocity at a fixed depth. Results for x = 50 m, 100 m and 200 m have been presented, the distance of 200 m giving the smallest standard deviation (±4.5 g/cm² yr) in the accumulation rate (Fig. 67). The apparent velocity V_{200} at the surface corresponds in this area to V_P at about 40-m depth.

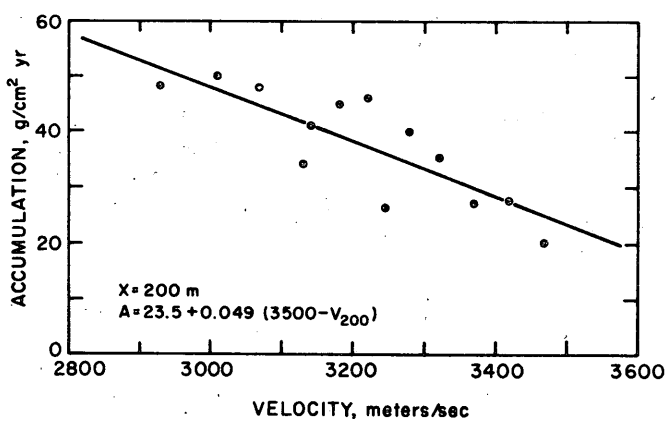

Figure 67. Accumulation rate as a function of the P*-wave velocity* V_x *at a distance of 200 m. (From Behrendt.*[13]*)*

Crary[54] has even extracted average accumulation rate from the area of worst scatter, the Victoria Land Plateau, by averaging temperature and density gradients $d\rho/dz$ obtained from velocities for the 25-m level ($\rho = 0.6$ g/cm^3) and applying densification theory. In earlier work by Robin[156] the depth-density data obtained from seismic refraction were used to test densification theory.

A still further and highly promising method for obtaining the accumulation rate from seismic data has been developed by Bentley[25]. It is based on the time intercept t_0 of the straight section of the travel-time curve corresponding to propagation in the fully densified ice at the depth of maximum penetration. The time intercept is obtained from long refraction lines directly, or by means of the travel-time difference of surface-reflected waves (p. 91). It is a measure of the total travel time through the region of firn densification and is small when the density increases rapidly with depth (high temperature and low accumulation rate), and vice versa. By least squares analysis a temperature dependency of

$$t_0' = t_0 + 3.42(T + 26.1) \tag{87}$$

has been found, where t_0' is the time intercept corrected to the temperature of −26.1°C. The regression line has then been forced through the point from Byrd Station, the only place where fully reliable information on the accumulation rate a is available, yielding

$$a = 14.4 + (2.91 \pm 0.17)(t_0' - 46.1) \text{ g/cm}^2 \text{ yr}. \tag{88}$$

Bentley's conclusion is that a long-term mean accumulation rate can be estimated more accurately from this formula than from pit measurements, provided it is possible to recognize anomalous values of t_0. A deviation can be caused by anisotropy or by the effect of strain.

There appears to be a systematic difference in depth-density and therefore depth-velocity relationships on shelves and glaciers compared with inland plateaus which are to a large extent related to horizontal strain.[23, 180] Crary et al.[53] have been able to correlate the firn densities at 40-m depth obtained by seismic refraction profiles to strains on the Ross Ice Shelf. A deviation from the ideally horizontal velocity structure almost universally found has also been reported on this shelf.

The increase of density and velocity with depth is less regular at temperatures close to the melting point than in polar snow. This is due to the infiltration of meltwater from the snow surface when melting occurs or when it rains. Ice layers form at various depths, some thick enough that they may be picked up by refraction.[160] The depth-velocity diagram of Figure 63a from the Hubbard glacier is a typical example for temperature very close to the melting point. The correlation between travel time at a fixed distance and firn facies in Greenland has been discussed by Brockamp.[36, 37]

On truly temperate snowfields there is always some water present at sufficient depth below the surface, the amount depending on the season. No unequivocal density-velocity relationship exists because of the presence of the liquid phase. A velocity of $V_P = 3000$ m/sec has been reported from brine-soaked snow on the McMurdo Ice Shelf,[15] which is the only record known to the author of the velocity in dense snow saturated with liquid. Since the snow is saturated with water at the transition zone from snow to glacier-ice on temperate glaciers it would be interesting to know more about the velocity in such a material.* Joubert[106] has found the water table at a depth of 33 m on the névé of Vallée Blanche in the French Alps, and the water-soaked layer was only about 3 m thick. The glacier ice below contained less than 1% of water. Thicker water-soaked layers have to be expected on larger snowfields with no crevasses, however.

* See ref. 56a.

Frozen ground

Barnes[9] has summarized the application of the refraction method on frozen ground in his review, *Geophysical Methods for Delineating Permafrost.* Probing for permafrost bodies in unfrozen strata or for unfrozen material in permafrost is one of the foremost applications of the refraction method in frozen ground environment. The principle of the method is based on velocity differences which depend on the frozen or non-frozen state of interstitial water. No such effect is therefore found in dry material. The frozen state, and not temperature, controls the velocity differences, so that the low velocities may persist at temperatures considerably below 0°C in the case of saline interstitial water or in very fine-grained rock where the freezing point is lowered by interfacial forces.

The depth to the frost table can be measured ideally by seismic refraction as shown in early Russian investigations and by Swartz and Shepard.[174] It may frequently turn out in practice, however, that simple probing rods are much more economical when the permafrost table is shallow. Barnes estimates that the seismic method may become competitive at depths below 1.8 m. Using delay-time techniques the thickness at each geophone location can be determined for each shot. Proper care has to be taken to place the geophones under comparable local conditions, such as are offered by the centers of fines in patterned ground.[162,163] In addition to determination of thickness, velocity changes in the thawed surface layer may be successfully interpreted to yield other information, as in the case of a groundwater layer above permafrost (Fig. 68). In areas of discontinuous permafrost it is usually possible to identify the frozen bodies, especially in the case of unconsolidated deposits, but it may not always be possible to distinguish them from bedrock, frozen or nonfrozen.

The bottom of the frozen layer cannot be determined by the refraction method and likewise *talik* cannot be identified.

Various attempts to measure the thickness of frozen unconsolidated deposits on bedrock have been made with variable success. The best results were probably obtained at very low temperatures,

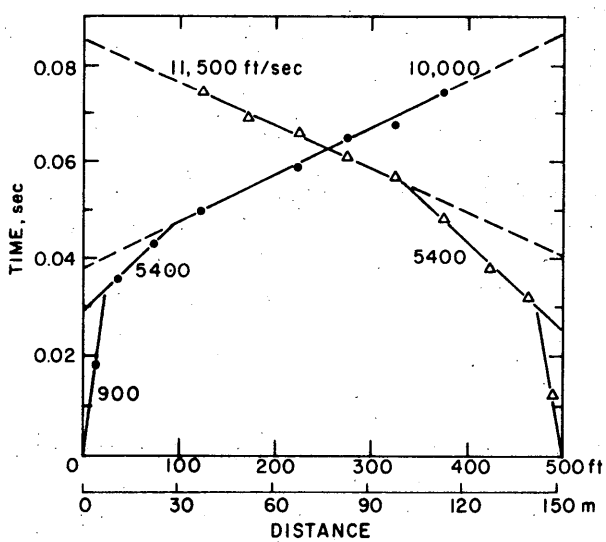

Figure 68. Seismic travel-time curves near Fairbanks, Alaska, from a refraction profile on 4.6 m of dry alluvium, overlying about 12 m of water-saturated sediments above permafrost (V_P = 3280 m/sec). (From Barnes.[9])

where the permafrost extends far down into the bedrock, as in the Thule area.[162 163] Figure 69 gives an example, in this case with 30 m of ice over the frozen till. Second arrivals could frequently be identified very shortly after the first arrivals due to the rapid decay of the latter (p. 91). Figure 69c shows a typical example of such a record. The best results were obtained when two shots were fired, a strong one for first arrivals and a weak one for the later events. (On one occasion in the Thule area the second arrival was identified as a wide-angle reflection rather than a refraction signal, where the underlying bedrock was shale with a lower velocity than the frozen

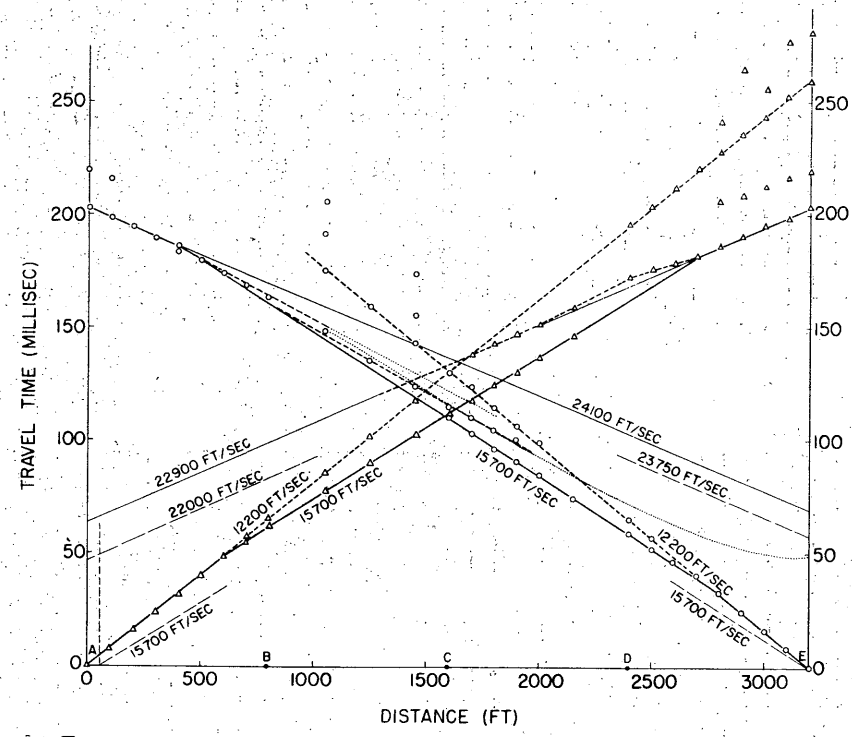

a. Time-distance curves from soundings through ice and frozen ground to bedrock near Thule, Greenland. Light solid and dashed lines show first approximation with topographic and top-layer corrections. Heavy dashed and dotted lines show alternative, and more elaborate, interpretations.

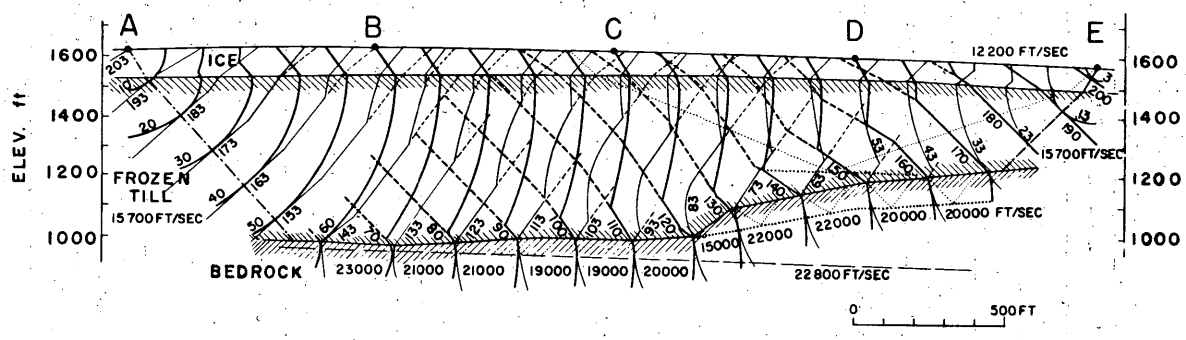

b. Interpretation of the travel-time curves of Figure 69a with wave fronts originating at A and E showing as index numbers the time, in millisec, elapsed after the shot. The solid, dotted and light dashed interfaces represent different interpretations.

Figure 69. Refraction soundings through frozen ground to bedrock. (From Roethlisberger.[162])

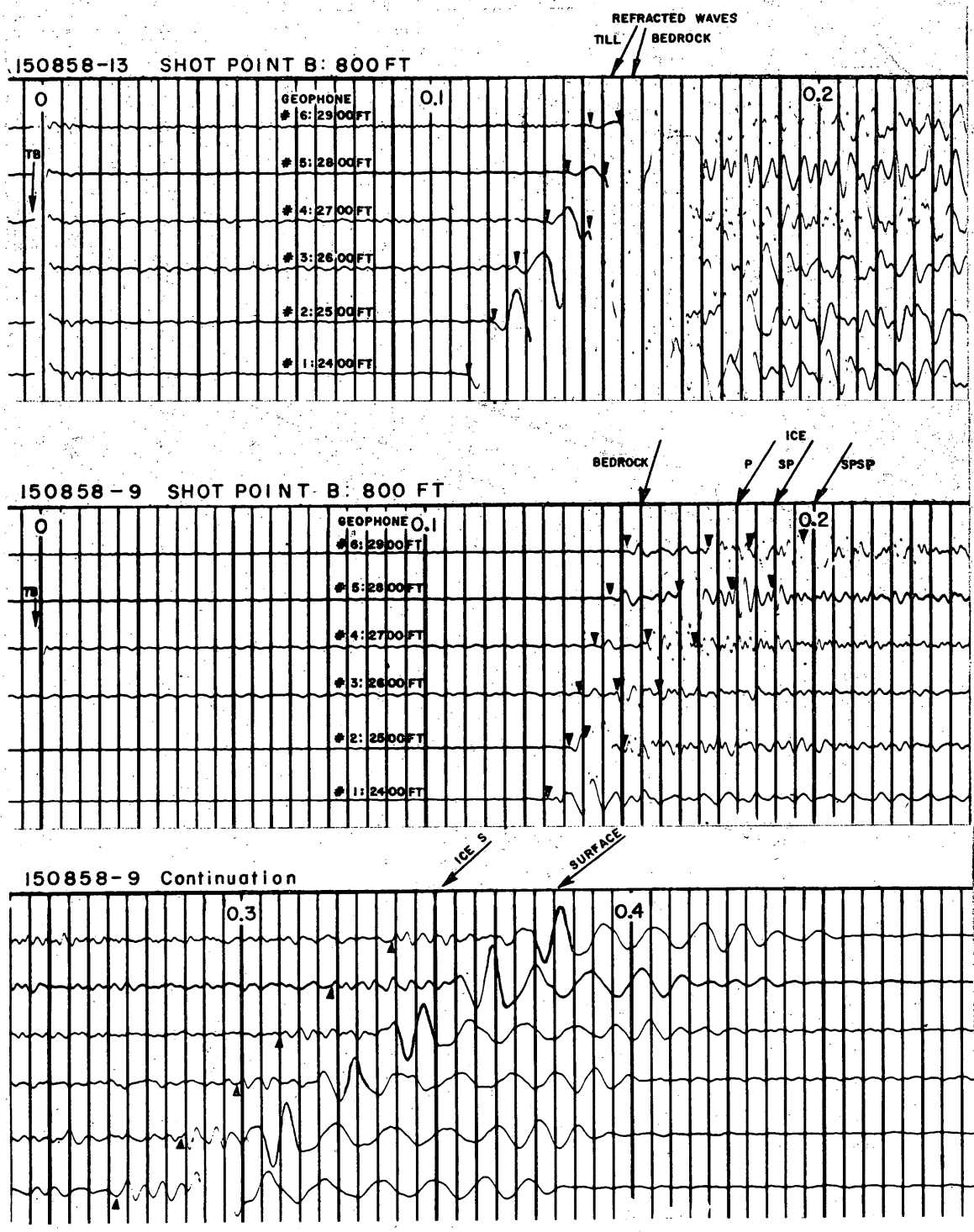

c. Refraction record on frozen till covered by 30 m of ice, overlying high velocity bedrock (top: heavy charge, center and bottom: light charge).

Figure 69 (cont'd). Refraction soundings through frozen ground to bedrock. (From Roethlisberger.[162])

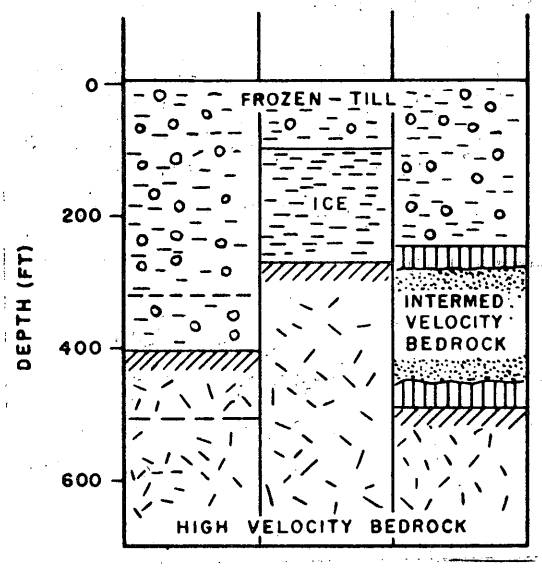

Figure 70. Accuracy and alternative interpretations of refraction data in the Thule area. (From Roethlisberger.[163])

outwash (p. 83).] The rapid decay of the permafrost wave has also been reported by Barnes and MacCarthy[8] at the much higher temperature of the Fairbanks area where the permafrost was about 24 m thick. The pronounced damping of the permafrost wave in the Thule area is much more remarkable than on thin permafrost, since one would expect the maximum velocity layer to be quite thick and the velocity gradient at the top of the inversion to be very small indeed from temperature alone. The fact that there was only about 50% saturation in the TUTO permafrost tunnel[175] while it is 100% at the frost table a short distance above implies a large gradient of ice content and thereby a relatively large negative velocity gradient with depth.

The rapid disappearance of the permafrost wave makes accurate velocity determinations sometimes quite difficult and leads to considerable uncertainty in the depth results (Fig. 70). The possibility of the presence of ice bodies makes the interpretation even more uncertain.

At temperatures close to the melting point and in areas of discontinuous permafrost the interpretation of the seismic data becomes more difficult because of velocity variations in the unconsolidated deposits. This is particularly true when the latter consist of fine-grained material. A refraction survey for placer deposits in the Fairbanks district by L.D. Leet and H.G. Taylor in 1938[98] was not successful because of the above reasons and because of the small velocity difference between frozen muck and gravel and the underlying schist bedrock. Even in thawed areas the accuracy was low because of deeply weathered bedrock, probably due to former frost action. Barnes and MacCarthy[9] and Sellmann[170] carried out successful refraction soundings in selected spots.

Bush and Schwarz[42] have found that the effect of thin zones of frozen material in the overburden upon the seismic data is small, but the effect of thick zones is much larger. They have been able to outline generally the lateral limits of areas of moderate to thick lenses of frozen overburden, based on the observations that high-frequency, high-velocity early arrivals attenuate rapidly into lower-frequency, lower-velocity energy, and that the total times from reversed refraction profiles are not the same, indicating that the waves travel along different paths depending upon the direction traveled. The early refraction arrivals from frozen ground were usually of higher frequency (in excess of 30 Hz) than those from bedrock (less than 20 Hz). Depth to rock calculations through frozen overburden have been found to be reasonably accurate but generally less accurate than those made over unfrozen overburden.

Bell[16] has measured the thickness of the dried-out surface layers in an ice-free area of McMurdo Sound, Antarctica, by refraction, and has used the results to estimate the minimum age of a moraine from assumptions about the diffusion of water vapors through till.

It can be concluded that the refraction method cannot be generally recommended for mapping the bedrock surface under frozen unconsolidated deposits, but that a survey may prove useful if carefully carried out under favorable circumstances. The accuracy of a refraction survey is hard to

assess because of the decreasing velocity with depth: the velocity determined by refraction in the horizontal direction at the top of a layer is higher than the average velocity of the waves going across the layer. A strong anisotropy has further been reported[98] with an effect in the same sense, both resulting in a larger computed depth than the true one. Particular care has to be taken with the interpretation when there is a chance of an unfrozen unconsolidated layer between frozen ground and bedrock.

SURFACE WAVES AND WAVES IN THIN FLOATING ICE

Surface Waves

Two types of surface waves are mentioned in textbooks: *Rayleigh waves* showing a retrograde rotational motion of particles in a vertical plane in the direction of propagation, and *Love waves* showing particle motion in a transverse direction in the horizontal plane. No Love waves exist in an infinite homogeneous medium with a free surface. In layered structures both types of surface waves are dispersive. Vertical geophones are insensitive to the Love wave motion, but pick up the Rayleigh waves; for a study of their complete motion the horizontal longitudinal component must also be measured, however. Rayleigh waves have been investigated in some detail by Jobert[97] and Bentley et al.[20] on the Greenland ice sheet. Bentley found some systematic deviation between observation and theory of dispersion, while Jobert obtained an excellent fit. She has described an additional surface wave showing rotational particle motion in the opposite sense to the Rayleigh wave, arriving before the latter. A compressional pseudo surface wave has been reported from the Ross Ice Shelf by Robinson,[158] who has explained it by constructive interference of low-frequency (25 to 35 Hz) components of multiply surface-reflected compressional waves. A corresponding wave train is absent on the records from the polar plateau because of different characteristics of the wave guide.

No practical use has been made of the surface waves since the information which might be gained on the parameters governing them is more readily obtained by refraction. It might nevertheless be feasible to study near-surface anisotropy (or with very low frequencies, even anisotropy at depth) by means of surface waves.[5 6] Robinson[158] has indeed been able to show a significant difference between Rayleigh wave dispersion on the Arctic Plateau and the Ross Ice Shelf. While an isotropic model was satisfactory in the first case he had to assume about 20% of anisotropy on the shelf. (His other statement, that the base of the wave guide would be deeper with lower velocities in the vertical than in the horizontal direction,is not correct; see p. 90). Anisotropy effects have been observed by Robinson for the Love wave also.

In regular seismic work, the surface waves can become detrimental when they are strong and not much attenuated, as on the high Antarctic Plateau attemperatures below -30°C. Robin[156] has discussed the general conditions under which a strong energy transformation from *P*- to surface waves may occur.

Surface waves can be propagated as flexural waves when a thin, high velocity layer overlies a low velocity medium, a typical condition in permafrost. Attempts were made to use flexural-wave dispersion to measure the thickness of frozen alluvium near Fairbanks, Alaska[55 98] but no satisfactory interpretation was possible. Dispersion measurements require that uniform permafrost thickness and elastic properties extend for such long distances that the method does not provide sufficient resolution for most site selection problems.[9] The basic problem is similar to that of flexural waves in floating ice in the following section.

Waves in Thin Floating Ice

The theory of waves in a thin floating ice sheet (sea, lake and river ice) has been treated for an isotropic infinite plate,[59 61 140 151] as well as for an anisotropic (transversely isotropic) infinite plate,[56] and experimental work has been done on lake and sea ice.* The simpler of the many

---

* Ref. 4, 38, 48, 50, 59, 60, 93, 148, 151.

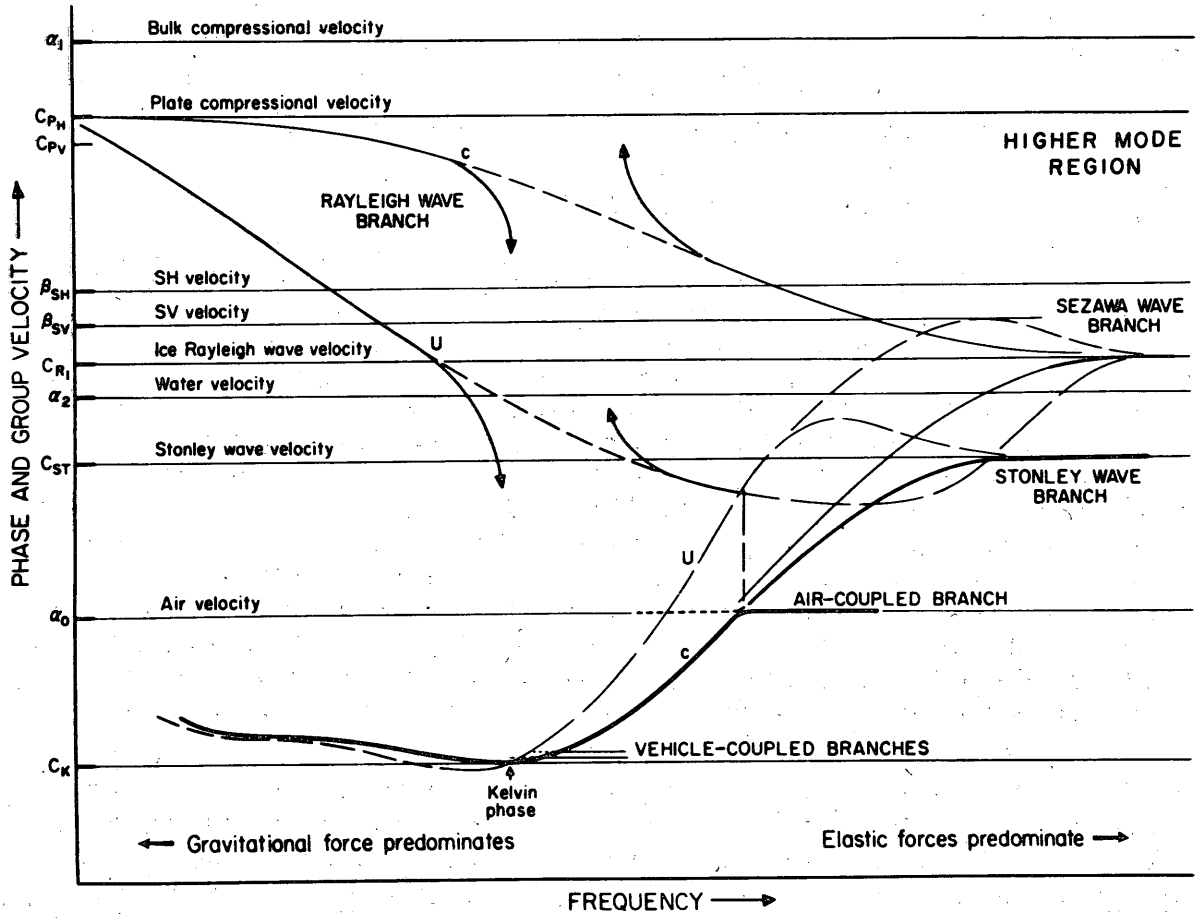

Figure 71. Dispersion curves of the lowest modes of elastic wave propagation in sea ice. (From Anderson.[6])

different waves that are theoretically possible are presented in Figure 71. Only a few are of practical interest: those which can easily be observed with commercially available equipment. Low-frequency or preferably wide-band seismic equipment is needed. At very low frequency (when investigating the waves related to moving vehicles) special deflectometers have been used.[4]

The waves that can easily be identified are described on the following pages.

Body waves

The *P*-wave can be measured only at relatively high frequencies and short distances. In pack ice about 3 m thick it has been observed to a distance of 90 m. The velocity of the *S*-wave is the same as that of the *SH* plate wave, which can usually be measured to greater distances. Body waves can serve to determine elastic parameters. They tend to give selectively high velocities, because the wave traveling in the layers with the highest velocities will arrive first. Body waves are also measured in most ultrasonic tests.

Plate waves

The compressional (longitudinal) plate wave of velocity $V_{PL} = \sqrt{E/\rho\,(1-\nu^2)}$ (eq 9), is the first event on the records at longer distances. On 3-m-thick pack ice it showed frequencies of about 100 Hz at 100 m from the shot point, and 25 Hz at 1000 m. A horizontally polarized shear

wave S_H occurs as a plate wave (isotropic media: $V_S = \sqrt{G/\rho}$); it can be excited strongly by a hammer blow to a vertical pit wall, the string of geophones being laid out in the direction of the wall. The plate-wave velocities are averaged over the thickness of the plate, probably weighted in favor of the faster velocities.

Flexural waves

The flexural waves are dispersive. The relation between the flexural wave phase velocity and the elastic constants is[59]

$$C^2 = \frac{\frac{1}{3}\pi^2\left(\frac{hf}{C}\right)^2 V_{PL}^2 + \left(\frac{\rho_w}{\rho_i}\right) g\lambda_0 \Big/ 4\pi^2\left(\frac{hf}{C}\right)}{1 + \left(\frac{\rho_w}{\rho_i}\right) \Big/ \left[2\pi\left(\frac{hf}{C}\right)\left(1 - \frac{C^2}{V_w^2}\right)^{1/2}\right]} \qquad (89)$$

where C = phase velocity
h = thickness of ice
f = frequency of wave
V_{PL} = velocity of compressional plate wave
g = acceleration of gravity
$\lambda_0 = C/f$ = wavelength
ρ_i = density of ice
ρ_w = density of sea water
V_w = velocity of sound in water.

The group velocity U is related to C by:

$$U = C + \left(\frac{hf}{C}\right) dC \Big/ d\left(\frac{hf}{C}\right) . \qquad (90)$$

Long trains of flexural waves are produced by placing the charge under the ice. While observed dispersions (velocity vs frequency) agreed well with computed ones on lake ice, a considerable discrepancy existed on sea ice. Part of the discrepancy is probably due to anisotropy,[5] but there is another reason. In flexural waves the elastic behavior of the entire sheet is important again, as in plate waves. However, in the flexural deformation a layer close to the center is in a neutral position, and the elastic reaction of the layers above and below is more important the further away the layers are from the neutral surface. Therefore the top and bottom layers of the ice have a much larger weight in the average elasticity controlling the flexural waves. The same is true in the case of flexural strength, and the flexural waves are therefore well suited to determine elastic parameters when the bearing capacity of ice is concerned. Determining the ice thickness from dispersion data and measured plate velocity is less satisfactory.

Air-coupled waves

These waves are a special type of flexural wave which are strongly excited by shooting at the ice surface or in the air. They consist of a train of vibrations of constant frequency preceding the arrival of the air blast. The frequency is found from eq 89 by setting $C = V_a$, where V_a is the velocity of sound in air. (The gravity term can usually be neglected.) The frequency of the air-coupled wave is easily measured, and so are the other parameters of the equation. If V_a is not

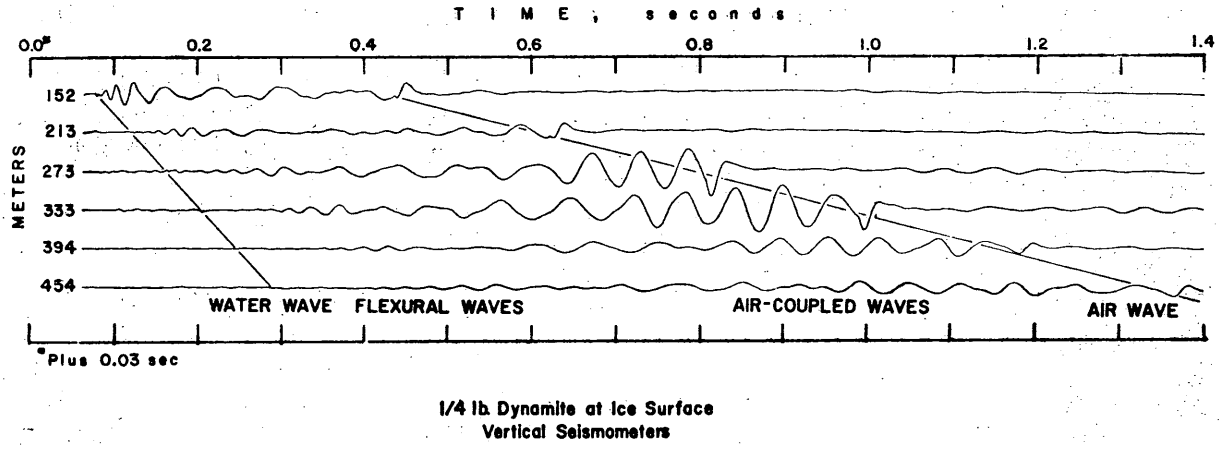

Figure 72. Elastic waves produced in sea ice by a surface explosion. (From Hunkins.[93])

directly observed, it may be computed from

$$V_a = 331 + 0.60\,T \quad \text{(m/sec)} \tag{91}$$

where T = air temperature in °C. Other parameters are (for the Arctic Ocean): V_W = 1440 m/sec, ρ_1/ρ_2 = 0.878, and V_{PL} varies, usually between 2000 and 3200 m/sec. If a fair estimate can be made of V_{PL}, then it would be sufficient to observe the frequency of the air-coupled wave to obtain the ice thickness. The method might be used to determine ice thickness from the air if a simple radio-equipped geophone could be air-dropped and a bomb were exploded at an appropriate distance. When used on the ground, the air-coupled wave is better suited to determining elastic parameters in flexure than ice thickness, as pointed out for the regular flexural waves. The length of the train of air-coupled waves depends on the distance from the shot or from open leads between shot and station. A record with typical flexural and air-coupled waves is given in Figure 72.

Reflected waves

A strong pulse at distances very many times the ice thickness has been observed on the floating ice island T-3.[50] It is known as the SV, or Crary, wave, and it appears shortly after the compressional wave with an almost constant frequency which was found to increase very slightly with time; a phase velocity close to V_{PL} was measured. The occurrence of the wave has been explained by constructive interference of S_V waves which are totally reflected at the upper and lower boundaries of the ice sheet at the critical angle γ, where $\sin\gamma = V_S/V_P$. The frequency f is simply related to the ice thickness h by the equation:

$$h = \frac{V_S}{f\cos\gamma}\,. \tag{92}$$

The explanation of the Crary wave by multiple S_V reflection (more correctly P refracted as S_V and then multiply reflected) leaves the change of frequency with time unanswered, and it is therefore more likely that interference of multiple converted reflections of type PS occurs. This question should be more closely looked into. Very strong single and multiple PS reflections of ultrasonic pulses have been observed in a lake ice sheet (Fig. 73). In this case the lake ice was used for seismic model studies in an anisotropic medium.[167]

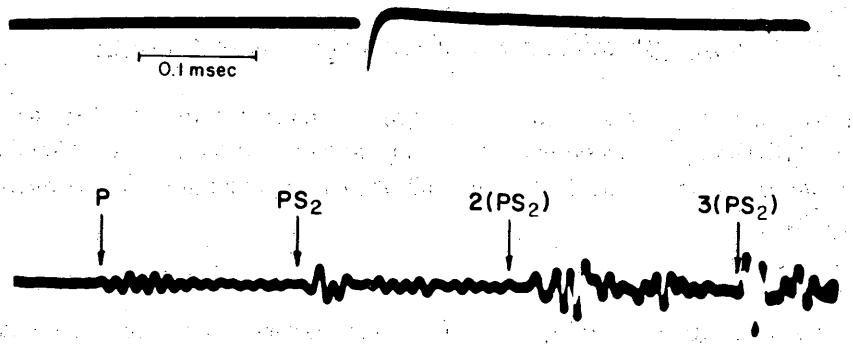

Figure 73. Multiple converted reflections (PS) of ultrasonic pulses in lake ice. (From Roethlisberger.[167])

SOME SPECIAL APPLICATIONS OF ELASTIC WAVES

Elastic waves have applications other than standard seismic surveys. Different frequencies can be used in various ways. Some special techniques and applications have been mentioned in relation to seismic methods. A few further procedures and experiments are described in the following paragraphs.

Echo sounding

Soundings by means of repeated sonic or ultrasonic pulses have become a standard technique for measuring water depth, and by using specific pulse sources it has been possible to penetrate lake and ocean bottom sediments as well. There is no reason why the method should not work on shallow ice, but there has been no need for much effort in this direction so far, since mechanical drilling is adequate for small depths. The use of high frequency sound waves at greater depth is limited by attenuation, which increases rapidly with higher frequency, as shown by Westphal.[191]

Akimov[2] has given examples of the successful use of echo sounding techniques in permafrost, in particular for delineating subaquatic permafrost on the shore of a lake.

Only the top of permafrost furnishes reflections. There is no sharp boundary at the lower surface. The shorter waves of the echo pulses are therefore even less likely to be reflected than regular seismic waves.

Well-logging by ultrasonic pulses

The measurement of travel time of ultrasonic pulses over fixed distances is one of a number of commonly used procedures in well-logging. It can be a particularly powerful method to distinguish between the frozen and unfrozen state of the soil or rock.[2 56] Information can be extracted not only from velocity, but also from attenuation characteristics.

Glacier-flow studies by an ultrasonic pulse technique

The basic idea developed by Millecamps and Lafargue[113 126 127] is to install ultrasonic ceramic transducers permanently in the ice. They serve alternately as transmitters and receivers, and the travel time between pairs of them can be measured. The positions of the transducers within the ice can be found from travel-time measurements if the transducers are placed on a suitable grid, and provided that the elastic wave velocity (V_P) is constant or changes with direction and location in a regular fashion. Changes of travel time can be interpreted in terms of displacement of the transducers, i.e. ice deformation, and possibly changes of velocity, when the survey is repeated after a given period of time. The French research group has installed their transducers on an Alpine glacier in four vertical drill holes forming a rectangular column in order to obtain a simple cubical grid. The side of their unit cell has been 10 m, and they have estimated that changes in length of the order of 1 cm could be detected. The evaluation has been found to be extremely cumbersome, and no final report seems to have come out.

Satisfactory results were obtained in Greenland with a similar technique in the much simpler two-dimensional case of ice flow around a rectangular ice tunnel by Roethlisberger.[164]

Acoustic surveys of the frozen zone around a freezing shaft

Travel-time measurements are well suited for observing the progress of artificial freezing for excavations in unstable ground as demonstrated by Müller.[130] He has used blasting caps as a source and well-geophones as receivers and has placed charges and geophones at variable depth

in drill holes to measure velocities in the horizontal direction. A favorable geometrical setup is described. The correlation between velocity and strength is discussed in a later paper.[185]

It is conceivable that ultrasonic techniques similar to those used for glacier flow studies, where the inexpensive ceramic transducers can be left in place, could be adapted to the above problem of observing the extent of freezing shields. Too strong an attenuation of the pulses might be a major obstacle, however.

Attenuation and particle motion

Attenuation measurements have been scarce. From the little information available it seems nevertheless possible to gain some insight into the structure of the materials penetrated by elastic waves by interpreting attenuation. Westphal[191] has been able to correlate the dependency of attenuation on frequency with average grain size in ice, using small explosions as a source and a pressure transducer in a water-filled drill hole as a pick-up. The Russians are making use of the fact that the frozen or non-frozen state of soils has a much stronger effect on attenuation than on velocity. Furthermore they are relating attenuation to heat conductivity.[2 196]

Particle motion has been investigated occasionally in relation to surface waves and flexural waves. Furthermore a systematic deviation of the direction of particle motion has been reported for body waves from the very early seismic work on glaciers with mechanical seismographs. It was attributed to ice structure.[72]

Continuous seismic waves

Johnson and Fischer[99] have experimented with continuous seismic waves (CSW) excited by special transducers in ice and permafrost, measuring velocities of elastic waves by observing phase shifts with distance, and observing attenuation. In addition they have observed transmission of pulsed waves. It seems that only shear waves and very slow surface waves, possibly related to surface conditions, have been observed, contrary to the interpretation given by the authors, which is unacceptable. The attenuation figures given are therefore useless, since it is not known to which mode they apply. The investigation shows that this type of work is extremely tricky since not only *P*- and *S*-waves but also various types of surface waves must be considered.

Ice tremors

Some elastic wave pulses in ice have a natural origin, such as the formation of cracks. Vibrations related to cracking may be clearly heard on glaciers in cold weather in the fall when the surface freezes, and they may be sufficiently abundant to interfere with seismic work.

A different type of tremor has been investigated on a glacier in Spitzbergen by Oelsner.[139] This work was done in summer, when thermal cracking must have been scarce or missing, at least at the lower station. Pulses of 0.3 to 0.5 sec duration showing a predominant frequency of 60 Hz (probably a local resonance phenomenon?) were observed, presumably originating from cracking related to the flow of the glacier. Pulses were counted at three stations over part of the month of August, and the frequency of the occurrence of the pulses was analyzed using pulse rates per three-hour period. With autocorrelation methods the pulse rate was not only correlated to temperature, but also to water discharge from the glacier. This is interpreted to indicate jerky motion of the glacier depending on water lubrication at the bed. The way the statistical methods are applied is subject to severe criticism and the conclusions reached are therefore highly questionable. Doubtless there is a strong diurnal variation of pulse rate with a certain time lag as compared to temperature, which may mean that a diurnal variation of glacier motion related to meltwater

drainage causes a daily variation of the intensity of surface cracking. Further investigations in this field would be of interest. (For a detailed account of further work see ref. 56a.)

Tremors in sea ice have also been observed.[51] They are probably caused by pressure from moving pack ice.

SELECTED BIBLIOGRAPHY

1. Abele, G. and G. Frankenstein (1967) Study of snow and ice properties as related to roads and runways in Antarctica. U.S. Army Cold Regions Research and Engineering Laboratory (USACRREL) Technical Report 176, p. 1-40. AD 665386

2. Akimov, A.T. (1964) Opyt primeneniia akusticheskikh i seismicheskogo metodov issledovaniia merzlykhgornykh porod (Experience in applying acoustical and seismic methods of permafrost exploration). Akademiia Nauk SSSR, Sibirskoe otdelenie, Institut merzlotovedeniia, Sovremennye voprosy regional'noi i inzhenernoi geokriologii (merzlotovedeniia) Izdatel'stvo *Nauka*, p. 167-180.

3. Allen, C.F. and S.W. Miller (1954) Seismic measurements on the Greenland ice cap. In *Final Report on the Scientific Program (Program B), Operation Ice Cap 1953.* Stanford Research Institute, p. 350-374.

4. Anderson, D.L. (1958) Preliminary results and review of sea ice elasticity and related studies. *Transactions of the Engineering Institute of Canada*, vol. 2, p. 116-122.

5. Anderson, D.L. (1961) Elastic wave propagation in layered anisotropic media. *Journal of Geophysical Research*, vol. 66, no. 9, p. 2953-2963.

6. Anderson, D.L. (1963) Use of long-period surface waves for determination of elastic and petrological properties of ice masses. In *Ice and Snow – Properties, Processes and Applications* (W.D. Kingery, Ed.). Cambridge, Mass.: MIT Press, p. 63-68.

7. Barnes, D.F. (1960) Seismic velocity measurements at the Ogotoruk Creek Chariot Site, Northwestern Alaska. In *Geological Investigations in Support of Chariot in the Vicinity of Cape Thompson, Northwestern Alaska – Preliminary Report, U.S. Geological Survey*, p. 62-78. U.S. Atomic Energy Commission, Technical Information Service, Oak Ridge, Tennessee.

8. Barnes, D.F. and G.R. MacCarthy (1964) Preliminary report on tests of the application of geophysical methods to arctic ground-water problems. U.S. Geological Survey Open-file report.

9. Barnes, D.F. (1965) Geophysical methods for delineating permafrost. *Proceedings of the Permafrost International Conference, 1963.* National Academy of Sciences – National Research Council Publication 1287, p. 349-355.

10. Barthelmes, A.J. (1946) Application of continuous profiling to refraction shooting. *Geophysics*, vol. 2, no. 1, p. 24-42.

11. Bass, R., D. Rossberg and G. Ziegler (1957) Die elastischen Konstanten des Eises (The elastic constants of ice). *Zeitschrift für Physik*, vol. 149, p. 199-203.

12. Behrendt, J.C. (1963) Seismic measurements on the ice sheet of the Arctic Peninsula. *Journal of Geophysical Research*, vol. 68, no. 21, p. 5973-5990.

13. Behrendt, J.C. (1964) Antarctic Peninsula traverse geophysical results relating to glaciological and geological studies. Geophysical Polar Research Center, Research Report ser. 64-1, p. 1-112, Wisconsin University, Department of Geology.

14. Behrendt, J.C. (1965) Densification of snow on the ice sheet of Ellsworth Land and the southern Antarctic Peninsula. *Journal of Glaciology*, vol. 5, no. 40, p. 451-460.

15. Bell, R.A.I. and A.J. Heine (1965) Seismic refraction measurements on the McMurdo Ice Shelf, Antarctica. *Journal of Glaciology*, vol. 5, no. 42, p. 880-881.

16. Bell, R.A.I. (1966) A seismic reconnaissance in the McMurdo Sound region, Antarctica. *Journal of Glaciology*, vol. 6, no. 44, p. 209-221.

17. Bender, J.A. (1957) Air permeability of snow. U.S. Army Snow, Ice and Permafrost Research Establishment (USA SIPRE) Research Report 37, p. 1-31. AD 158193

18. Bender, J.A. and A.J. Gow (1961) Deep drilling in Antarctica. IUGG General Assembly of Helsinki, International Association of Scientific Hydrology, vol. 55, p. 132-141.

19. Bennett, H.F. (In prep.) Measurements of ultrasonic wave velocities in ice cores from Greenland and Antarctica. USACRREL Research Report 237.

19a. Bennett, H.F. (1968) An investigation into velocity anisotropy through measurements of ultrasonic wave velocities in snow and ice cores from Greenland and Antarctica. Ph.D. Thesis, University of Wisconsin.

20. Bentley, C.R., P.W. Pomeroy and H.J. Dorman (1957) Seismic measurements on the Greenland icecap. Part I: Studies at 76°59'N 56°05'W; Part II: Reflection studies. *Annales de Geophysique*, vol. 13, p. 253-275, 276-285.

21. Bentley, C.R. and N.A. Ostenso (1961) Glacial and subglacial topography of West Antarctica. *Journal of Glaciology*, vol. 3, no. 29, p.882-911.

22. Bentley, C.R. (1962) Glacial and subglacial geography of Antarctica. In *Antarctic Research*, p. 11-25. Geophysical Monograph no. 7, American Geophysical Union, Wash.

23. Bentley, C.R. (1964) The structure of Antarctica and its ice cover. In *Research in Geophysics, Vol. 2: Solid Earth and Interface Phenomena* (H. Odishaw, Ed.). Cambridge, Mass.: MIT Press, p. 335-389.

24. Bentley, C.R. (1965) The land beneath the ice. In *Antarctica* (Trevor Hatherton, Ed.). New York: Frederick A. Praeger, chap. 10, p. 259-277.

25. Bentley, C.R. (In press) Seismic anisotropy in the West Antarctic ice sheet. American Geophysical Union Antarctic Research Series, Glaciology II.

25a. Bentley, C.R. (In press) Seismic evidence for moraine within the basal Antarctic ice sheet. Contribution 227 of the Geophysical and Polar Research Center, University of Wisconsin.

26. Berckhemer, H. and J. Oliver (1955) Zur Deutung seismischer Einsätze mit parallelen Laufzeitkurven (An explanation of seismic onset with parallel travel time curves). *Zeitschrift für Geophysik*, vol. 21, p. 152-164.

27. Berzon, I.S., L.I. Bokanenko and V.S. Isaev (1959) Seismicheskie issledovaniia na lednike Tuiuksu (Seismic studies on Tuyuksu glacier). Akad. Nauk SSSR, Meezhduved, Komit. Proved. MGG, IX i XII Razdely Programmy MGG, vol. 3, p. 1-67.

28. Berzon, I.S., V.A. Pak and V.N. Iakovlev (1960) Seismicheskoe zondirovanie lednika Fedchenko (Seismic sounding of Fedchenko glacier). In *Glatsiologicheskaia Ekspeditsiia na Lednik Tedchenko*, p. 84-109. Izdat. Akad. Nauk Uzbekskoi SSR, Tashkent.

29. Borovinsky, B.A. (1963) Izuchenie lednikov Zailiiskogo Alatau geofizicheskimi metodami: Glatziologiya i seismologiya, IX i XII Razdeli Programmi MGG (Study of Zailyskiy Alatau glaciers by geophysical methods: Glaciology and seismology, Sections IX and XII of IGY Program). Results of Researches of the Program of IGY, vol. 10 and 5, p. 1-112. Izdat. Akad. Nauk SSSR, Moskva.

30. Brockamp, B. and H. Mothes (1939) Seismische Untersuchungen auf dem Pasterzegletscher, I (Seismic investigations on the Pasterze glacier, I). *Zeitschrift für Geophysik*, vol. 6, p. 482-500.

31. Brockamp, B. (1931) Seismische Untersuchungen auf dem Pasterzegletscher, II (Seismic investigations on the Pasterze glacier, II). *Zeitschrift für Geophysik*, vol. 7, p. 232-240.

32. Brockamp, B., E. Sorge and K.K. Wölcken (1933) Wissenschaftliche Ergebnisse der Deutschen Grönland – Expedition Alfred Wegener 1929 und 1930/31, Band II., Seismik (Scientific results of the German Greenland Expedition Alfred Wegener 1929 and 1930/31, Vol. II, Seismic investigations). p. 1-160, Brockhaus, Leipzig.

33. Brockamp, B. (1958) Reflektionsseismische Wiederholungsmessungen auf dem Pasterzegletscher und ihre Bedeutung für die Feststellung von Gletscher- und Inlandeisschwankungen (Repeated seismic reflection measurements on Pasterze glacier and their importance for the determination of glacier and icecap variations). IUGG General Assembly of Toronto, International Association of Scientific Hydrology, vol. 46, p. 509-513.

34. Brockamp, B. and H. Querfurth (1964) Untersuchungen über die Elastizitätskonstanten von See und Kunsteis (Investigations of the elastic constants of lake and artificial ice). *Polarforschung*, vol. 5, no. 34, 1/2, p. 253-262.

35. Brockamp, B. and Kohnen (1965) Ein Beitrag zu den seismischen Untersuchungen auf dem Grönländischen Inlandeis (Seismic investigations on the Greenland ice sheet). *Polarforschung*, vol. 6, no. 35, 1/3, p. 2-12.

36. Brockamp, B. (1965) Ueber einige geophysikalische Ergebnisse der internationalen Grönland – Expedition EGIG 1959 (Some geophysical results of the international Greenland expedition EGIG 1959). *Polarforschung*, vol. 6, no. 35, 1/2, p. 42-66.

37. Brockamp, B. and P. Pistor (1967) Ein Beitrag zur seismischen Erforschung der Struktur des Grönländischen Inlandeises (Seismic investigation of the structure of the Greenland ice sheet). *Polarforschung*, vol. 6, no. 37, 1/2, p. 133-146.

38. Brown, J.H. (1963) Elasticity and strength of sea ice. In *Ice and Snow – Properties, Processes and Applications* (W.D. Kingery, Ed.). Cambridge, Mass.: MIT Press, p. 79-106.

39. Bruggeman, D.A.G. (1930) Elastizitätskonstanten von Kristall-Aggregaten (Elastic constants of crystal aggregates). Diss. Rijks-Universitet Utrecht, p. 1-104, J.B. Wolters, Groningen.

40. Bruggeman, D.A.G. (1937) Berechnung verschiedener physikalischer Konstanten von heterogenen Substanzen, III. Die elastischen Konstanten der quasi-isotropen Mischkörper aus isotropen Substanzen (Analysis of various physical constants of heterogeneous substances, III. The elastic constants of pseudo-isotropic aggregates of isotropic substances). *Annalen der Physik*, 5. F., vol. 29, p. 160-178.

41. Bull, C. (1956) British North Greenland Expedition 1952-54. IV. Seismic investigations on the northern part of the Greenland ice-sheet. *Geographical Journal*, vol. 122, p. 219-225.

42. Bush, B.O. and S.D. Schwarz (1965) Seismic refraction and electrical resistivity measurements over frozen ground. *Proceedings of the Canadian Regional Permafrost Conference, 1964*, National Research Council of Canada Technical Memo 86, p. 32-39.

43. Chalmers, H.B., Jr. (1949) Report of well velocity of Fish Creek Test Well no. 1. U.S. Geological Survey Open-file report, United Geophysical Co. Report 49-21.

44. Clarke, G.K.C. (1964) Geophysical measurements on the Kaskawulsh and Hubbard glaciers, Yukon Territory, Canada. Master Thesis, Department of Physics, University of Toronto.

45. Clarke, G.K.C. (1966) Seismic survey Northwest Greenland, 1964. USACRREL Research Report 191. AD 640454

46. Clarke, G.K.C. (1967) Geophysical measurements on the Kaskawulsh and Hubbard Glaciers, Yukon Territory. Arctic Institute of North America Technical Paper 20, p. 1-36.

47. Collins, F.R. (1958) Test wells, Umiat area, Alaska, with micropaleontologic study of the Umiat Field, Northern Alaska (by H.R. Bergquist). U.S. Geological Survey Professional Paper 305-B, p. 71-206.

48. Cook, J.C. (1963) Seismic reconnaissance on an ice-covered Antarctic sea. *Journal of Glaciology*, vol. 4, no. 35, p. 559-568.

49. Crary, A.P., R.D. Cotell and T.F. Sexton (1952) Preliminary report on scientific work on "Fletcher's Ice Island." *Arctic*, vol. 5, p. 211-223.

50. Crary, A.P. (1954) Seismic studies on Fletcher's ice island, T-3. *Transactions of the American Geophysical Union*, vol. 35, p. 293-300.

51. Crary, A.P. (1955) A brief study of ice tremors. *Bulletin of the Seismological Society of America*, vol. 45, p. 1-9.

52. Crary, A.P. (1956) Arctic ice island research. *Advances in Geophysics*, vol. 3, p. 1-41.

53. Crary, A.P., E.S. Robinson, H.F. Bennett and W.W. Boyd, Jr. (1962) Glaciological studies of the Ross Ice Shelf, Antarctica, 1957-1960. IGY Glaciological Report 6, p. 1-193. IGY World Data Center A, Glaciology, American Geographical Society, New York.

54. Crary, A.P. (1963) Results of United States traverses in East Antarctica, 1958-1961. IGY Glaciological Report 7, p. 1-144. IGY World Data Center A, Glaciology, American Geographical Society, New York.

55. Crowley, F.A. and R.E. Hansen (1956) Seismic measurements in permafrost areas of interior Alaska. *Proceedings of the 7th Alaskan Science Conference*, p. 54.

56. Desai, K.P. and E.J. Moore (1967) Well log interpretation in permafrost. *Transactions of the 8th Annual Logging Symposium, Denver, Colorado, 1967.* Society of Professional Well Logging Analysts, Houston, Texas.

56a. Dewart, G. (1968) Seismic investigation of ice properties and bedrock topography at the confluence of two glaciers, Kaskawulsh glacier, Yukon Territory, Canada. Institute of Polar Studies, Report no. 27, p. 1-207, The Ohio State University.

57. Dobrin, M.B. (1960) *Introduction to Geophysical Prospecting.* New York, Toronto, London: McGraw-Hill, Inc., 2nd ed., p. 1-446.

58. Doell, R.R. (1963) Seismic depth study of the Salmon glacier, British Columbia. *Journal of Glaciology*, vol. 4, no. 34, p. 425-437.

59. Ewing, M., A.P. Crary and A.M. Thorne, Jr. (1934) Propagation of elastic waves in ice, Part I. *Physics*, vol. 5, p. 165-168.

60. Ewing, M. and A.P. Crary (1934) Propagation of elastic waves in ice, Part II. *Physics*, vol. 5, p. 181-184.

61. Ewing, W.M., W.S. Jardetzky and F. Press (1957) *Elastic Waves in Layered Media.* New York: McGraw-Hill.

62. Förtsch, O., H.J. Schneider and H. Vidal (1955) Seismische Messungen auf dem Gepatsch- und Kesselwandferner in den Oetztaler Alpen (Seismic measurements of the Gepatsch and Kesselwand glaciers in the Oetztaler Alps). *Gerlands Beitr. Geophys.*, vol. 64, p. 233-261.

63. Förtsch, O. and H. Vidal (1956) Die Ergebnisse der seismischen Messungen auf dem Hintereisferner in den Oetztaler Alpen 1954 (Results of seismic measurements of Hintereis glacier in the Oetztaler Alps in 1954). *Gerlands Beitr. Geophys.*, vol. 65, p. 131-156.

64. Förtsch, O. and H. Vidal (1958) Die seismische Vermessung des grossen Gurgler Ferners in den Oetztaler Alpen im Spätsommer 1956, mit Vorwort von H. Reich (Seismic survey of Grosser Gurgler glacier in the Oetztaler Alps in late fall of 1956, with introduction by H. Reich). *Gerlands Beitr. Geophys.*, vol. 67, p. 1-30.

65. Förtsch, O. and H. Vidal (1958a) Beiträge zur Erforschung subglazialer Talformen und der in ihnen liegenden Ablagerungen (Studies of subglacial valley forms and the deposits they contain). IUGG General Assembly of Toronto, 1957, International Association of Scientific Hydrology, vol. 46, p. 553-562.

66. Förtsch, O. and H. Vidal (1968) Die Existenz, Beschaffenheit und Bedeutung einer Zwischenschicht zwischen Gletschereis und Felsuntergrund (Existence, nature and importance of an intermediate layer between glacier ice and bedrock). *Geol. Rundschau*, vol. 57, no. 3, p. 1019-1033.

67. Frankenstein, G. and R. Garner (1967) Linear relationship of brine volume and temperature from -0.5 to -22.9C for sea ice. *Journal of Glaciology*, vol. 6, no. 48, p. 943-944.

68. Frankenstein, G. and R. Garner (1967a) Dynamic Young's modulus of sea ice. USACRREL Technical Note (unpublished).

69. Gassmann, F. (1951) Ueber die Elastizität poröser Medien (Elasticity of porous media). *Vierteljahrsschrift der Naturforschenden Gesellschaft in Zürich*, vol. 96, p. 1-23.

70. Gassmann, F. (1964) Introduction to seismic travel time methods in anisotropic media. *Pure and Applied Geophysics*, vol. 58, p. 63-113.

71. Gassmann, F. (In prep.) Seismische Prospektion (Seismic prospecting).

72. Gerecke, F. and H.K. Müller (1932) Seismische Untersuchungen des Geophysikalischen Institutes in Göttingen, I. Messungen auf dem Rhonegletscher (Seismic investigations of the Geophysical Institute Göttingen, I. Studies on the Rhone glacier). *Zeitschrift für Geophysik*, vol. 8, p. 65-71.

73. Giese, P. (1963) Some results of seismic refraction work at the Gepatsch glacier in the Oetztal Alps. IUGG General Assembly of Berkeley, 1963, International Association of Scientific Hydrology, vol. 61, p. 154-161.

74. Giovinetto, M.B. (1960) Glaciology Report for 1958, South Pole Station. USNC-IGY Antarctic Glaciological Data. Report no. 2: Field Work 1958, Part IV. Ohio State University Research Foundation, p. 1-104.

75. Goldthwait, R.P. (1936) Seismic soundings on South Crillon and Klooch glaciers. *Geographical Journal*, vol. 87, p. 596-611.

76. Goldthwait, R.P. (1960) Study of ice cliff in Nunatarssuaq, Greenland. USA SIPRE Technical Report 39. AD 091484

77. Goodman, B. (1963) *The Radio Amateur's Handbook.* 40th edition.

78. Gow, A.J. and R. Rowland (1965) On the relationship of snow accumulation to surface topography at "Byrd Station," Antarctica. *Journal of Glaciology*, vol. 5, no. 42, p. 843-847.

79. Gow, A.J. (1968) Deep core studies of the accumulation and densification of snow at Byrd Station and Little America V, Antarctica. USACRREL Research Report 197. AD 669240

80. Gow, A.J. (In press) Deep core drilling at Byrd Station: Preliminary results of core studies. Scientific Committee on Antarctic Research (SCAR), IS-AGE, Hanover, NH, Sept 1968.

81. Green, R.E., Jr. and L. Mackinnon (1956) Determination of the elastic constants of ice single crystals by an ultrasonic pulse method. *Journal of the Acoustical Society of America*, vol. 28, p. 1292.

82. Greszczuk, L.B. (1966) Effect of foreign inclusions on properties of solids. *Proceedings of the American Society of Civil Engineers, Journal of the Engineering Mechanics Division*, vol. 92, EM 6, p. 63-78.

83. Hagedoorn, J.G. (1959) The plus-minus method of interpreting seismic refraction sections. *Geophysical Prospecting*, vol. 7, no. 2, p. 158-182.

84. Hattersley-Smith, G. (1959) Operation Hazen, narrative and preliminary reports 1957-58. Operation Hazen, D, Phys. R(G), Hazen, vol. 4, p. 1-88. Defence Research Board, Ottawa.

85. Hattersley-Smith, G. (1960) Operation Hazen, glaciological studies: snow cover, accumulation and ablation. Operation Hazen, D, Phys. R(G), Hazen, vol. 10, p. 1-13. Defence Research Board, Ottawa.

86. Helbig, K. (1958) Elastische Wellen in anisotropen Medien, Teil I und II (Elastic waves in anisotropic media, Part I and II). *Gerlands Beitr. Geophys.*, vol. 67, p. 177-211, 256-288.

87. Hobbs, P.V. (1965) The effect of time on the physical properties of deposited snow. *Journal of Geophysical Research*, vol. 70, no. 16, p. 3903-3907.

88. Hobson, G.D. (1962) Seismic exploration in the Canadian Arctic Islands. *Geophysics*, vol. 27, no. 2, p. 253-273.

89. Holtzscherer, J.-J. (1953) Sondages séismiques (Seismic soundings). In *Campagne au Groenland 1951*, Rapports préliminaires sér. sci., vol. 16, p. 45-58, Expeditions Polaires Francaises, Paris.

90. Holtzscherer, J.-J. (1954) Mesures séismiques (Seismic measurements). In *Contribution à la connaissance de l'inlandsis du Groenland*, p. 1-28, Expéditions Polaires Francaises, Paris.

91. Holtzscherer, J.-J. (1954) Seismic investigations in Inglefield Land. In *Final report on the scientific program (Program B), Operation Ice Cap 1953*, p. 287-299. Stanford Research Institute, Stanford, California.

92. Holtzscherer, J.-J. and G.deQ. Robin (1954) Depth of polar ice caps. *Geographical Journal*, vol. 120, p. 193-202.

93. Hunkins, K. (1960) Seismic studies of sea ice. *Journal of Geophysical Research*, vol. no. 10, p. 3459-3472.

94. Hunkins, K. (1962) Waves on the Arctic Ocean. *Journal of Geophysical Research*, vol. 67, no. 6, p. 2477-2489.

95. Hunkins, K. et al. (1962) Geophysical studies of the Chukchi Cap, Arctic Ocean. *Journal of Geophysical Research*, vol. 67, no. 1, p. 235-247.

96. Imbert, B. (1953) Sondages séismiques en Terre Adélie (Seismic soundings in Adelie Land). *Annales de Géophysique*, vol. 9, p. 85-92.

97. Jobert, N. (1953) Dispersion des ondes de surface dans la couche superficielle du glacier du Groenland (Dispersion of surface waves in the superficial layer of the Greenland glacier). *Annales de Géophysique*, vol. 9, p. 345-357.

98. Joesting, H.R. (1954) Geophysical exploration in Alaska. *Arctic*, vol. 7, p. 165-175.

99. Johnson, R.F. and W.H. Fischer (1966) Seismic propagation studies in the Arctic region using novel type of electromechanical transducer. U.S. Army Electronics Command, TR ECOM-2713, p. 1-38.

100. Jona, F. and P. Scherrer (1952) Die elastischen Konstanten von Eis-Einkristallen (Elastic constants of ice single crystals). *Helvetica Physica Acta*, vol. 25, p. 35-54.

101. Joset, A. (1950) Sondages séismiques (Seismic soundings). In *Campagne au Groenland 1950*, Rapports préliminaires sér. sci., vol. 15, p. 43-56. Expéditions Polaires Francaises, Paris.

102. Joset, A. and J.-J. Holtzscherer (1953) Etude des vitesses de propagation des ondes séismiques sur l'Inlandsis du Groenland (Study of the propagation velocity of seismic waves on the Greenland inland ice). *Annales de Géophysique*, vol. 9, p. 330-344.

103. Joset, A. and J.-J. Holtzscherer (1954) Détermination des épaisseurs de l'Inlandsis du Groenland (Determination of the thickness of the Greenland ice cap). *Annales de Géophysique*, vol. 10, p. 351-381.

104. Joset, A. and J.-J. Holtzscherer (1954) Expédition Franco-Islandaise au Vatnajökull mars-avril 1951. Résultats des sondages séismiques (French-Icelandic expedition to Vatnajökull in March-April 1951. Results of seismic soundings). *Jökull*, vol. 4, p. 1-33

105. Jost, W. (1936) Die seismischen Eisdickenmessungen am Rhonegletscher 1931 (Seismic thickness measurements of the Rhone glacier in 1931). *Denkschriften der Schweizerischen Naturforschenden Gesellschaft*, vol. 71, p. 29-42.

106. Joubert, J-L (1963) Stratigraphie de la glace tempérée à l'aide de la teneur en eau liquide (Stratigraphy of temperate ice by means of the content of liquid water). Comptes Rendues Acad. Sci. Paris, vol. 257, p. 3638-3639.

107. Kapitza, A.P. and O.G. Sorokhtin (1963) On errors in interpretation of reflection seismic shooting in the Antarctic. IUGG General Assembly of Berkeley, 1963, International Association of Scientific Hydrology, vol. 61, p. 162-164.

108. Kapitza, A.P. (1967) Antarctic glacial and subglacial topography. In *Proceedings of the Symposium on Pacific-Antarctic Sciences*, p. 82-91. JARE Sci. Reports, Special Issue 1, Tokyo.

109. Kaplar, C.W. (1965) Laboratory determination of the dynamic moduli of frozen soils and of ice. *Proceedings of the Permafrost International Conference 1963*, National Academy of Sciences – National Research Council, Publication 1287, p. 293-301.

110. Kaplar, C.W. (1968) Laboratory determination of the dynamic moduli of frozen soils and of ice. USACRREL Research Report 163. AD 686282

111. Kreis, A. (1944) Seismische Sondierungen auf dem Morteratschgletscher (Seismic soundings on Morteratsch glacier). *Verhandlungen der Schweizerischen Naturforschenden Gesellschaft*, vol. 124, p. 95.

112. Kreis, A., R. Florin and A. Süsstrunk (1952) Die Ergebnisse der seismischen Sondierungen des Unteraargletschers 1936-1950 (Results of seismic soundings of the Unteraar glacier 1936-1950). *Verhandlungen der Schweizerischen Naturforschenden Gesellschaft*, vol. 132, p. 125-126.

113. Lafargue, M. and R. Millecamps (1958) Sur l'application d'une méthode électroacoustique originale à des mesures physiques et mécaniques de glaciologie (Application of a new electroacoustic method for physical and mechanical measurements in glaciology). *Comptes Rendues*, 246, p. 970-973.

114. Lange, G.R. (1965) Refrigerated fluids for drilling and coring in permafrost. *Proceedings of the Permafrost International Conference 1963*, National Academy of Sciences – National Research Council Publication 1287, p. 375-380.

115. Lavergne, M. (1966) Réfraction de long des bancs minces rapides et effet d'écran pour les marqueurs profonds (Refraction in the case of thin high velocity layers...). *Geophysical Prospecting*, vol. 14, p. 504-527.

116. Langleben, M.P. and E.R. Pounder (1963) Elastic parameters of sea ice. In *Ice and Snow – Properties, Processes and Applications* (W.D. Kingery, Ed.). Cambridge, Mass.: MIT Press, p. 69-78.

117. Lee, T.-M. (1963) Method of determining dynamic properties of viscoelastic solids employing forced vibration. *Journal of Applied Physics*, vol. 34, p. 1524-1529. Also USACRREL Research Report 122. AD 434085

118. Legge, I.A., Jr. (1947/48) Report of well velocity survey of Umiat Test Well No. 2. U.S. Geological Survey Open-file Report, United Geophys. Co., Report 47-8 and 48-1.

119. Lin'kov, E.M. (1958) Izuchenie uprugikh svoistv ledianogo pokrova v Arktike (Study of the elastic properties of an ice cover in the Arctic). *Vestnik Leningradskogo Universiteta*, vol. 13, no. 4, p. 17-22.

220. Lliboutry, L. (1965) *Traité de Glaciologie*, Tome II (*Handbook of Glaciology*, Vol. II). Paris: Masson & Cie.

221. Lliboutry, L. (1966) Bottom temperatures and basal low-velocity layer in an ice-sheet. *Journal of Geophysical Research*, vol. 71, no. 10, p. 2535-2543.

222. Lotze, W. (1957) Schallgeschwindigkeitsmessungen von Eis in Abhängigkeit von Druck und Temperatur (Sound velocity measurements on ice as dependent on pressure and temperature). *Zeitschrift für Geophysik*, vol. 23, no. 5, p. 242-249.

123. Mackenzie, J.K. (1950) The elastic constants of a solid containing spherical holes. *Proceedings of the Physical Society (London), Series B*, vol. 63B, no. 1, p. 2-11.

124. Mason, W.P. (1958) *Physical Acoustics and the Properties of Solids*. Princeton: Van Nostrand Co., p. 1-402.

125. Mellor, M. (1964) Properties of snow. Cold Regions Science and Engineering (F.J. Sanger, Ed.), USACRREL Monograph III-A1, p. 1-105. AD 611023

126. Millecamps, R. and M. Lafargue (1957) Sur la propagation des ultrasons dans un glacier (Propagation of ultrasonic waves in a glacier). *Compt. Rend.*, vol. 244, p. 2824-2827.

127. Millecamps, R. and M. Lafargue (1958) Présentation d'une méthode électro-acoustique originale pour l'étude du mécanisme de l'écoulement et des déformations de la glace sur l'épaisseur d'un glacier (An account of a new electro-acoustical method for the study of the mechanism of ice flow and deformation in the thickness of a glacier). Symposium of Chamonix, 1958, International Association of Scientific Hydrology, vol. 47, p. 370-382.

128. Mothes, H. (1927) Seismische Dickenmessungen von Gletschereis (Seismic thickness measurements of glacier ice). *Zeitschrift für Geophysik*, vol. 3, p. 121-134.

129. Mothes, H. (1929) Neue Ergebnisse der Eisseismik (New results of seismic ice thickness measurements). *Zeitschrift für Geophysik*, vol. 5, p. 120-144.

130. Müller, G. (1961) Geschwindigkeitsbestimmungen elastischer Wellen in gefrorenen Gesteinen und die Anwendung akustischer Messungen auf Untersuchungen des Frostmantels an Gefrierschächten (Velocity determinations for elastic waves in frozen rocks and the application of acoustic surveys for investigation of the frozen zone around a freezing shaft). *Geophysical Prospecting*, vol. 9, no. 2, p. 276-295.

131. Musgrave, M.J.P. (1954) On the propagation of elastic waves in aeolotropic media. I. General principles; II. Media of hexagonal symmetry. *Proceedings of the Royal Society (Ser. A)*, vol. 226, p. 339-366.

132. Musgrave, M.J.P. (1961) Elastic waves in anisotropic media. *Progress in Solid Mechanics*, vol. 2, p. 61-85.

133. Myers, W.H. (1951) Geophysical prospecting for oil through permafrost. *Bulletin of the National Research Council*, vol. 122, p. 73-74.

134. Nafe, J.E. (1957) Reflection and transmission coefficients at a solid-solid interface of high velocity contrast. *Bulletin of the Seismological Society of America*, vol. 47, no. 3, p. 205-219.

135. Nakaya, U. (1959) Visco-elastic properties of snow and ice in the Greenland ice cap. USA SIPRE Research Report 46. AD 226274

136. Nakaya, U. (1959) Visco-elastic properties of processed snow. USA SIPRE Research Report 58. AD 235329

137. Nakaya, U. (1961) Elastic properties of processed snow with reference to its internal structure. USACRREL Research Report 82. AD 277541

138. Northwood, T.D. and F.W. Simpson (1948) Depth measurements in the Seward ice field by sonic echo ranging. National Research Council of Canada, Division of Physics, Report PS 300.

139. Oelsner, C. (1965) Seismoakustik, eine neue Messmethode für die Gletschermechanik (Seismo-acoustics, a new technique in glacier mechanics research). *Polarforschung*, vol. 6, no. 35, p. 19-27.

140. Oliver, J., A.P. Crary and R. Cotell (1954) Elastic waves in Arctic pack ice. *Transactions of the American Geophysical Union*, vol. 35, p. 282-292.

141. Omote, S., Y. Yamazaki, N. Kobayashi and I. Murauce (1955) Ice tremors generated in the floating lake ice. *Tokyo University Earthquake Research Institute Bulletin*, vol. 5, no. 33/4, p. 663-679.

142. Paterson, W.S.B. and J.C. Savage (1963) Geometry and movement of the Athabaska glacier. *Journal of Geophysical Research*, vol. 68, no. 15, p. 4513-4520.

143. Pickett, G. (1945) Equations for computing elastic constants from flexural and torsional resonant frequencies of vibration of prisms and cylinders. *Proceedings of the American Society of Testing Materials*, vol. 45, p. 846-865.

144. Poulter, T.C. (1947) Seismic measurements on the Ross shelf ice – Part I and II. *Transactions of the American Geophysical Union*, vol. 28, p. 162-170, 367-384.

145. Poulter, T.C. (1950) *Geophysical studies in the Antarctic.* Stanford Research Institute, Stanford, California, p. 1-180.

146. Poulter, T.C., C.F. Allen and S.W. Miller (1950) Seismic measurements of the Taku glacier. In *Geophysical Studies in the Antarctic*, Appendix III. Stanford Research Institute, Stanford, California.

147. Pounder, E.R. and P. Stalinsky (1961) Elastic properties of Arctic sea ice. IUGG General Assembly of Helsinki, International Association of Scientific Hydrology, vol. 54, p. 35-39.

148. Pounder, E.R. (1962) The physics of sea-ice. In *The Sea, Vol. I, Physical Oceanography.* New York: Interscience, Chap. 7, p. 826-838.

149. Pounder, E.R. and M.P. Langleben (1964) Arctic sea ice of various ages. II. Elastic properties. *Journal of Glaciology*, vol. 5, no. 37, p. 99-105.

150. Pratt, J.G.D. (1960) Trans-Antarctic Expedition 1955-1958, No. 3, Seismic soundings across Antarctica. Trans-Antarctic Expedition Committee, London, p. 1-69.

151. Press, F., M. Ewing, A.P. Crary, S. Katz and J. Oliver (1950) Air-coupled flexural waves in floating ice. *Transactions of the American Geophysical Union*, vol. 32, p. 166-172; Lamont Geological Observatory, Geophysical Research Paper 6, p. 1-46; Air Force Cambridge Research Laboratory, Cambridge, Mass., p. 1-46.

152. Ragle, R.H., B.L. Hansen, A.J. Gow and R.W. Patenaude (1960) Deep core drilling in the Ross Ice Shelf, Little America V, Antarctica. USA SIPRE Technical Report 70. AD 648511

153. Redpath, B.B. (1965) Seismic investigations of glaciers on Axel Heiberg Island. Axel Heiberg Island Research Reports, McGill University, *Geophysics*, vol. 1, p. 1-26.

154. Riznichenko, IU.V. (1942) O seismicheskikh svoistvakh sloia vechnoi merzloty (Seismic properties of permafrost). *Izvestiia Akademii Nauk SSSR, Seriia Geograficheskaia i Geofizicheskaia*, vol. 6, p. 263-274.

155. Robin, G.deQ. (1953) Measurements of ice thickness in Dronning Maud Land, Antarctica. *Nature*, vol. 171, p. 55-58.

156. Robin, G.deQ. (1958) Seismic shooting and related investigations, Glaciology III. Norwegian-British-Swedish Antarctic Expedition 1949-52. *Scientific Results*, vol. 5, p. 1-134.

157. Robinson, E.S. (1962) Results of geophysical studies on the McMurdo to South Pole traverse. Geophysical Polar Research Center Research Report Ser. 62-6, p. 1-49, Wisconsin University, Department of Geology.

158. Robinson, E.S. (1968) Seismic wave propagation on a heterogeneous polar ice sheet. *Journal of Geophysical Research*, vol. 73, no. 2, p. 739-753.

159. Robinson, F.M. (1959) Test wells, Simpson area, Alaska, with a section on core analysis by S.T. Yuster. U.S. Geological Survey Professional Paper 305-J, p. 523-568.

160. Roethlisberger, H. (1955) Studies in glacier physics on the Penny ice cap, Baffin Island, 1953. Part III. Seismic sounding. *Journal of Glaciology*, vol. 2, no. 18, p. 539-552.

161. Roethlisberger, H. (1959) TUTO seismic survey. USA SIPRE Technical Report 64, p. 1-13. AD 135203

162. Roethlisberger, H. (1961) The applicability of seismic refraction soundings in permafrost near Thule, Greenland. USA CRREL Technical Report 81, p. 1-35. AD 276607

163. Roethlisberger, H. (1961) Seismic refraction soundings in permafrost near Thule, Greenland. In *Geology of the Arctic. Proceedings of the 1st International Symposium on Arctic Geology*, vol. 2, p. 970-980. Toronto: University of Toronto Press.

164. Roethlisberger, H. (1963) Ultrasonic measurements of deformation around a rectangular ice tunnel. In *Ice and Snow – Properties, Processes and Applications* (W.D. Kingery, Ed.). Cambridge, Mass.: MIT Press, p. 187-211.

165. Roethlisberger, H. (1964) Reflection and transmission coefficients at the interface ice-solid. USACRREL Research Report 110, p. 1-17. AD 602414

166. Roethlisberger, H., C.R. Bentley and H. Bennett (1965) Movement studies by seismic soundings on the Greenland ice sheet. USACRREL Research Report 161, p. 1-25. AD 617618

167. Roethlisberger, H. (1966) Ultrasonic pulse measurements in anisotropic lake ice. USA CRREL Research Report 126, p. 1-21. AD 642110

168. Rüter, H. (1967) Berechnung der Richtungsabhängigkeit der P-Wellen-Geschwindigkeit in polykristallinen Eisproben mit vorgegebener C-Achsen-Verteilung aus den elastischen Konstanten des Einkristalls (Computation of the P-wave velocity in function of direction for polycrystalline ice samples with known c-axes distribution from the elastic constants of monocrystals). *Polarforschung*, vol. 6, no. 37, p. 175-177.

169. Sandstrom, H. (1959) Geophysical methods in glaciology. Operation Hazen, D Phys R(G) Hazen, vol. 3, p. 1-52. Defence Research Board, Ottawa.

170. Sellmann, P.V. (1967) Geology of the USACRREL permafrost tunnel, Fairbanks, Alaska. USACRREL Technical Report 199, p. 1-26. AD 660310

171. Sorge, E. (1930) Die ersten Dickenmessungen des grönländischen Inlandeises (The first thickness determinations of the Greenland ice sheet). *Zeitschrift für Geophysik*, vol. 6, no. 1, p. 22-31.

172. Sorokhtin, O.G., O.K. Kondrat'ev and IU.N. Avsiuk (1960) Metodika i osnovnye resul'taty seismicheskikh i gravimetricheskikh issledovaniia stroeniia Vostochnoi Antarktidy (Methods and principal results of seismic and gravimetric studies of eastern Antarctica).

Izvestiia Akademii Nauk SSSR, Seriia Geofizicheskaia, vol. 3, p. 396-401. Translated in *Bulletin of the Academy of Sciences, USSR, Geophys. Ser. 3*, p. 265-268.

173. Süsstrunk, A. (1951) Sondage du glacier par la méthode seismique (Sub-surface glacier investigations: seismic soundings). *La Houille Blanche*, vol. 6, p. 309-317.

174. Swartz, J.H. and E.R. Shepard (1946) Report on a preliminary investigation of the possible application of geophysical methods to studies of permafrost problems in Alaska. Corps of Engineers, St. Paul District, p. 1-67.

175. Swinzow, G.K. (1964) Tunneling in permafrost. USACRREL Technical Report 91, p. 1-18. AD 435608

176. Tarrant, L.H. (1956) A rapid method of determining the form of a seismic refractor from line profile results. *Geophysical Prospecting*, vol. 4, no. 2, p. 131-139.

177. Thiel, E., C.R. Bentley, N.A. Ostenso and J.C. Behrendt (1959) Oversnow traverse programs, Byrd and Ellsworth Stations, Antarctica, 1957-1958; Seismology, gravity and magnetism. IGY Glaciological Report Ser. 2, IGY World Data Center A, Glaciology, American Geographical Society.

178. Thiel, E. and J. Behrendt (1959) Seismic studies on the Filchner ice shelf, Antarctica, 1957-1958. See Thiel et al.[177]

179. Thiel, E. and J. Behrendt (1959) Seismic studies at the Ellsworth snow pit. See Thiel et al.[177]

180. Thiel, E. and N.A. Ostenso (1961) Seismic studies on Antarctic ice shelves. *Geophysics*, vol. 26, no. 6, p. 706-715.

181. Thornburgh, H.R. (1930) Wave-front diagrams in seismic interpretation. *Bulletin of the American Association of Petroleum Geologists*, vol. 14, no. 2.

182. Thyssen, F. (1967) Die Temperaturabhängigkeit der P-Wellen geschwindigkeit in Gletschern und Inlandeisen (Temperature dependency of the P-wave velocity in glaciers and continental ice sheets). *Zeitschrift für Geophysik*, vol. 33, p. 65-69.

183. Vallon, M. (1967) Etude de la Mer de Glace, 4: Le glacier du Tacul (Investigations of Mer de Glace, 4: Glacier du Tacul). Rapport. Sci. Laboratoire Géophys. et Glaciol. Grenoble, vol. 102.

184. Voigt, W. (1928) *Lehrbuch der Kristallphysik (Handbook of Crystal Physics)*. Teubner, Leipzig and Berlin, 2nd ed., p. 1-978.

185. Wachholz, H. and G. Müller (1964) The relationship of the ultimate strength and sound velocity in frozen layers of soil with regard to the construction of frozen shafts. *Zeitschrift für Geophysik*, vol. 30, no. 3, p. 127-139.

186. Weber, J.R. and H. Sandstrom (1960) Geophysical methods in glaciology, Part II: Seismic measurements on Operation Hazen in 1958. Operation Hazen, D Phys R(G), Hazen, vol. 6, p. 1-9. Defence Research Board, Ottawa.

187. Weber, M. (1957) Die abschnittweise Darstellung einer gemessenen Laufzeitkurve mit abgebrochenen Potenzreihen und ihre Auswertung in der Refraktionsseismik (Sector by sector approximation of observed travel time curves by incomplete power series and application to refraction soundings). *Geofisica Pura e Applicata*, vol. 38, no. 3, p. 57-80.

188. Weeks, W.F. and A. Assur (1967) The mechanical properties of sea ice. Cold Regions Science and Engineering (F.J. Sanger, Ed.), USACRREL Monograph II-C3, p. 1-94. AD 662716

189. Weihaupt, J.G. (1961) Geophysical studies in Victoria Land, Antarctica. Geophysical Polar Research Center, Research Report ser. 61-1, p. 1-123. Wisconsin University, Department of Geology.

190. Weihaupt, J.G. (1963) Seismic and gravity studies at the South Pole. *Geophysics*, vol. 28, no. 4, p. 582-592.

191. Westphal, J.A. (1965) In situ acoustic attenuation measurements in glacial ice. *Journal of Geophysical Research*, vol. 70, no. 8, p. 1849-1853.

192. Wiancko, E. (1950) Report of well velocity survey on Minga Velocity Test no. 4. U.S. Geological Survey Open-file Report, United Geophys. Co., Report 50-7.

193. Willie, M.R.J., A.R. Gregory and L.W. Gardner (1956) Elastic wave velocities in heterogeneous and porous media. *Geophysics*, vol. 21, p. 41-70.

194. Woolson, J.R. et al. (1962) Seismic and gravity surveys of Naval Petroleum Reserve no. 4 and adjoining areas, Alaska. U.S. Geological Survey Professional Paper 304-A, p. 1-25.

195. Wyrobek, S.M. (1956) Application of delay and intercept times in the interpretation of multilayer refraction time distance curves. *Geophysical Prospecting*, vol. 4, no. 2, p. 112-130.

196. Zykov, IU.D. (1966) Primenenie ul(trazvuka dlia izucheniia fiziko-mekhanischeskikh svoistv merzlykh porod i proiskhodiaschikh v nikh protsessov (Ultrasonic study of physical and mechanical properties of frozen rocks and the internal processes). Moskov. Gosud. Univ., Merzlotnye Issledovaniia, Vyp. 6, p. 184-198.

197. Crary, A.P., R.D. Cotell and Jack Oliver (1952) Geophysical studies in the Beaufort Sea, 1951. *Transactions of the American Geophysical Union*, vol. 33, p. 211-216.

APPENDIX A: COMPUTATION OF RAY VELOCITY AS A FUNCTION OF DIRECTION FOR UNIAXIALLY ANISOTROPIC MEDIA

(Roethlisberger[167])

The problem of the propagation of elastic waves in anisotropic media was mathematically treated by Rudzki as far back as the end of the last century and, more completely, in 1911. More recent treatments followed by Musgrave,[131 132] Miller and Musgrave, Postma, Helbig,[86] Buchwald, and Gassmann.[70] Beryl, which is very similar to ice in its elastic anisotropy, is often used as an example for hexagonal symmetry, i.e. uniaxial anisotropy.

Helbig's presentation served as a guide to set up programs for a Bendix G-15D electronic computer.* The following equations were used to compute ray velocities from the elastic constants c_{11}, c_{33}, c_{44}, c_{12} and c_{13} and the density ρ, with $c_{66} = (c_{11} - c_{12})/2$, $A = c_{13} + c_{44}$, $B = c_{11} - c_{44}$, $C = c_{33} - c_{44}$ and $E^2 = BC - A^2$:

$$\frac{\rho}{c_{66}} z_1^{(1)2} + \frac{\rho}{c_{44}} z_3^{(1)2} = 1 \tag{93}$$

$$\left.\begin{aligned} n_1^{(2)2} &= \frac{C w^{(2)} + A w^{(2)2}}{A c_{44} + (c_{11} c_{33} - c_{44}^2 - A^2) w^{(2)} + A c_{44} w^{(2)2}} \\ n_3^{(2)2} &= \frac{A + B w^{(2)}}{A c_{44} + (c_{11} c_{33} - c_{44}^2 - A^2) w^{(2)} + A c_{44} w^{(2)2}} \end{aligned}\right\} \tag{94}$$

$$\left.\begin{aligned} z_1^{(2)} &= n_1^{(2)} \left[c_{44} + \frac{E^2}{C + 2A w^{(2)} + B w^{(2)2}} \right] \frac{1}{\sqrt{\rho}} \\ z_3^{(2)} &= n_3^{(2)} \left[c_{44} + \frac{E^2 w^{(2)2}}{C + 2A w^{(2)} + B w^{(2)2}} \right] \frac{1}{\sqrt{\rho}} \end{aligned}\right\} \tag{95}$$

$$\left.\begin{aligned} n_1^{(3)2} &= \frac{C w^{(3)} + A w^{(3)2}}{A c_{33} + (c_{11} c_{33} - c_{44}^2 + A^2) w^{(3)} + A c_{11} w^{(3)2}} \\ n_3^{(3)2} &= \frac{A + B w^{(3)}}{A c_{33} + (c_{11} c_{33} - c_{44}^2 + A^2) w^{(3)} + A c_{11} w^{(3)2}} \end{aligned}\right\} \tag{96}$$

$$\left.\begin{aligned} z_1^{(3)} &= n_1^{(3)} \left[c_{11} - \frac{E^2}{C + 2A w^{(3)} + B w^{(3)2}} \right] \frac{1}{\sqrt{\rho}} \\ z_3^{(3)} &= n_3^{(3)} \left[c_{33} - \frac{E^2 w^{(3)2}}{C + 2A w^{(3)} + B w^{(3)2}} \right] \frac{1}{\sqrt{\rho}} \end{aligned}\right\} \tag{97}$$

* Some misprints were discovered in his paper. The second line of his equation 74 should contain c_{33} instead of c_{11}. In equation 75, c_{11} should replace c_{44} in the numerator and $[B - (E^2/c_{33})]$ replace $[B + (E^2/c_{44})]$ in the denominator, and the whole expression must be multiplied by c_{11}/c_{33}.

The expressions $z_1^{(i)}$ and $z_3^{(i)}$ are components of the ray velocity in cylindrical coordinates, where $z_3^{(i)}$ is parallel to the crystallographic c-axis ($n_1^{(i)}$ and $n_3^{(i)}$ are similar components of the index vector). The index i, $i = 1, 2, 3$, corresponds to three different types of waves, namely (1) a true shear wave S_1 polarized perpendicular to the plane through the ray and c-axis, (2) and (3) a quasi-transverse wave S_2 and a quasi-longitudinal wave P respectively, polarized in the plane through the ray and the c-axis. The parameters $w^{(2)}$ and $w^{(3)}$ can be arbitrarily chosen and vary in the interval $0 \leq w^{(i)} \leq \infty$.

APPENDIX B: VARIOUS METHODS FOR DETERMINING ELASTIC AND SEISMIC PROPERTIES OF ICE, IN PARTICULAR THOSE APPLICABLE ON FLOATING ICE SHEETS

(From Anderson[4])

Elasticity – Methods of Measurement

I. Laboratory (Small Scale) Methods

- A. Static determinations – stress-strain relations measured directly
  1. Linear extension, contraction, and "bulging" due to load
  2. Volume change due to confining pressure
  3. Bending or flexural tests
  4. Torsion or twisting
- B. Dynamic determinations
  1. Natural (resonant) frequencies of transverse, torsional, flexural, and longitudinal vibrations
  2. Direct seismic velocities through small samples

II. Field Methods

- A. Static
  1. Deflection of beam, plate, edge or sector under a load
     - (a) Measurement of deflection
     - (b) Measurement of "wavelength" of deflection
     - (c) Measurement of deflection dish profile
     - (d) Measure to maximum moment (breaking point)
- B. Dynamic.
  1. Moving load
     - (a) "Wavelength" of deflection
     - (b) Wave shape
     - (c) Amplitude of deflection
     - (d) Resonance curve, critical velocity
     - (e) Flexural wave dispersion
     - (f) Forced vibration of sheet to obtain resonant frequency
  2. Seismic measurements
     - (a) Velocity
       - (1) *P* wave
       - (2) *S* wave
       - (3) Surface and flexural waves
     - (b) Dispersion and frequency measurements
       - (1) Flexural wave dispersion
       - (2) Air-coupled flexural wave frequency
       - (3) Multi-reflected waves

Internal Friction – Methods of Measurement

I. Laboratory Methods

- A. Decay of oscillation of freely vibrating specimen
- B. Sharpness of resonance curve under forced vibration
- C. Heat produced when specimen taken around a stress cycle
- D. Attenuation of stress wave when it travels through a solid
- E. Spreading of a stress pulse as it propagates
- F. Viscoelastic dispersion of seismic wave
- G. Viscous coupling
- H. Phase lag of strain to stress on cyclic loading
- I. Dynamic stress-strain measurements

II. Field Methods

- A. Deflection measurements
  1. Decay of free oscillation-sudden loading and unloading
  2. Amplification at resonance
  3. Forced vibration of sheet to obtain natural frequency, damping and shape of resonance curve
     - (a) Vibrator
     - (b) Moving load
  4. Sag of sheet under load, recovery after load removal
- B. Seismic
  1. Attenuation, spreading and shifting of pulses

APPENDIX C: SPATIAL SOLUTIONS FOR REFLECTION SOUNDINGS

Analytical Method for an *L*-Spread on a Gently Sloping Surface[160, 169]

The method is based on the assumption that the reflections come from a plane rock surface. The extended ray paths of the reflected waves to all geophones intersect in a point which is the mirror image of the shot point with respect to the reflecting plane. The reflection times of three geophones are used for the analysis, say the ones at the apex (G_o) and at both ends of the *L*-spread (G_u, G_v), of which the horizontal projection is rectangular. It is assumed that they are set up on a fairly level surface. An approximately rectangular coordinate system (u, v, w) is introduced with the origin in G_o and the u and v axes through G_u and G_v respectively. The rectangular coordinate system (x, y, z) has the same origin G_o, vertical z-axis, and x and y are the horizontal projections of u and v respectively. The following additional symbols are used (Fig. C1).

S = shot point

P = image shot point

R = reflection point

c = distance $G_o G_u = G_o G_v$

δ_u = angle from x to u measured in the (x, z)-plane = slope of u-axis, positive for down-slope

δ_v = angle from y to v measured in the (y, z)-plane = slope of v-axis, positive for down-slope

s = distance between 0 and S

p = distance between 0 and $P = Vt_0$

r = distance between G_u and $P = Vt_u$

q = distance between G_v and $P = Vt_v$

V = velocity V_P or V_S (for converted PS-reflections see below)

$\cos\alpha_u$, $\cos\alpha_v$, $\cos\alpha_w$ = direction cosines of the ray $G_o RP$ in the (u, v, w)-system

$\cos\alpha_x$, $\cos\alpha_y$, $\cos\alpha_z$ = direction cosines of the ray $G_o RP$ in the (x, y, z)-system

The direction cosines of the ray from G_o to the image point P are given by:

$$\left.\begin{aligned} \cos\alpha_u &= \frac{p^2 - r^2 + c^2}{2pc} \approx \frac{V(t_u - t_o)}{C} \\ \cos\alpha_v &= \frac{p^2 - q^2 + c^2}{2pc} \approx \frac{V(t_v - t_o)}{C} \\ \cos\alpha_w &= \sqrt{1 - \cos^2\alpha_u - \cos^2\alpha_v} \end{aligned}\right\} \qquad (98)$$

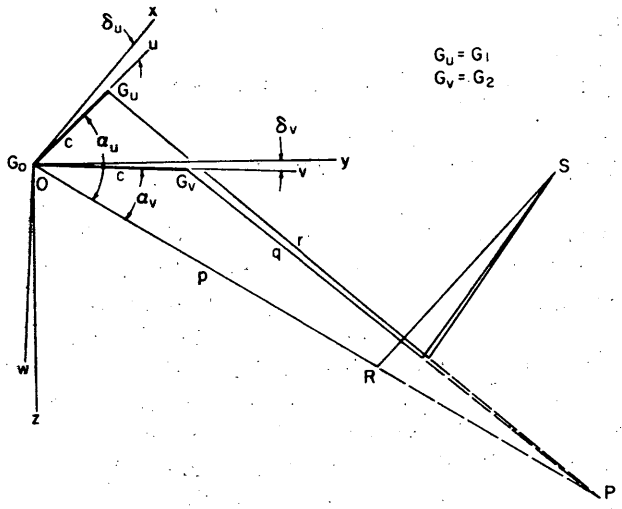

a. *3-dimensional space diagram for reflection calculations when using an* L-*shaped geophone spread.*

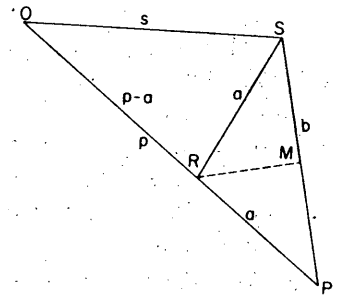

b. *Diagram for calculating the position of* R.

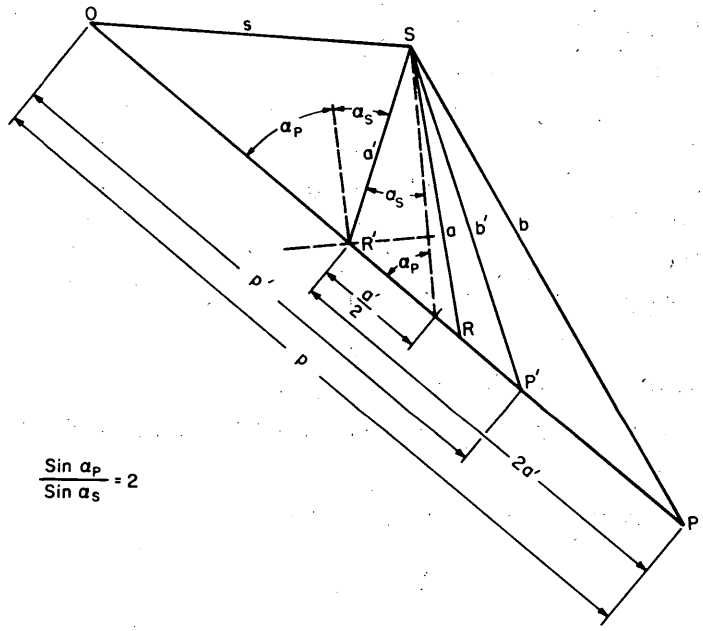

c. *Diagram and symbols for calculating an* SP *reflection.*

Figure C1. Diagrams for analytical solution for 3-dimensional reflection soundings. (After Sandstrom[169]*)*

if $c \ll p$, q, r and $|t_u - t_o| \ll t_o$, or, in the (x, y, z) coordinate system from coordinate transformation, by

$$\left.\begin{aligned} \cos\alpha_x &= \cos\alpha_u \cos\delta_u - \cos\alpha_w \sin\delta_u \\ \cos\alpha_y &= \cos\alpha_v \cos\delta_v - \cos\alpha_w \sin\delta_v \\ \cos\alpha_z &= \sqrt{1 - \cos^2\alpha_x - \cos^2\alpha_y} \end{aligned}\right\}. \qquad (99)$$

The coordinates of P in the (x, y, z) system are:

$$\left.\begin{aligned} x_p &= p\cos\alpha_x \\ y_p &= p\cos\alpha_y \\ z_p &= p\cos\alpha_z \end{aligned}\right\} . \qquad (100)$$

The coordinates of the reflection point R are found from eq 53 and 54, or explicitly from further geometric considerations (Fig. C1b), based on the common angle of the triangles OSR and OSP:

$$\left.\begin{aligned} x_r &= Kx_p \\ y_r &= Ky_p \\ z_r &= Kz_p \end{aligned}\right\} \qquad (101a)$$

where

$$K = \left(1 - \frac{a}{p}\right) = \frac{p^2 - s^2}{b^2 + p^2 - s^2} \qquad (101b)$$

$$b^2 = (x_s - x_p)^2 + (y_s - y_p)^2 + (z_s - z_p)^2. \qquad (101c)$$

(It may be noticed that the shot point enters only now into the computation and not before, and that placing it at a certain relation to the spread, i.e. on one of the axes, is only a minor simplification.) The dip angle θ of the reflecting plane and the direction of the dip ϕ are found from eq 55 and 56 (see Fig. 35b).

For the solution of the problem of the converted reflection R_{SP} equation 101a for the reflection point has to be replaced by (see Fig. C1c)

$$\left.\begin{aligned} x_r' &= K'x_p \\ y_r' &= K'y_p \\ z_r' &= K'z_p \end{aligned}\right\} \qquad (102a)$$

where

$$K' = 1 - \frac{2a'}{p} \qquad \text{since } V_P = 2V_S \qquad (102b)$$

and

$$a' = \frac{f}{3Kp} - \sqrt{\left(\frac{f}{3Kp}\right)^2 - \frac{f}{3}\left(\frac{1-K}{K}\right)} \qquad (102c)$$

with $f = p^2 - s^2$ and K from eq 101. For dip and strike an additional point P'' is computed:

$$\left.\begin{aligned} x_p'' &= K'' x_p \\ y_p'' &= K'' y_p \\ z_p'' &= K'' z_p \end{aligned}\right\} \qquad (103a)$$

where

$$K'' = 1 - \frac{3a'}{2p} \qquad (103b)$$

and dip and direction of dip are computed with eq 55 and 56, where the coordinates of P are replaced by those of P''. Equations similar to 102 and 103 can be developed for R_{PS}.

Graphical Method for 4 Geophones on a Plane of Arbitrary Slope

The projections G_1', G_2', G_3', G_4' of the 4 geophones G_1, G_2, G_3 and G_4 form a square in the horizontal x, y plane in the illustration (Fig. C2), but this is by no means a requirement for the graphical method. With only slight modifications it can be applied to a group of only three geophones, which must not be on one line, however. The following is one of many ways to proceed in the geometrical construction of reflection point, dip and strike. The method is shown in multiple steps, but in practice all the construction can be carried out on a single sheet. The steps are:

1. Construct the intersection (a) of the plane containing the geophones with the x, y plane; find the azimuth ϕ_0, and the slope θ_0 of the geophone plane (Fig. C2a).

2. Construct in the geophone plane: the true position of the geophones; the intersections of the spheres r_1, r_2, r_3, r_4 with each other and the "square" determined by the intersections (test square of Lliboutry graphically solved; it is not exactly a square because the geophones are not located on a square); and the center C of this "square." Construct further in the plane perpendicular to the geophone plane through O and C: the depth g of the image shot point P below the geophone plane (Fig. C2b).

3. Construct in the plane perpendicular to (a) through C: the new position of P and the intersection of this plane with the x, y plane, read z_p; construct the projection P' of the image point in the x, y plane, read x_p, y_p, (Fig. C2c).

4. Plot $S^*(x_s, y_s)$ in the x, y plane and indicate the direction ϕ of the dip = direction $(P'S')$; construct the true distance $\overline{SP}$ in a vertical plane through S' and P' and indicate the dip angle θ (Fig. C2d).*

5. Determine the true distance $\overline{OS}$ in a vertical plane through O and S'. Construct the triangle OSP in the tilted plane containing the three points from the true lengths, and find R at the intersection of $\overline{OP}$ with the median perpendicular to $\overline{PS}$. Find the coordinates of R, z_r in the vertical plane through O and P', x_r and y_r in the x, y plane (Fig. C2e); plot strike and dip at the projection R'.

---

* S is in no way related to the geophone array and can therefore be chosen in a survey, without complication for the graphical solution as presented here.

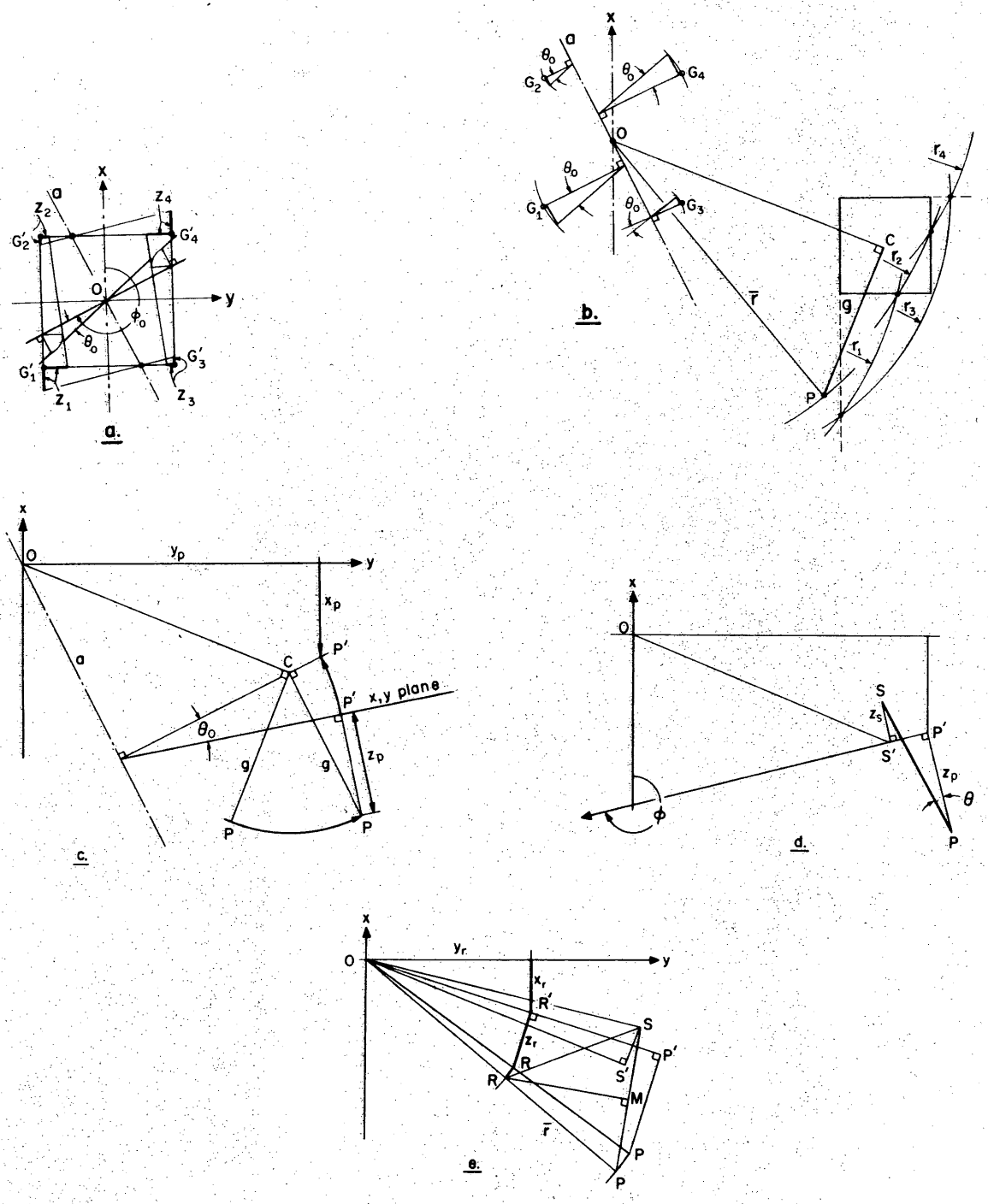

Figure C2. Graphical solution for 3-dimensional reflection soundings. (Explanations see text.)

APPENDIX D: GLOSSARY

(Pratt[150])

The technical terms used in seismic work need explanations, both for the benefit of the layman who has not the least idea what any of them mean, and also for the expert who knows only too well that different writers use them with different meanings.

Arrival	The first arrival of a pulse of seismic vibrations at a geophone. As there are many possible routs by which a pulse can travel from a shot to the geophones, one shot will give many successive arrivals; the very first of all these is termed the "first break."*
Arrival correction (ΔT_a)	The arrival itself is rarely measurable on a record; some later event nearer the middle of a pulse of vibrations has to be measured. The arrival correction allows for the difference in time between these two. [See ref. 150, Pt. II, Sect. 2.2.]
Arrival velocity (V_a)	The velocity with which a single pulse of vibrations travels along a line of geophones.
Camera	The part of the apparatus which actually produces a paper record photographically. It comprises far more equipment than the purely photographic device suggested by the name.
Central geophone	A geophone very close to the shot point, and intended to record reflections like all the others. It is very rarely used in the field, but appears mainly as a useful concept in interpretation. Not to be confused with the up-hole geophone (q.v.).
Central ray	A ray from the shot which is reflected back along its own path so as to be recorded by the central geophone.
Central time (T_0)	The time for an arrival to reach the central geophone
Channel	One of a number of identical sections of the apparatus, comprising one or more geophones, an amplifier with various filters, etc., and a galvanometer with optical parts in the camera.
Correction	An adjustment made to a time read from a record, so as to bring it into line with the idealized conditions envisaged during interpretation. Positions of geophones and of the shot may also have corrections applied to them for the same reason.
Direct wave	A wave which goes from the shot to a geophone without going deep enough to encounter a refractor, that is, a bed at the top surface of which abrupt refraction can occur. Although it therefore always remains comparatively close to the surface a direct wave has no connection with surface waves (q.v.).
Dip	This differs from the geological usage, which normally means the angle at which a bed or surface slopes down, measured in the direction for which the slope is steepest. In seismic work the dip does not usually mean this greatest value of the slope, but a lesser one measured in a plane normal to the bed and which contains the geophone line.

* Not in this Monograph, where "first break" is used for the onset of a signal.

First break	The very first arrival of a pulse of vibrations at a geophone. It always corresponds to a ray which has suffered refraction but no reflection. (See footnote on p. 135.)
Geophone	A device for converting seismic vibrations into electrical oscillations. A common design resembles a moving coil microphone in principle, but is made for much lower frequencies.
Geophone string	A set of geophones permanently connected together by lengths of wire.
Intercept time (T_i)	An extrapolated and hypothetical arrival time for the central geophone position beside the shot point. The extrapolation is carried out from the times of refraction arrivals recorded by more or less distant geophones.
Jumper	A short length of cable with plugs, sockets or clips on its ends so that it can be inserted into the apparatus to make a connection that is only occasionally required.
Line	A line marked out with a series of positions for geophones and shot points, so designed as to be covered continuously by a succession of spreads.
Mix	The combination electrically of the outputs of two or more channels. The apparatus provided for several different ways of doing this mixing, the one required being selected by a switch. Mixing seeks to achieve the same sort of effect as the use of multiple geophones (q.v.), and has the advantage of easy control by a switch. Its disadvantage is that relatively few kinds of mixing can be built in to the apparatus, and that far better results can consequently be obtained by multiple geophone arrays designed on the spot to suit local conditions.
Moveout	The increase in time needed for a reflected pulse to reach a distant geophone as compared with one at the shot point.
Multiple geophones	A group of geophones all connected to the input of the same channel; the group is usually wired up into a permanent geophone string (q.v.) with a single pair of connectors brought out, so that the whole lot can be treated as a single unit. The object is to lay out the geophones forming the group in a suitable pattern so as to strengthen the reception of a reflected seismic pulse more than the reception of noise.
Noise	Unwanted vibrations which tend to cover up reflections and refractions on a record, and which make the important arrivals difficult to pick. This term describes something closely analogous to noise in a street or a crowded room, which makes it difficult to hear faint but interesting sounds.
Offset	The horizontal distance covered by a seismic ray which is not following an interface between two layers. For example, the horizontal distance between the point where a ray leaves a refractor, and a geophone where it ends on the surface, is known as the geophone offset.

Overburden	The medium lying on top of a seismic reflector or refractor. Quite often the term refers to a simplified version of the true medium – for instance, an imaginary bed having the same dimensions as the real overburden but with a constant velocity throughout. In such a case the constant velocity is in the nature of an average of all the velocities in the real overburden, its value being chosen so as to reproduce some important seismic property; this average is termed the "overburden velocity" V_0 or $\bar{V}$ if it is especially desired to emphasize that it is an average and not anything physically real.
Peak	A point on a record where a trace rises towards the top of the paper and then falls again. Depending on the type of geophone and the rest of the circuit it may represent the instant when the ground is moving down fastest, when it has its greatest upward acceleration, or some other such situation.
Pick	To choose an event or series of events on a record with a view to measurement and interpretation of their significance.
Reflection	Three meanings are current. (i) The turning back of a pulse of seismic vibrations when it meets a discontinuity, etc., in accordance with ordinary ray- or wave-theory. (ii) A system of seismic prospecting based on the study of pulses which have undergone reflection in the above sense. (iii) The disturbance which shows on a record when a pulse reaches the geophones after being reflected.
Reflector	A discontinuity or region of rapidly changing properties which is able to reflect seismic pulses.
Refraction	Two meanings are current. (i) The bending either gradually or abruptly of a seismic ray as it traverses regions of changing propagation velocity, in accordance with ordinary ray- or wave-theory. (ii) A system of seismic prospecting based on the study of rays which have not undergone reflection.
Refractor	Two meanings are current. (i) An interface across which abrupt refraction can occur. (ii) A bed whose top surface can act as a refractor in the first sense.
Shot point	A position marked on the surface of the ground at which, or underneath which, an explosive charge is to be fired.
Shot signal	An electrical signal originated by the shot-firing apparatus at the exact instant of the explosion, and which is used to make a mark of some kind on the record.
Spread	A complete layout of all the apparatus needed to record a shot. In the case of reflection work, where the shot point is in amongst the geophones, the shooting arrangements are also included in the spread.
Spread cable	A long cable containing many pairs of insulated wires, used for connecting the recording apparatus to the geophones laid out on the spread. The spread cable incorporates suitable electrical connectors at the ends and at intervals along its length where the geophones are placed.

Surface wave	A type of wave motion which can only exist in the neighborhood of a free surface; not to be confused with direct wave (q.v.).
Take-out	A point along the length of a spread cable at which connectors are fitted for joining to a geophone.
Time break	The mark produced on a record by the shot signal.
Time break correction (ΔT_t)	On a record times are measured from a quite arbitrary origin; this correction adjusts the times so as to make them refer to the instant of firing the shot. [See ref. 150, Pt. II, Sect. 2.1.]
Timing lines	Lines placed right across a record at regular intervals of time.
Trace	A line running along the length of a record and which constitutes a graph of the signal passing through one channel, or of mixed signals from two or more channels.
Trough	A point on a record where a trace falls towards the bottom of the paper and then rises again. It is the opposite of a peak (q.v.).
Two-way time	The time needed for a seismic pulse to go from a shot to a reflector and then back up to a geophone, as distinct from one-way time which covers only the journey from the shot to the reflector.
Up-hole geophone	A geophone placed close to the opening of a shot hole, and intended only to pick up the first vibrations which have travelled almost vertically up to it. No attempt is made to record any later event by means of this geophone.
Weathering	A region extending not very far below the surface in which abnormally low seismic velocities predominate. It has nothing to do with the surface decay as implied by weathering in geology or physiography.

DOCUMENT CONTROL DATA - R & D

(Security classification of title, body of abstract and indexing annotation must be entered when the overall report is classified)

1. ORIGINATING ACTIVITY *(Corporate author)*
U.S. Army Cold Regions Research
and Engineering Laboratory
Hanover, New Hampshire 03755

2a. REPORT SECURITY CLASSIFICATION
Unclassified

2b. GROUP

3. REPORT TITLE

SEISMIC EXPLORATION IN COLD REGIONS

4. DESCRIPTIVE NOTES *(Type of report and inclusive dates)*
Monograph

5. AUTHOR(S) *(First name, middle initial, last name)*

Hans Roethlisberger

6. REPORT DATE
October 1972

7a. TOTAL NO. OF PAGES
139

7b. NO. OF REFS
198

8a. CONTRACT OR GRANT NO.

b. PROJECT NO. DA Project 4A062112A894
Task 20

c.

d.

9a. ORIGINATOR'S REPORT NUMBER(S)
Monograph II-A2a

9b. OTHER REPORT NO(S) *(Any other numbers that may be assigned this report)*

10. DISTRIBUTION STATEMENT

Approved for public release; distribution unlimited.

11. SUPPLEMENTARY NOTES

12. SPONSORING MILITARY ACTIVITY
U.S. Army Cold Regions Research
and Engineering Laboratory
Hanover, New Hampshire 03755

13. ABSTRACT
This Monograph contains a comprehensive review of the use of seismic methods and related techniques based on elastic waves, to gain information on the geometry and physical properties of the substrata in cold regions, particularly snow, ice and frozen ground. Pertinent elastic properties of these materials are described and methods for determining seismic velocities are summarized. Theories and application of reflection and refraction soundings on glaciers, continental ice sheets, ice shelves, and frozen ground are reviewed. Surveys employing surface waves, and special application of elastic waves, are described. Included with the text are 73 figures and about 200 selected references.

14. KEY WORDS

Elastic waves
Frozen soils
Geophysical surveys
Glaciers
Land ice
Sea ice
Seismic reflection method
Seismic refraction method
Seismic surveys
Subsurface investigations

DD FORM 1 NOV 65 1473 REPLACES DD FORM 1473, 1 JAN 64, WHICH IS OBSOLETE FOR ARMY USE.